TECHNICAL REPORT STANDARD TITLE PAGE

1. Report No.	2. Government Accession No.	3. Recipient's Catalog No.
FHWA/TX-86/68+382-1		

4. Title and Subtitle	5. Report Date
RESPONSE OF HIGHWAY BARRIERS TO REPEATED IMPACT LOADING: STEEL POST BARRIERS	November 1985
	6. Performing Organization Code

7. Author(s)	8. Performing Organization Report No.
K. S. Armstrong, R. E. Klingner, and M. A. Steves	Research Report 382-1

9. Performing Organization Name and Address	10. Work Unit No.
Center for Transportation Research The University of Texas at Austin Austin, Texas 78712-1075	11. Contract or Grant No. Research Study 3-5-84-382
	13. Type of Report and Period Covered Interim
12. Sponsoring Agency Name and Address Texas State Department of Highways and Public Transportation; Transportation Planning Division P. O. Box 5051 Austin, Texas 78763	14. Sponsoring Agency Code

15. Supplementary Notes

Study conducted in cooperation with the U. S. Department of Transportation, Federal Highway Administration

Research Study Title: "Resistance of Anchor Bolts to Impact Loading"

16. Abstract

A series of static and impact tests were carried out on a steel barrier post (T101 type) anchored to a 10-in. reinforced concrete deck. Slab reinforcement was modified in an attempt to produce a test specimen which would fail by yielding of the tension anchors. Analytical models were developed for various failure modes.

The primary objective of this research was to study the behavior of the anchorage under repeated impact loading. Repeated impact at low to moderate load levels proved not to be a problem for either the anchorage or the concrete deck; the response was very stable.

At higher load levels, however, all tests resulted in brittle failures. In most cases, this was attributed to a local diagonal tension failure near the slab edge. Since reinforcement is not effective in preventing this type of failure, it could not have been eliminated without changing the distance which the post base plate is set back from the free edge of the slab.

17. Key Words	18. Distribution Statement
	No restrictions. This document is available to the public through the National Technical Information Service, Springfield, Virginia 22161.

19. Security Classif. (of this report)	20. Security Classif. (of this page)	21. No. of Pages	22. Price
Unclassified	Unclassified	270	

Form DOT F 1700.7 (8-69)

RESPONSE OF HIGHWAY BARRIERS TO REPEATED IMPACT LOADING:

STEEL POST BARRIERS

by

K. S. Armstrong, R. E. Klingner, and M. A. Steves

Research Report No. 382-1

Research Study 3-5-84-382
Resistance of Anchor Bolts to Impact Loading

Conducted for

Texas
State Department of Highways and Public Transportation

In Cooperation with the
U.S. Department of Transportation
Federal Highway Administration

by

CENTER FOR TRANSPORTATION RESEARCH
BUREAU OF ENGINEERING RESEARCH
THE UNIVERSITY OF TEXAS AT AUSTIN

November 1985

The contents of this report reflect the views of the authors who are responsible for the facts and accuracy of the data presented herein. The contents do not necessarily reflect the views of policies of the Federal Highway Administration. This report does not constitute a standard, specification or regulation.

PREFACE

Steel post traffic barriers on our nation's highways are routinely subjected to high impact loads. Successful performance of a barrier requires inelastic deformation of the barrier system. In order to sustain large inelastic deformations while retaining structural integrity, the barrier system must possess a high degree of ductility.

In current design practice, steel post barriers are connected to bridge decks by anchor bolts. This study addresses the connection of steel post guardrail supports to concrete bridge decks. Its objectives are:

1) to provide information on the behavior of barrier to bridge deck connections;

2) to provide a basis for predicting the behavior of existing barrier anchorages; and

3) to propose recommendations for the design of ductile anchorages.

SUMMARY

A series of static and impact tests were carried out on a steel barrier post (T101 type) anchored to a 10-in. reinforced concrete deck. Slab reinforcement was modified in an attempt to produce a test specimen which would fail by yielding of the tension anchors. Analytical models were developed for various failure modes.

The primary objective of this research was to study the behavior of the anchorage under repeated impact loading. Repeated impact at low to moderate load levels proved not to be a problem for either the anchorage or the concrete deck; the response was very stable.

At higher load levels, however, all tests resulted in brittle failures. In most cases, this was attributed to a local diagonal tension failure near the slab edge. Since reinforcement is not effective in preventing this type of failure, it could not have been eliminated without changing the distance which the post base plate is set back from the free edge of the slab.

IMPLEMENTATION

The current Texas SDHPT design detail for anchorage of steel post highway barriers (T101 type) is non-ductile. Work should begin immediately on the development of a barrier which will fail in a ductile manner under lateral loads.

One way of achieving this is to modify the current anchorage detail by the most practical and economical combination possible of:

1) increased post set-back;

2) increased slab thickness; and

3) decreased anchor sizes, offset by increased length of base plate or decreased post spacing.

Otherwise, the steel-post barrier system should be replaced with a barrier system which does not present such a severe ductility problem. Research should be directed toward the development of a ductile steel-post barrier system to replace the current non-ductile design.

TABLE OF CONTENTS

CHAPTER 1

INTRODUCTION

1.1 General

Traffic barriers on our nation's highways are routinely subjected to high impact loads. Successful performance of a barrier requires that large amounts of energy be dissipated under impact loading. A primary source of such energy dissipation is inelastic deformation of the barrier system. In order to sustain large deformations while retaining structural integrity, the barrier system must possess a high degree of ductility; that is, it must be able to deform to several times its yield displacement without losing a significant portion of its maximum strength. This ability to deform inelastically while maintaining strength offers an additional advantage. After sufficient deformation, load will be redistributed from the heavily stressed portion of the system to adjacent sections, thus increasing the system's capacity.

The AASHTO bridge design specifications [1] call for an elastic design of traffic barriers with a transverse load of 10 kips applied to the barrier. The intent of those provisions is to contain the average vehicle. In more severe loading situations, however, the behavior of the system at its ultimate capacity must be assessed. As previously stated, ductility is an important aspect of this behavior.

In current design practice, barriers are connected to bridge decks by anchor bolts (Fig. 1.1). This connection is often the least ductile element of the barrier system. The anchorage can fail either by tensile yielding of steel or by tensile failure of the concrete at the anchorage. This second mode is a brittle type of failure and must be avoided. Ideally, the anchor bolts should yield before substantial damage to the concrete bridge deck occurs. In this case, repair would require only replacement of the damaged bolts. Failure of the concrete deck, on the other hand, leads to costly and time-consuming repairs. Unfortunately, deck failure is a prevalent failure mode for existing barrier installations [2].

1.2 Purpose of Investigation

Results from this study are intended to:

1) provide information on the behavior of barrier to bridge deck connections;

2) provide a basis for prediction of the behavior of existing barrier anchorages; and

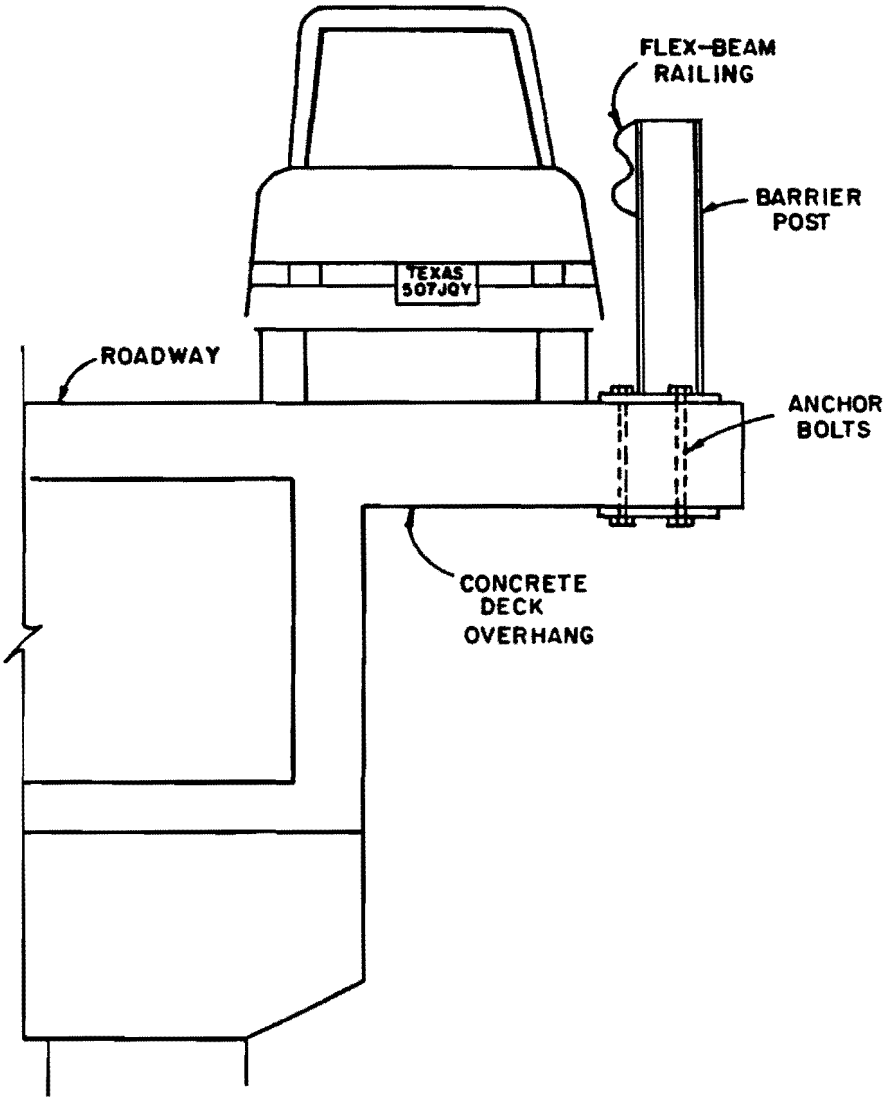

Fig. 1.1 Typical Steel Barrier System for Bridges

3) lead to recommendations for the design of ductile anchorages.

Increased understanding of the behavior of anchorages under impact load should lead to the use of safer anchorage systems and decrease repair costs.

1.3 Scope of Investigation

This study addresses the connection of steel post guardrail supports to concrete bridge decks. The anchorage of concrete barriers, sometimes referred to as "safety shapes" or "New Jersey barriers," is investigated by Steves [3] in a separate study. Both studies are part of a research program, funded by the Federal Highway Administration and the Texas State Department of Highways and Public Transportation, concerning the behavior of anchor bolts under impact loading.

The particular barrier system investigated here conforms to Texas SDHPT Type T101, and consists of a "flex-beam" shaped metal railing supported by W6x20 steel posts bolted to the bridge deck (Fig. 1.2). Although the original scope of the project involved only evaluation of the performance of the current anchorage design under impact loading, it was soon discovered that the existing design would probably be inadequate under static loading. Thus, the scope was expanded to include redesign as well as testing of the anchorage. All trial modifications to the Texas SDHPT standard design were approved by that organization.

All anchorages considered in this study make use of anchor bolts or studs which are either embedded in the concrete deck or inserted through the deck and fastened underneath. As referred to in this report, anchor bolts or studs are those connectors which resist pullout primarily by means of a mechanical anchoring device, such as a bolt head or steel plate, rather than by bond along their length.

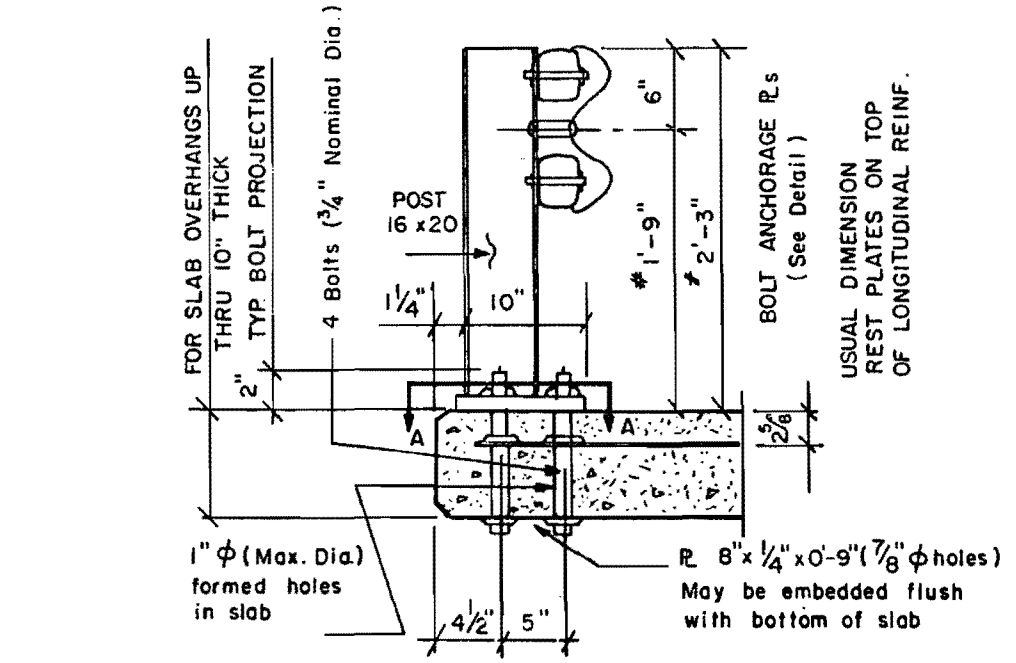

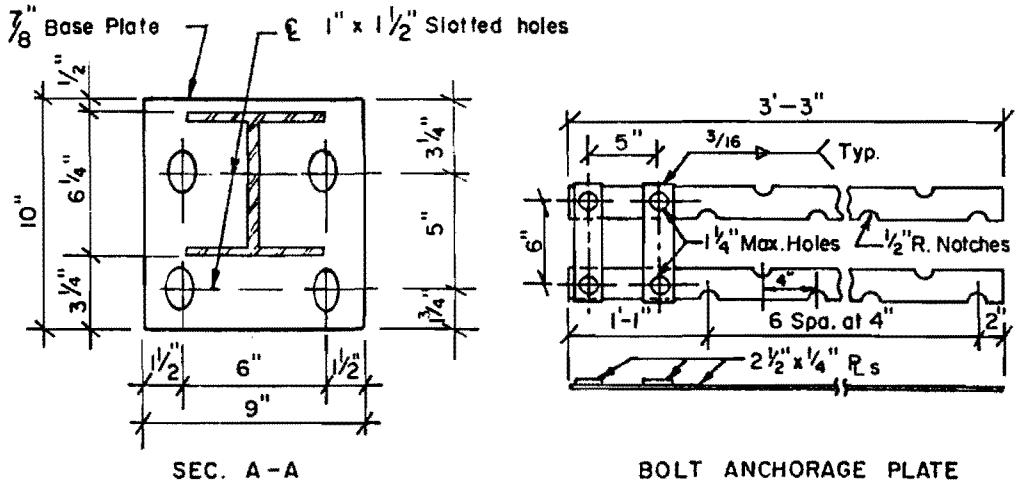

Fig. 1.2 Texas SDHPT Type T101 Barrier System.

CHAPTER 2

BACKGROUND

2.1 Traffic Barrier and Impact Loads

The basic function of the traffic barrier is to redirect vehicles which have come too close to the edge of a bridge or roadway. In so doing, the barrier is subjected to impact loading. When barrier systems are designed, much attention is given to the safety aspects of the system's performance. Under relatively light loads, such as those caused by the average passenger vehicle, the system should deform sufficiently to inflict little damage on the vehicle. At the same time, the barrier must be strong enough to contain heavy vehicles such as buses and semi-trailer trucks. New systems are often given crash tests before being put into service.

A report by Bryden and Hahn [4] describes a typical crash test program, conducted on a steel post, thrie-beam railing barrier system. The authors of that study felt that the anchorage of the system to the bridge deck did not need to be modeled, since previous tests and field experience had shown existing details to be adequate. Therefore, the posts were anchored with three 1-in. diameter by 17-in. long anchor bolts (A36) to a 3-ft wide by 3-ft deep concrete footing embedded 2 ft 6 in. into the ground. The behavior of the anchorage was similarly removed as a test parameter from programs carried out on other proposed barrier systems.

That a problem with barrier anchorages does, in fact, exist has come to the attention of Texas SDHPT. A study conducted by Arnold and Hirsch [2] of existing Texas SDHPT anchorage details is described in Section 2.3. For additional information on anchorage behavior it is necessary to look at work done in fields not directly related to the area of transportation structures.

2.2 Basic Principles of Anchorage Design

Some of the earliest investigations into the behavior of short anchor bolts and welded studs were carried out in the 1960's and early 1970's by the Nelson Stud Company (now a subsidiary of TRW, Inc.) [5,6,7,8]. In a 1974 publication [8], they presented a model for tensile pullout which is similar to the currently accepted model discussed in subsection 2.2.1.

Nelson Stud/TRW sponsored tests by Ollgaard, Slutter and Fisher [9] in 1971, and by McMackin, Slutter and Fisher [10] in 1973, which resulted in the development of empirical formulas for the shear

capacity of anchors. These formulas were incorporated into the 1974 TRW report [8] as well as into the 1978 PCI Design Handbook [11], the 1977 PCI Manual for Structural Design [12], and the 1978 AISC specifications [13]. Work done at the University of Tennessee for TVA from 1975 to 1977 [14,15,16] resulted in the development of a semiconical failure model (described in subsection 2.2.2) for anchors close to a free edge which are loaded in shear.

The growth of the nuclear power industry in the late 1970's provided the impetus for renewed interest in the behavior of anchors. Because of increased emphasis on ductility and quality assurance, ACE Committee 349, in its "Proposed addition to Code Requirements for Nuclear Safety Related Structures" [17], included an appendix which summarized state-of-the-art design procedures for anchorages, incorporating more conservative capacity reduction factors. The work of the committee was presented as a "Guide to the Design of Anchor Bolts and Other Steel Embedments" [18] in a 1981 edition of Concrete International.

Two papers by Klingner and Mendonca [19,20], published in 1982, compare existing procedures for predicting tensile and shear capacities of anchorages in the light of available test data. The results of those studies indicate that, with some modifications, tensile and shear capacity as governed by the anchor itself is most reliably calculated using the methods presented in the PCI publications [11,12] and in a 1981 paper by Klingner, Mendonca and Malik [21]. Capacity as governed by concrete failure is most reliably calculated using the method of ACI Committee 349. These methods are presented in subsections 2.2.1 and 2.2.2.

2.2.1 Tensile Loading Condition. A typical headed anchor, embedded in a block of unreinforced concrete and subjected to a tensile load, is shown in Fig. 2.1. If the depth of embedment and edge distance are sufficient, the capacity of the anchorage can be computed as the cross-sectional area of the anchor times its specified minimum yield strength [19]. For threaded anchors, the nominal tensile stress area should be used. If the anchor steel does not exhibit a definite yield plateau, yield strength can safely be taken as 90 percent of the specified minimum ultimate tensile strength [19]. For design of anchorage steel, the nominal tensile capacity should be modified by a capacity reduction factor of 0.90 [19]. Thus,

$$P_u \geq \phi_s P_s \qquad (2.1)$$

$$P_s = A_s f_y \qquad (2.2)$$

If the depth of embedment is inadequate, concrete tensile failure will occur before the anchor has yielded. Whether the anchor

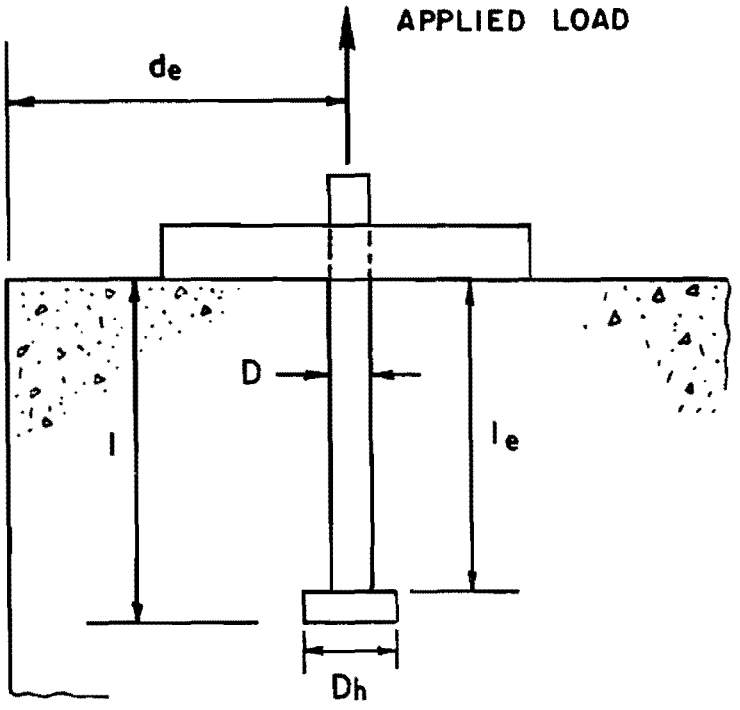

Fig. 2.1 Typical Tension Anchor

is initially bonded or unbonded along its length, the entire tensile load will eventually be transferred into the concrete by the anchor head (Fig. 2.2). Cracking begins around the perimeter of the anchor head and propagates to the surface at an angle, producing a conical failure surface often referred to as a "pullout cone."

The applied load is resisted by tensile stresses acting perpendicular to the failure surface. The resultant force, however, acts in the direction of the applied load since all stresses acting perpendicular to the applied load are self-equilibrating (Fig. 2.3b). Thus, pullout strength can be calculated as the resultant of tensile stresses directed parallel to the applied load and acting on the surface area of an idealized truncated cone, or equivalently, on its projected area (Fig. 2.3a). The magnitude of stress is assumed to vary from zero at the concrete surface to a typical value for concrete tensile strength of $6\text{-}7\sqrt{f'_c}$ (psi) at the anchoring device. A uniform nominal stress of $4\sqrt{f'_c}$ (psi) may conservatively be assumed to act on the failure surface [17,18,19] (Fig. 2.3c).

If the state of stress in the concrete is produced by tension on the anchor alone, the initial inclination of the failure surface will be at about 45° to the direction of the applied load [17,18]. As the crack nears the surface, the uncracked concrete above deforms in flexure, producing a state of compression in the concrete near the leading edge of the crack. For embedments less than about 5 in., the resistance due to this flexural action exceeds the cone pullout resistance, increasing the failure load. If the value of $4\sqrt{f'_c}$ is retained as a uniform stress, the angle of inclination of the failure surface is effectively increased. The use of a 45° inclination for all anchors is recommended, however, since surface cracking may prevent development of the flexural mechanism for shallow depth anchors [17,18,19].

If the inclination of the failure surface is assumed to be 45°, pullout strength can also be calculated as the resultant of stresses acting parallel to the applied load on the surface area of a hypothetical cylinder with radius equal to the average radius of the idealized truncated cone (Fig. 2.3d). This is analogous to the procedure recommended by ACI [22] for calculating punching shear in slabs and footings. Derivations of the three procedures for calculating pullout strength of concrete are presented in Appendix A.1.1.

When multiple anchors are used at close spacings, a single failure surface will develop which will offer less resistance than the sum of individual anchor capacities. The overlapping portions of the projected stress cones must be omitted from the area calculations, as in Fig. 2.4a. If a plate is used as an anchoring device for multiple anchors, the trapezoidal failure surface (Fig. 2.4b) can be assumed, as long as failure by punching of the bolt head through the anchoring plate has been prevented.

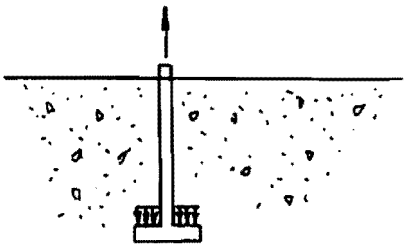

ANCHOR INITIALLY UNBONDED

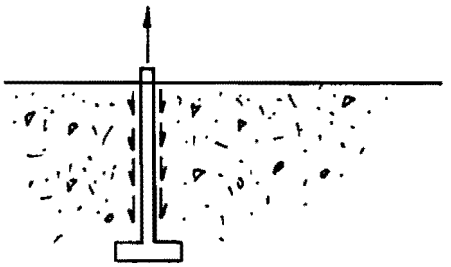

ANCHOR INITIALLY BONDED

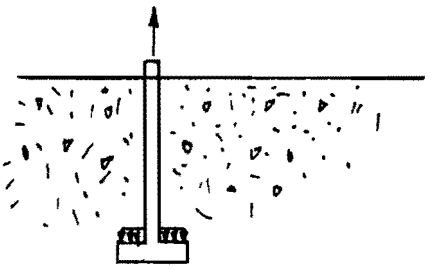

AFTER BOND HAS BEEN BROKEN

Fig. 2.2 Transfer of Load to Concrete

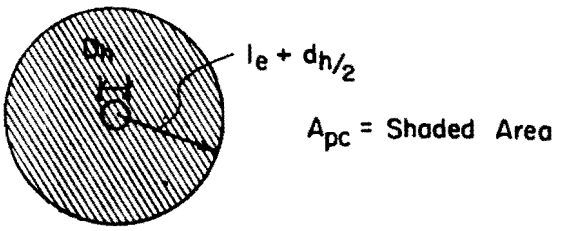

a. Projected Area

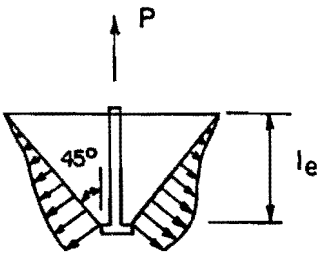

b. Failure Cone With Assumed Stress Distribution

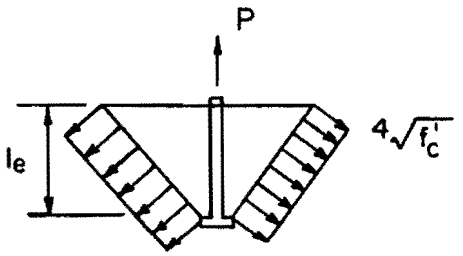

c. Equivalent Uniform Stress Distribution

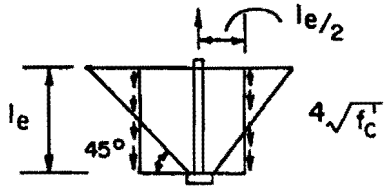

d. Cylindrical Failure Surface (Equivalent For 45° Cone)

Fig. 2.3 Failure Surface of Single Tension Anchor

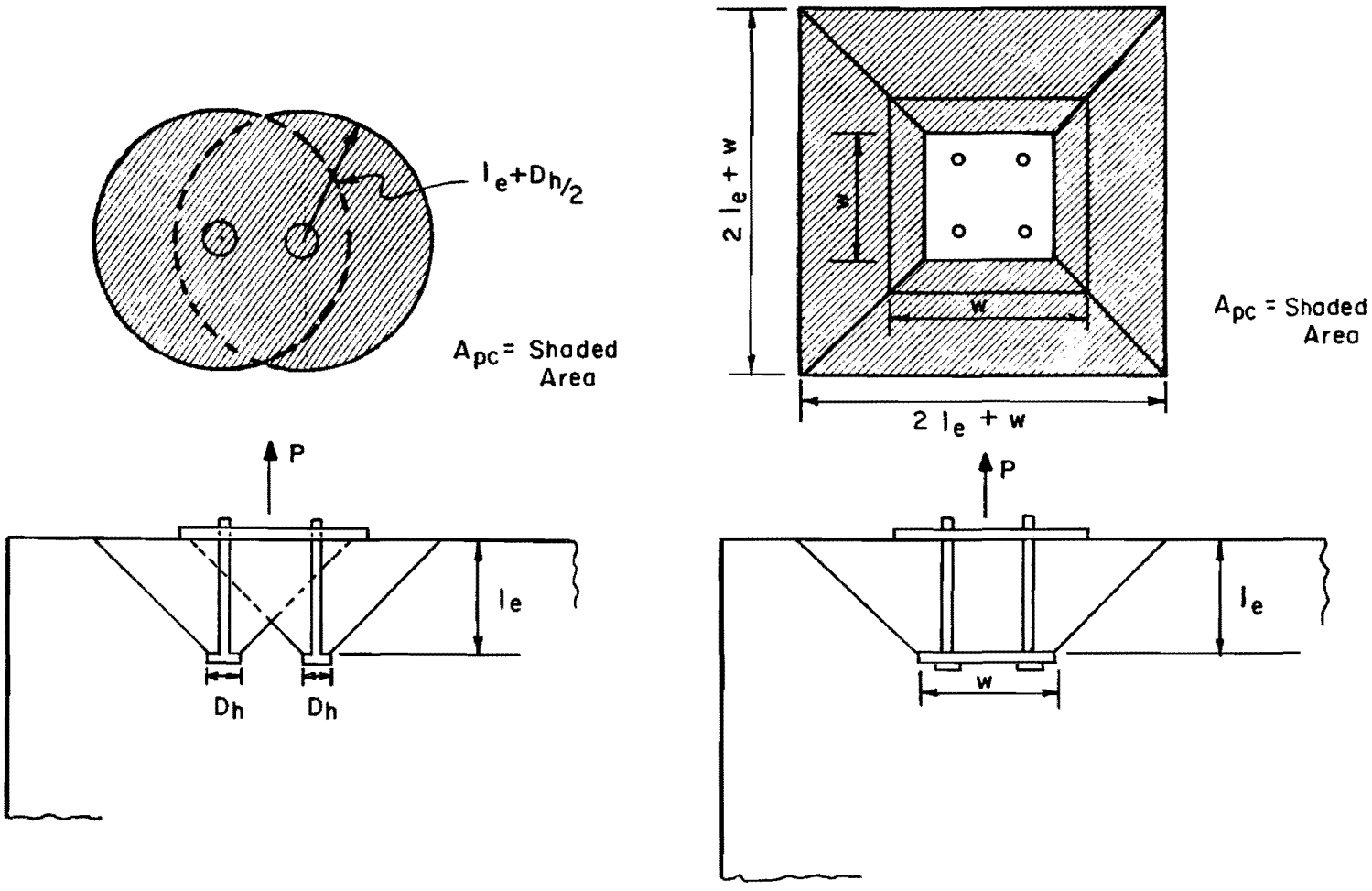

Fig. 2.4 Typical Failure Surfaces for Multiple Tension Anchors

For either single or multiple anchors, portions of the projected failure cone or trapezoid which extend beyond the edge of the concrete should be excluded from the area calculation. This situation is illustrated in Fig. 2.5. It should be emphasized that since failure begins at the periphery of the anchoring device, the area of the anchor head or plate must also be subtracted. The projected tensile stress area of an anchorage can be computed by a combination of simple geometric formulas. Sample calculations of effective projected area are presented in Appendix A.2.1.

Tensile capacity of the anchorage as governed by concrete failure is computed as

$$P_u \leq \phi_c P_c \tag{2.3}$$

$$P_c = 4\sqrt{f'_c}\, A_{pc} \tag{2.4}$$

The understrength factor should be taken as 0.65 for normal weight concrete [19].

For anchors very near an edge, lateral bursting of concrete in the region of the anchor head is a possible failure mode [17,18]. The minimum edge distance required to prevent this type of failure can be found by equating the lateral bursting force to the tensile capacity of the concrete. The lateral force can be conservatively taken as one-fourth of the tensile capacity of the anchor, while the concrete capacity is calculated in a manner analogous to that used for computing pullout capacity, with the height of the conical failure surface taken as the edge distance, d_e [17,18]. Applying a conservative reduction factor of 0.65 to the concrete capacity gives

$$d_e = (A_s f_{ut} / 32 \sqrt{f'_c})^{1/2} \tag{2.5}$$

with A_s equal to the nominal tensile stress area for threaded anchors. A derivation of this is presented in Appendix A.1.2. Sample capacity calculations for an anchorage loaded in tension are presented in Appendix A.2.2.

2.2.2 Shear Loading Condition. The capacity of an individual anchor loaded in direct shear depends on depth of embedment, edge distance, and the strength of the anchor itself. To develop the ultimate shear capacity of an anchorage, sufficient embedment length must be provided to prevent a pullout failure. As in the tensile loading condition, the resistance over a conical failure surface must exceed the tensile capacity of the anchor steel. Partially embedded

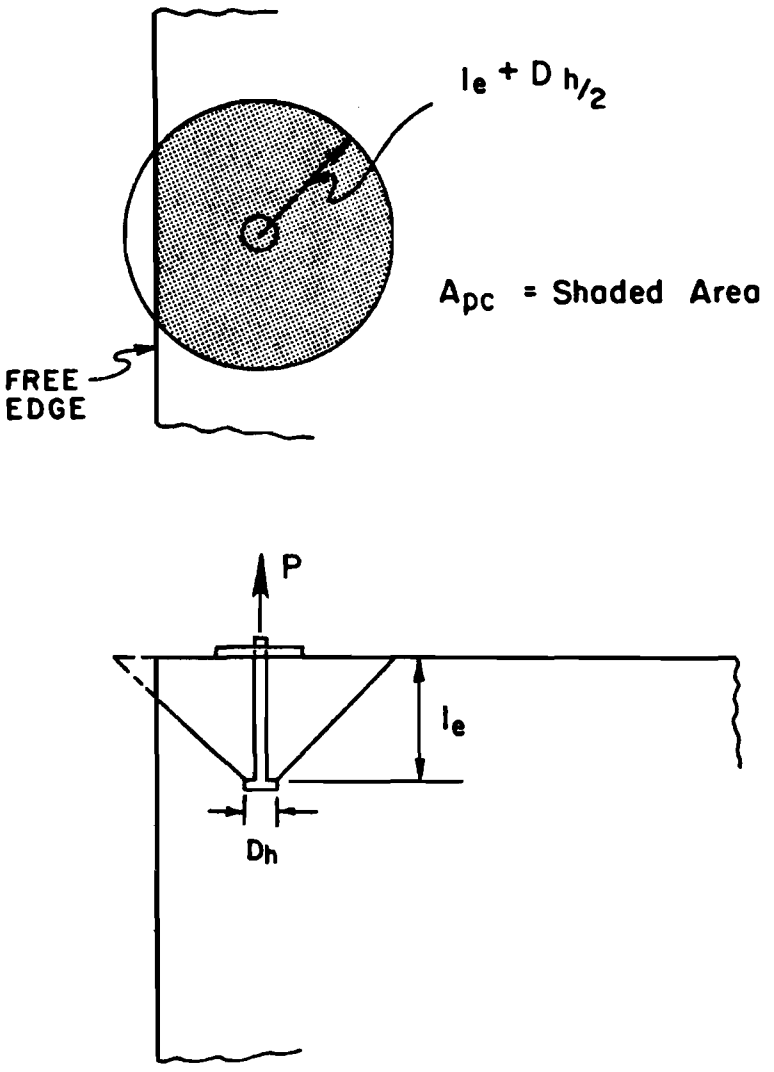

Fig. 2.5 Tension Anchor with Limited Edge Distance

anchors (those for which pullout failure has not been prevented) are beyond the scope of this report.

For a fully embedded anchor far from a free edge, ACI Committee 349 [17] applies the shear-friction concept to the transfer of shear from anchor steel to concrete. According to this theory, shear is transmitted to the concrete by bearing of the anchor on the surface of the concrete, forming a shallow wedge (Fig. 2.6). In order for the wedge to move laterally, it must also move upward against the base plate. This upward force on the base plate produces tension in the anchor and in turn increases the clamping force on the wedge.

The clamping force is a function of the coefficient of friction, μ, whose magnitude depends on the location of the plane of shear transfer. Accepted values of μ are 0.7 for a flush mounted plate; 0.9 for a plate embedded so that its exterior surface is flush with the surface of the concrete; and 0.55 for a plate mounted on a grout pad exterior to the concrete surface [17]. The shear strength of the anchorage is then given as

$$V_s = \mu A_s f_y \tag{2.6}$$

In tests by Klingner, Mendonca, and Malik [21] such a clamping force mechanism was not observed. Rather than resisting movement of the anchor and concrete wedge, the loading plate either slid easily along the concrete surface or rotated away from it. The failure mechanism observed was a combination of shear and flexure in the anchor itself, producing a "kink" in the anchor (Fig. 2.7).

A report by Adihardjo and Soltis [23], describing their tests of grouted base details, includes photographs of anchor bolts which also exhibited this kinking mechanism. Although loads were applied at angles of 0 to 90° to the vertical in these tests, Adihardjo and Soltis propose that slip between the base plate and grout surface was induced by the shear component of the load, producing moment in the anchor bolt. Thus, the location of the shear transfer plane plays a role in both the bolt kinking theory and the shear-friction concept. As previously mentioned, the coefficient of friction is related to the location of the shear transfer plane in the shear-friction mechanism. In terms of the kinking theory, on the other hand, a transfer plane at a greater distance from the embedded end of the anchor increases the effective length of the anchor subjected to bending. Adihardjo and Soltis conclude that additional study is necessary to develop a method for the design of anchor bolts which is consistent with the kinking mechanism. Effective length and end fixity are the major parameters to be defined.

Klingner, Mendonca and Malik [21] have proposed expressions for design of anchor steel based on the direct shear capacity of the

Fig. 2.6 Shear Friction Mechanism

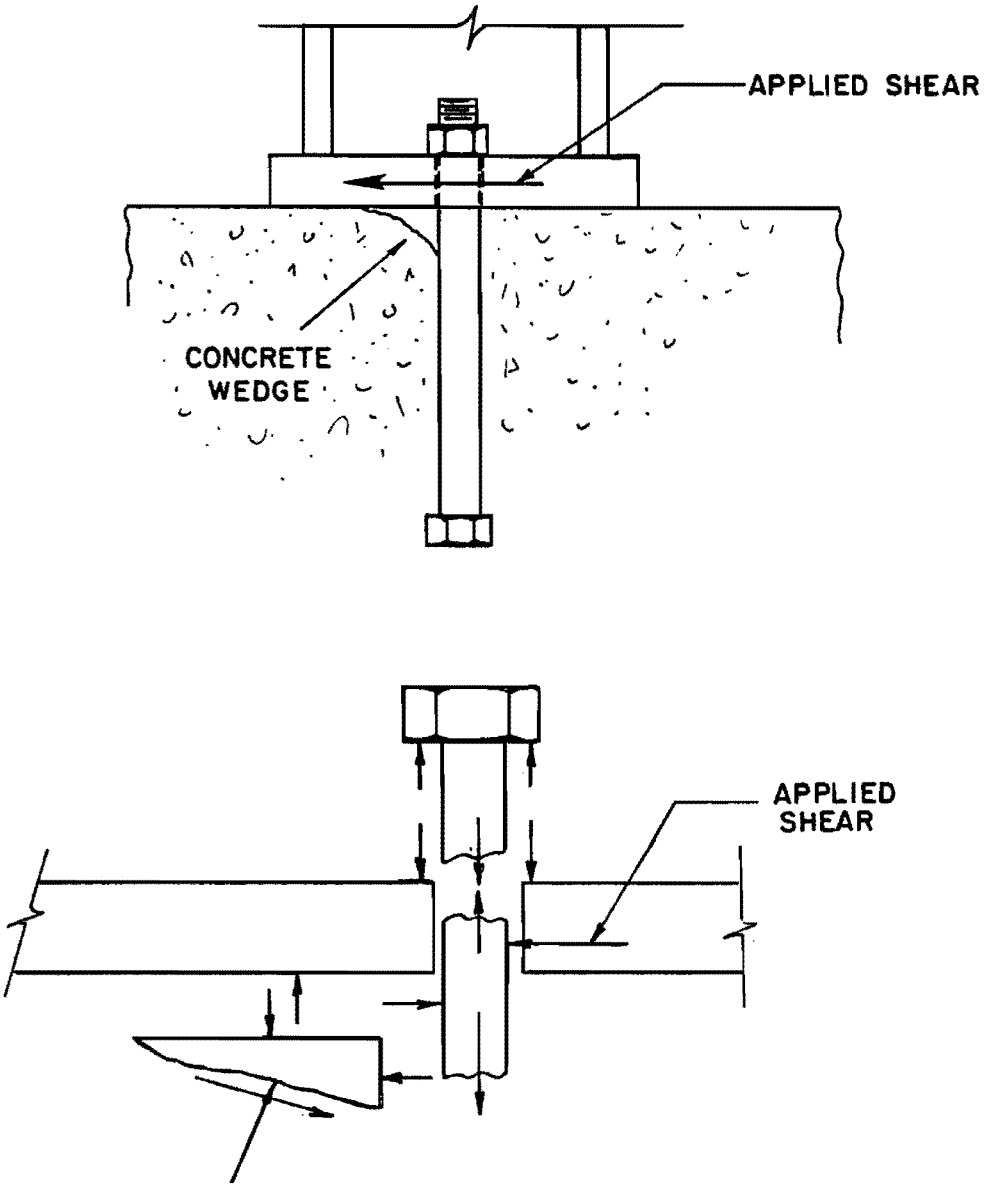

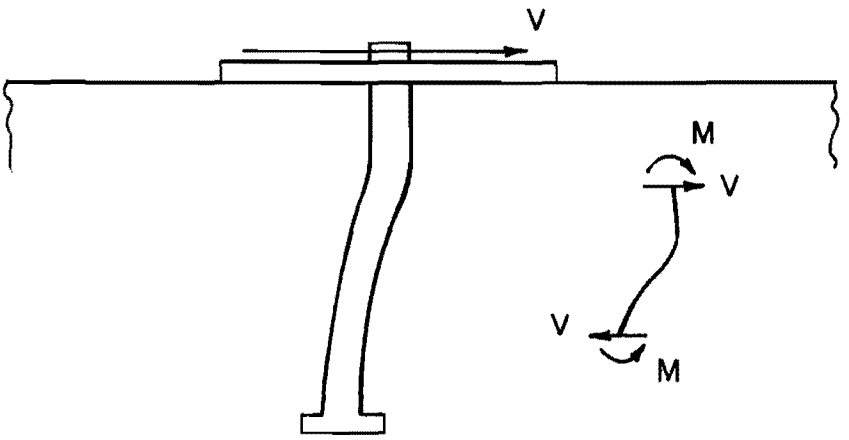

Fig. 2.7 Bolt Kinking Mechanism

anchor. Shear capacity is calculated as the appropriate cross-sectional area of the anchor times its minimum yield strength, in shear. Since information on the shear strength of an anchor is not ordinarily available to the designer, it must be derived from values for tensile strength. Shear yield strength, f_{yv}, for anchor steel exhibiting a definite yield plateau can be taken as $1/\sqrt{3}$ times the minimum specified tensile yield strength, f_y, in accordance with the von Mises failure theory. When the material does not exhibit a definite yield plateau, yield strength should be taken as 0.90 times the minimum specified ultimate tensile strength, f_{ut}. In this case, yield strength in shear can be computed as 0.75 times the tensile yield strength; that is, f_y equals 0.75 (0.90 f_{ut}), or 0.67 f_{ut}.

Design of anchor steel for shear is then based on the following expressions:

$$V_u \leq \emptyset_s V_s \tag{2.7}$$

$$V_s = A_s f_{yv} \tag{2.8}$$

where the shear yield strength, f_{yv}, is calculated as recommended above. The capacity reduction factor $\emptyset_s$ is taken as 0.90. These expressions correlate well with available test data, and provide a conservative estimate of the actual failure load [21].

The direct shear method can be compared with the shear-friction method of ACI 349 [17]. For a base plate flush with the concrete surface the shear-friction theory gives

$$V_s = \mu A_s f_y \tag{2.6}$$

$$V_s = (0.7)A_s(5/6)f_{ut} = 0.58\ A_s f_{ut} \qquad \text{(2.7) repeated}$$

Where $\mu = 0.7$ and fy is taken as 5/6 f_{ut}.

The direct shear method gives

$$V_s = A_s f_{yv} \qquad \text{(2.8) repeated}$$

$$f_{yv} = (0.67)f_{ut} \tag{2.9a}$$

$$V_s = (0.67)A_s f_{ut} \tag{2.9b}$$

Reference 20 proposes that the direct shear method is sufficiently conservative and more rational than the shear-friction theory.

If edge distance is inadequate, the anchorage capacity will be limited by the tensile strength of the concrete. The resulting failure surface can be idealized as a semicone with a total central angle of 90° radiating from the anchor at the surface of the concrete toward the free edge (Fig. 2.8). The failure load can be computed as the resultant of stresses equal in magnitude to the maximum tensile strength of the concrete, taken as $4\sqrt{f'_c}$, and acting on the projected area of the idealized semicone. For design purposes,

$$V_u \leq \phi_c V_c \tag{2.10}$$

$$V_c = 4\sqrt{f'_c}\, A_{vc} \tag{2.11}$$

The capacity reduction factor ϕ_c is taken as 0.65.

When the applied shear is resisted by more than one anchor in a plane parallel with the edge of the concrete, the effect of overlapping failure surfaces must be considered for computing Avc (Fig. 2.9a). Similarly, when multiple anchors are placed in the plane of the applied shear, only the anchor farthest from the free edge will be effective in resisting concrete failure, since its failure surface will envelope those of each forward anchor (Fig. 2.9b).

When edge distance is limited, reinforcement must be used to prevent pullout of a shear cone. ACI Committee 349 [17] recommends the use of reinforcement placed so as to restrain tensile cracking along the assumed failure surface (Fig. 2.10a). They caution that adequate development length for the reinforcement must be provided on either side of the crack.

An alternate reinforcing scheme recommended by Klingner, Mendonca and Malik [21] transfers shear load directly from the anchor to the reinforcement. The load is then resisted by bond along the surface of the reinforcment, rather than by the tensile strength of the unreinforced concrete. The reinforcement is placed so as to restrain the anchor, on a plane as near as possible to the plane on which the shear is applied. Such an arrangement, often referred to as hairpin reinforcement, is shown in Fig. 2.10b. The strength of the reinforcement can be taken as the cross-sectional area of the two hairpin legs times the specified minimum yield strength of the reinforcing steel. That is,

$$V'_s = A_h f_{yh} \tag{2.12}$$

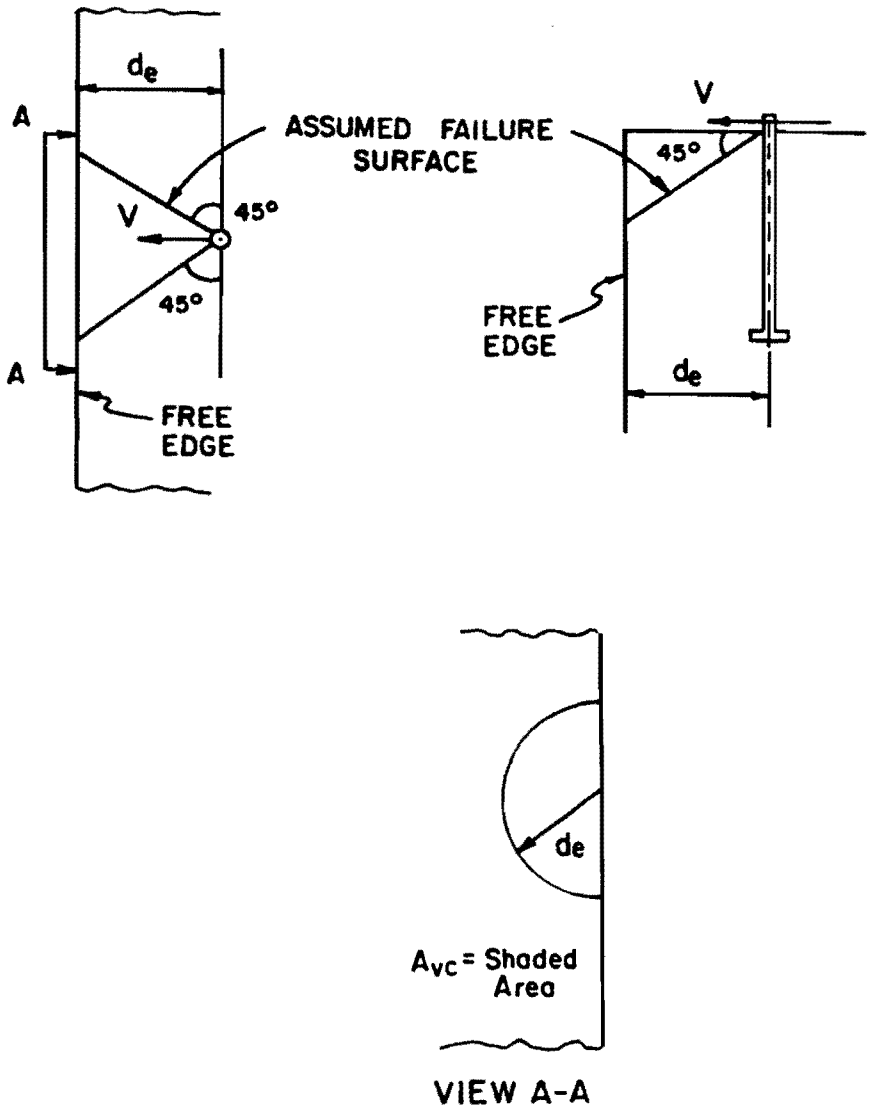

Fig. 2.8 Semi-conical Failure Surface for Shear Anchors

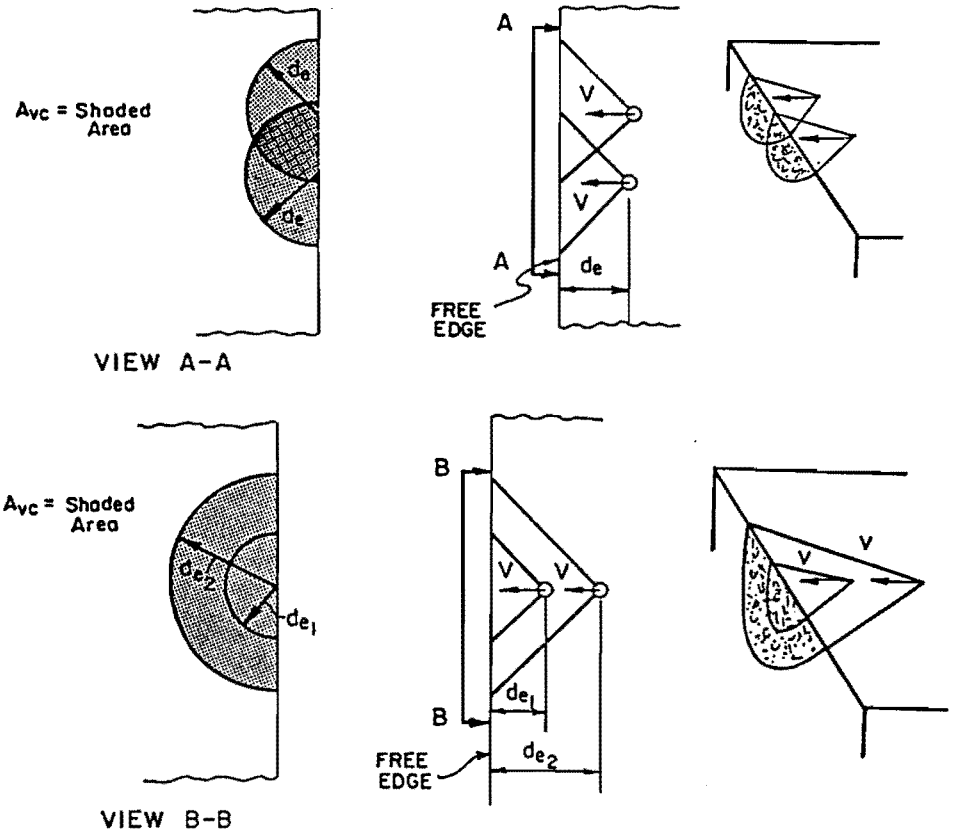

Fig. 2.9 Typical Failure Surface for Multiple Shear Anchors

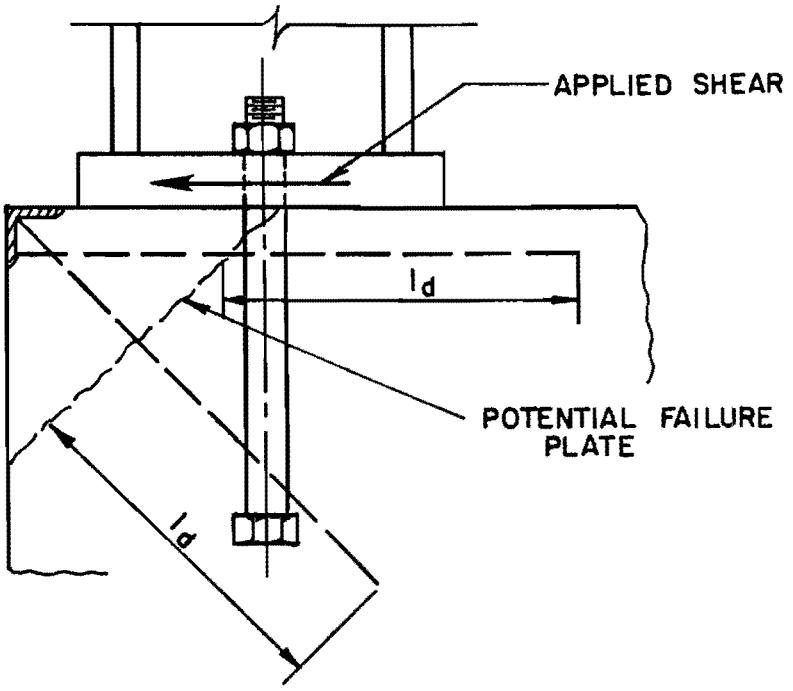

Fig. 2.10a Reinforcement for Shear.

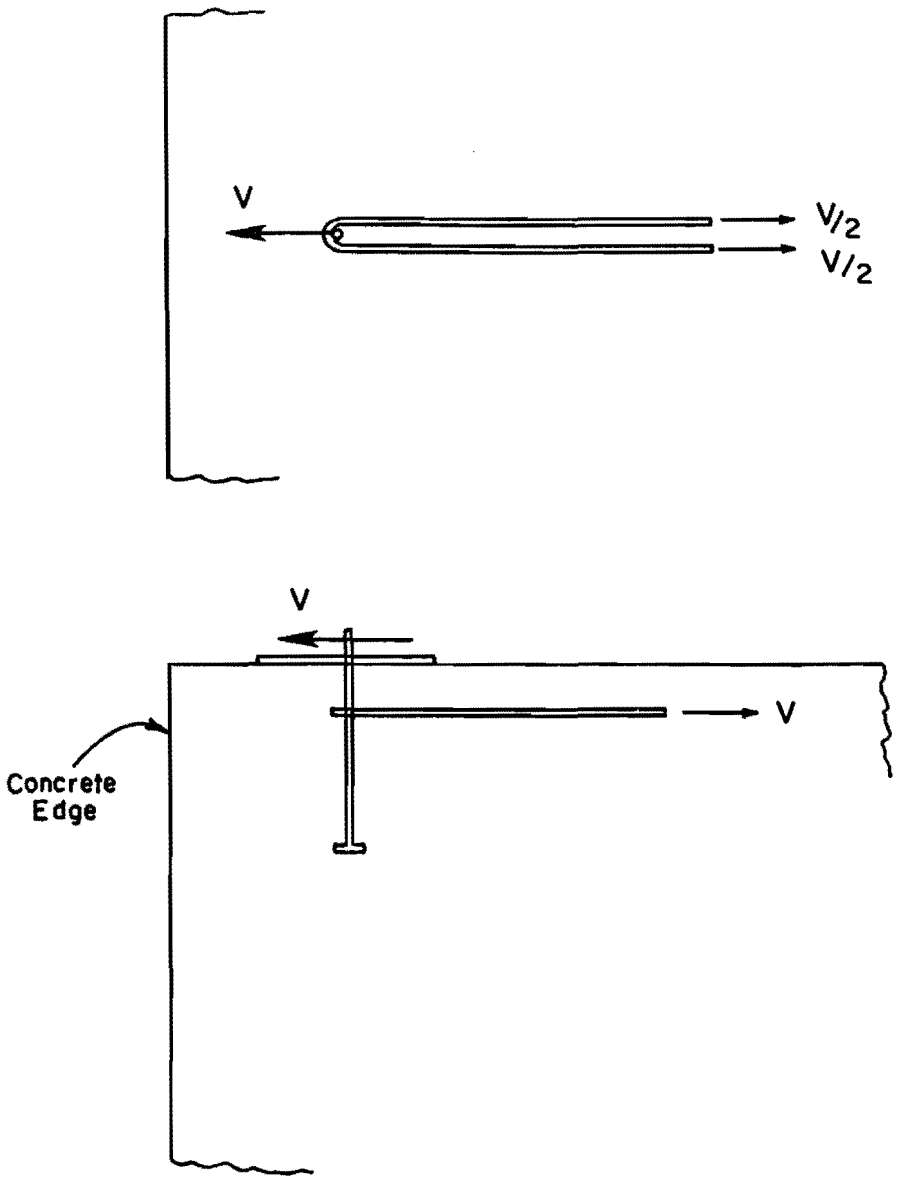

Fig. 2.10b Reinforcement for Shear (cont.).

Development length should be provided in accordance with ACI provisions [22].

While reinforcement can prevent concrete failure due to inadequate edge distance, some spalling of the edge must still be expected when the tensile capacity of the concrete is reached [21]. Furthermore, although concrete tensile failure can be controlled by reinforcement, the capacity of the anchor bolt will be reduced due to bending between the shear plane and the top layer of reinforcement or hairpins. Thus, it is desirable to provide adequate edge distance whenever possible. Shear reinforcement, if necessary, should be placed as near as possible to the shear plane to reduce bending stresses in the anchors.

Sample capacity calculations for an anchorage loaded in shear are presented in Appendix A.2.2.

2.2.3 Combined Tension and Shear. The behavior of anchors subjected to a combination of tension and shear is more complex than that of anchors under pure tension or shear. Since the anchor actually resists the applied shear by a combination of direct shear and tension due to flexure, the full tensile capacity of the anchor will not be available for resisting the tensile load component.

Relatively few investigations have been made into the behavior of anchor bolts under combined loading. McMackin, Slutter and Fisher [10] presented an interaction equation which represented the best fit to results obtained from their tests of individual anchors under combined loading.

$$(P_u/\phi_s P_s)^{5/3} + (V_u/\phi_s V_s)^{5/3} \leq 1 \qquad (2.14)$$

In this expression the tensile capacity of the anchor, P_c, was determined by the pullout cone method of Subsection 2.2.1. The shear capacity, V_c, on the other hand, was based on an empirical formula which has been largely replaced by the more rational method of subsection 2.2.2. This interaction equation is not valid with a different expression for V_c.

In 1979, Adihardjo and Soltis [23] conducted tests on individual anchors with base plates resting on 1-in. grout pads. They proposed a failure model which treats the anchor as a fixed-end member subjected to moment and axial tension. Rather than deriving an interaction equation, they recommended further investigation to determine such parameters as effective length and end fixity with regard to the proposed failure model.

Since the behavior of anchors under combined loading is not well understood, ACI Committee 349 has proposed a conservative straight-line addition of the pure tensile and shear capacities. That is,

$$(P_u / \phi_s P_s) + (V_u / \phi_s V_s) \leq 1 \qquad (2.14)$$

The shear and tensile capacities should be computed as recommended in subsections 2.2.1 and 2.2.2 (also see Appendix A.2.2), and the capacity reduction factor ϕ_s taken as 0.90.

Note that the required tensile and shear capacities are those of the anchor steel. Concrete failure is assumed to be prevented if depth of embedment is adequate to develop the full tensile capacity of the anchor, since the actual tensile load must necessarily be less than the tensile capacity of the anchor.

2.2.4 Load Sharing. When multiple anchors are used in a connection, the applied load is distributed in some manner among the individual anchors. The actual resistance mechanism is quite complex, involving the stiffnesses and strengths of the individual anchors and also their interaction with the load plate and with the concrete.

Even when dealing with the relatively well defined problem of a row of connectors loaded in shear (Fig. 2.11), a typical analysis requires that several simplifying assumptions be made. The results of such analyses have been found to be inconsistent with experimental values [24]. Fortunately, the assumption that the stress at failure is uniformly distributed among the bolts, seems to be borne out by experimental evidence [25]. Apparently, only a relatively small amount of plastic deformation is necessary to permit a uniform distribution of load among the bolts [25].

It seems reasonable to expect that if the connection behaves in a ductile manner, plastic deformation will allow redistribution of the loads among individual anchors. In the terminology of limit design, any possible resistance mechanism which satisfies statics represents a lower bound to the actual capacity [26]. A value for the actual failure load of the connection can be arrived at by considering the most efficient mechanism for resisting the applied loads.

For a connection loaded in pure tension or shear, the most efficient resistance mechanism would be one in which all anchors would carry a share of the load in proportion to their individual capacities. Theoretically, all anchors would then reach their full capacities. This represents the maximum possible capacity of such a connection.

An anchorage subjected to an overturning moment caused by an eccentrically applied shear must do two things. It must resist the applied shear, and also provide a force couple to equilibrate the overturning moment. The force couple is provided by tension in the anchors on one side of the connection and by bearing of the base plate on the concrete surface at the other side. The situation is similar to that of a beam resisting bending moment, and the normal beam model can

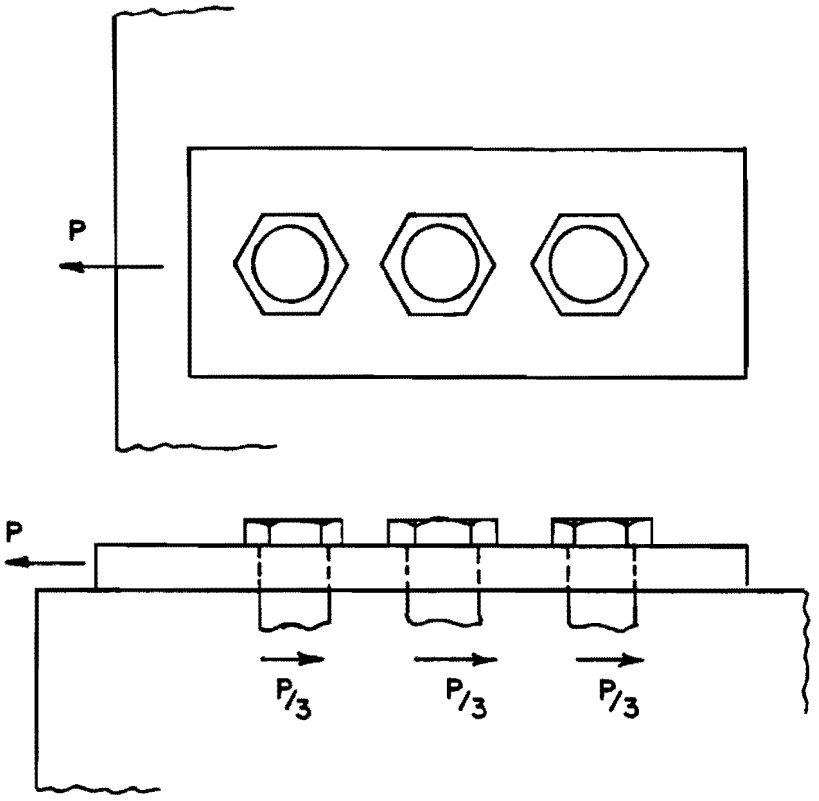

Fig. 2.11 Load Distribution to Multiple Anchors

be used to determine the magnitude of the forces and the length of the internal lever arm. From Fig. 2.12

$$T = C = 0.85\, f'_c\, ab \qquad (2.15)$$

$$M = T(d-a/2) \qquad (2.16)$$

The remaining question is then the manner in which the shear load is resisted. Unlike the case of a group anchorage resisting pure shear, the most efficient distribution of load is not immediately apparent. As a first approximation, it is convenient to assume that the entire shear load is resisted by the anchors in the compression zone (Fig. 2.13). If the load level corresponding to yielding in the tension bolts does not cause the bolts carrying the shear load to exceed their capacities, then the most efficient resistance mechanism has been found. In this case, strength of the connection is limited by the capacity of the tension bolts.

If, on the other hand, the shear capacity of the bolts in the compression zone is reached before the tension bolts yield, then some of the shear load can be redistributed (Fig. 2.13). The "tension" bolts would then be carrying a combination of tension and shear. The combined load-carrying capacity of the bolts is determined as in subsection 2.2.3, using Eq. 2.14.

The maximum capacity of the connection can be found by trial and error. A trial value is chosen for the magnitude of the applied shear load. The shear load carried by the tension bolts is assumed to be the trial value less the total shear capacity of the bolts in the compression zone. The tension in the bolts is then determined from Eqs. 2.15 and 2.16. The combined stresses due to tension and shear are evaluated using Eq. 2.14, and the magnitude of the applied shear is adjusted so that this sum approaches unity. A sample calculation of this type is presented in Appendix A.2.2.

The work of Hawkins, Mitchell and Roeder [27] compared two different models for load-sharing in connections subjected to eccentric shear. The plastic distribution method is as described above, while the rigid plate method requires that the applied shear be distributed elastically to all anchors in the connection with no redistribution of load. For the connections tested, the plastic distribution method gave ratios of measured to predicted strengths which were closer to unity, and which were always conservative. The predicted strengths were based on the interaction equation of McMackin, Slutter and Fisher [10]. If strength predictions had been made using the more conservative straight-line formula (Eq. 2.14) of ACI Committee 349 [17], the ratios of measured to predicted strength would probably have been higher.

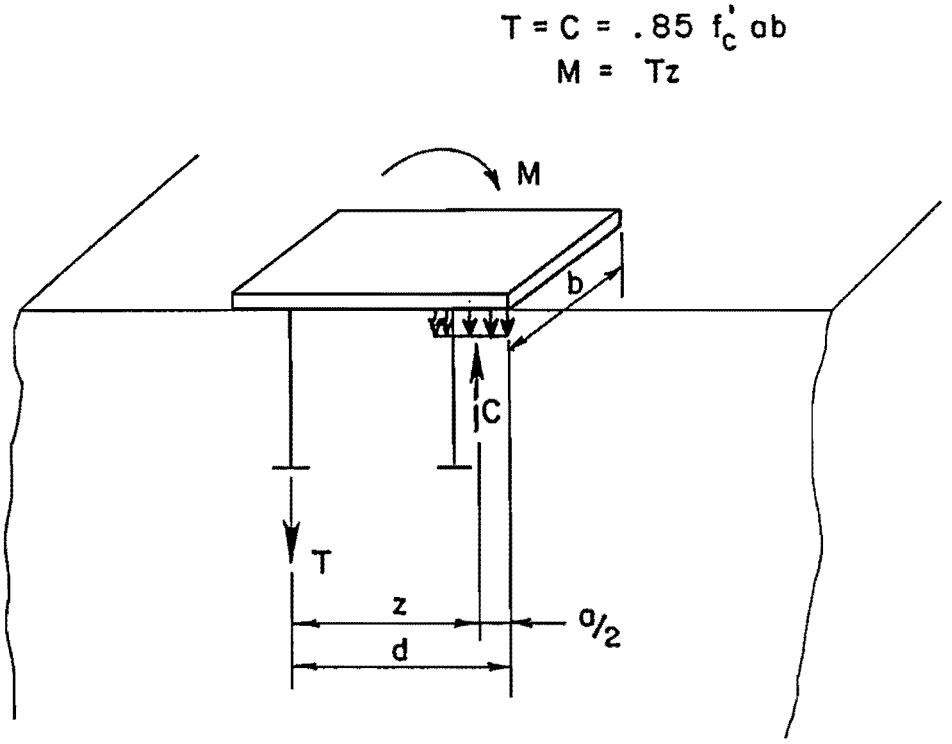

Fig. 2.12 Assumed Stress Distribution for Anchorage Subjected to Overturning Moment

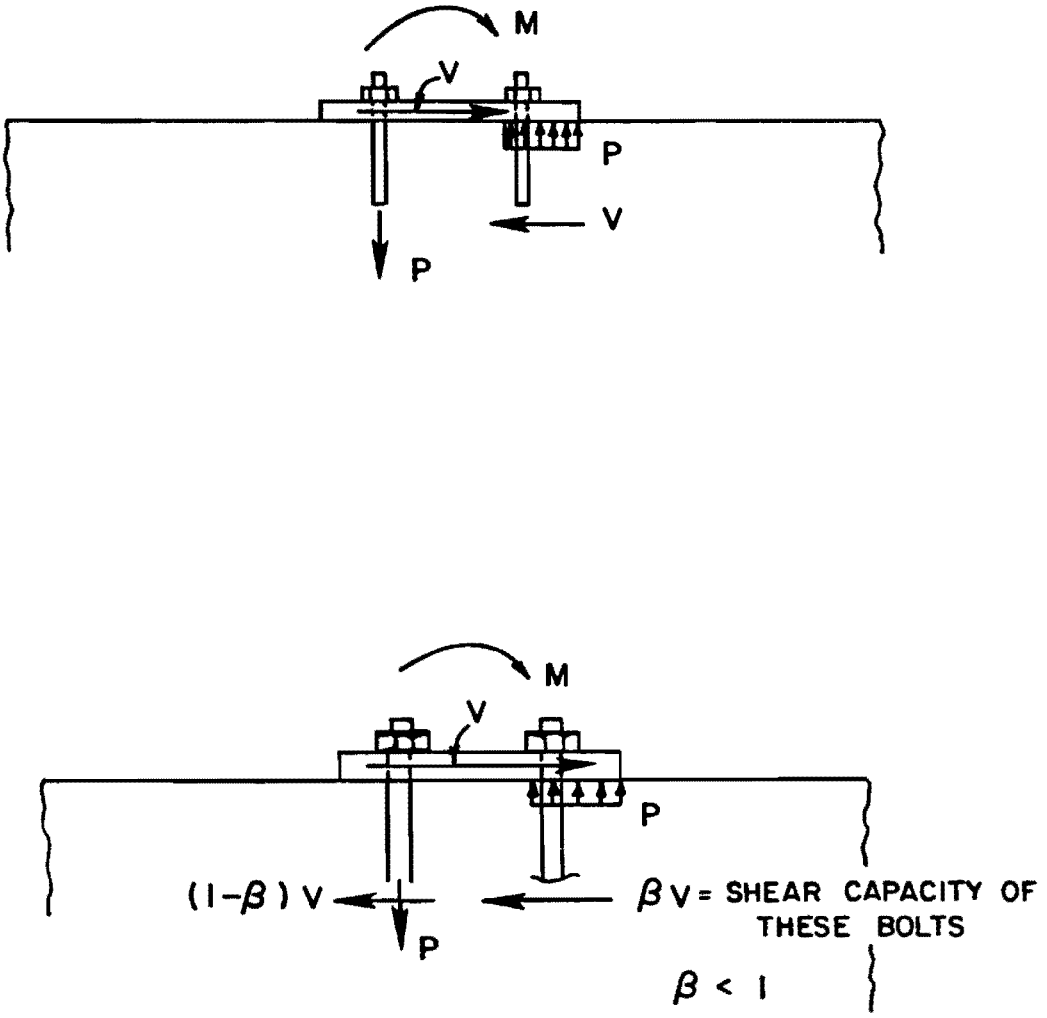

Fig. 2.13 Distribution of Shear Load

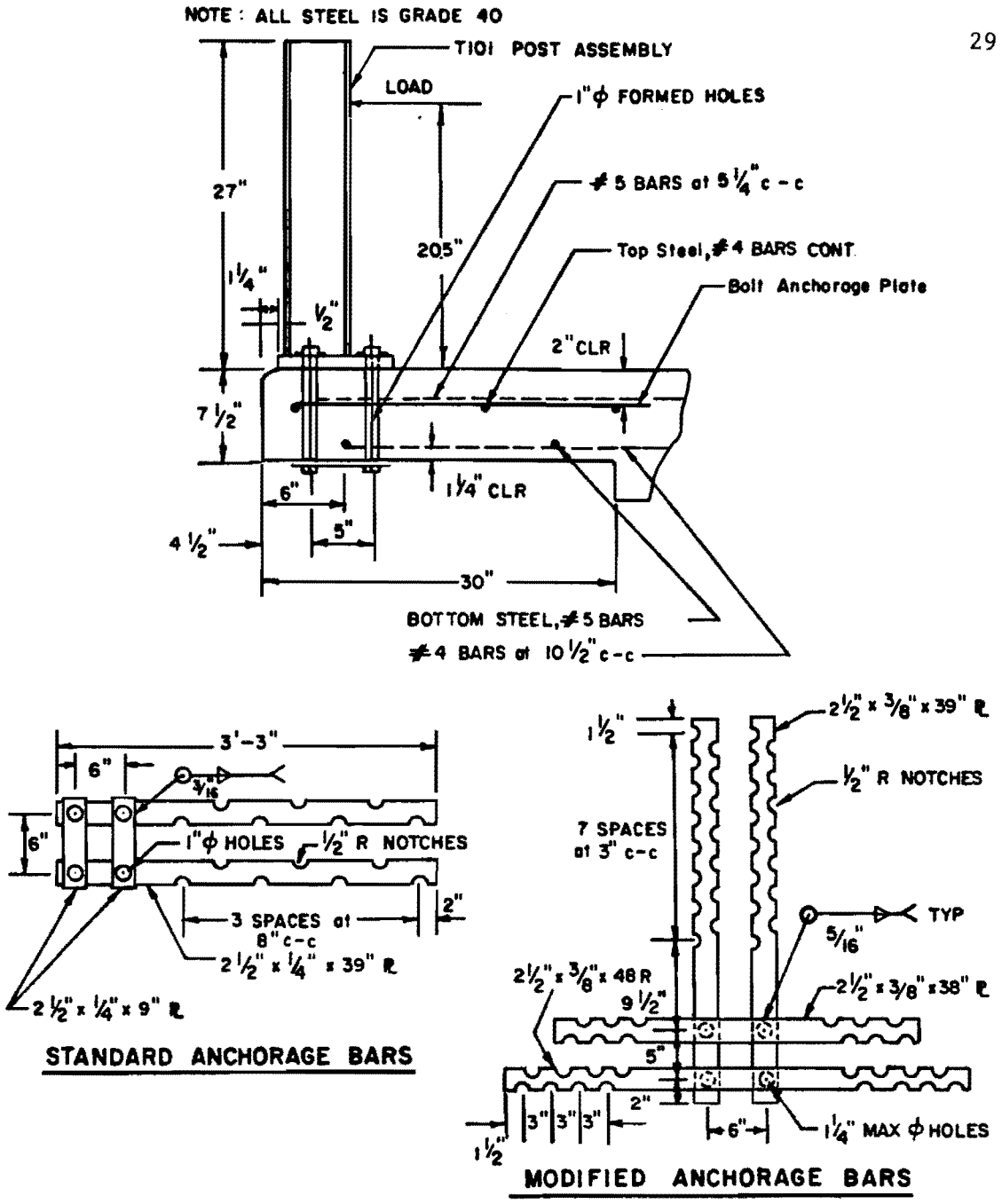

Fig. 2.14 Test Setup and Anchorage Bars used in Tests of Reference 2

Since the interaction of tension and shear in an anchor is not well understood at this point, comparisons of this type cannot give a definitive answer to the question of load distribution in the connection. For now, the plastic distribution method seems to be the most logical approach to the problem. It should be emphasized, however, that redistribution of load is possible only as long as the connection remains ductile. Brittle failure of the concrete must be prevented.

2.2.5 Design Criteria. In establishing guidelines for the design of anchorages, ACI Committee 349 requires that the failure mechanism be yielding of the anchor steel. Because of their improved energy absorption characteristics, ductile anchorages are very desirable for systems subjected to impact loads [17]. Furthermore, in the event of an overload, ductility allows the system to redistribute load to less heavily stressed anchorages. Thus, the anchorage of traffic barriers to bridge decks is an application where ductility is of particular importance.

By providing ductility, the designer can influence the behavior of the system at failure. The objective is to increase the likelihood that the system will fail in the manner preferred by the designer. This is accomplished by providing the system with a capacity in the preferred failure mode which is greater than the design load and less than that of all possible brittle failure modes. Additional conservatism is incorporated by calculating the capacity in the preferred mode with probable rather than minimum strength values and no understrength factor. The capacities in the undesirable modes are calculated in the usual manner.

ACI Committee 349 [17] and Klingner and Mendonca [19,20,21] have proposed that the nominal tensile and shear capacities of the anchorage as governed by concrete failure exceed the specified minimum tensile strength of the anchor steel. Thus,

$$\phi_c P_c \geq A_s f_{ut} \tag{2.17}$$

$$\phi_c V_c \geq A_s f_{ut} \tag{2.18}$$

Alternatively, if hairpin reinforcement is used to carry the shear load, the second requirement becomes

$$\phi_s V'_s \geq A_s f_{ut} \tag{2.19}$$

These requirements are intended to prevent tensile failure of the concrete at anchors loaded in tension, shear, or a combination of the two. They also provide the necessary ductility to make possible the redistribution of load in multiple anchor connections.

To summarize, design of an anchorage should begin with the sizing of anchor bolts or studs to resist the applied loads. The other elements of the design, such as edge distance, depth of embedment and spacing of anchors, should then be selected so that the resistance of the anchorage to tensile failure of the concrete exceeds the ultimate strength of the anchor steel. An example of this type of design procedure is given in Appendix A.2.2.

2.3 Observed Failure Modes

All of the tests mentioned thus far involved anchorage to monolithic concrete. The failure modes observed have been yielding of the anchor steel and tensile failure of concrete in the zone of the anchorage if either embedment length or edge distance was inadequate. While reinforcement was provided in some cases (to prevent development of a semiconical failure surface at an anchor loaded in shear), the overall strength of the concrete block was not in question.

Arnold and Hirsch [2] performed static and dynamic tests on full scale models of the standard Texas SDHPT Type T101 traffic rail assembly, attached to concrete decks of various thicknesses. Two static tests were performed with the standard T101 assembly attached to a 7-1/2-in.-thick deck (Fig. 2.14). The bolts were placed through formed holes in the deck with load plates provided at both sides of the connection. The deck thickness and connection detail are typical for most Texas SDHPT applications. In both tests, the post punched through the deck before either tensile failure of the bolts or development of the usual pullout or shear failure surface had occurred. The resulting crack pattern is shown schematically in Fig. 2.15. Dynamic tests produced the same failure mode.

These tests indicate that for typical highway applications, the capacity of the barrier is limited by the strength of the slab in the region of the connection. Thus, punching of the post through the slab must be considered as a possible failure mode. Unfortunately, the mechanism is not well understood. Arnold and Hirsch felt that it was caused by a high concentration of stress under the post base plate.

Several modifications to the standard detail were made in an effort to spread out the load. Static tests were conducted on a 7-1/2-in. deck and a 10-in. deck, each having a 48-in. by 18-in. welded wire fabric mat (D20) placed on top of the existing steel, as well as additional longitudinal steel. To eliminate bolt fracture as a failure mode, the usual 3/4-in. diameter, A325 bolts were replaced with 7/8-in. diameter bolts. Although the strength of the system was increased, the crack patterns were identical to those of the earlier tests. An 8-in. and a 10-in. slab were tested with the welded wire fabric mat replaced by an enlarged anchor plate (Fig. 2.14). Anchor bolts of 3/4-in diameter were used. Both specimens failed by bolt fracture, but not until the typical crack pattern had developed.

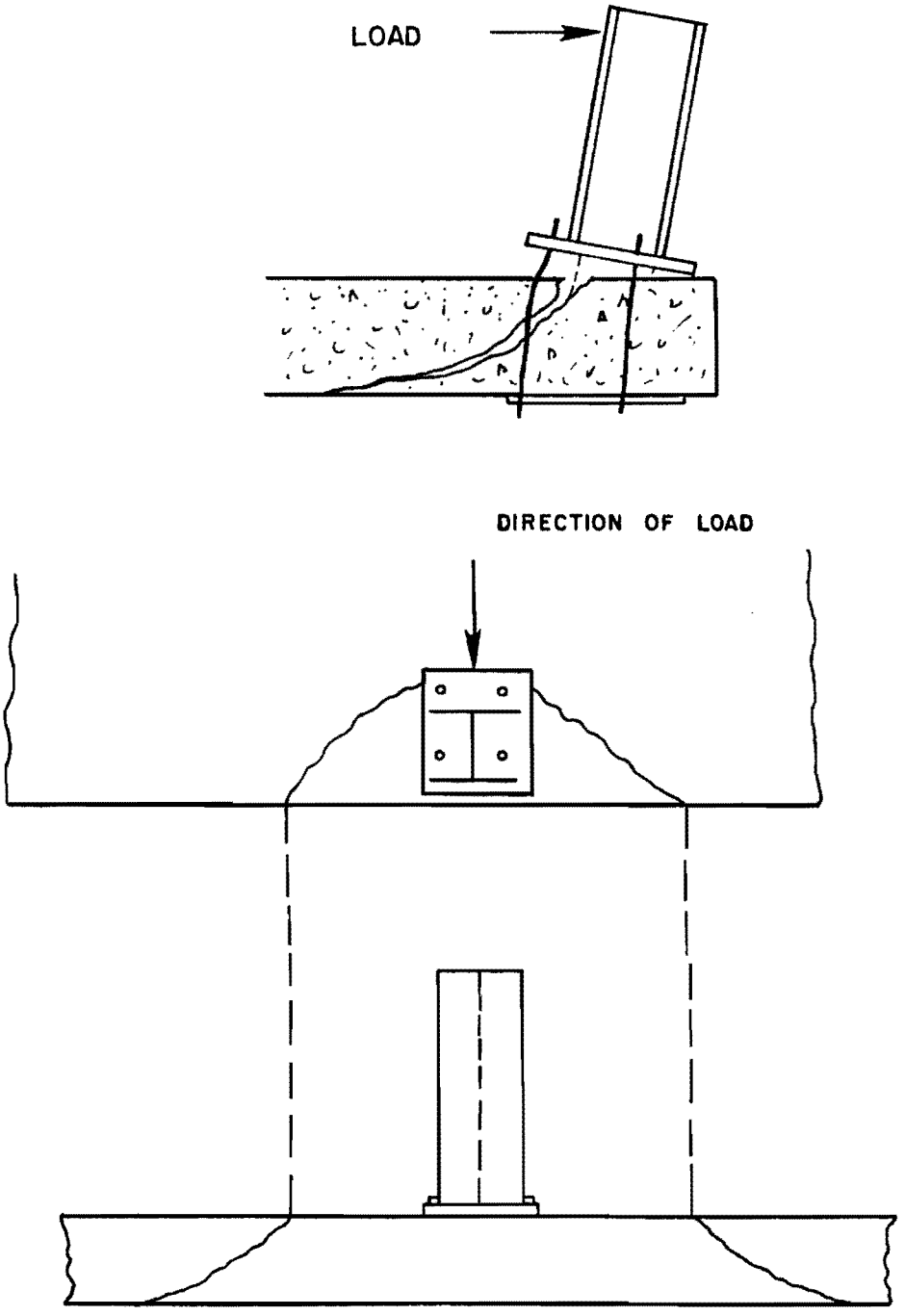

Fig. 2.15 Schematic of Typical Crack Pattern

In the final two tests of the series, the post edge distance was increased from 1-3/4 in. to 3-1/2 in. Though the typical crack pattern developed, cracking was not as severe at failure as it had been in the previous tests.

The exact nature of the failure mechanism is not evident from the results of these tests. It is clear, however, that an appropriate model must be developed so that the rational design of steel-post traffic barriers may be approached as discussed in subsection 2.2.5, with the designer setting the desired level for each failure mode. Development of a behavioral model for this type of failure is discussed in Chapter 3.

One other test carried out by Arnold and Hirsch [2] involved a post connected to a rigid foundation using the standard base plate and bolt arrangement. Failure occurred when the washers on the tension bolts pulled down through the 1x1-1/2 in. slotted holes in the post base plate. The holes, which are in accordance with the Texas SDHPT standard, are larger than recommended by AISC [13] for the 3/4-in. diameter bolts which were used. AISC further recommends use of a 5/16-in. minimum thickness bar or washer on all long-slotted holes, rather than the standard washers used. This failure mode was also observed in the final test of the series, which involved increased post edge distance.

In light of this, all tests in the current study were performed on specimens having standard 13/16-in. diameter holes in the base plate and hardened washers on the tension bolts. This was done to eliminate the possibility of this failure mode occurring and to ensure that data were obtained on the types of failure which are the focus of this study. It is clear, however, that further study of the slotted-hole problem should be undertaken.

CHAPTER 3

DEVELOPMENT OF TEST SPECIMEN

3.1 General Design Criteria

The major elements of the test specimen are shown in Fig. 3.1; the setup is similar to that used for the tests of Ref. 2. To observe the response of the slab in the region of the anchorage, and also the behavior of the anchorage itself, it was necessary to model the deck overhang. For testing purposes, the overhang was supported by a block of concrete which was tied to the laboratory floor.

It was decided that a single specimen should be developed which would permit the testing of several different anchorages. This would reduce the cost and time required for specimen construction. To determine the extent of the slab area which would be affected by load applied at a single post, a finite element analysis was performed using the SAP IV program. The results indicated that if the posts to be tested were attached to the specimen at a spacing of 4 ft or more, the affected slab regions would not overlap. The length of the specimen was decreased significantly by not using the 8ft, 4in. post spacing typical of actual construction.

As is discussed below, both the anchorage detail and the deck section were modified in an effort to produce a more ductile system. In all other respects, the specimen was as near as possible to a typical Texas SDHPT Type T101 installation.

In developing the test specimen, certain goals were set for its performance. The plastic moment capacity of the W6x20 A36 steel post was calculated to be 522 kip-in., which corresponds to a load of 26.6 kips applied at the top of the post. The ultimate capacity of the post ($M_u = Zxf_{ut}$ with $f_{ut} = 58$ ksi for A36 steel) corresponds to a load of 42.9 kips applied at the top of the post. It was decided that the capacity of the system as governed by bolt fracture should fall within those limits.

Placing the tension bolts 9-1/4 in. from the back of the base plate (Fig. 3.2) and retaining the 3/4-in. diameter A325 bolts of the standard detail, results in a probable failure load of 37 kips (applied at the top of the post). For this calculation, the base plate was assumed to be 9 in. wide and f_{ut} for the A325 bolts was taken as 140 ksi. The design capacity of this system as governed by bolt fracture is computed from the equations of Subsection 2.2.1.

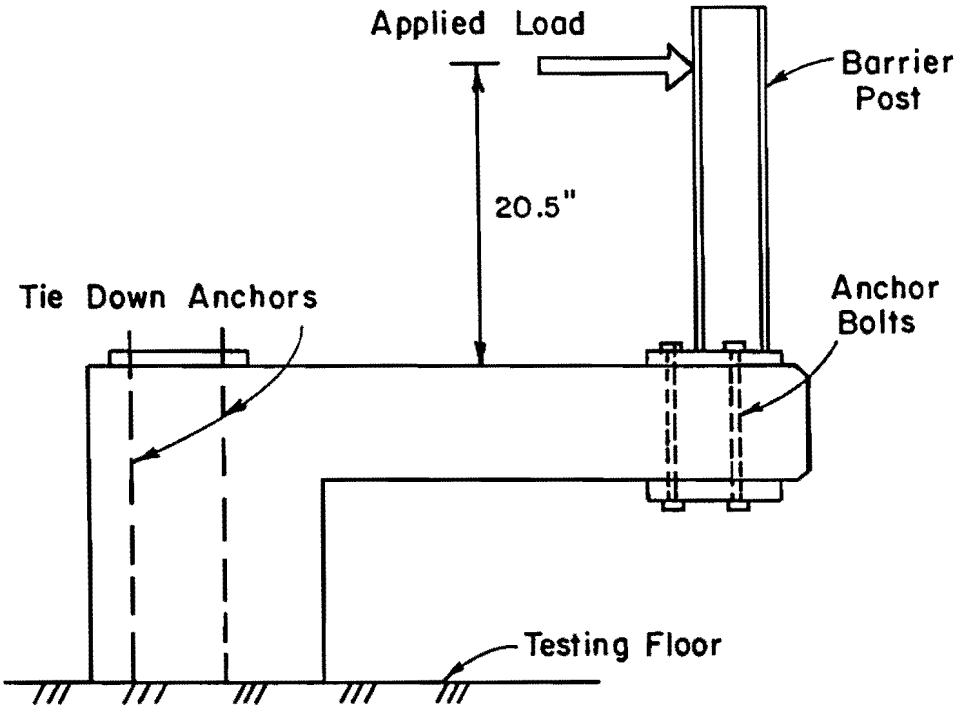

Fig. 3.1 Test specimen

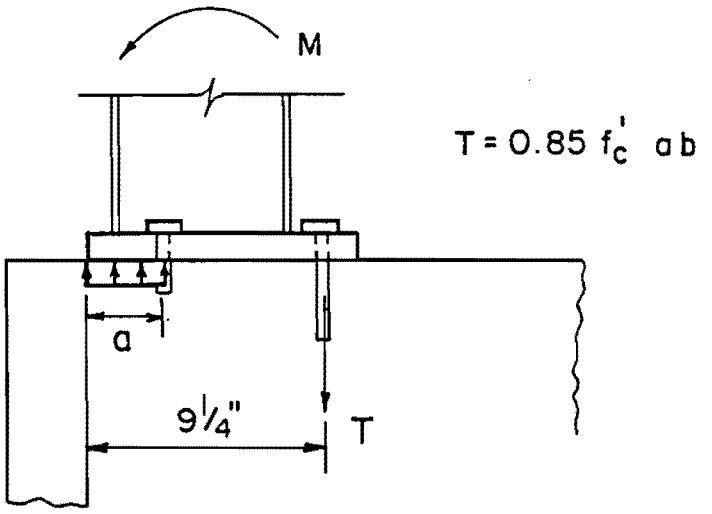

Fig. 3.2 Tension Bolt Placement for Test Specimen

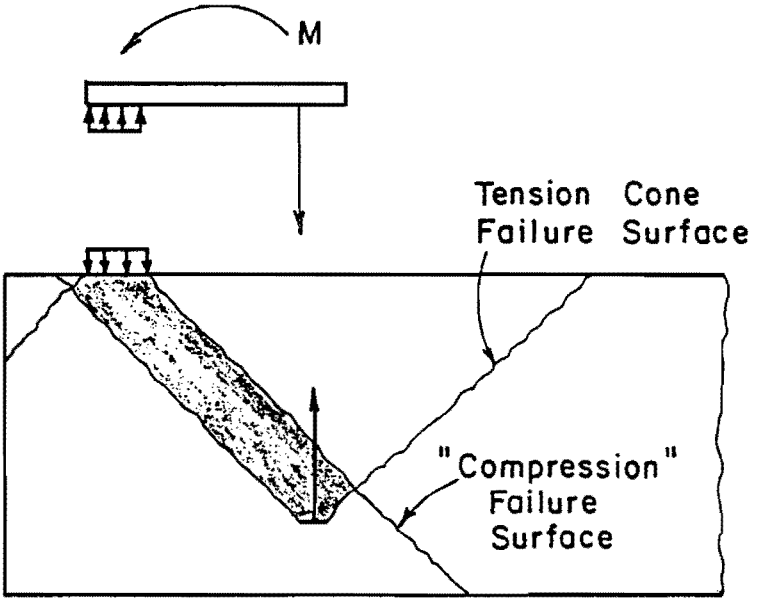

Fig. 3.3 Preliminary Failure Hypothesis

$$P_u \leq \phi_s P_s \qquad (2.1), \text{ repeated}$$

$$P_s = A_s f_y \qquad (2.2), \text{ repeated}$$

$$f_{ut} = 120 \text{ ksi}$$

$$f_y = 0.9 f_{ut} = 108 \text{ ksi}$$

The limiting tensile load in the bolts is 65 kips, which corresponds to a load of 27 kips applied to the post. This is near the plastic capacity of the post and well above the current design load of 10 kips.

The shear capacity of the two back bolts is calculated as

$$V_u \leq \phi_s V_s \qquad (2.7), \text{ repeated}$$

$$V_s = A_s f_{yv} \qquad (2.8), \text{ repeated}$$

where $$f_{yv} = 0.67 f_{ut} \qquad (2.9), \text{ repeated}$$

This gives a maximum capacity of 49 kips for the post. Thus, the design load can be set at 27 kips, with the entire shear load being taken by the back bolts. The procedure of subsection 2.2.5 is followed to complete the design.

The failure modes which have not yet been considered in this design are tensile and shear failure as governed by the capacity of the concrete, and the flexure-torsion failure exhibited by the specimens of Ref. 2. These failure modes are all somewhat related, involving the thickness, edge distance, and reinforcement of the concrete deck section. A failure model was developed for the flexure-torsion type failure and compared with the results obtained by Ref. 2. Design of the specimen was based on this model. The shear and tensile capacities of the anchorage as governed by concrete were checked separately.

3.2 Development of Model

The simplest failure model computes flexure-torsion capacity in a manner analogous to that used for computing tensile capacity. A roughly trapezoidal section of concrete is pushed down by the compressive stress concentrated near the back end of the base plate (Fig. 3.3). Failure occurs when the compressive force exceeds the resultant of tensile stresses acting on the assumed failure surface. A uniform nominal failure stress of $4\sqrt{f'_c}$ is assumed. Pullout of the tension anchors is checked independently, and the lower of the two capacities controls the design.

For a 7-1/2 in. slab conforming to the Texas SDHPT standard, the model predicts post failure at a lateral load of 14.6 kips.

Actual tests of this system resulted in failure loads of 18.6 and 19.0 kips [2]. This seems to indicate that the model is overly conservative, and that perhaps another mechanism aids in resisting the downward force.

In Fig. 3.3 it can be seen that for a typical anchorage, the compressive and tensile failure surfaces overlap; compression and tension occur simultaneously when the post is loaded. In the shaded region, the downward force must overcome the upward force produced by the tension bolts for failure to occur. The moment produced by this force couple must be balanced by compressive and tensile stresses on the failure surface. The body is then in equilibrium with respect to rotation about a horizontal neutral axis (Fig. 3.4).

The cracking load can be obtained by equating the flexural stress ($\sigma = M_y/I$) with an assumed value for the tensile strength of concrete. The centroid and moment of inertia are computed for the projected shape of the failure surface (Fig. 3.5). When tensile strength is conservatively assumed as $7.5\sqrt{f'_c}$, the cracking load for the 7-1/2 in. thick deck discussed above is calculated to be 8.4 kips. A more probable concrete strength of $10.5\sqrt{f'_c}$ gives a value of 11.7 kips. This is approximately the point at which first cracking occurred in the Arnold and Hirsch tests [2].

The ultimate strength of the section can be estimated using a beam bending analogy (Fig. 3.6). Reinforcement is provided to carry the tensile stress induced in the region above the neutral axis. The compressive force is taken as $0.85 f'_c ab'$, where b' is the average width of the trapezoidal compression face. If the overturning moment is the result of an eccentrically applied shear load, the shear force must be included in the model.

Using this analysis, the failure load for the 7-1/2 in. thick section was calculated to be 16.4 kips. The reinforcement which was considered to be effective in this analysis included both the transverse slab reinforcement within the failure surface (#5 Grade 40 reinforcing bars at 5-1/4 in.), and the bolt anchorage bars lying in the direction of the load (two 2-1/2 in. by 1/4 in. A36 bars). Taking the probable yield strength of both types of reinforcement as 42 ksi, the calculated failure load is 18.1 kips, close to the observed failure loads of 18.6 and 19.0 kips [2].

3.3 Specimen Design

Design of the test specimen was based on the failure model described above and in Figs. 3.4 through 3.6. To better control the severe diagonal cracking reported in the tests of Ref. 2, the use of torsional or cage reinforcement was investigated. In Fig. 3.7, bars placed such that the vertical leg crosses the failure surface are labeled V-bars. Those bars which have the vertical leg fully contained

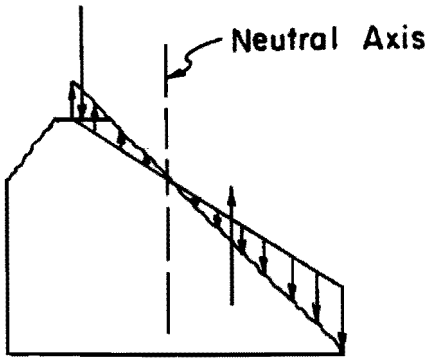

Fig. 3.4 Body in Equilibrium about Neutral Axis

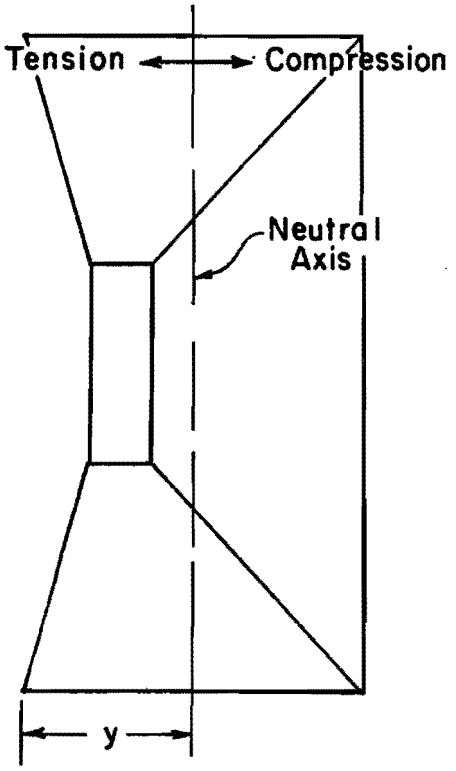

Fig. 3.5 Projected Shape of Failure Surface

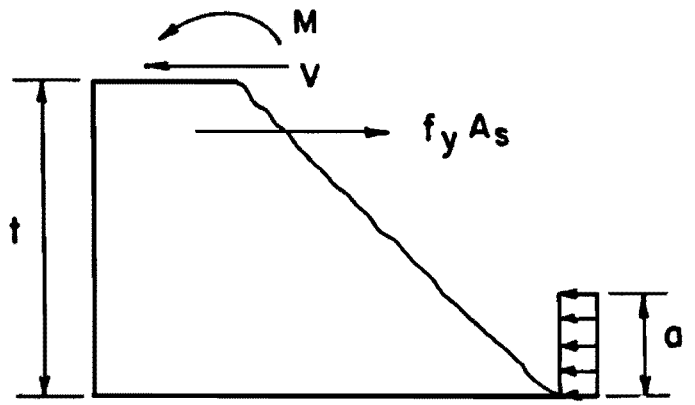

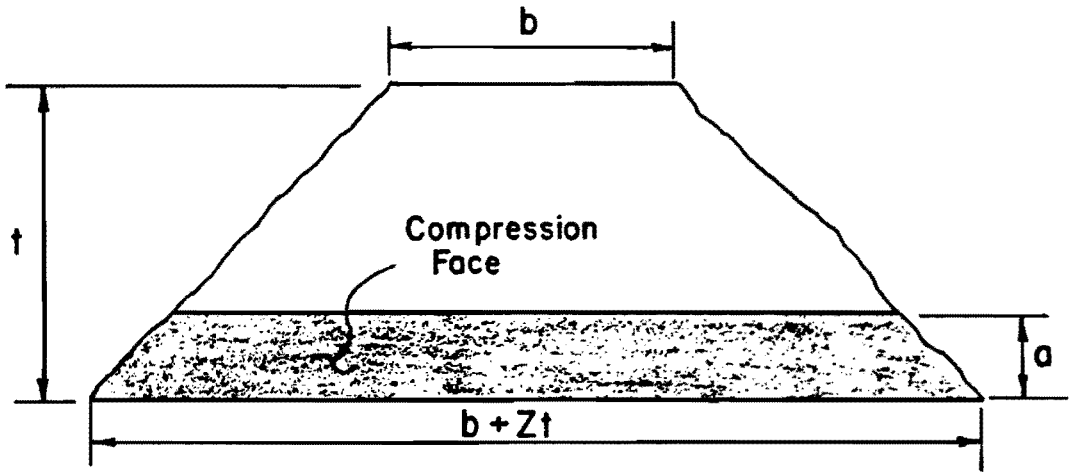

Compression Area = 1/2 a [(b+2t) + (b+2t-2a)]

= a (b + 2t - a)

= a b'

Fig. 3.6 Beam Model

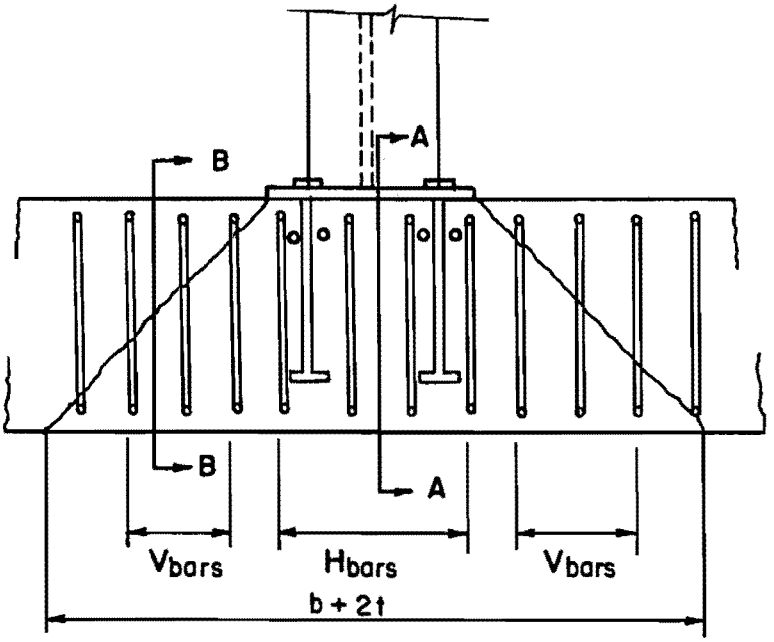

ELEVATION OF SLAB

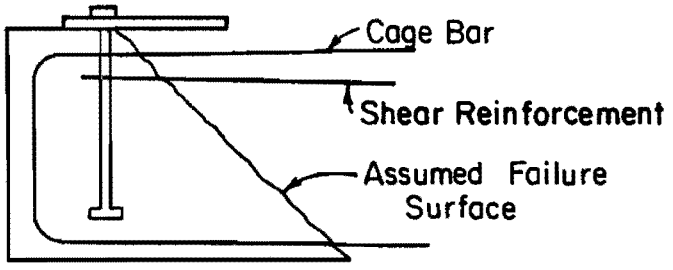

SECTION A-A

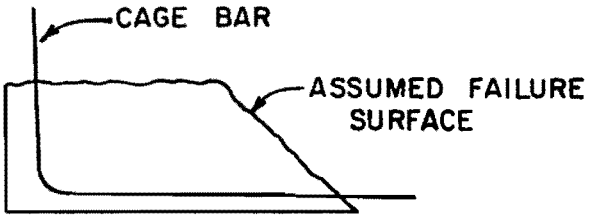

SECTION B-B

Fig. 3.7 Cage Reinforcement

within the failure surface are labeled H-bars. Note that only the top horizontal legs of the H-bars are effective in resisting this type of failure, and only the vertical legs of the V-bars are effective. The bottom horizontal leg of each cage bar also crosses the failure surface, but is not highly stressed.

The model was modified to include shear stresses acting on the inclined failure surface in the compression zone. In this analysis, the three equilibrium equations are used to determine the unknowns: the applied shear, V; the depth of the compression block, a; and the inclined shear force, V_i. Since it is possible that not all of the reinforcement will reach yield, the stress in each leg of the cage reinforcement and that in the hairpin or shear reinforcement is determined by using compatibility equations to compute each unknown stress in terms of its distance from the neutral axis.

From Fig. 3.8,

$$\sum F_x = 0 = n_h A_c f_{s2} + (n_v+n_h)A_c f_{s3} + A_h f_{sh} - V - V_i \cos 45^o - 0.85 f'_c ab' \cos 45^o \quad (3.1)$$

$$\sum F_y = 0 = n_v A_c f_{s1} + V_i \sin 45^o - 0.85 f'_c ab' \sin 45^o \quad (3.2)$$

Taking moments about the centroid of the compression block,

$$\sum M = 0 = \lambda V + (t-1/2\ a \sin 45^o)V - n_v A_c f_{s1}(h_1-1/2\ a \cos 45^o) - n_h A_c f_{s2}(h_2-1/2\ a \sin 45^o) - A_h f_{sh}(h_h-1/2\ a \sin 45^o) - (n_v+n_h)A_c f_{s3}(h_3-1/2\ a \sin 45^o) \quad (3.3)$$

In Fig. 3.9, ε_c is the strain in the concrete at one of the reinforcement locations.

$$(\varepsilon_u/c) = (\varepsilon_c / (h/\sin 45^o - c)) \quad (3.4a)$$

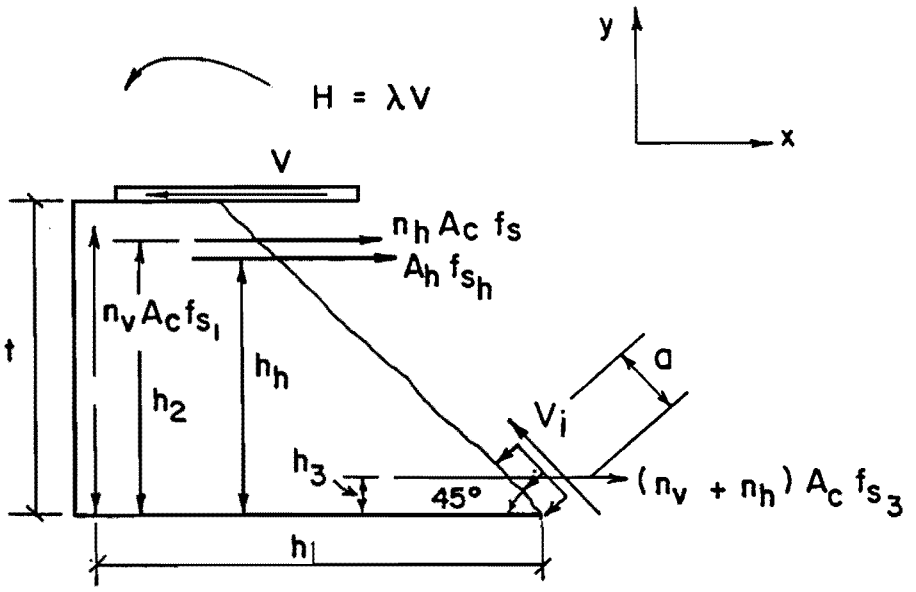

A_c = cross-sectional area of one cage bar

A_h = total area of shear or hairpin reinforcement

f_{s1} = stress in vertical leg of cage bar

f_{s2} = stress in top horizontal leg of cage bar

f_{s3} = stress in bottom horizontal leg of cage bar

f_{sh} = stress in shear or hairpin reinforcement

n_v = number of V-bars (Fig. 3.7)

n_h = number of H-bars (Fig. 3.7)

λ = distance from point of application of shear load to top of slab

h_1, h_2, h_3, h_4: distance from center line of reinforcement to point shown

Fig. 3.8 Flexure-Torsion Failure Model

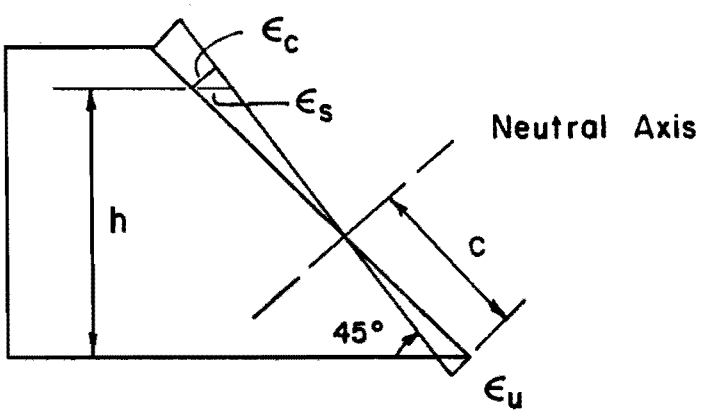

Fig. 3.9 Strain Diagram for Failure Model

and

$$\varepsilon_c = (h/\sin 45^o)(\varepsilon_u/c) - \varepsilon_u \qquad (3.4b)$$

Putting this in terms of the variable, a,

$$a = \beta_1 c \qquad (3.4c)$$

$$\varepsilon_c = (\beta_1 h \varepsilon_u / a \sin 45^o) - \varepsilon_u \qquad (3.4d)$$

The direction of strain in the steel is at a 45^o angle to the direction of strain in the concrete. Using Mohr's Circle, or another procedure for transforming strains,

$$\varepsilon_s = \varepsilon_c/2 \qquad (3.4e)$$

and

$$\varepsilon_s = (\beta_1 h \varepsilon_u / 2 a \sin 45^o) - \varepsilon_u/2 \qquad (3.4f)$$

Then the steel stress is given by

$$f_s = (E_s \beta_1 h \varepsilon_u / 2 a \sin 45^o) - (E_s \varepsilon_u / 2) \qquad (3.4g)$$

A computer program was written to carry out this analytical procedure, permitting a large number of designs to be tried. Originally, the program simply solved for the seven unknowns. In some cases, the resulting value for the inclined shear stress exceeded the maximum available shear stress on the inclined surface, taken as 800 to 1200 psi [22], and the solution was considered invalid.

This analysis requires that the compression force ($0.85f_{\text{ab}}$' $\sin 45^o$) be balanced by the force in the vertical leg of the cage bars, and by the vertical component of the inclined shear force. When the vertical reinforcement is inadequate, the inclined shear force becomes excessive. Although it is not possible for such a section to carry the applied shear load determined in such an analysis, the section is capable of withstanding a lower level of load.

To solve this problem, the program was modified to compute the equilibrium forces over a range of maximum concrete strains.

Originally, the maximum concrete strain (ε_u in Eq. 3.4) had been taken as 0.003. In the revised procedure, the stress at each strain level is determined using the Hognestad stress-strain diagram for concrete. Instead of assuming a rectangular stress block, the compressive force in the concrete is determined by integration of the stress diagram. Thus, the analysis is valid at lower strain levels, allowing the maximum load to be determined in all cases. A program listing is included in Appendix A.3.2, along with sample results.

The design resulting from this analysis is shown in Figs. 3.10 and 3.11. Note that neither bolt anchorage bars nor hairpin reinforcement are used. It was felt that the longitudinal slab steel, which passes behind the vertical leg of the U-shaped bars and in front of the bolt, would be able to restrain the bolt, transferring load to the U-bars and thus to the concrete. The four #4 bars (two for each bolt) which function in this manner provide a shear capacity of 48 kips, or 43.2 kips when reduced by the understrength factor for steel. This exceeds the 37-kip load corresponding to the ultimate tensile capacity of the anchors.

The remaining failure mode to be considered is cone pullout due to the tensile load in the front bolts. Given the 10- in. slab thickness shown in Fig. 3.10, a 7/8-in. thick anchor plate was provided on the underside of the slab, to prevent the bolt from pulling through.

Figure 3.12 shows the capacity of the design section in each failure mode. The nominal capacities correspond to nominal yield strengths for Gr. 60 reinforcement and A36 steel, nominal ultimate tensile strength for A307 anchors, a diagonal tensile strength for concrete of $4\sqrt{f'_c}$, and no understrength factors. The probable capacities were computed similarly, except that the yield strengths of Gr. 60 reinforcement and A36 steel were increased to probable values of 67 and 42 ksi, respectively.

To complete the design of the test specimen, it was necessary to provide reinforcement in the region beyond the assumed failure surface which would give the slab a transverse flexural capacity equivalent to that of the Texas Highway Department's standard design. In other words, a 4-ft section of the test specimen, with a post in the middle, should have the same transverse flexural capacity as an 8-ft, 4-in. section of the standard design. This was accomplished by using #4 U-bars spaced at 5 in., as shown in Fig. 3.13.

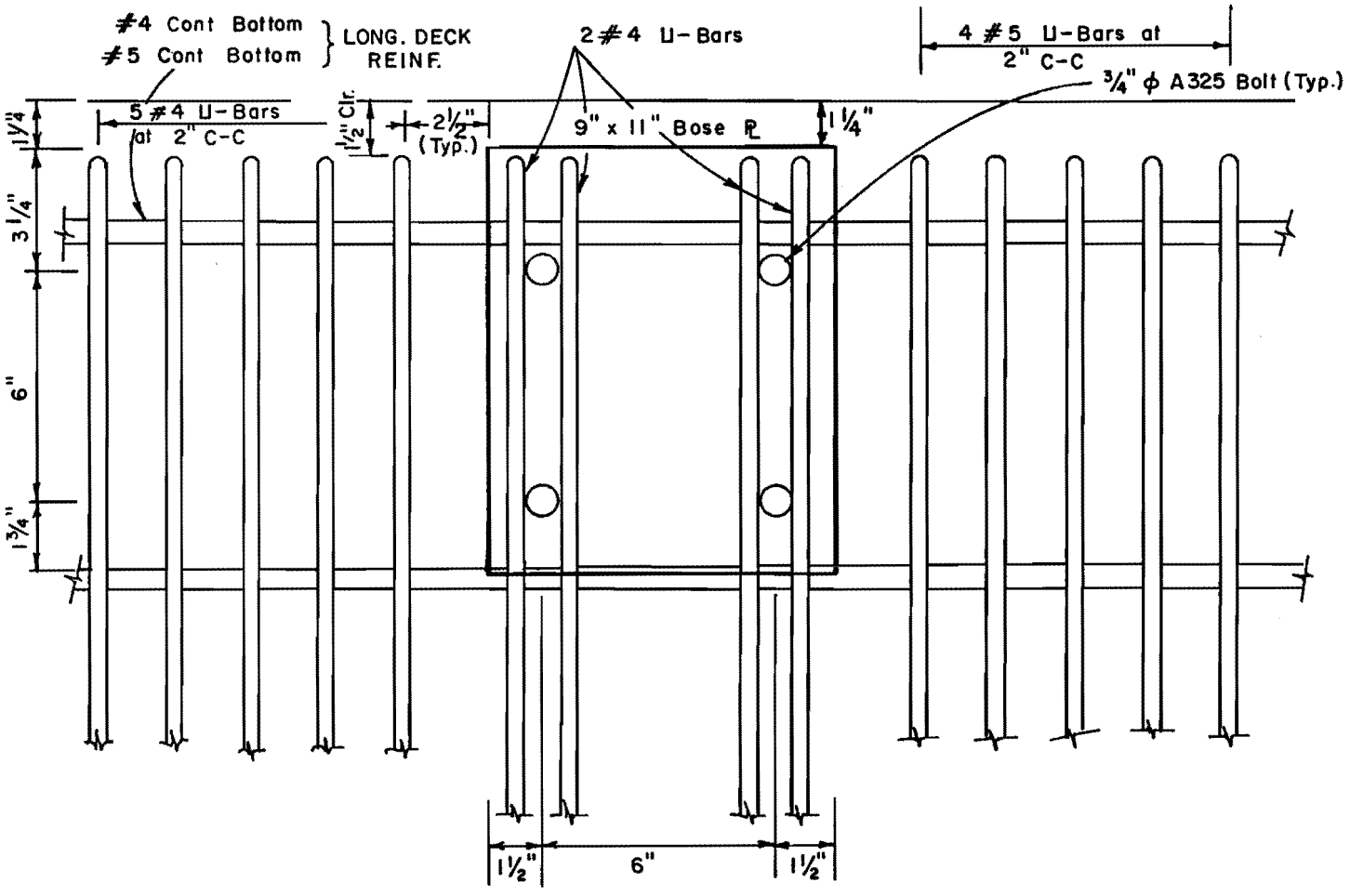

Fig. 3.10 Design section: Plan View

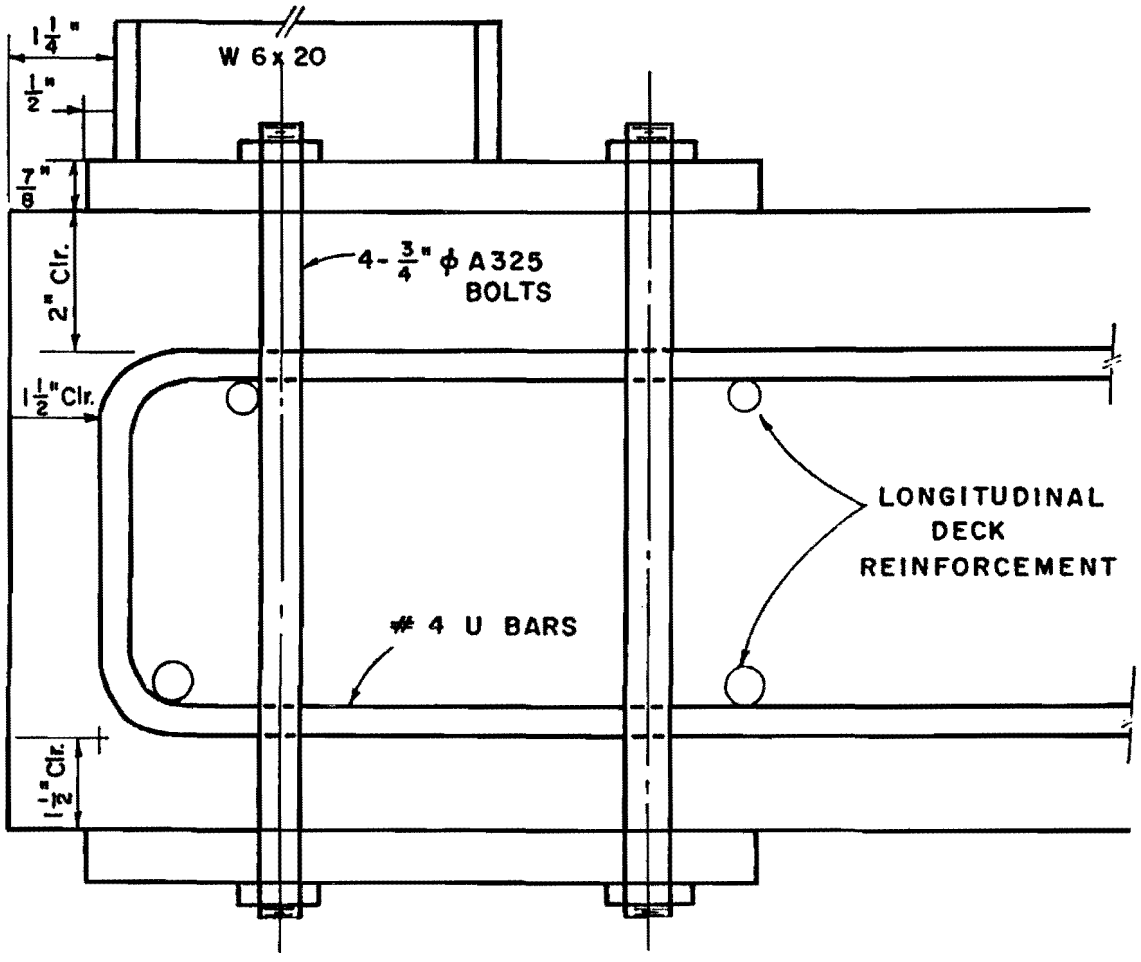

Fig. 3.11 Design Section: Side View

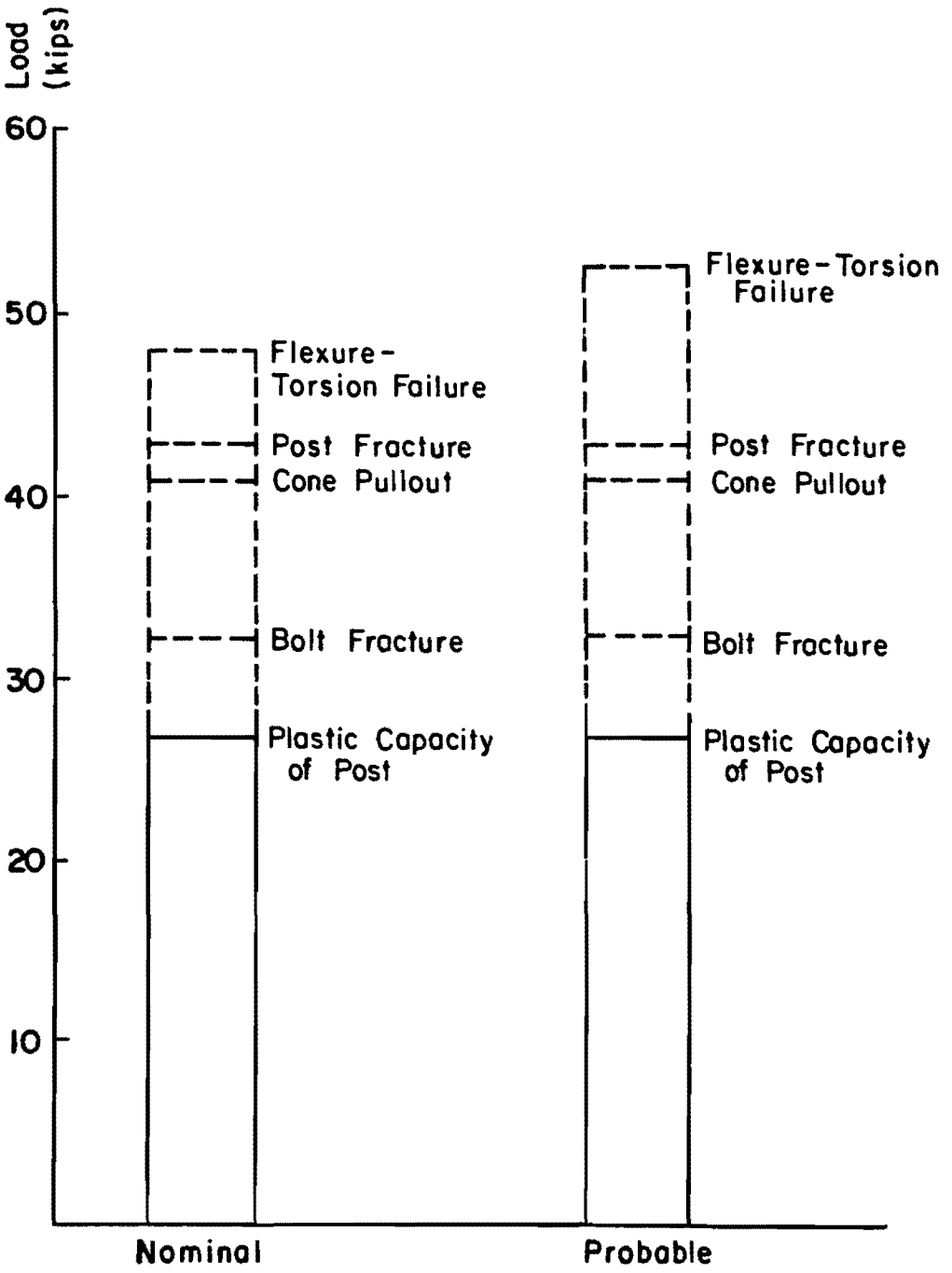

Fig. 3.12 Capacity of Design Section

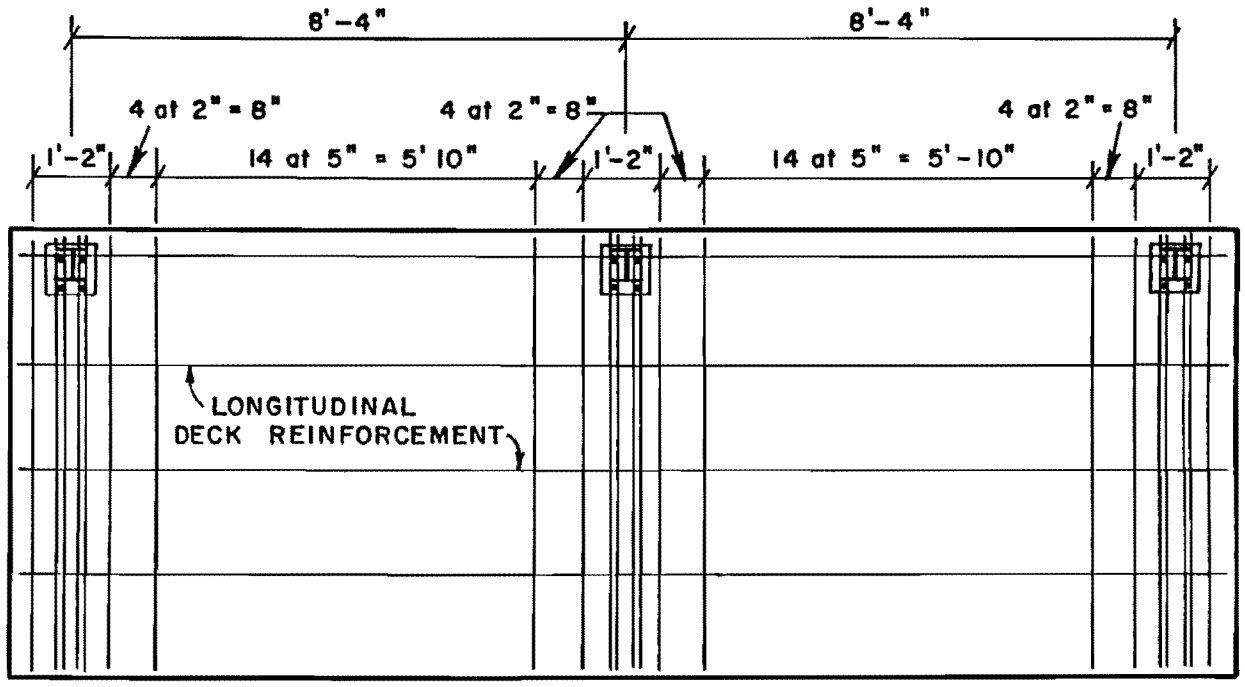

Fig. 3.13 Reinforcement Layout for Test Specimen

CHAPTER 4

SPECIMEN PREPARATION AND TESTING PROCEDURE

4.1 Materials

4.1.1 Concrete. The concrete used conformed to Texas SDHPT requirements for Class C concrete. It was designed to have a 4000-psi compressive strength, using a cement content of 6 sacks per cubic yard of concrete. When the concrete arrived at the laboratory from the ready-mix plant, it had very low slump. The water-cement ratio appeared to be much lower than called for. Some water was added, but it was felt that adding a large amount of water would be unwise. The concrete was quite stiff when placed.

The 28-day strength of the concrete was 5920 psi. By the time testing started, the strength had risen to 6720 psi, considerably higher than the design strength of 4000 psi. A plot of concrete strength versus time is shown in Fig. 4.1. The splitting tensile strength was found to be 520 psi.

As explained leter, the governing failure made for all barrier specimens was diagonal tension failure of the concrete. Diagonal tensile strength of concrete is usually proportional to $\sqrt{f'_c}$, and the specimens as tested were therefore considerably stronger than specified in diagonal tension. Since even these stronger specimens failed in diagonal tension, specimens with only the minimum specified concrete strength would also have failed in the same way. Test results from the stronger specimens are therefore still indicative of the probable performance of specimens with lower concrete strength.

4.1.2 Reinforcing Steel. Grade 60 deformed steel bars were used for all reinforcement. All bars were #4, and were from the same heat. Random bars were selected for tension tests. The measured yield strength was 54 ksi; the ultimate strength was 85 ksi. The stress-strain relationship is shown in Fig. 4.2.

4.1.3 Anchors. All anchors were threaded rods conforming to ASTM A193 Grade B7. The rods had 2H heavy hex nuts and A325 hardened flat washers at each end. The first part of the testing program used 3/4-in. diameter rods. Since these were all taken from the same heat, rods were randomly selected for tensile tests. Based on nominal cross-sectional areas, the yield strength and ultimate strength were 125 and 139 ksi, respectively. The stress-strain relationship is shown in Fig. 4.3. The last two tests were conducted using 1/2-in. diameter rods. These rods did not come from the same heat, and so were individually tested. Based on nominal cross-sectional areas, the average yield

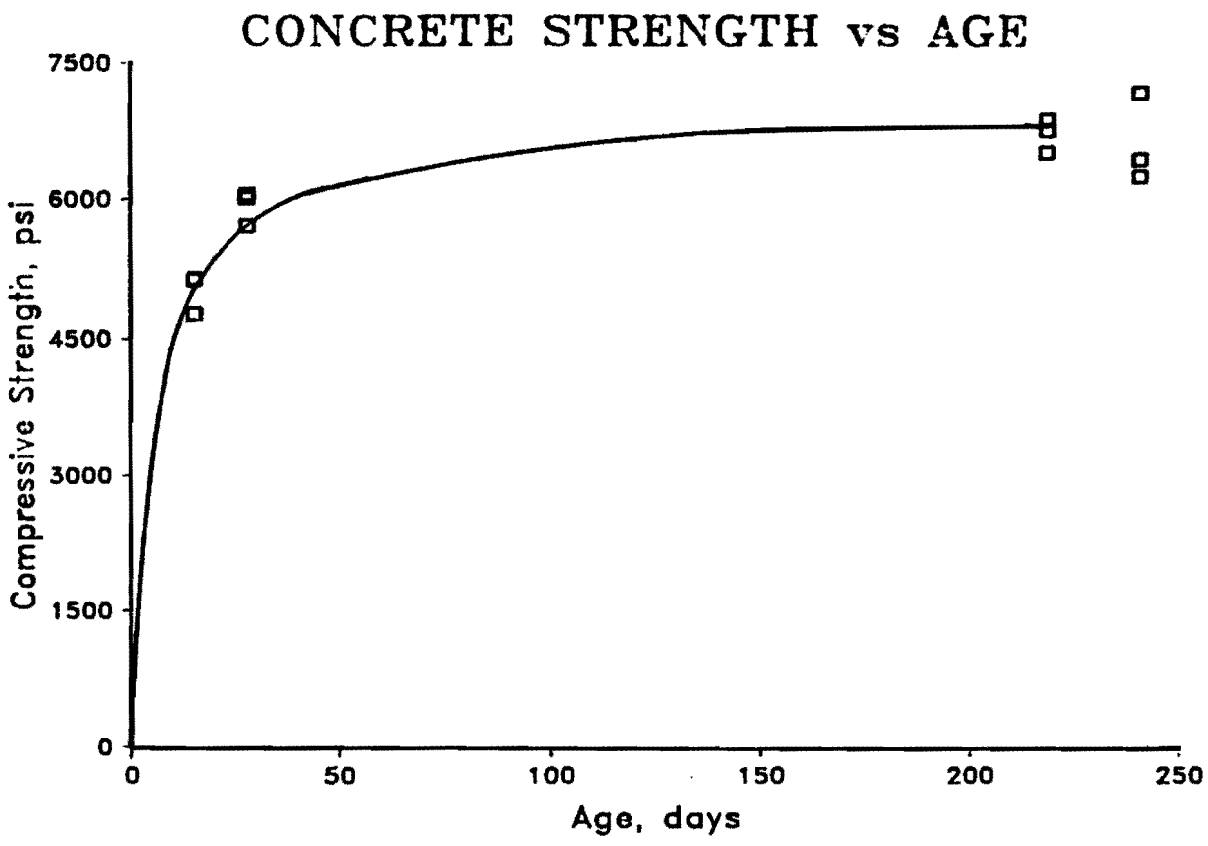

Fig. 4.1 Concrete Strength vs. Time

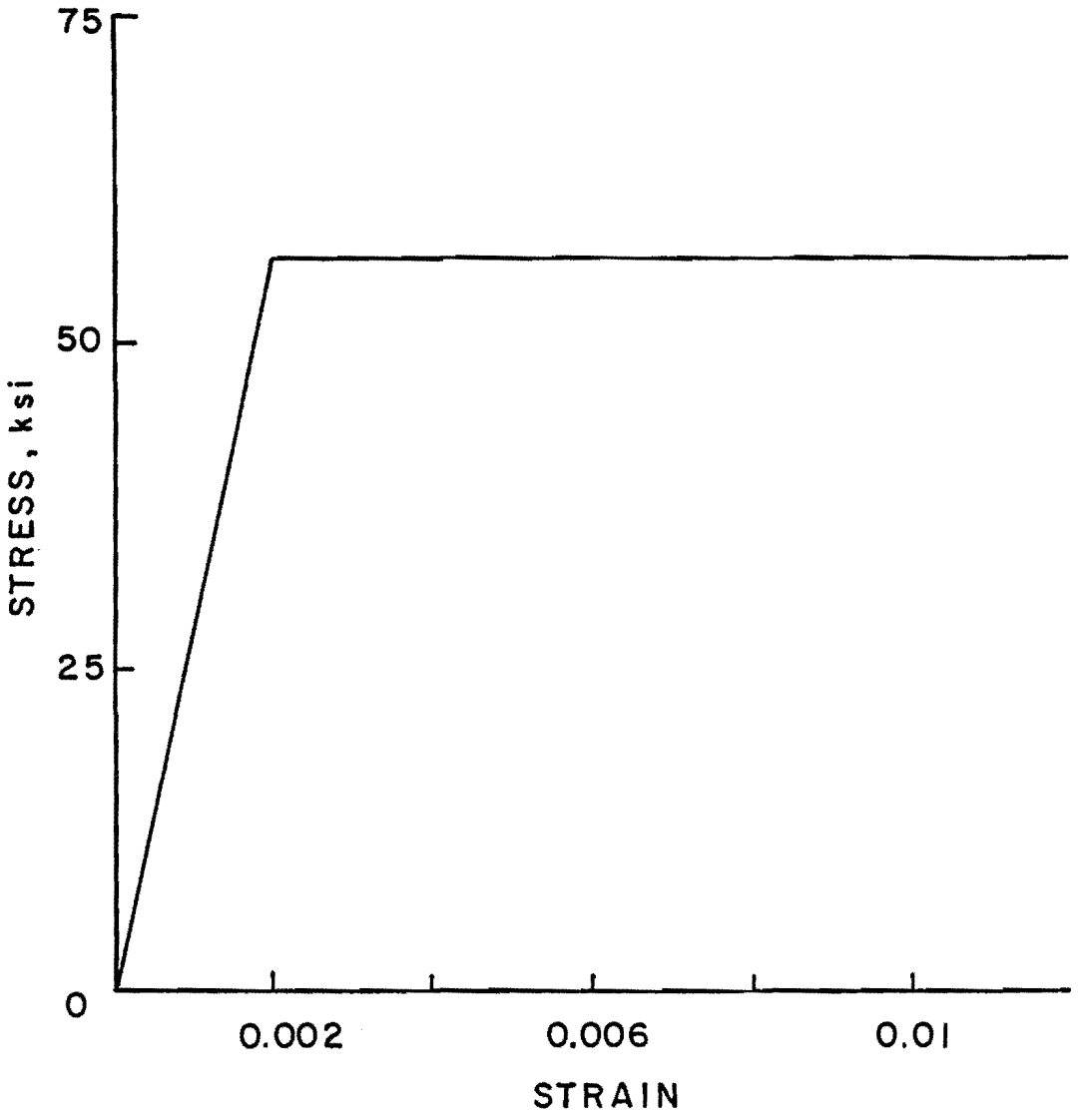

Fig. 4.2 Stress vs. Strain Curve for Reinforcing Steel

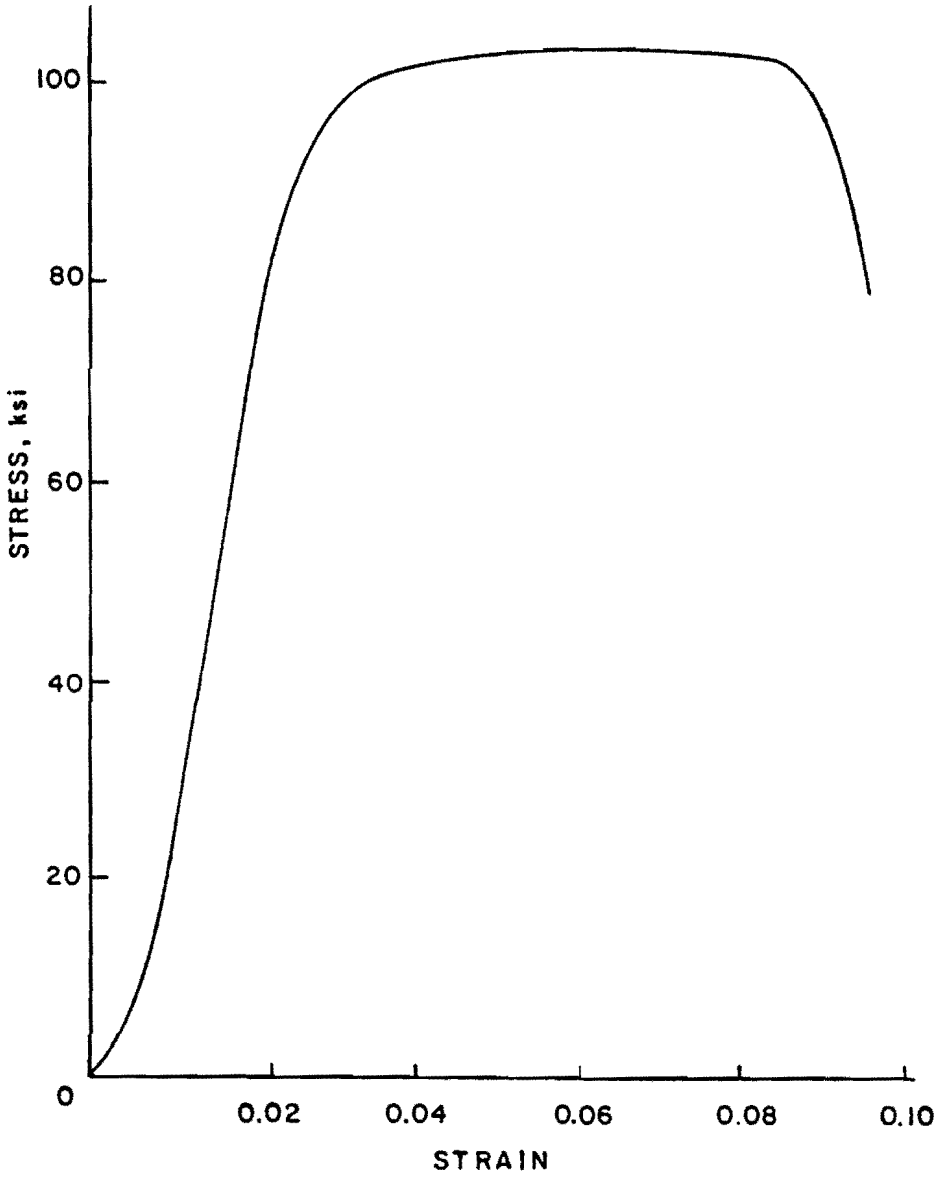

Fig. 4.3 Stress vs. Strain Curve for 3/4-in. Diameter Anchors

strength was 78 ksi, and the average ultimate strength, 84 ksi. A typical stress-strain diagram is shown in Fig. 4.4.

4.1.4 Structural Steel. The W6x20 posts, base plates, load plates, and stiffeners were all of A36 steel.

4.2 Specimen Detail and Construction

4.2.1 Specimen Details. Overall nominal dimensions for the specimen are shown in Fig. 4.5. The three barrier posts are equally spaced at 48 in. center to center. Note that the edge distance is less on the west end of the specimen. The edge distance on the east end of the specimen was chosen to ensure the development of a complete flexural-torsional failure surface as shown in Fig. 3.5 The effects of reduced edge distance were to be investigated at the west-end post location.

The specimen reinforcement is shown in Fig. 4.6. Construction of the reinforcing cage is shown in Fig. 4.7.

4.2.2 Formwork. The formwork was constructed using 3/4- in. exterior grade plywood with 2- by 4-in. bracing. Holes for the anchors were formed by placing sections of 3/4-in. I.D. PVC pipe in the hole locations. The pipes were held in place at top and bottom by wooden dowels about 1/4 in. thick, and with diameters equal to the inside diameter of the pipe. The bottom dowels were nailed to the bottom of the form, while the top dowels were mounted on wooden platforms which were suspended from 2- by 4-in. braces which spanned the form (Fig. 4.8). Holes for the tie-down rods were formed in the same manner using 1-1/2 in. I.D. pipe. The forms were lacquered and oiled prior to casting.

4.2.3 Casting. The specimen was cast on December 12, 1984. The concrete was placed in one lift and mechanically vibrated. The surface was screeded and troweled.

4.3 Test Setup and Loading Apparatus

4.3.1 Test Setup. The test setup is shown in Figs. 4.9 and 4.10. The specimen was anchored to the laboratory floor using 1-in. diameter rods tensioned to 25 kips.

The test frame was fabricated from two C10x15.3 sections back to back, and using two C6x13 sections for the diagonal. Stiffeners were added at the load point and at the connection of the diagonal. The frame was tied to the laboratory floor with 1-in. diameter threaded rods, each tensioned to 25 kips.

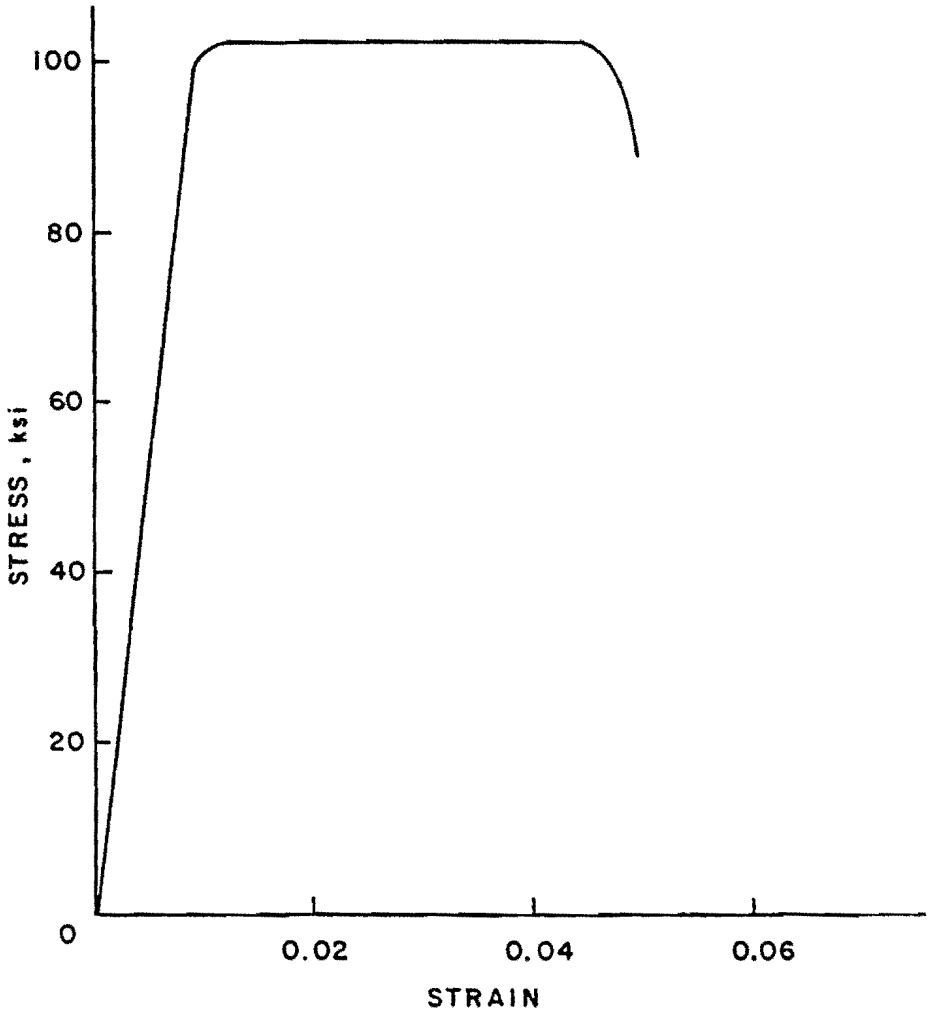

Fig. 4.4 Stress vs. Strain Curve for 1/2-in Diameter Anchors

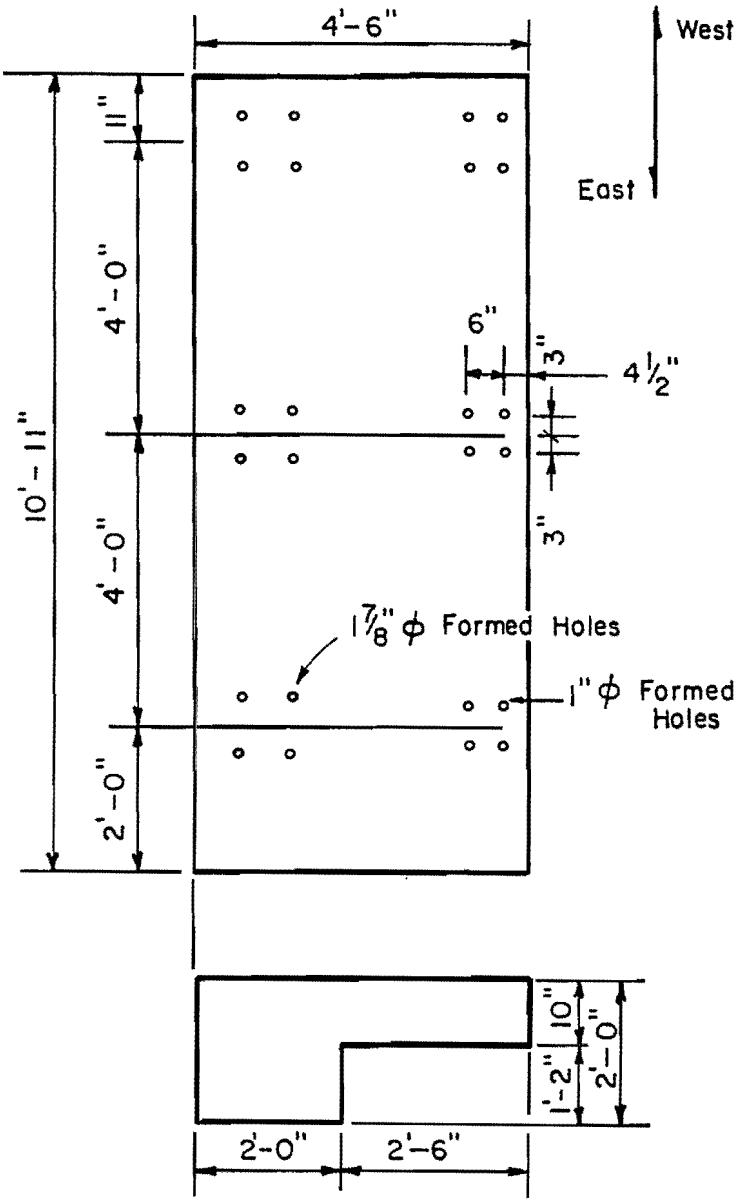

Fig. 4.5 Test Specimen

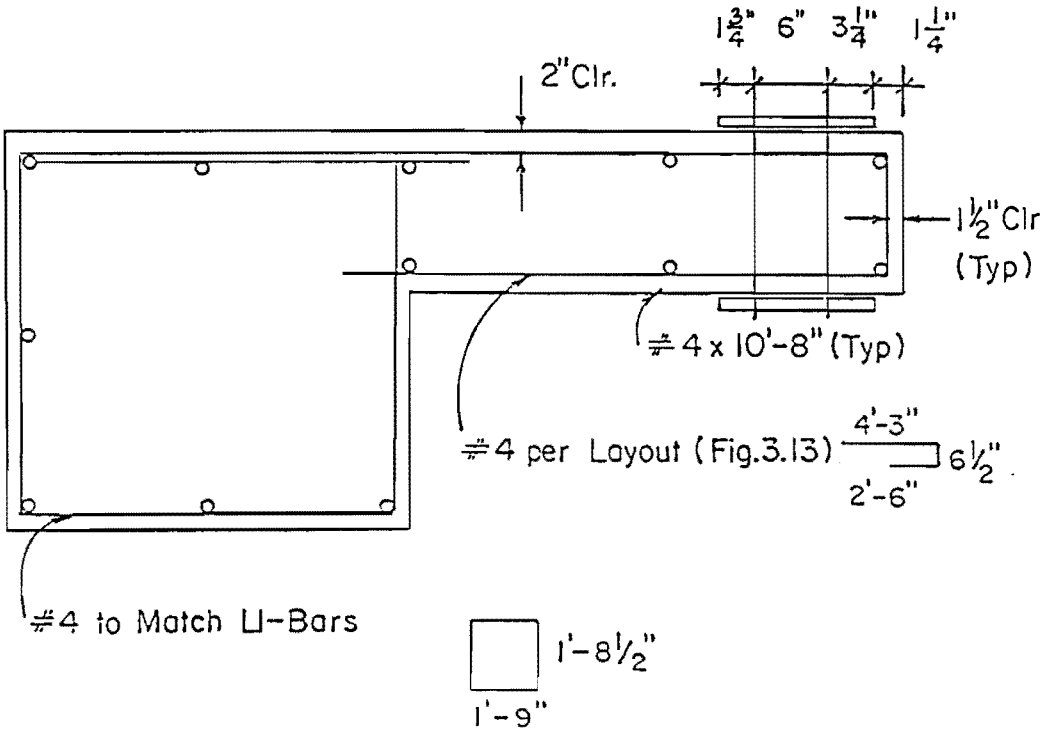

Fig. 4.6 Specimen reinforcement

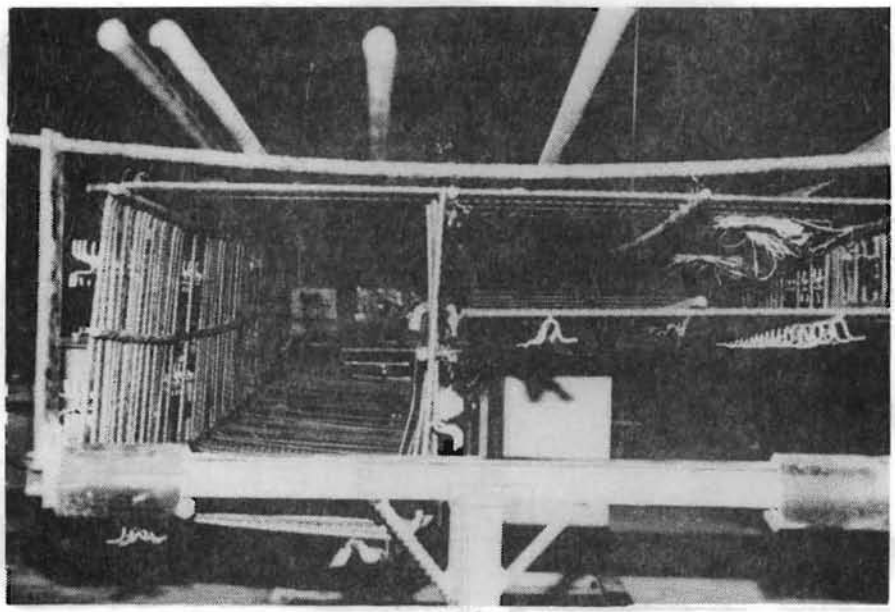

Fig. 4.7 Construction of Reinforcing Cage

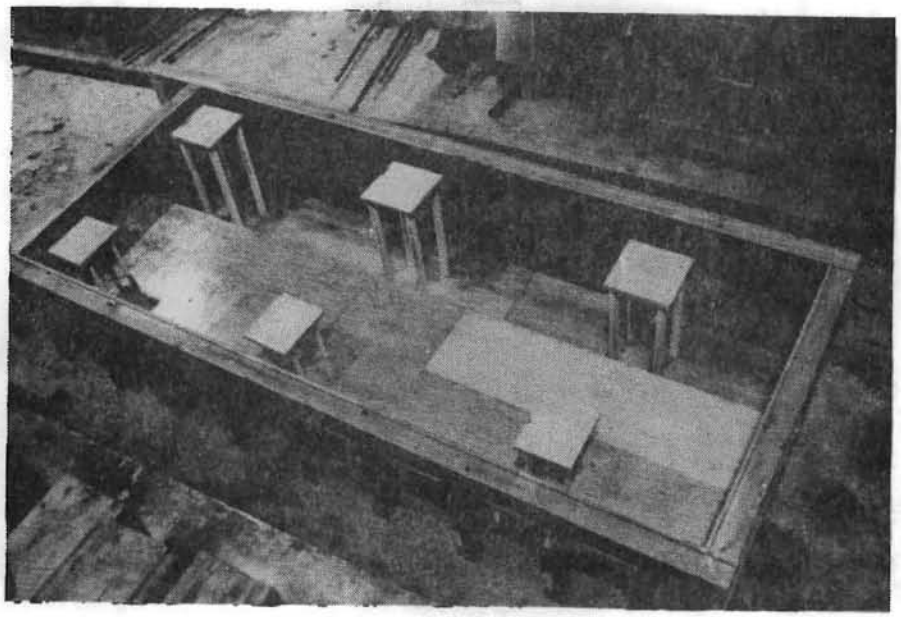

Fig. 4.8 Formwork

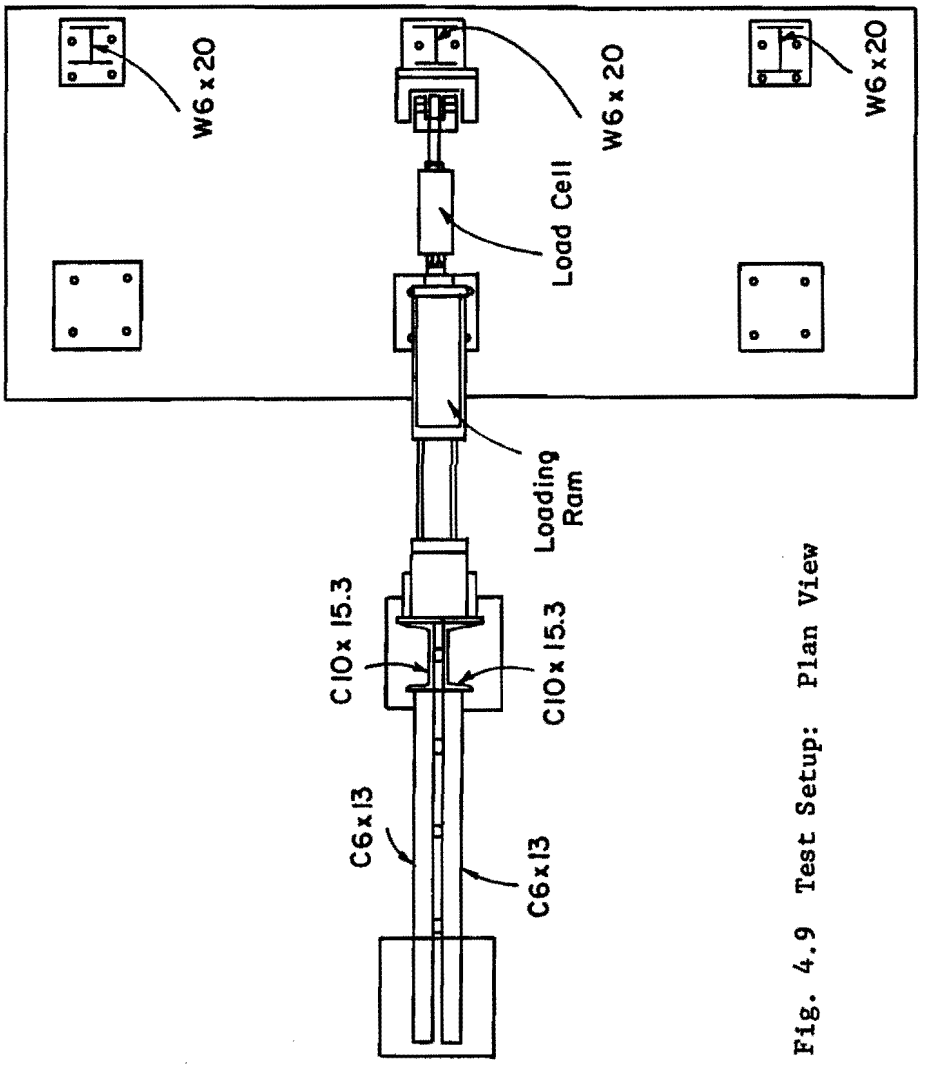

Fig. 4.9 Test Setup: Plan View

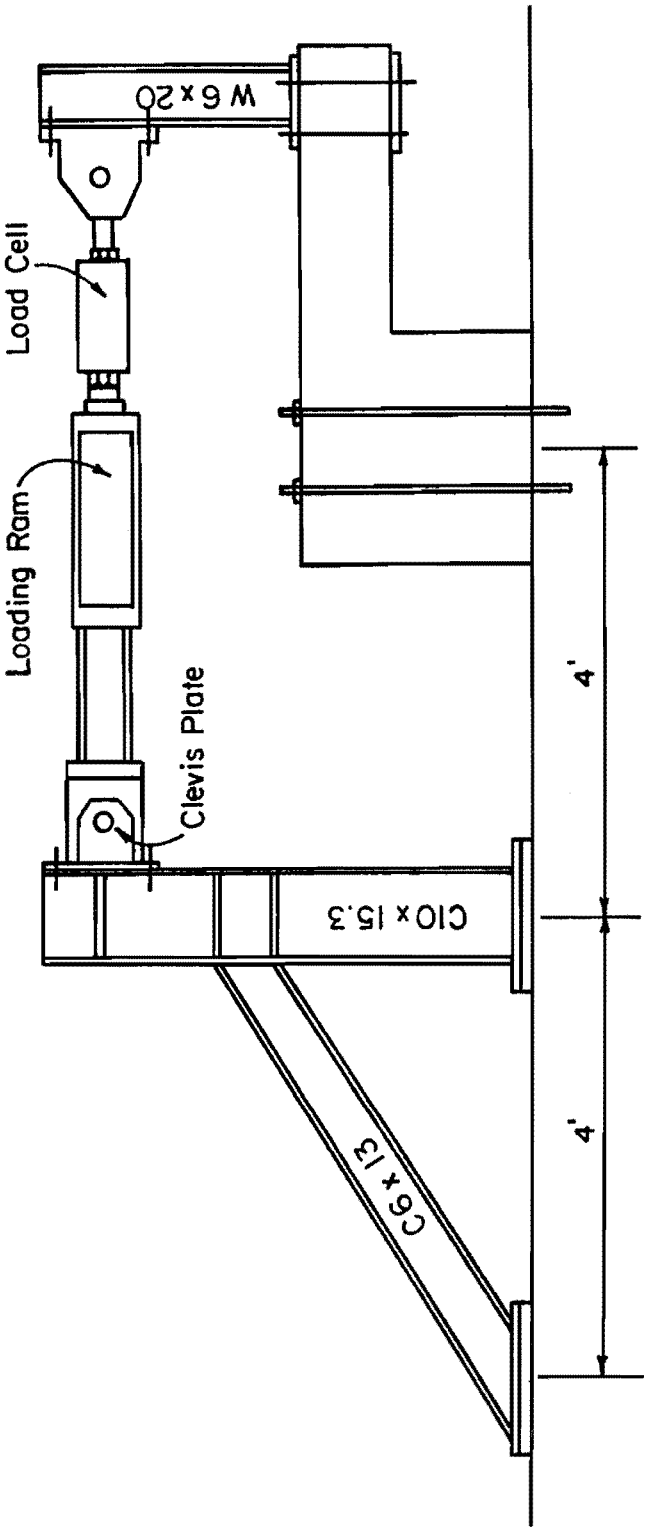

Fig. 4.10 Test Setup: Side View

The 100-kip capacity, double-ended ram was bolted to a loading plate mounted on the test frame. It was temporarily supported by a steel frame which rested on the specimen. The other end of the ram was bolted to a load plate on the W6x20 post. Both ends of the ram were equipped with clevises which allowed the ram to rotate once deflection of the post began.

4.3.2 Impact Loads.

Crash Test Results

Buth et al. performed a series of tests in which various types of vehicles were driven into a wall instrumented with load cells and accelerometers [28]. Both the vehicle's speed and its angle of impact were varied. Plots of lateral force versus time indicate that two impacts occurred in each test. The first was a relatively long but low-intensity pulse, produced as the front of the vehicle scraped along the wall. The second impulse, very sharp and of greater intensity, corresponded to the impact of the back end of the vehicle, as the front end bounced off the wall. A typical load versus time curve is shown in Fig. 4.11a.

It was decided that the second, more intense, impact was more critical, and would be modeled in the current test program. Note that the load variation over time is virtually triangular, and can be closely simulated by a triangular pulse (Fig. 4.11b).

Hydraulic System

The loads measured in the crash test program had a total duration on the order of 0.05 to 0.15 sec (for the second pulse). A hydraulic loading system was chosen because the application of the load could be carefully controlled and monitored. The traditional method of applying impact loads by means of a pendulum is very difficult to control. The major drawback of the hydraulic system is that the speed with which load can be applied is limited by the rate at which hydraulic fluid can be input to the actuator. The magnitude of the applied load depends on the maximum flow rate, the duration of the loading and the flexibility of the barrier system.

It was not considered feasible to match the load duration of the crash test program for all test pulses. Instead, a hydraulic system which would maximize flow rate was developed from the available equipment. This system is shown schematically in Fig. 4.12.

The shortest pulse duration over which this system could apply a load of a given magnitude was limited by the flow rate of the servovalves. The valves used have a rated capacity of 15 gpm. Although a larger valve was available, its response time is so long that the pulse duration could not have been decreased at the required

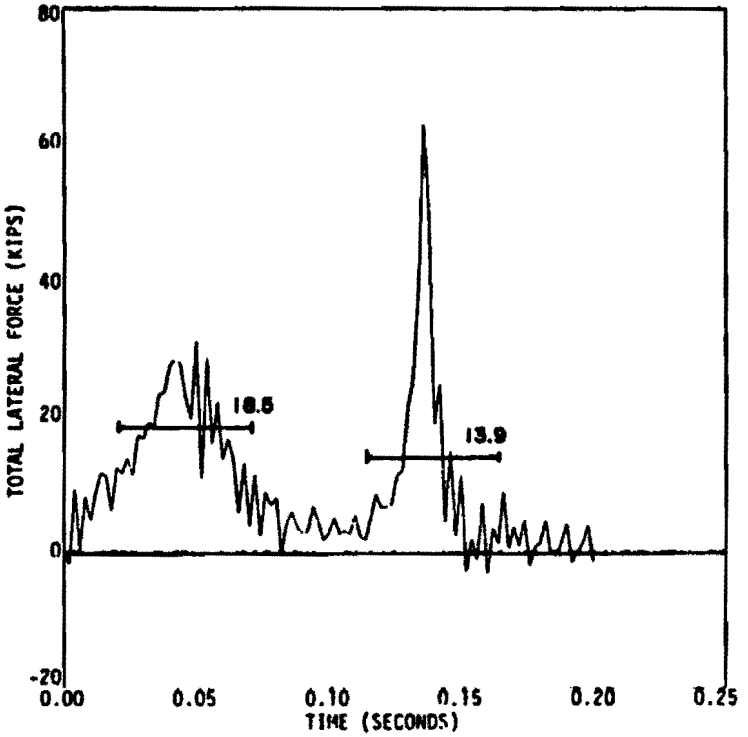

Measured Impact Load from Crash Test [28]

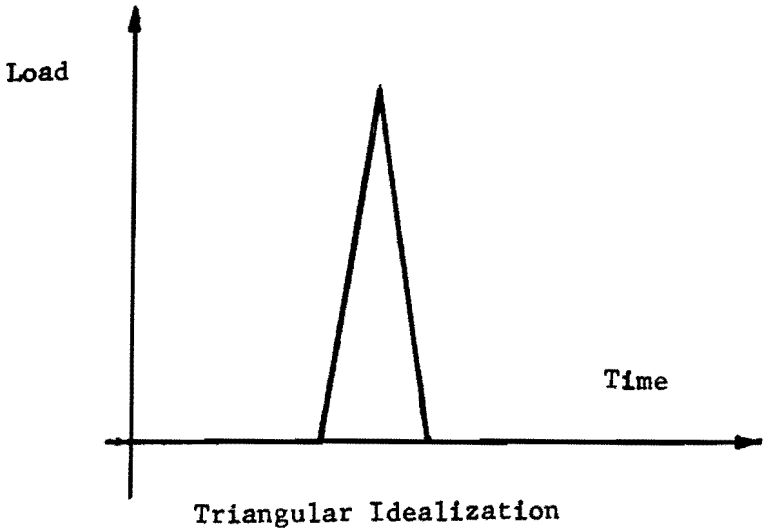

Triangular Idealization

Fig. 4.11 Impact Load

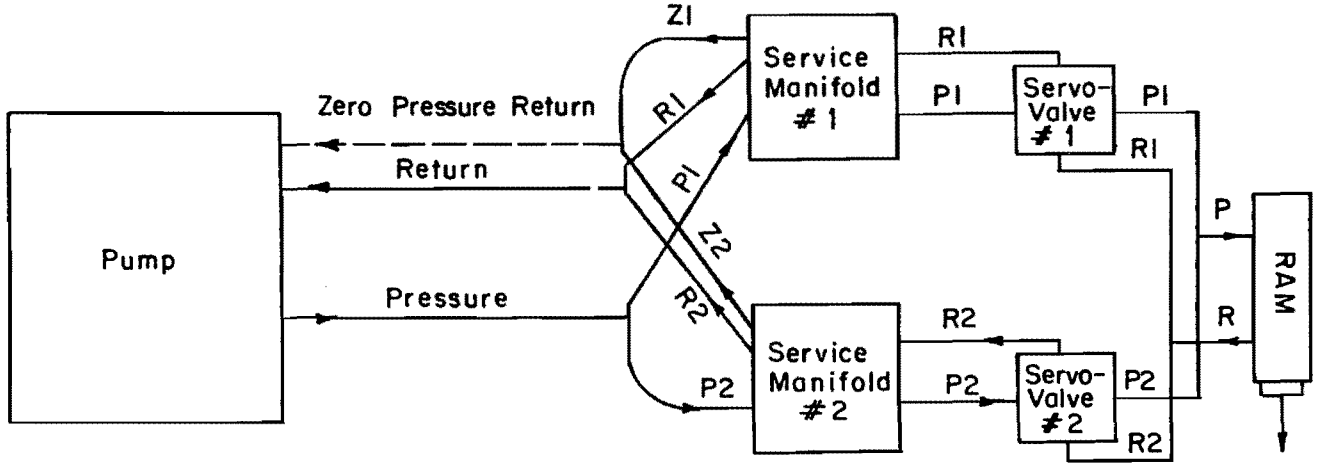

Fig. 4.12 Hydraulic System

load levels. To increase capacity without sacrificing responsiveness, two 15-gpm valves were used in parallel.

Before entering the servovalves, each pressure line passes through a service manifold containing a rubber bladder which fills with fluid and then discharges to the system. This minimizes pressure fluctuations in the system and increases the amount of fluid available for short-duration pulses. Pulse durations used in the testing program ranged from 0.1 sec to 0.8 sec. The longer-length pulses were required only after significant deterioration of the test specimens had occurred.

Load Control

A schematic of the load control system is shown in Fig. 4.13. An electronic function generator is set to deliver a triangular pulse of the desired duration. This signal is sent to the servocontroller which opens or closes the servovalve to produce the required load. The actual load is monitored by a load cell mounted between the ram and the post. This signal is continuously fed back to the servocontroller which responds by adjusting the position of the servovalve to minimize the difference between the measured load and the programmed load.

4.3.3 Static Loads. The system just described was also used to produce static loads. The function generator was not used. Instead, a constant load was set on the servocontroller. Otherwise, the system functioned in the same manner, with the servocontroller making adjustments to keep the load constant. As is discussed later, in one of the static tests, the load was deflection-controlled. A target deflection was set on the servocontroller, and a linear potentiometer was mounted on the ram to monitor the actual deflection.

4.4 Instrumentation

Electrical resistance strain gages were placed on the vertical and top horizontal legs of selected U-shaped reinforcing bars. These locations were chosen because they were predicted by the failure model to be the most highly stressed in the failure model. At each post location, the two U-bars between the bolts, and the first U-bar beyond the base plate on each side of the post were gaged. In each test, only four of the eight gages were connected. The duplicate gages were put in as backups, since gages can be damaged during placing of the concrete.

A strain gage was also placed on each post, about 1 in. above the base. During the static tests, this was used to determine whether the post had yielded. Since only eight channels of data acquisition were available for the impact tests, this gage was not connected for those tests, and yielding was determined by inspection of the post.

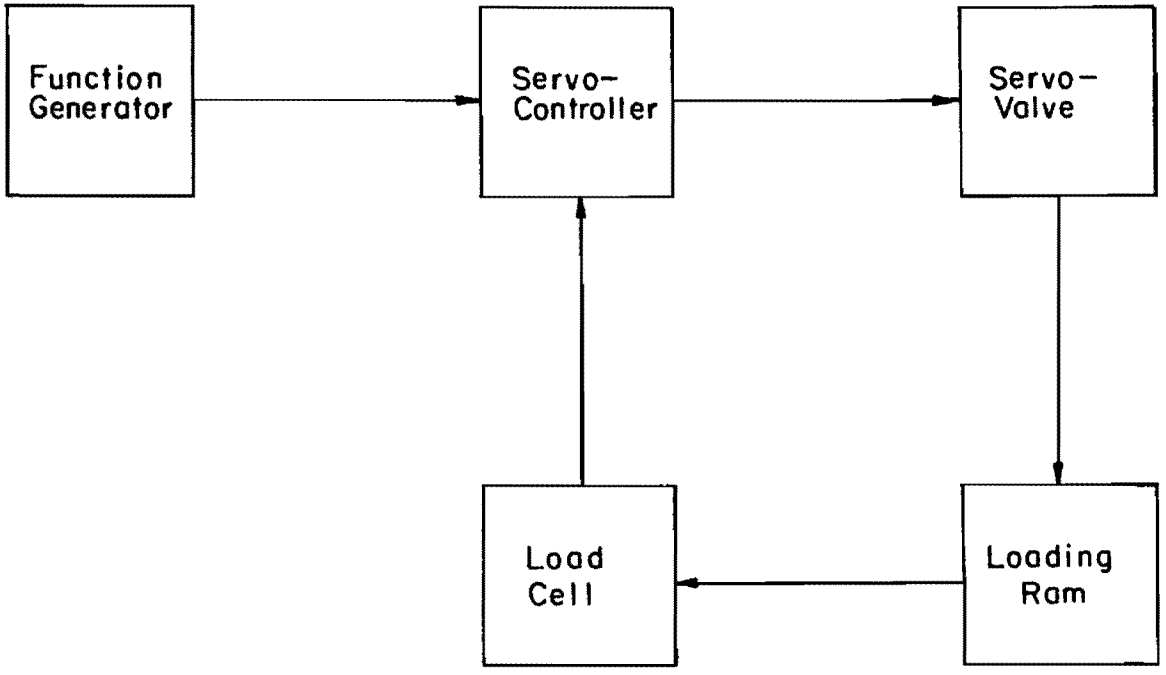

Fig. 4.13 Load Control System

A 100-kip capacity load cell was mounted between the actuator and the post to measure the applied load. A linear potentiometer was attached to the actuator to measure the deflection of the post. The load cell used had the capability of measuring load on two channels simultaneously and independently. Thus, one channel was fed into the data acquisition system, while the other channel monitored the load for the load control system. For the deflection-controlled test, a second linear potentiometer was added.

The tension in the front bolts was measured by load cells placed between the bottom of the slab and the bottom nut on the anchor. Each load cell consisted of four strain gages connected to form a full bridge and mounted on a piece of round mechanical tubing made of high strength carbon steel. The tubing was placed over the anchor and held in place by a plate washer and the anchor nut (Fig. 4.14). Prior to use, the load cells were calibrated using a center-hole actuator. The compressive force in the load cell was assumed to equal the tensile force in the anchor bolt.

4.5 Data Acquisition

4.5.1 Static Tests. The responses of the strain gages, linear potentiometer, and load cells, were continuously monitored during testing by a Hewlett Packard 3497A high-speed data acquisition system. A zero reading was first taken, and scans were made when a load was initially applied. If a significant amount of time elapsed between load stages, a second scan was made before applying the next increment of load.

4.5.2 Impact Tests. Data from the impact tests were recorded on two Data Precision D6000 digital oscilloscopes. Each machine can measure and store the output from four transducers. The load and displacement data were recorded on one machine while the strain gage data were recorded on the other. Both machines were triggered by a signal from the load cell channel. Once the signals for a test had been internally recorded, they were transferred to computer diskettes for permanent storage and further reduction.

4.6 Test Sequence

4.6.1 Planned Test Sequence. The test program originally planned was as follows:

(1) Static test of center post: load-deflection response

(2) Replace center post; repeated impact at moderate load levels; impact at ultimate

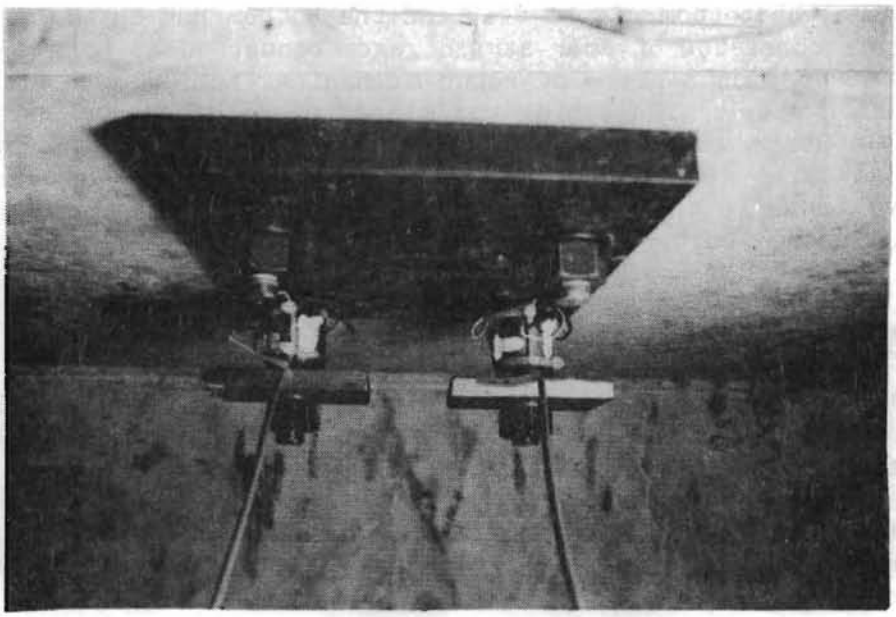

Fig. 4.14 Load Cells on Tension Anchors

(3) Impact test at ultimate load - east end post

(4) Replace east end post; repeated impact at moderate load levels; impact at ultimate load

(5) Static test of west end post

(6) Replace west end post; impact test at ultimate load

Once testing began, this program did not prove to be feasible. The actual test program and the reason for the change are described below.

4.6.2 Actual Test Sequence. The static test of the center post resulted in a brittle failure. The test is described in detail in Chapter 5. Damage to the slab was so great that further tests could not be carried out at this location. Since the actual failure, due to fracture of the weld between the post and base plate, occurred before anchorage failure, the test was inconclusive. It was therefore decided that a second static test should be performed before proceeding with the impact tests.

The west-end post location was chosen for this test since it was deemed necessary to preserve one location for an impact test where the slab had not been damaged, and where edge effects would not be a problem. The edge effect investigation originally planned for the west-end post was a secondary objective. The static test on the west-end post also produced a nonductile failure, but was terminated before very severe damage to the slab had occurred.

An impact test was then performed at the west location. To produce a ductile failure, the anchors were changed to 1/2 in. diameter threaded rods. A series of tests was carried out at increasing load levels until an anchor fractured. Finally, the as yet undamaged east-end post location was tested in the same manner. Again, 1/2-in. diameter anchors were substituted for those originally specified.

The actual test sequence was then as follows:

(1) Static test of center post

(2) Static test of west end post

(3) Impact test of west end post

(4) Impact test of east end post

The sequence is illustrated in Fig. 4.15.

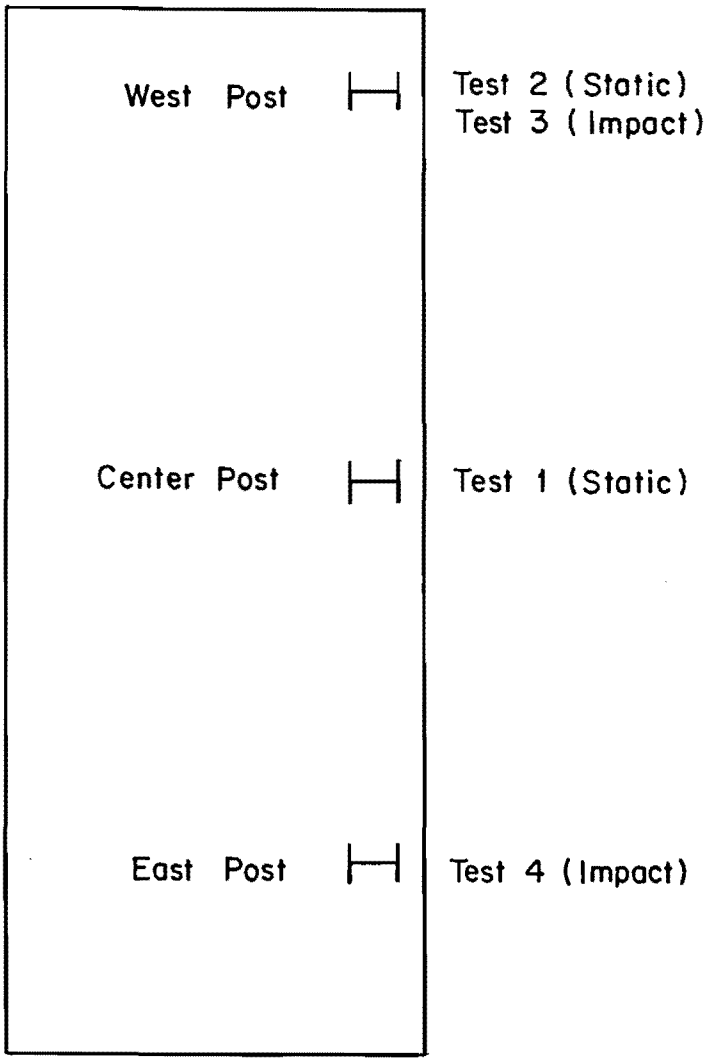

Fig. 4.15 Testing Sequence

CHAPTER 5

TEST RESULTS

5.1 Description of Static Tests and Results

5.1.1 Static Test of Center Post. The first static test was performed at the center post location. Results from the static tests of the center and west-end posts are presented in Figs. 5.1 through 5.7. In Fig. 5.2, the anchor load is the sum of the loads measured in the two tension anchors. The stress in the U-shaped reinforcing bars near the post is plotted as a function of displacement in Figs. 5.4 through 5.7. The corresponding strain gage locations are given in Table 5.1.

Load was applied in approximately 2-kip increments. When the load reached 12 kips, the base plate slipped laterally (0.01 - 0.05 in) on the hydrostone pad. The first significant cracks began to show at the 14-kip load stage (Fig. 5.8). The cracks developed as expected, extending diagonally from the compression zone beneath the base plate. By a load of 18 kips, the cracks had extended to the bottom of the deck section (Fig. 5.9). As shown in Fig. 5.10, the crack extending from the east edge of the post was at a steeper angle than the assumed 45°.

When the 20-kip load was first applied, a vertical crack developed, centered on the post and extending the full thickness of the deck (Fig. 5.11). At the next load stage (22 kips), the fillet weld connecting the post to the base plate broke suddenly. Since the test was load-controlled, a large error was created between the desired and applied loads. The servocontroller shut off, and the load immediately dropped off to 2 kips (Fig. 5.12).

When the weld broke, the point of application of the compressive stress block acting on the slab shifted further toward the slab edge. A 2-or3-in. deep section at the slab edge was pushed down and away from the remainder of the deck, resulting in cracks 1/8 to 1/4 in. wide (Fig. 5.13). Until this point, the cracks had been well defined but less than 0.015 in. wide.

The two 3/4-in. diameter front bolts, which were subjected to tension, were still intact at failure, though they had yielded in bending.

5.1.2 Static Test of West-end Post. The second static test was performed at the west-end post. Because the previous load-controlled test had resulted in a brittle failure, the servo-controlled loading system was modified to operate under displacement control. As explained in section 4.2.1, this post was located closer to the side

edge of the slab than the minimum required distance as calculated by analysis. Results are presented in Figs. 5.14 to 5.20. The second static test involved unloading and reloading of the specimen after some strain gages had broken. Since the strain gage data recorded under this circumstance are not valid, those portions of the curves have been omitted from Figs. 5.17 and 5.18. First cracking occurred at a load of approximately 12 kips with the vertical leg of the reinforcement under the base plate showing a large increase in stress. On the interior side of the post, cracking began as in the previous test. On the exterior side, however, the crack extended from the front of the compression zone near the base plate, to the west edge of the slab (Fig. 5.21). That is, the crack propagated perpendicular to the direction of loading, rather than angling toward the north edge of the slab in the usual manner. The crack then extended toward the bottom and back of the slab at about a 45^{o} angle.

At a load of about 17 kips, cracks began developing near the tension bolts (Fig. 5.22). At this point, the widest crack was 0.013 in. wide. At a load of 17.7 kips the base plate slipped about 0.1 in. on the grout pad.

After reaching a load of 17.9 kips, the specimen was unloaded. It was then reloaded, but the linear potentiometer was not functioning properly and the test was stopped. The specimen was again reloaded. By the 12-kip load stage, the base plate had begun to bend. At the peak load of 13.5 kips the concrete failure surface had fully developed, and cracks were quite wide.

Subsequent loading produced a series of cracks behind the base plate, perpendicular to the direction of loading (Fig. 5.23). A flexural inelastic hinge had developed in the slab behind the post attachment, permitting the post and surrounding slab to move as a rigid body. A permanent deformation had occurred in the top slab reinforcement, resulting in a permanent deflection at the top of the post of about 0.3 in. in the direction of load. The test was terminated since it was evident that the post-slab system would not carry additional load. The two 3/4-in. diameter tension rods remained intact throughout the test.

5.2 Description of Impact Tests

5.2.1 General. A series of impact tests were performed under load control, using monotonically increasing values of peak load. Corresponding to each peak load, several tests were carried out. In the following discussion, those tests are referred to using the following notation: a number (indicating the peak load in kips), followed by a letter (indicating the test, starting at A and going toward Z). For example, Tests 12A, 12B and 12C were the first 3 tests involving a peak target load of 12 kips.

Because of limitations in the flow rates of the two servovalves, it was not possible to apply very large peak loads in short-duration pulses. The loads actually applied were in many cases considerably below the target values. Therefore, Tests 12A, 12B and so forth might actually involve peak loads lower than 12 kips. The test results are always discussed in terms of the actual applied load. However, the test names, and the corresponding figure titles, refer to the nominal (target) values.

5.2.2 Impact Test of West-end Post. After the test described in the previous section was terminated, the loading system was again modified to produce a triangular pulse loading of variable duration, under load control. In addition, the 3/4-in. diameter rods were replaced with 1/2-in. diameter rods, in an attempt to force the anchorage to exhibit a ductile failure mode. The maximum load level was increased in approximately 2-kip increments.

Figures 5.24 through 5.30 show the results of impact tests performed at the west-end post location. Due to the considerable damage caused by the earlier static test at this location, only the main load cell (Channel 1) and linear potentiometer (Channel 2) gave meaningful data. A different notation was used for the names of tests conducted on the west-end post--the tests were simply numbered in the order they were conducted.

A typical curve of applied load vs. time is shown in Fig. 5.24. This particular test (Test 8) had a peak applied load of 9.8 kips and a 0.8-sec pulse duration. Figure 5.25 shows a similar loading history for Test 10, which had a peak load of 11.5 kips. The sudden drop to a load of 6 kips corresponds to fracture of one of the two tension anchors.

Load-displacement curves for several tests are shown in Fig. 5.26. In tests 1 through 6, the response of the system was essentially elastic, with the displacement vs. time curves conforming to the shape of the load vs. time curves. The first permanent deformation occurred in Test 7. A picture of the displacement history of the system can be gathered from Figs. 5.27 through 5.30. The specimen had been badly damaged by the previous static test, and repeated impacts widened the pre-existing cracks (Fig. 5.31). When a 12-kip maximum load was applied, one of the two tension anchors fractured (Figs. 5.32, 5.33). The post did not yield.

5.2.3 Impact Test of East-end Post. The procedure of the previous test was repeated at the east-end post location. Again, 1/2-in. diameter bolts were used. The first tests were performed with a 0.2-second pulse duration. Figure 5.34 shows a typical load curve. It can be seen that the actual peak load (7.6 kips) closely approximates the target load. As testing progressed, the actual load began to drop off with respect to the target load. At Test 12D, the pulse duration was changed to 0.4 second. Actual load again approached the target

load, dropping off slightly as the testing proceeded. A typical 0.4 second pulse (Test 14A) is shown in Fig. 5.35. For ease in interpreting this and other figures referring to impact tests on the east-end post, the channel descriptions are given in Table 5.2.

The load vs. time curve for the following test (14B) shows a sudden drop in load (Fig. 5.36) at a value of 11.7 kips. This corresponds to first cracking of the specimen. Due to the large increase in displacement following that cracking, Tests 14C and 16A resulted in peak loads of only 9 kips and 10.5 kips, respectively. For test 16B and 18A the pulse duration was increased to 0.8 seconds (Fig. 5.37). The system had lost much of its stiffness, and it became very difficult to produce any increase in load. A 1.6-second pulse was used for Test 18B, and a 2.4-second pulse for Test 18C. This last test finally fractured the tension anchors.

The typical displacement vs. time curves of Figs. 5.38 and 5.39 are similar in form to the load vs. time curves of Figs. 5.34 and 5.35. The response in these tests was essentially elastic. The displacement curve for Test 14B (Fig. 5.40) shows about a 0.2-in. permanent displacement, corresponding to first cracking. From this point, the permanent deformation increased with each successive impact (Fig. 5.41).

The load in the tension anchors for a low level impact is shown in Figs. 5.42 and 5.43. Note that the anchor of Channel 3 does not show significant tension until its initial pretension is exceeded. The anchor loads for Test 14B, shown in Figs. 5.44 and 5.45, reflect the sharp decrease in anchor load when cracking of the specimen occurred.

Stresses in the reinforcement are presented in Figs. 5.46 through 5.56 for Tests 14A, 14B and 18A. Because it was necessary to measure a very low level response, a great deal of background noise was also recorded, and is reflected in the graphs.

A series of load-deflection curves for different tests are shown in Fig. 5.57.

First cracking occurred at a load of 11.5 kips (Test 14B). On the exterior side of the post, cracking began near the back edge of the base plate (side nearest slab edge) and extended immediately to the slab edge at an angle of about 20^{o} (Fig. 5.58). A second crack extended from the center of the back edge of the base plate, roughly parallel to the first crack. On the interior side of the post, a crack extended to about the top quarter of the slab thickness. When the next load was applied (Test 14C) the crack reached the bottom of the slab (Fig. 5.59). At this point, the major cracks were about 1/4 in. wide. The cracks are illustrated in Fig. 5.60. It can be seen that the interior crack (c) is consistent with the theoretical failure surface

discussed in Chapter 3, while cracks a and b on the exterior side represent a more localized failure.

At a load of 11.65 kips (Test 16B), the strip of concrete between cracks a and b (in Fig. 5.60) began to spall. Three 11.8- kip loads were then applied to the post. The second of these (Test 18B) caused yielding of the tension anchors and a permanent rotation of the post and base plate. The back edge of the base plate became embedded in the cracked concrete. Both tension anchors fractured when the third 11.8-kip load was applied (Test 18C). Cracks were quite wide, with reinforcement exposed in some areas (Figs. 5.61, 5.62 and 5.63).

TABLE 5.1

STRAIN GAGE LOCATIONS

Notation	Test	
	First Static	Second Static
Bar Stress 1	Vertical Leg-West Inside Bar	Vertical Leg-West Inside Bar
Bar Stress 2	Vertical Leg West Outside Bar	Vertical Leg-West Outside Bar
Bar Stress 3	Top Horiz Leg-West Outside Bar	Top Horiz Leg-East Outside Bar
Bar Stress 4	Top Horiz Leg-West Inside Bar	Top Horiz Leg-East Inside Bar

TABLE 5.2

Channel	Descriptions
1	Load applied to post
2	Horizontal displacement at top of post
3	Load in East tension anchor
4	Load in West tension anchor
5	Stress in top horizontal leg of West inside bar
6	Stress in vertical leg of West inside bar
7	Stress in top horizontal leg of East outside bar
8	Stress in vertical leg of West outside bar

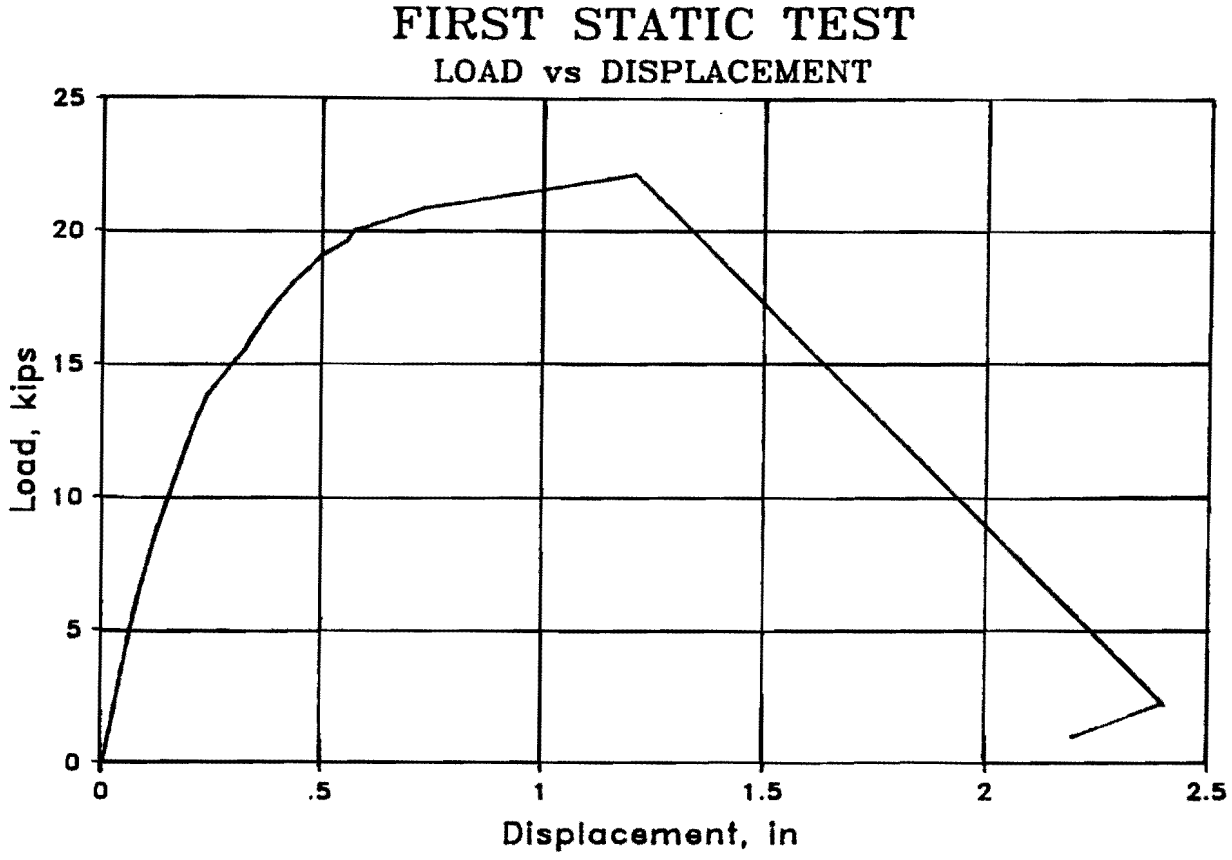

Fig. 5.1 Applied load vs. post displacement, first static test

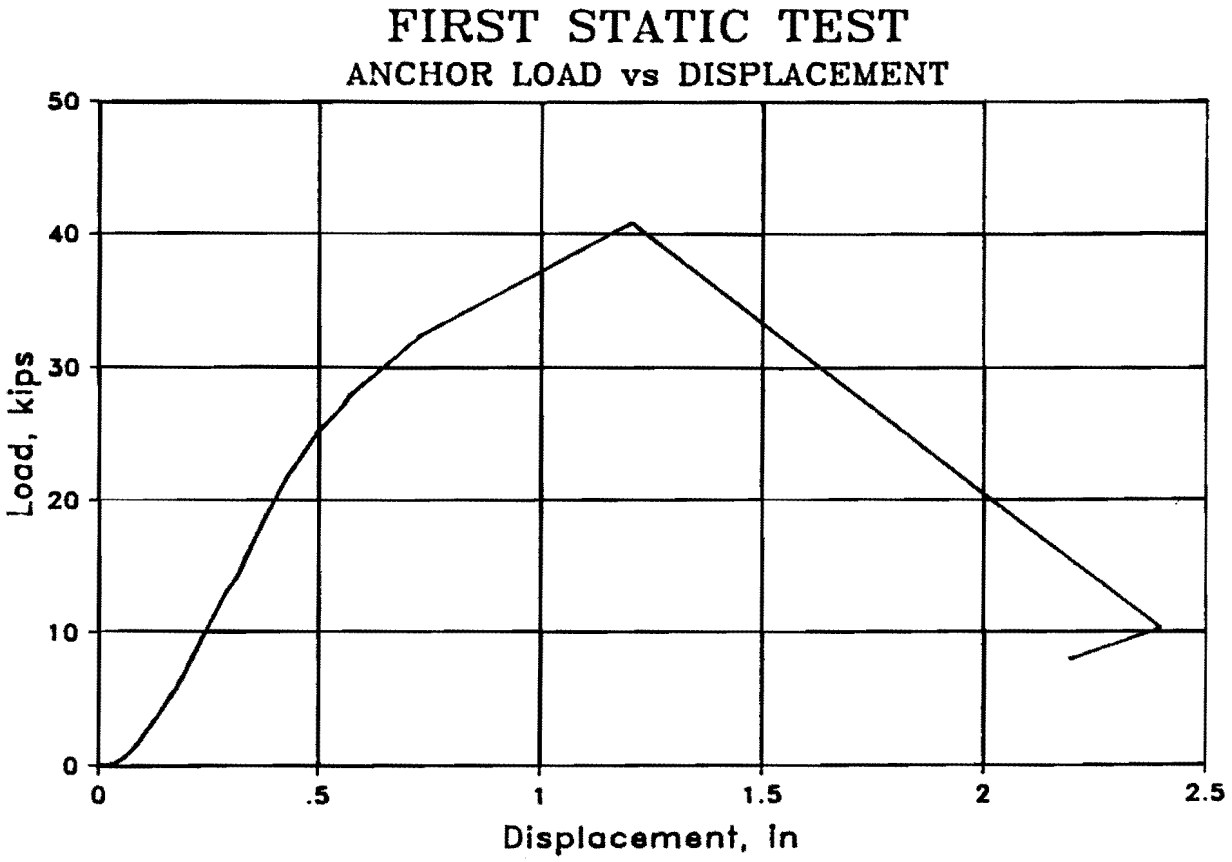

Fig. 5.2 Anchor load vs. post displacement, first static test

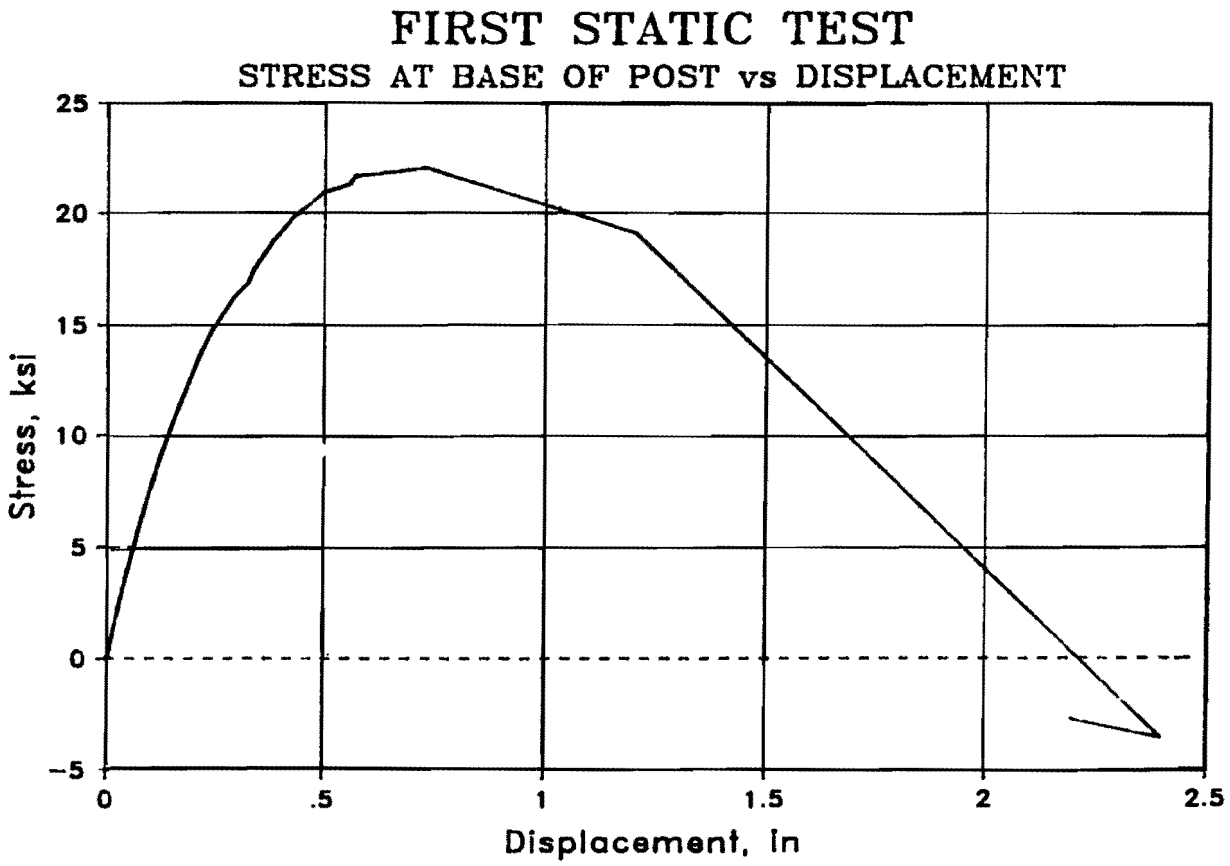

Fig. 5.3 Stress at base of post vs. post displacement, first static test

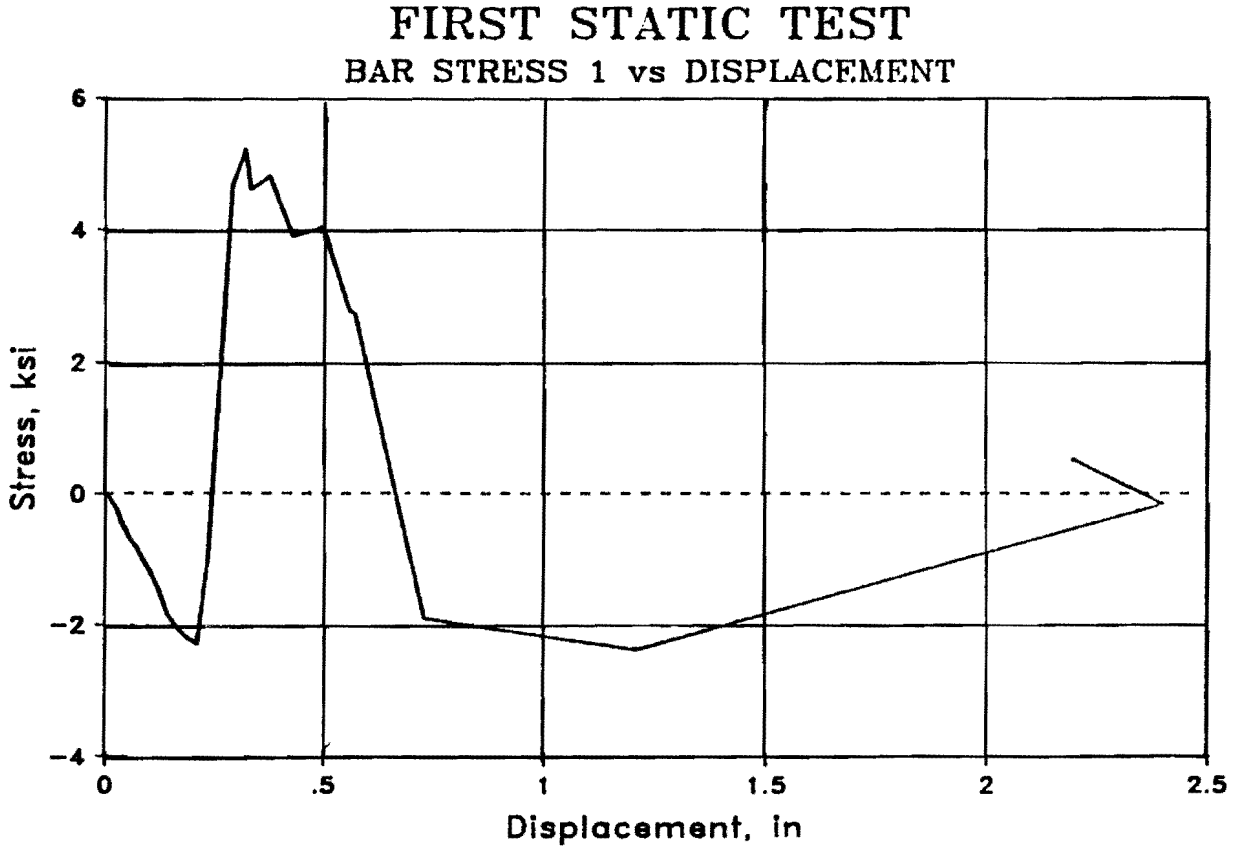

Fig. 5.4 Bar stress 1 vs. post displacement, first static test (see Table 5.1)

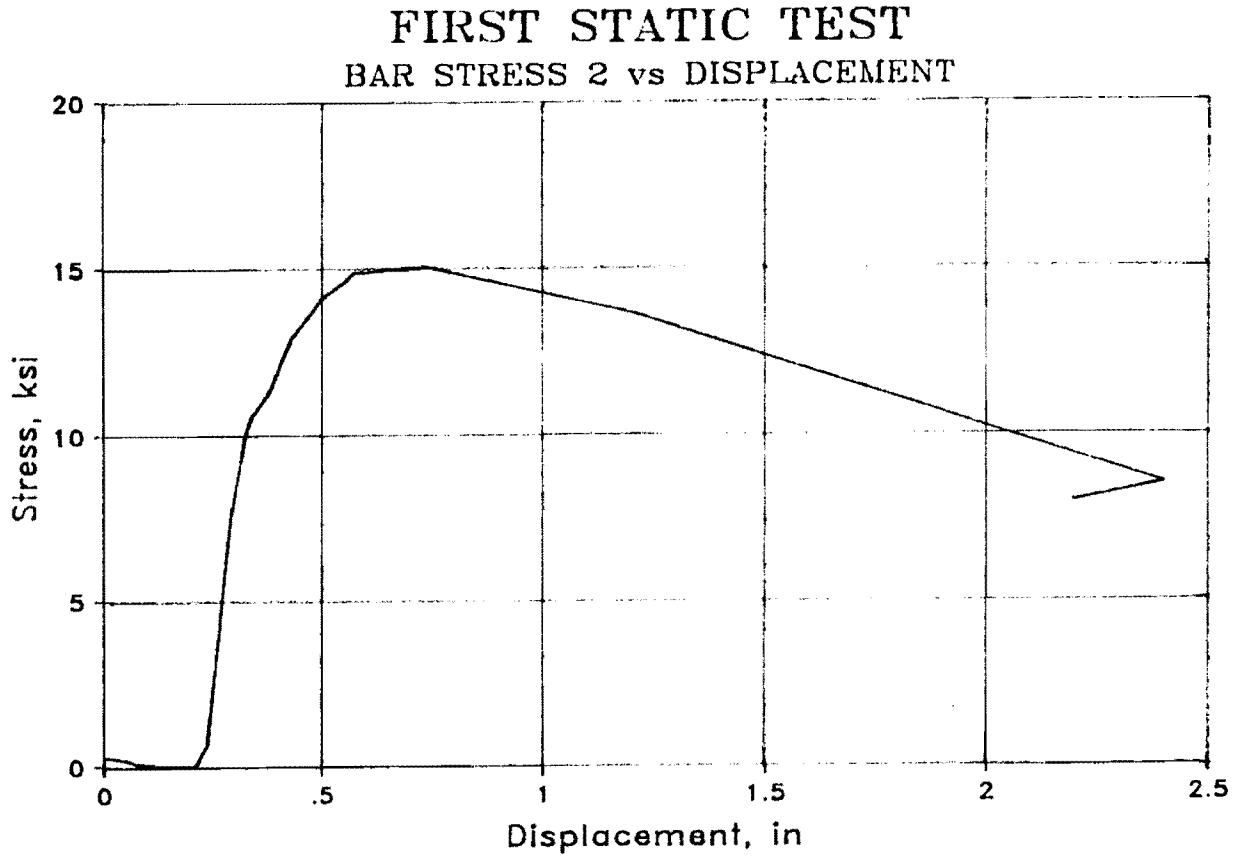

Fig. 5.5 Bar stress 2 vs. post displacement, first static test (see Table 5.1)

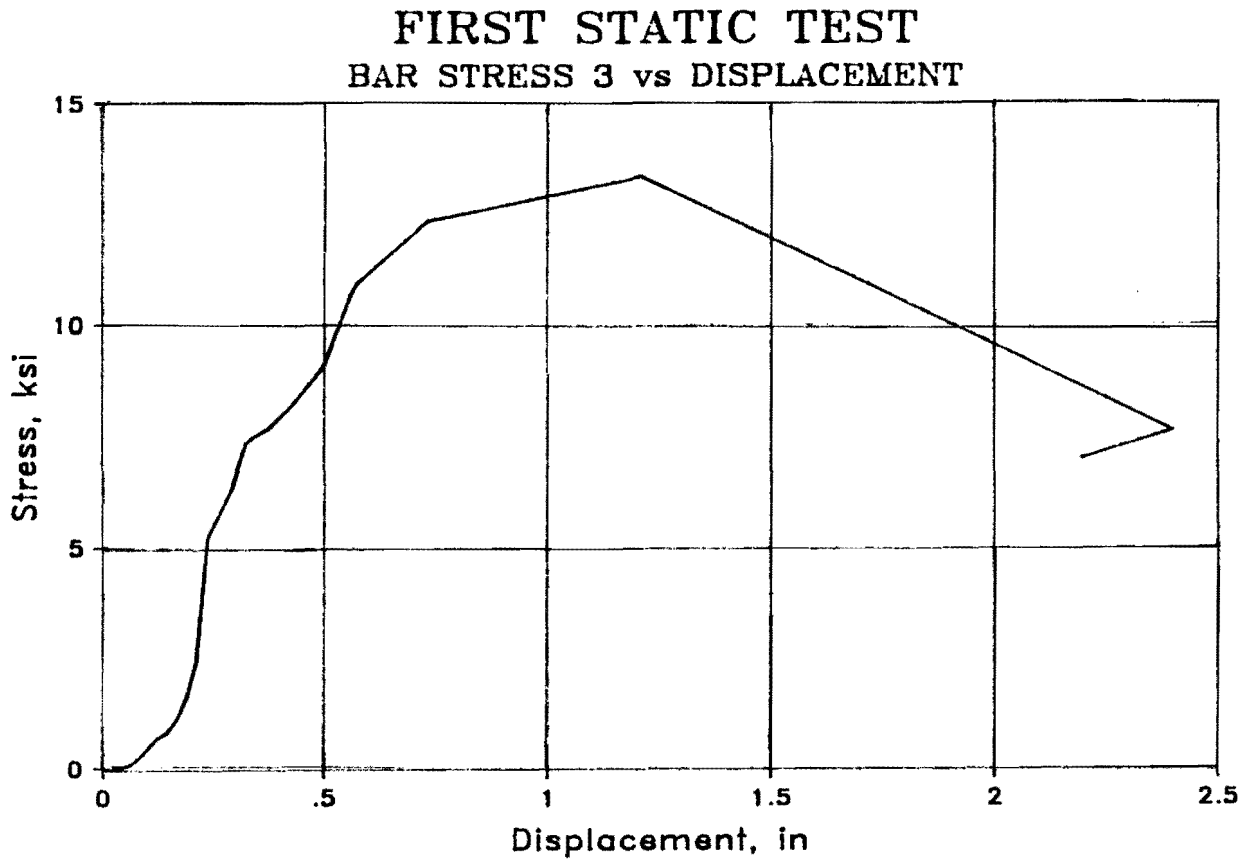

Fig. 5.6 Bar stress 3 vs. post displacement, first static test (see Table 5.1)

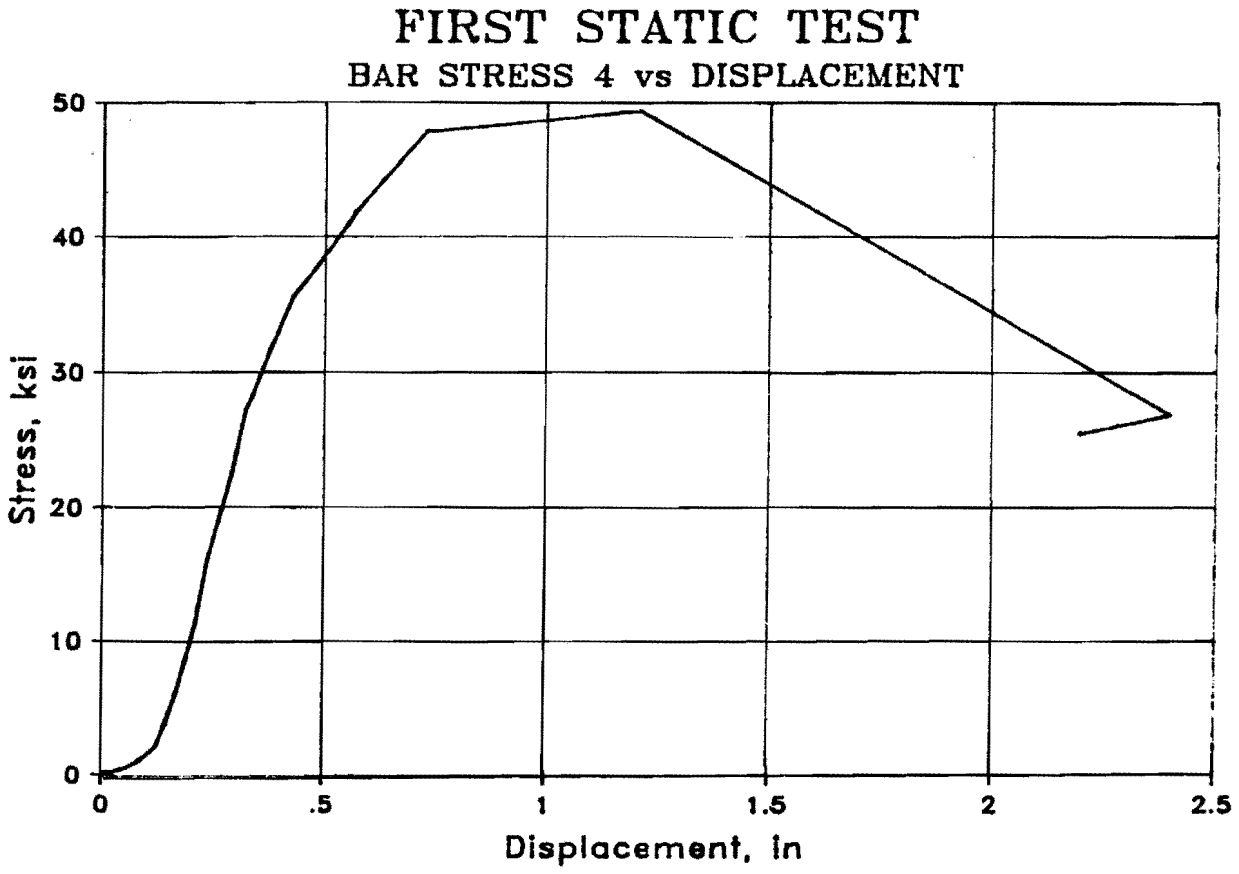

Fig. 5.7 Bar stress 4 vs. post displacement, first static test (see Table 5.1)

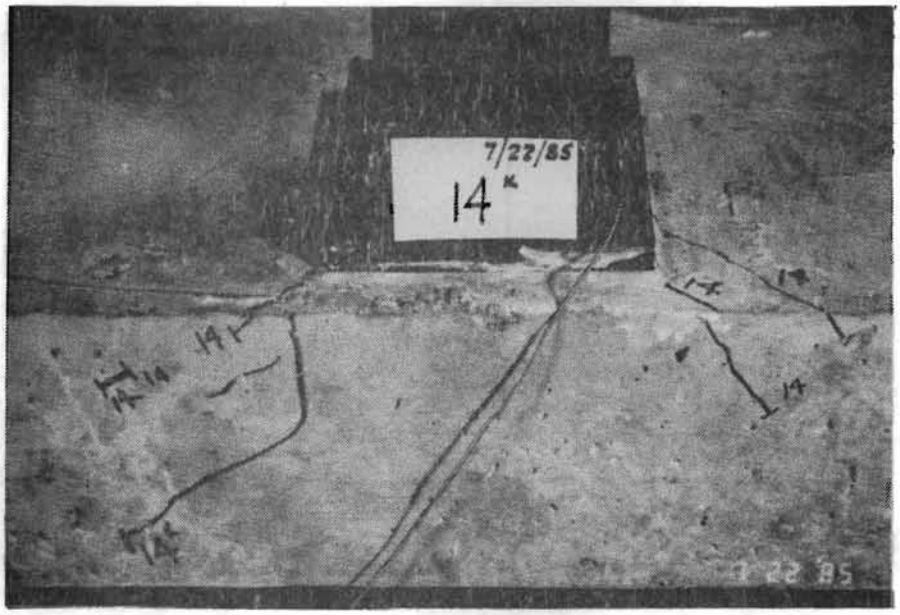

Fig. 5.8 Initial diagonal cracking at center post location

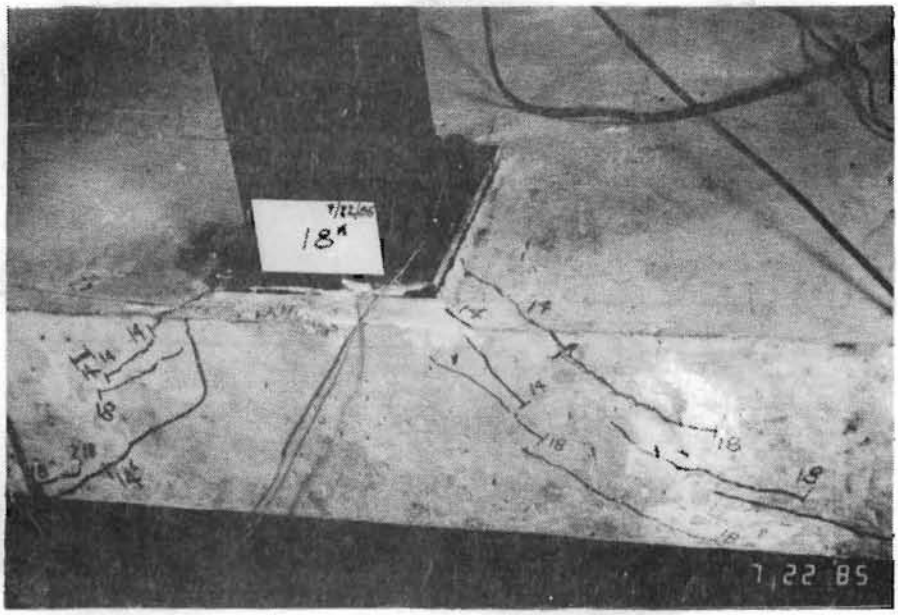

Fig. 5.9 Diagonal cracking at center post location

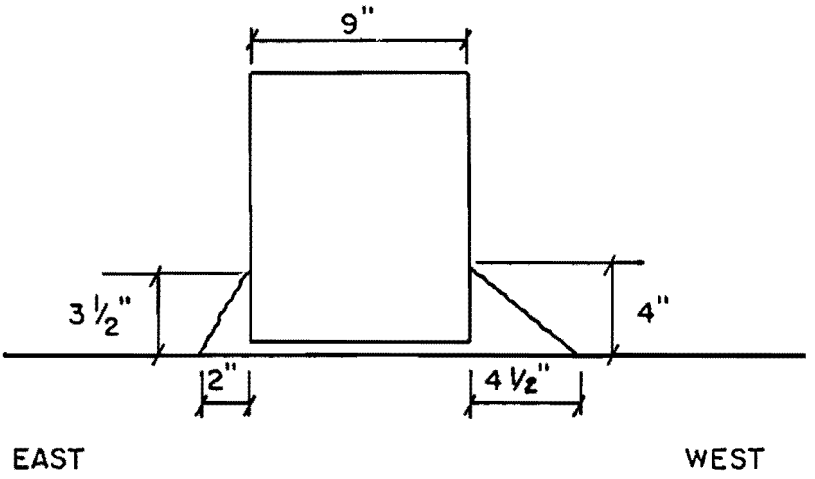

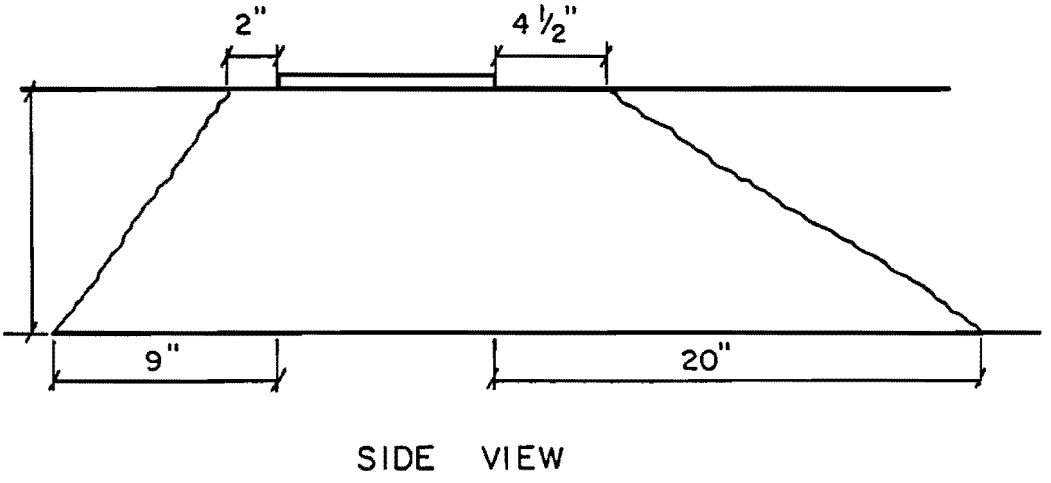

Fig. 5.10 Cracking pattern at center post

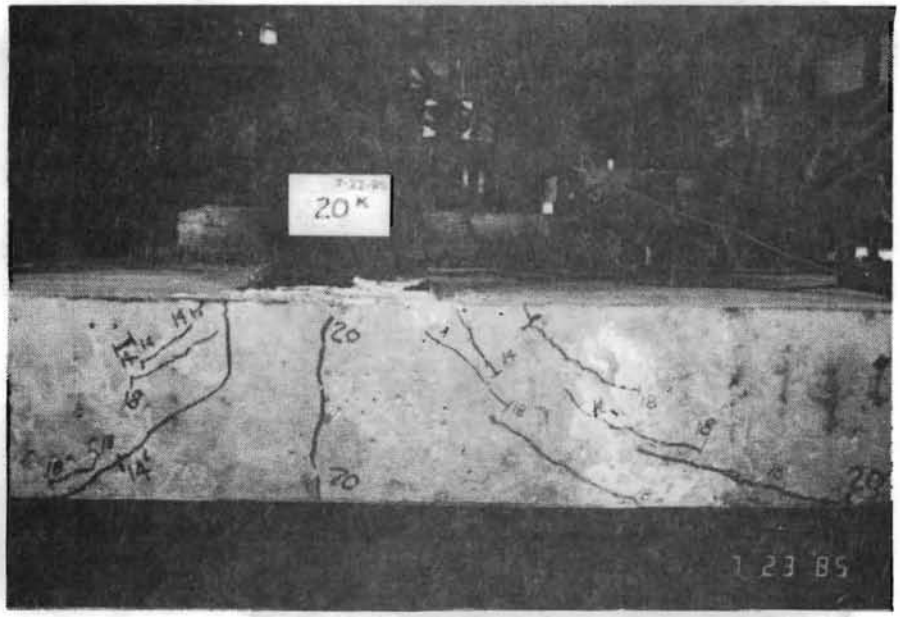

Fig. 5.11 Development of vertical crack under center post

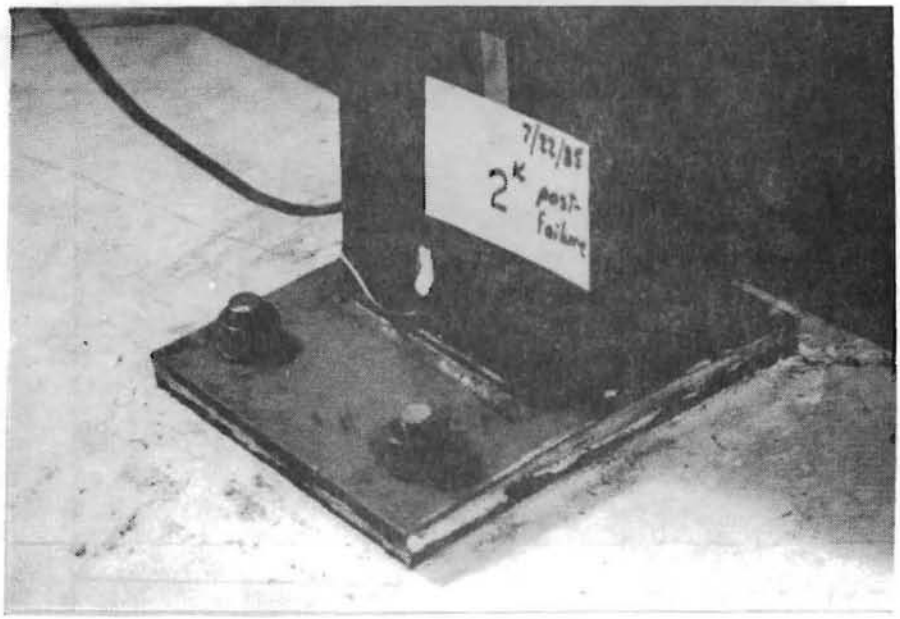

Fig. 5.12 Center post after weld failure

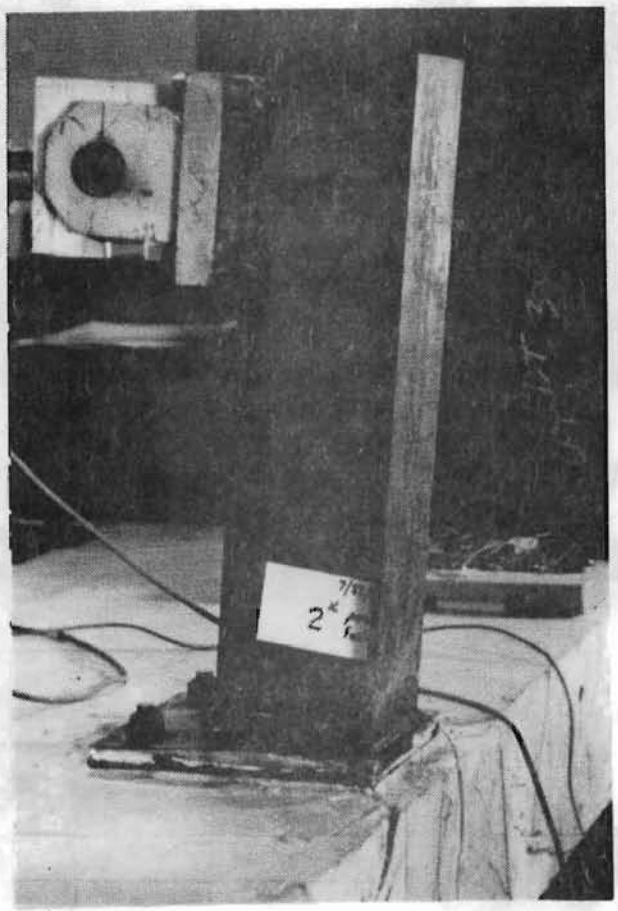

Fig. 5.13 Large diagonal cracks at center post location

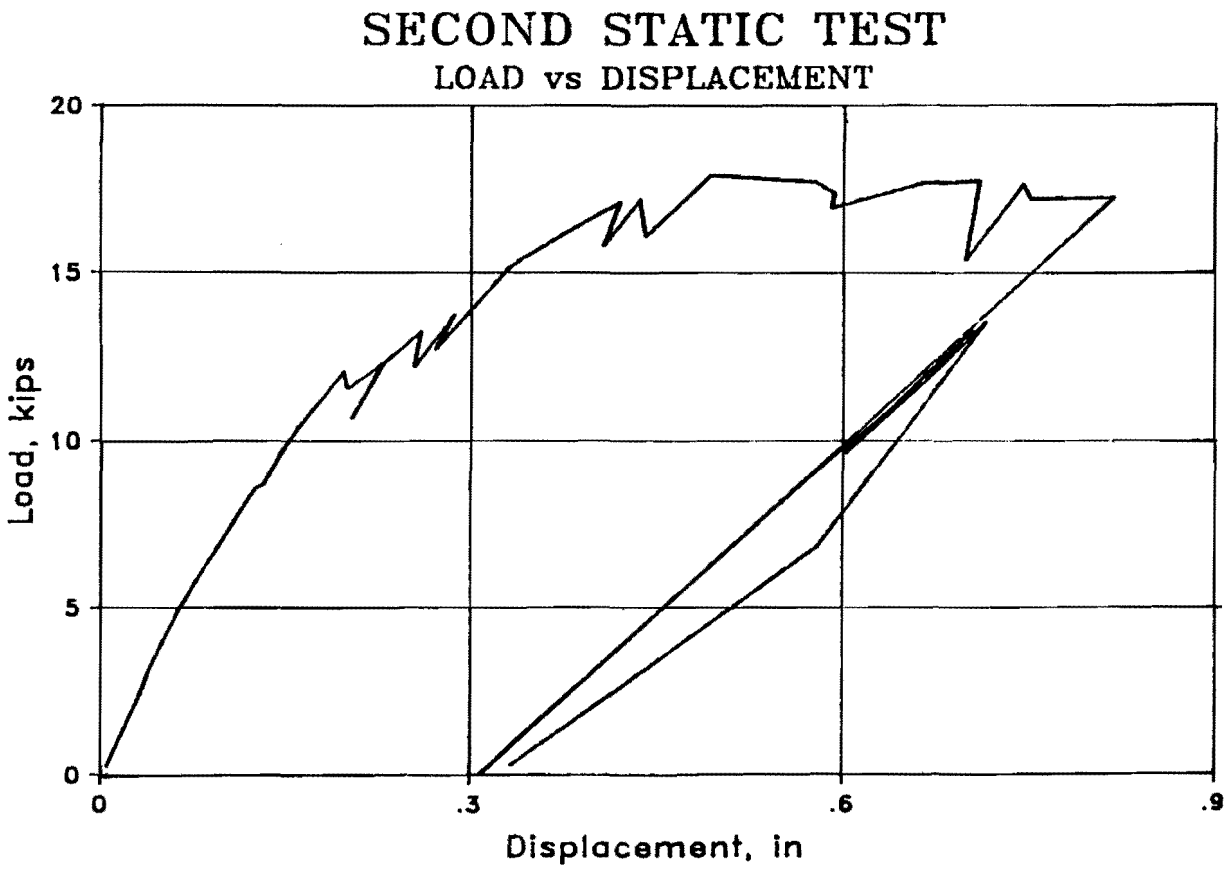

Fig. 5.14 Applied load vs. displacement, second static test

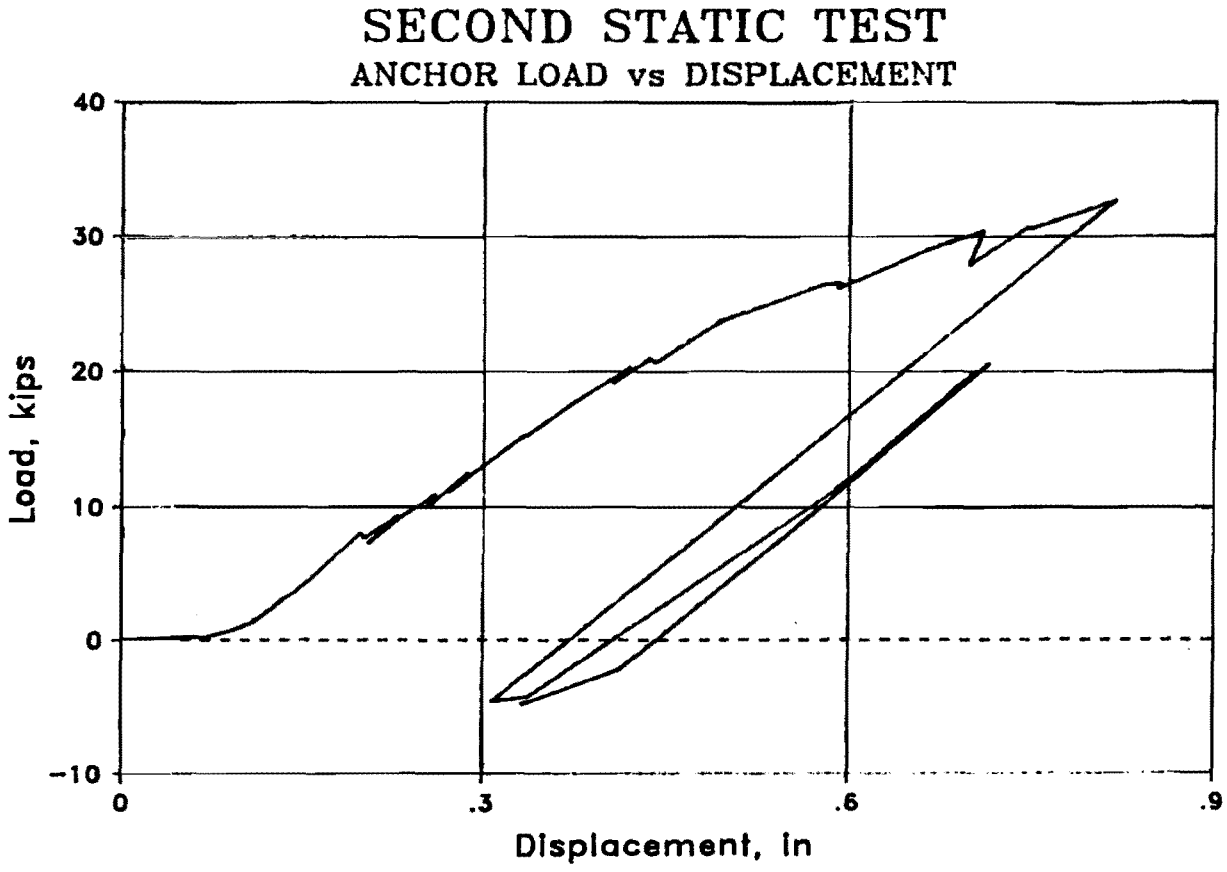

Fig. 5.15 Anchor load vs. post displacement, second static test

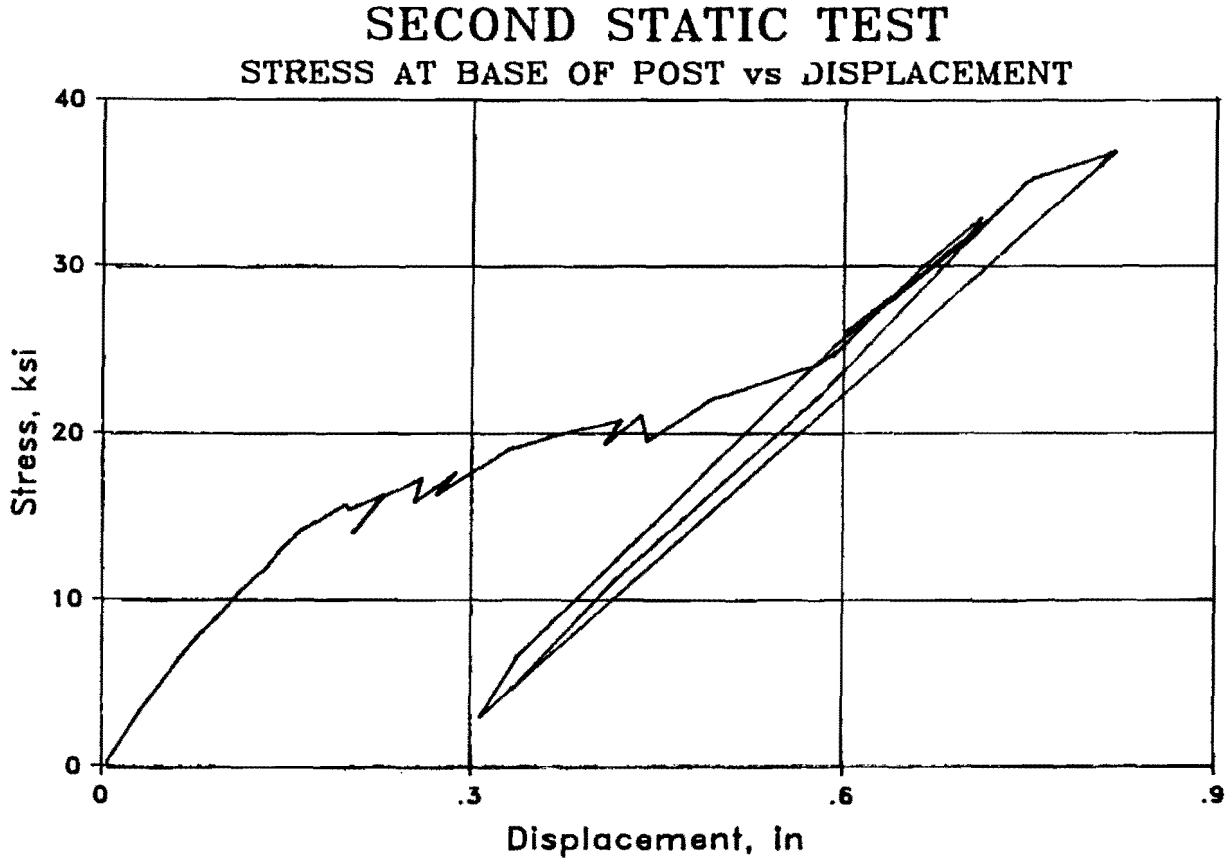

Fig. 5.16 Stress at base of post vs. post displacement, second static test

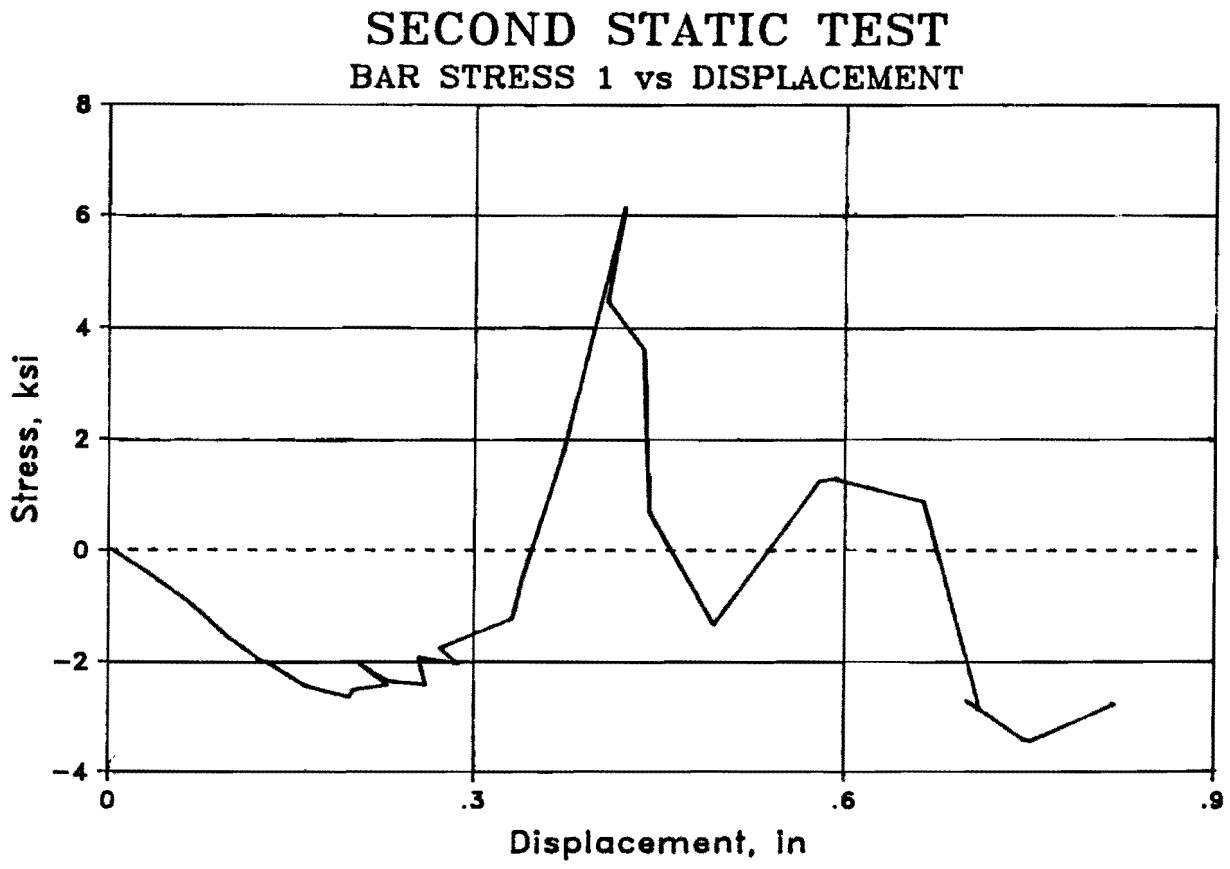

Fig. 5.17 Bar stress 1 vs. post displacement, second static test (see Table 5.1)

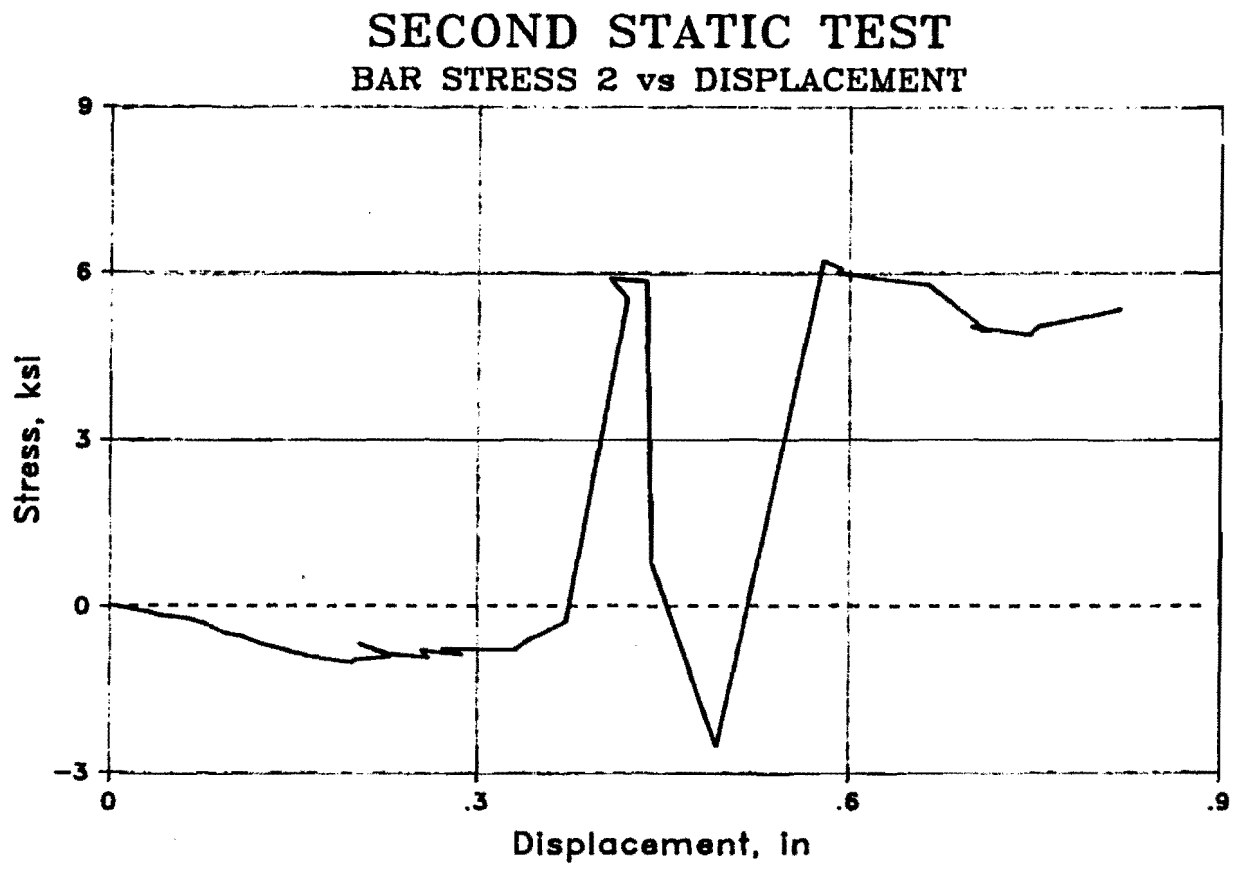

Fig. 5.18 Bar stress 2 vs. post displacement, second static test (see Table 5.1)

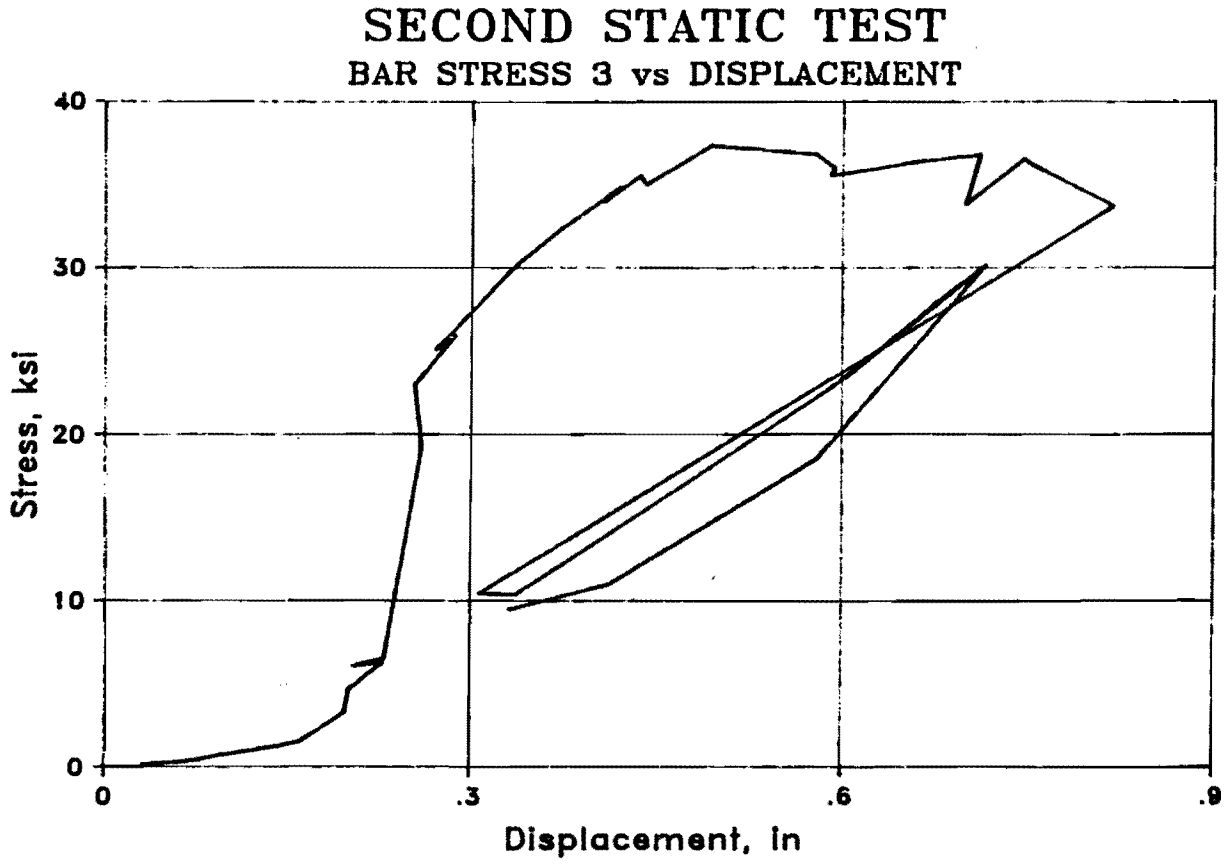

Fig. 5.19 Bar stress 3 vs. post displacement, second static test (see Table 5.1)

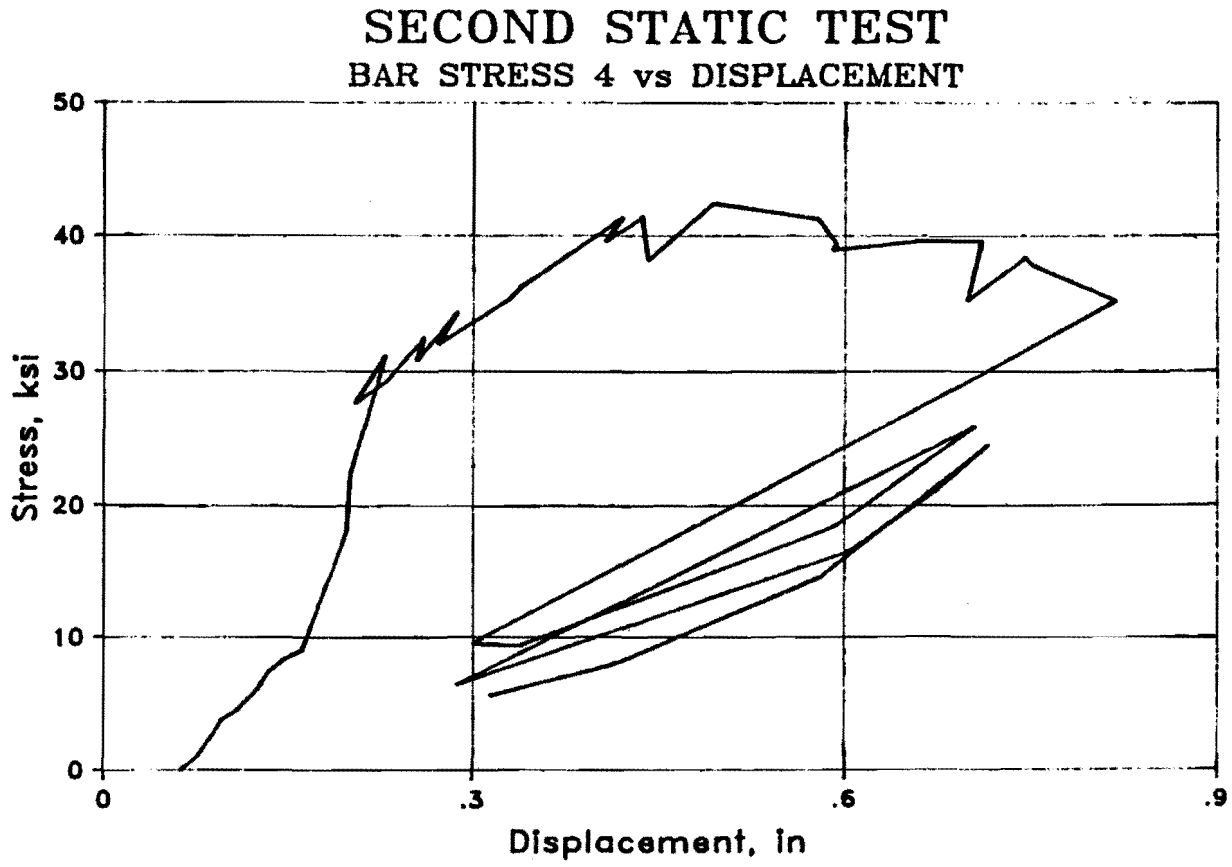

Fig. 5.20 Bar stress 4 vs. post displacement, second static test (see Table 5.1)

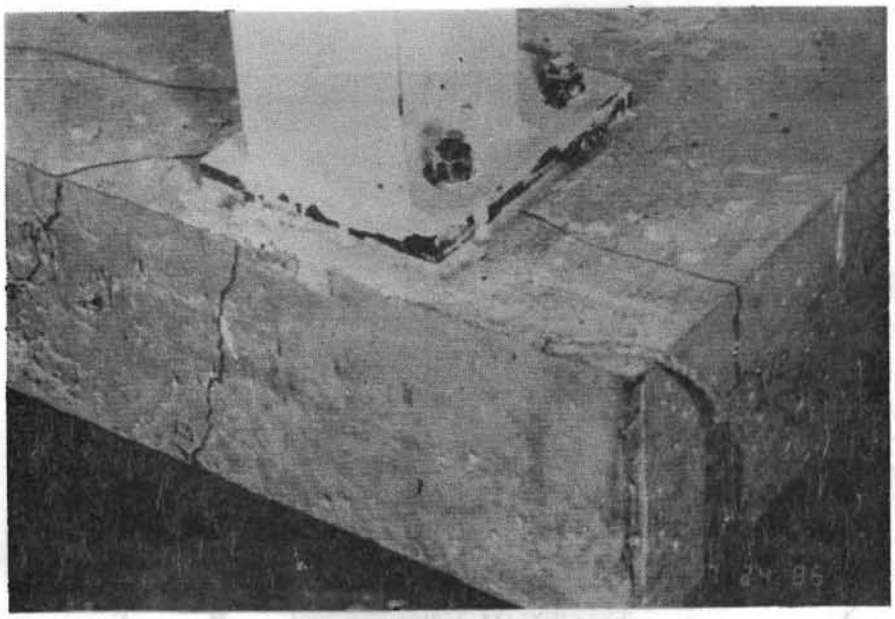

Fig. 5.21 Initial cracking at west-end post location

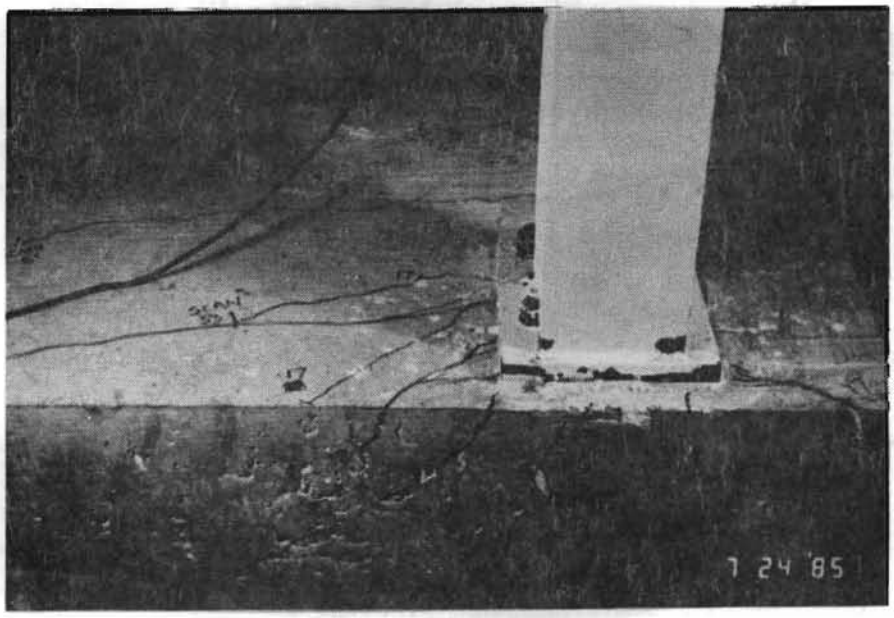

Fig. 5.22 Cracking near tension bolts of west-end post

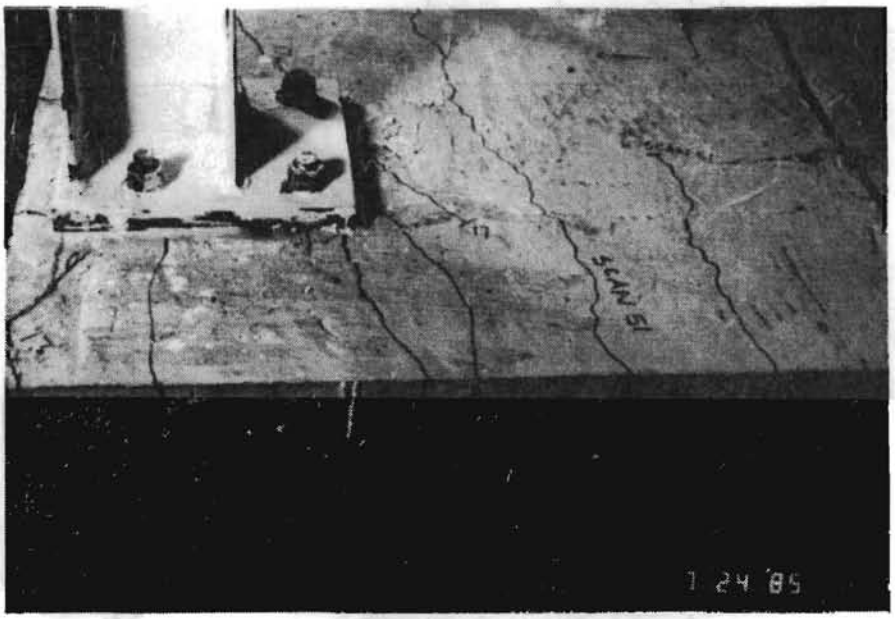

Fig. 5.23 Flexural cracking behind west-end base plate

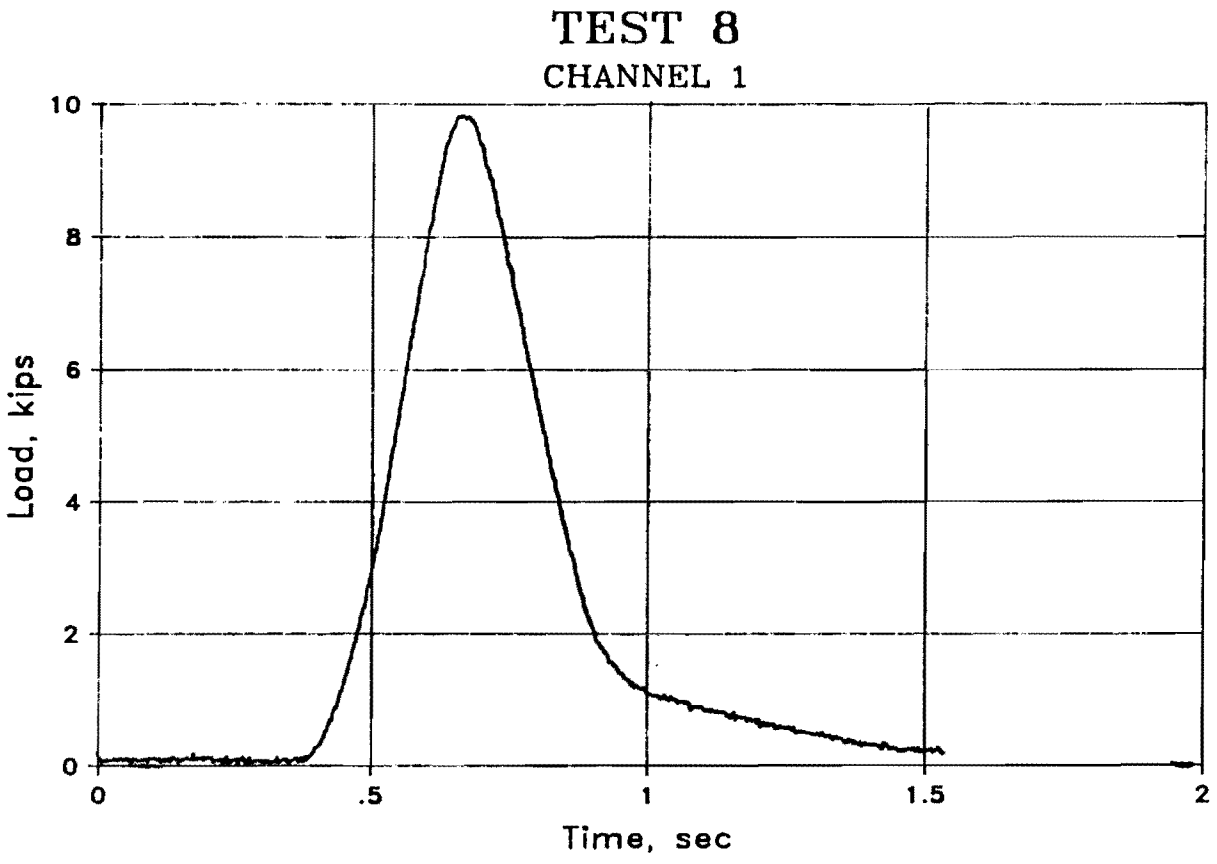

Fig. 5.24 Applied load vs. time, impact test on west-end post (Test 8)

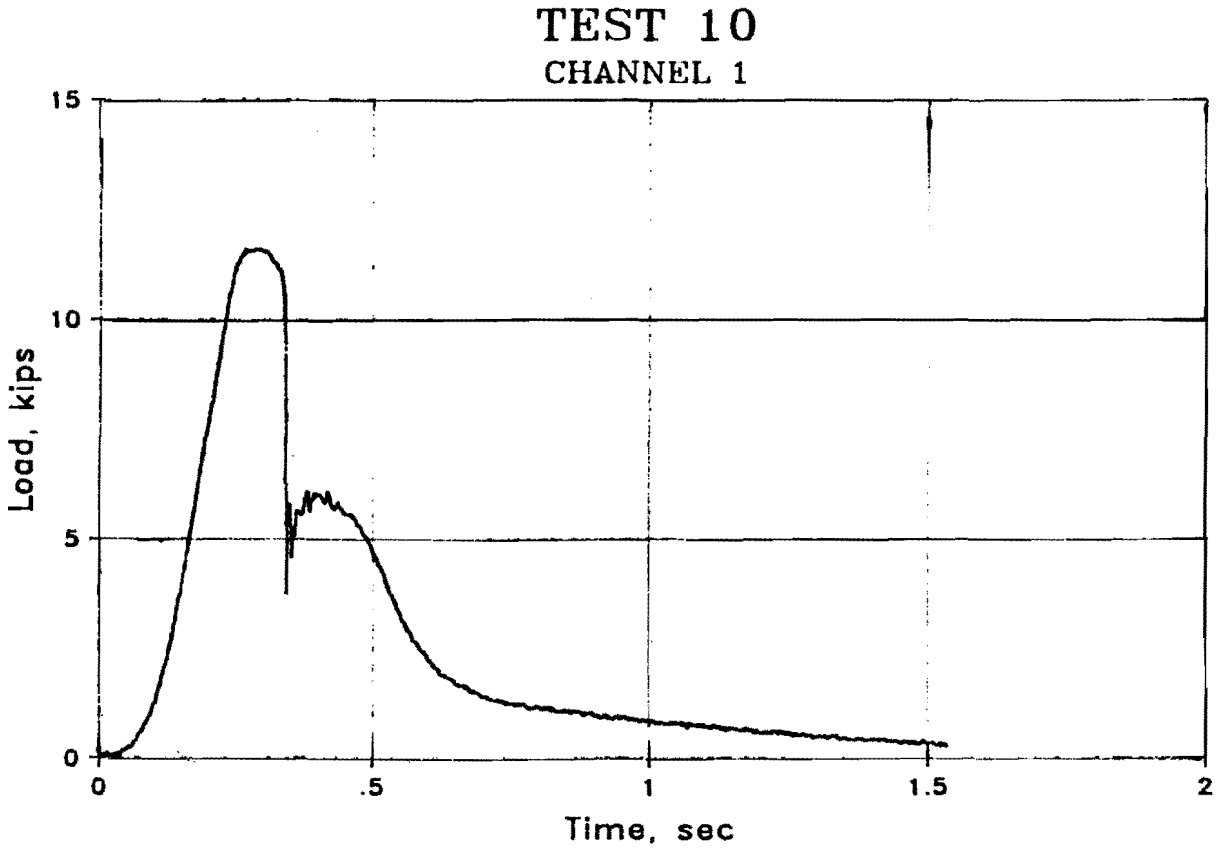

Fig. 5.25 Applied load vs. time, impact test on west-end post (Test 10)

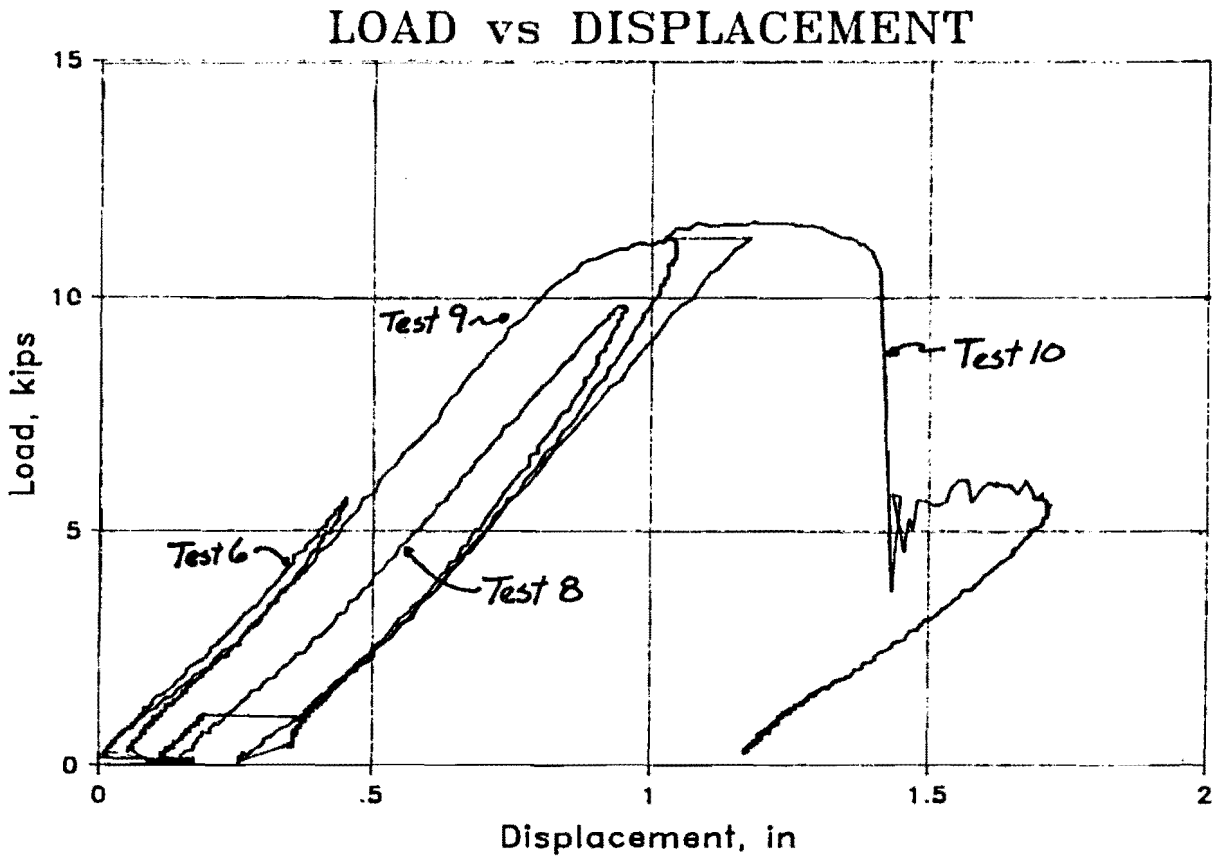

Fig. 5.26 Applied load vs. post displacement, impact tests on west-end post (Tests 6, 8, 9, 10)

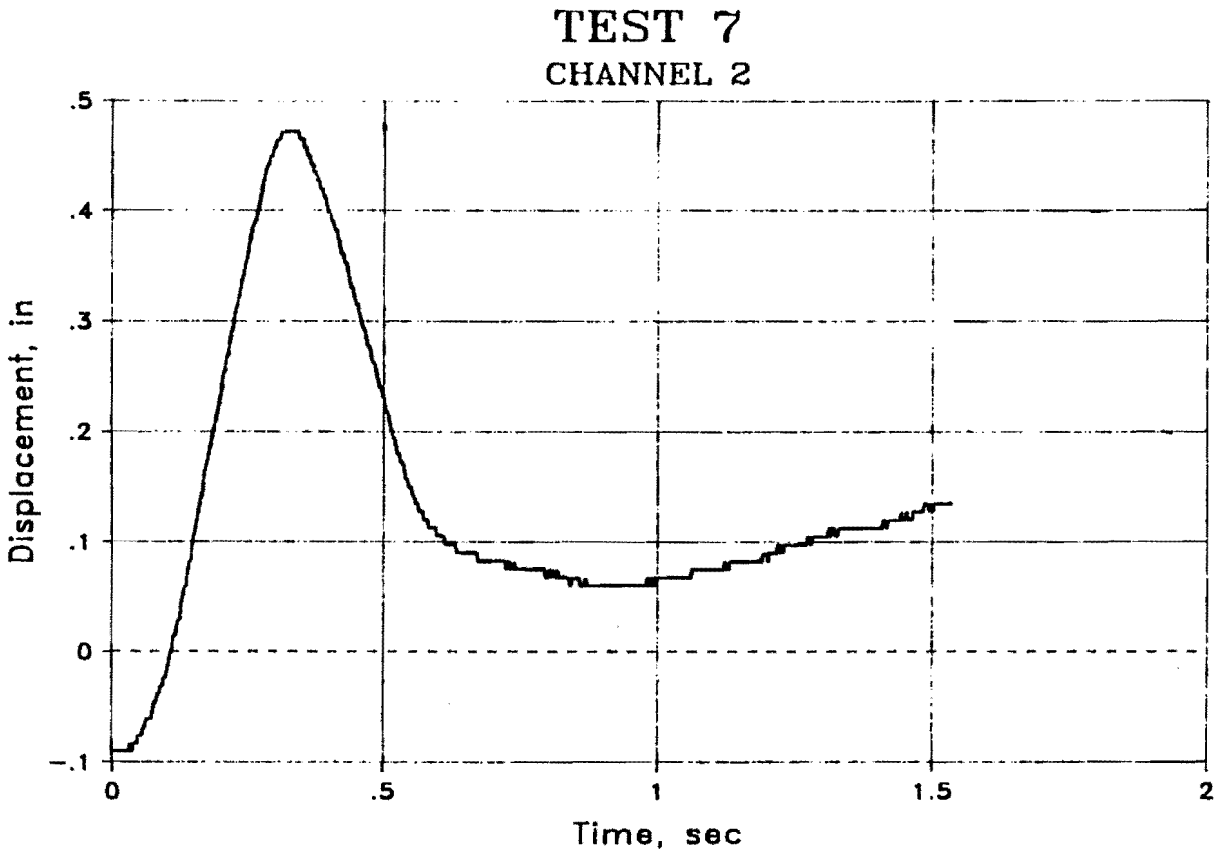

Fig. 5.27 Post displacement vs. time, impact test on west-end post (Test 7)

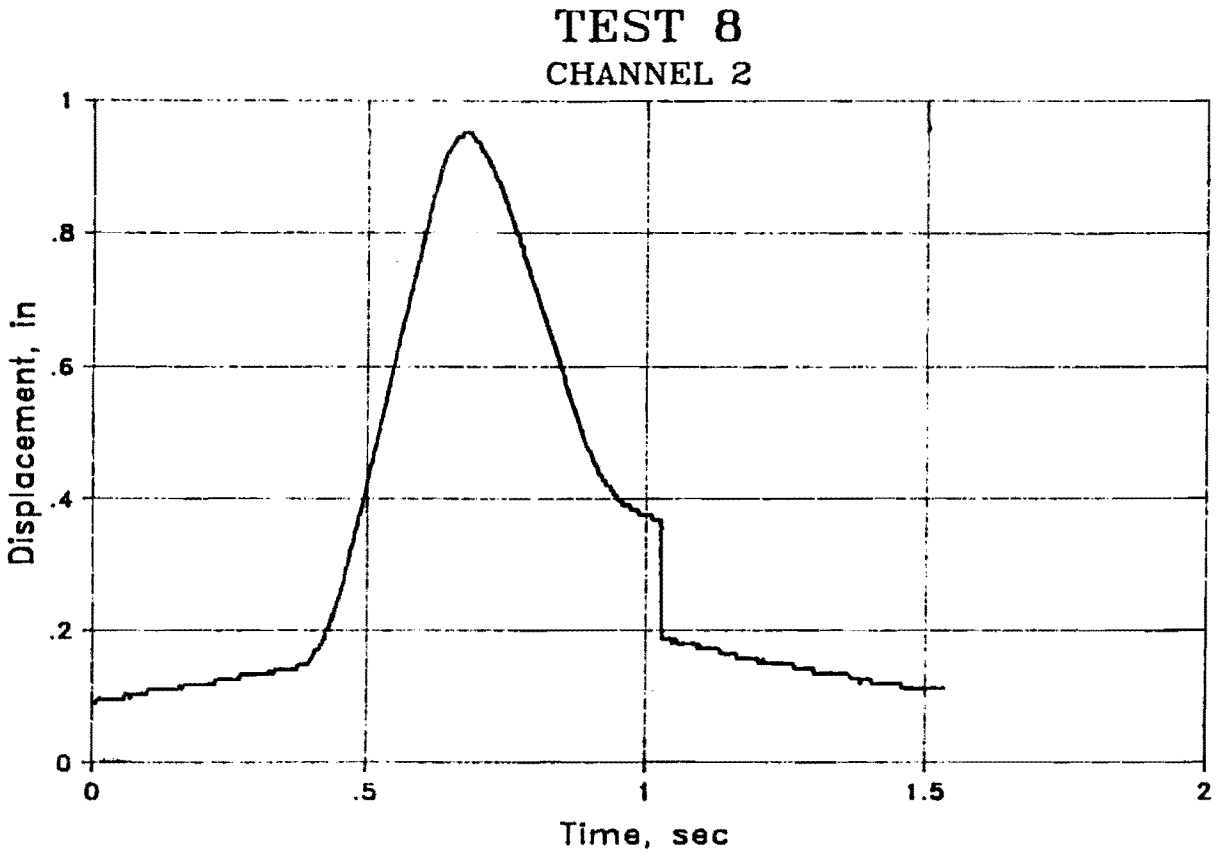

Fig. 5.28 Post displacement vs. time, impact test on west-end post (Test 8)

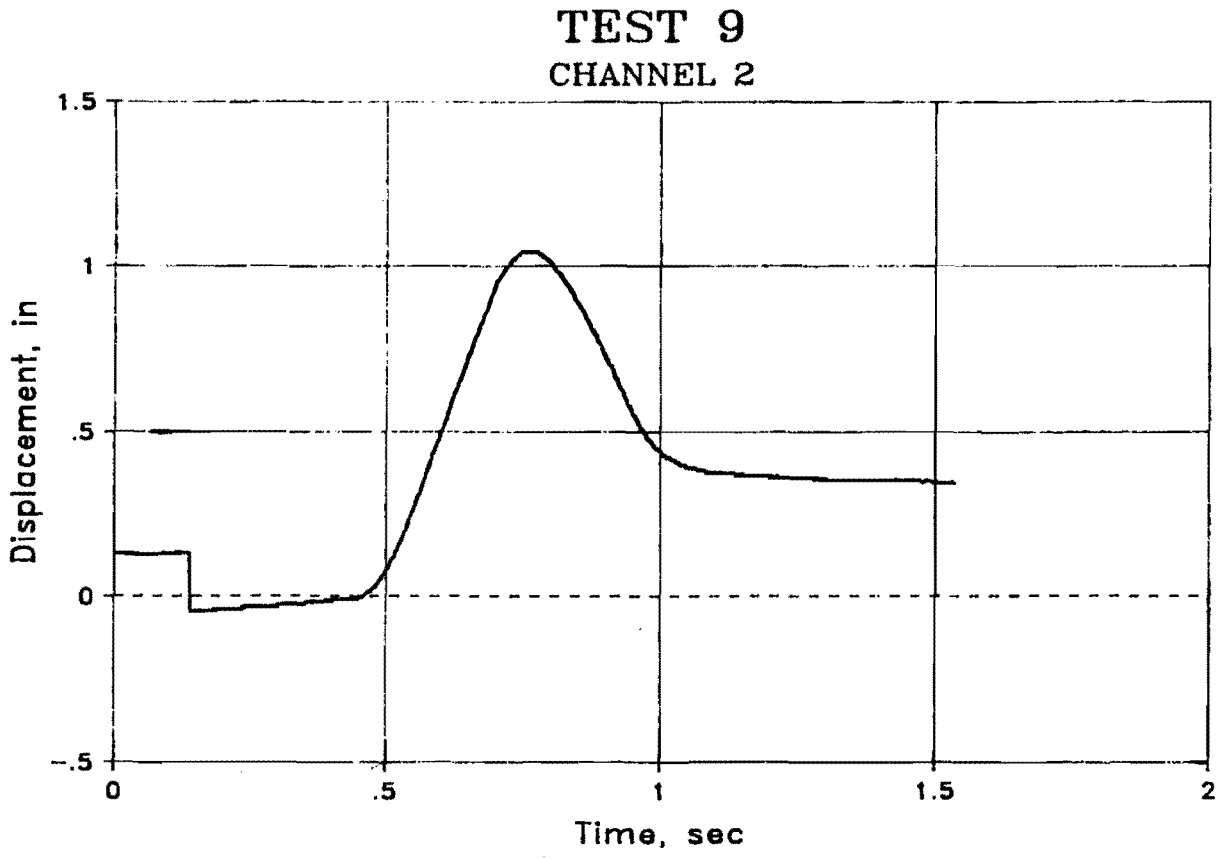

Fig. 5.29 Post displacement vs. time, impact test on west-end post (Test 9)

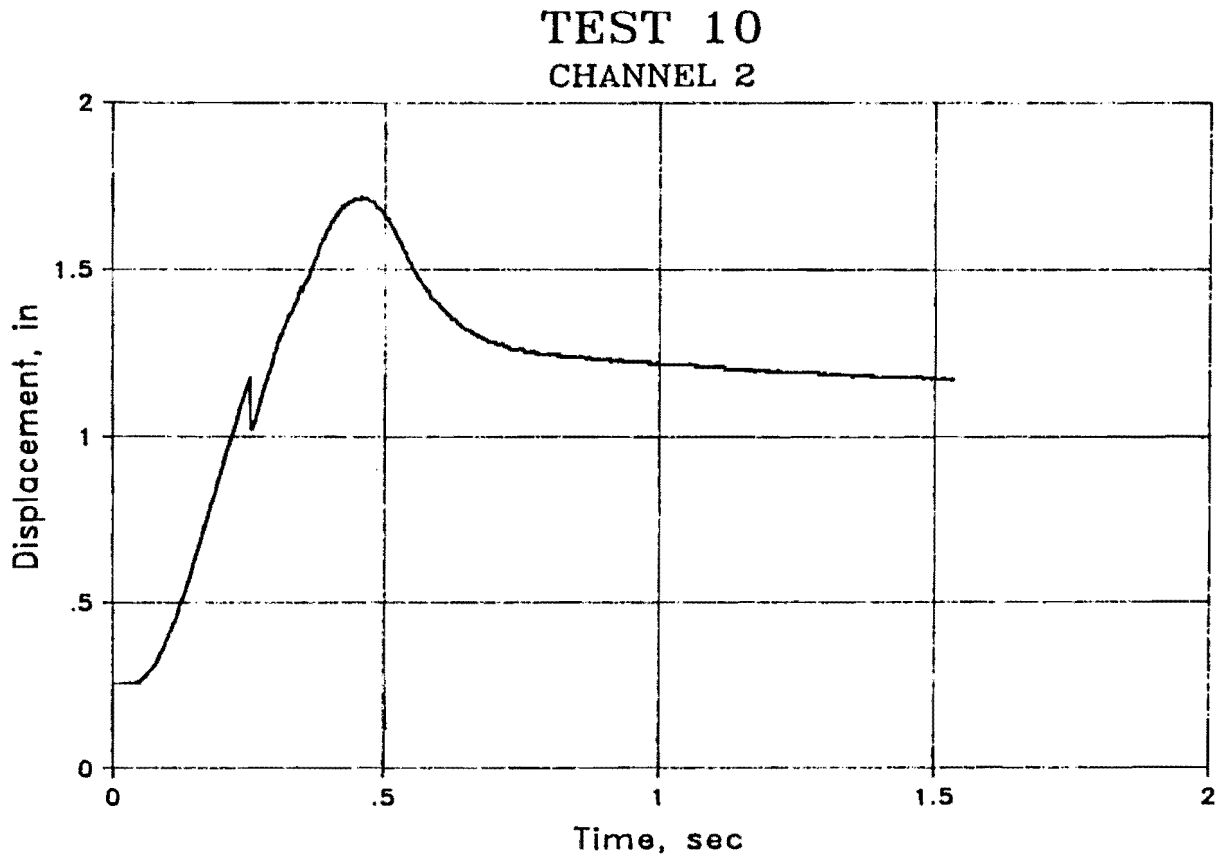

Fig. 5.30 Post displacement vs. time, impact test on west-end post (Test 10)

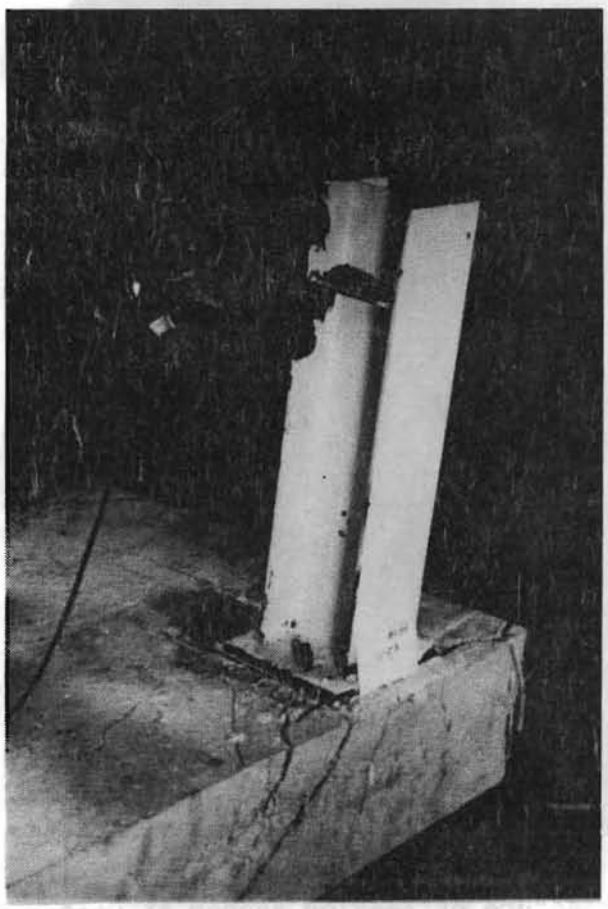

Fig. 5.31 Widening of cracks at west-end post location

Fig. 5.32 Fracture of tension anchor at west-end post

Fig. 5.33 Fractured tension anchor at west-end post

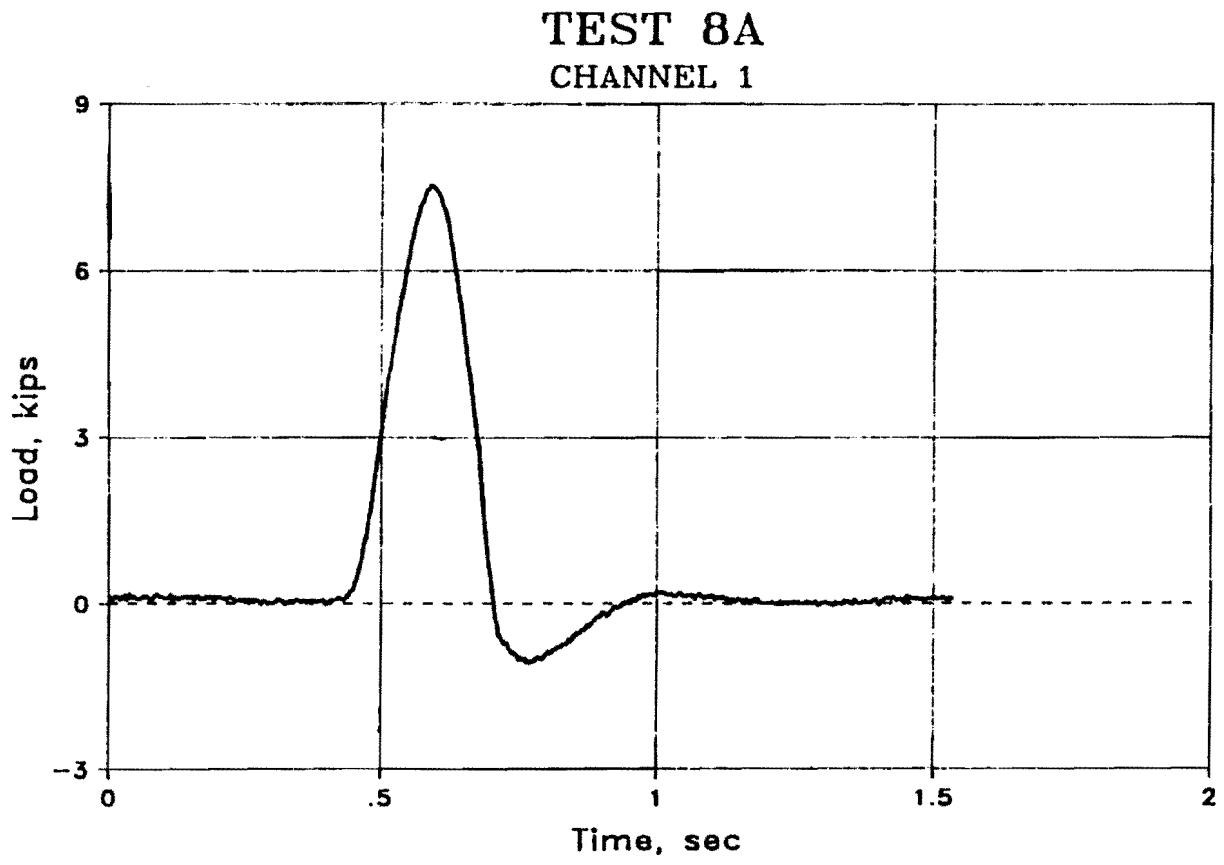

Fig. 5.34 Applied load vs. time, impact test on east-end post (Test 8A)

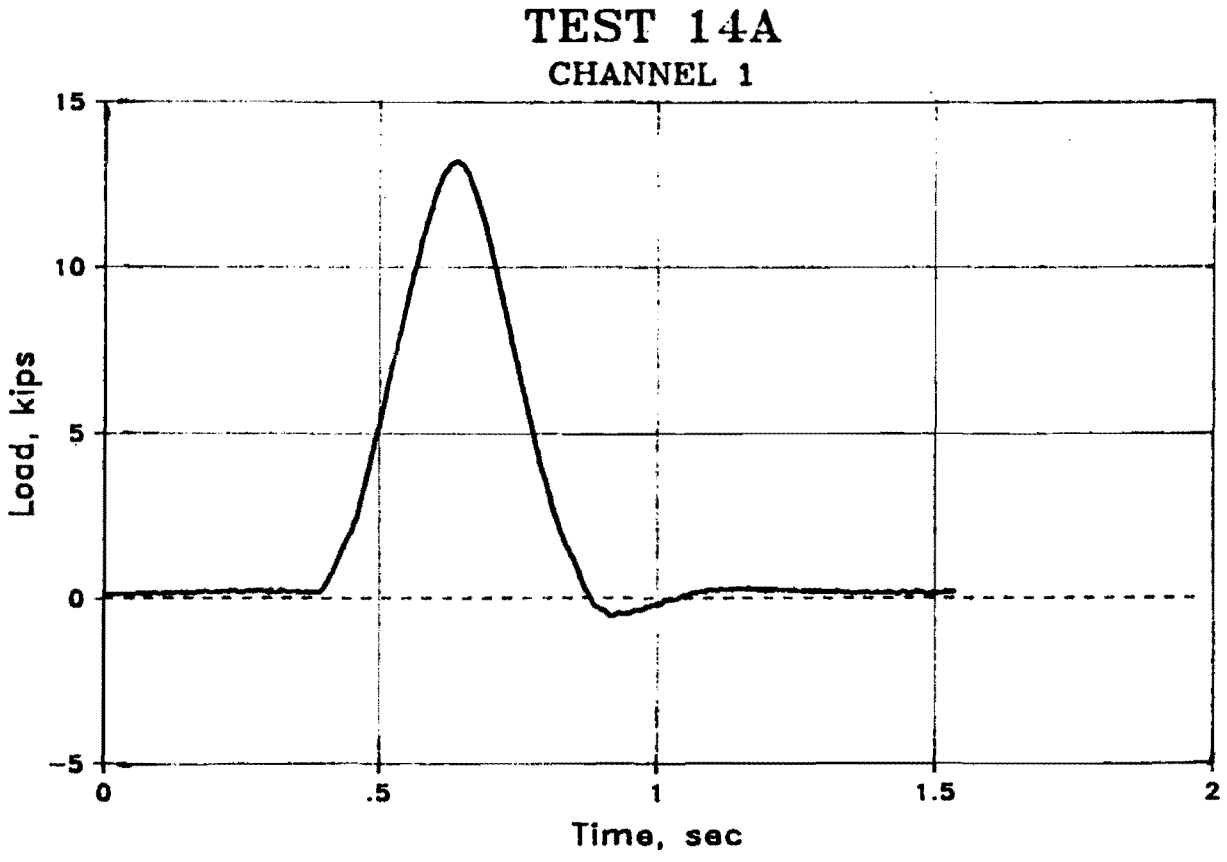

Fig. 5.35 Applied load vs. time, impact test on east-end post (Test 14A)

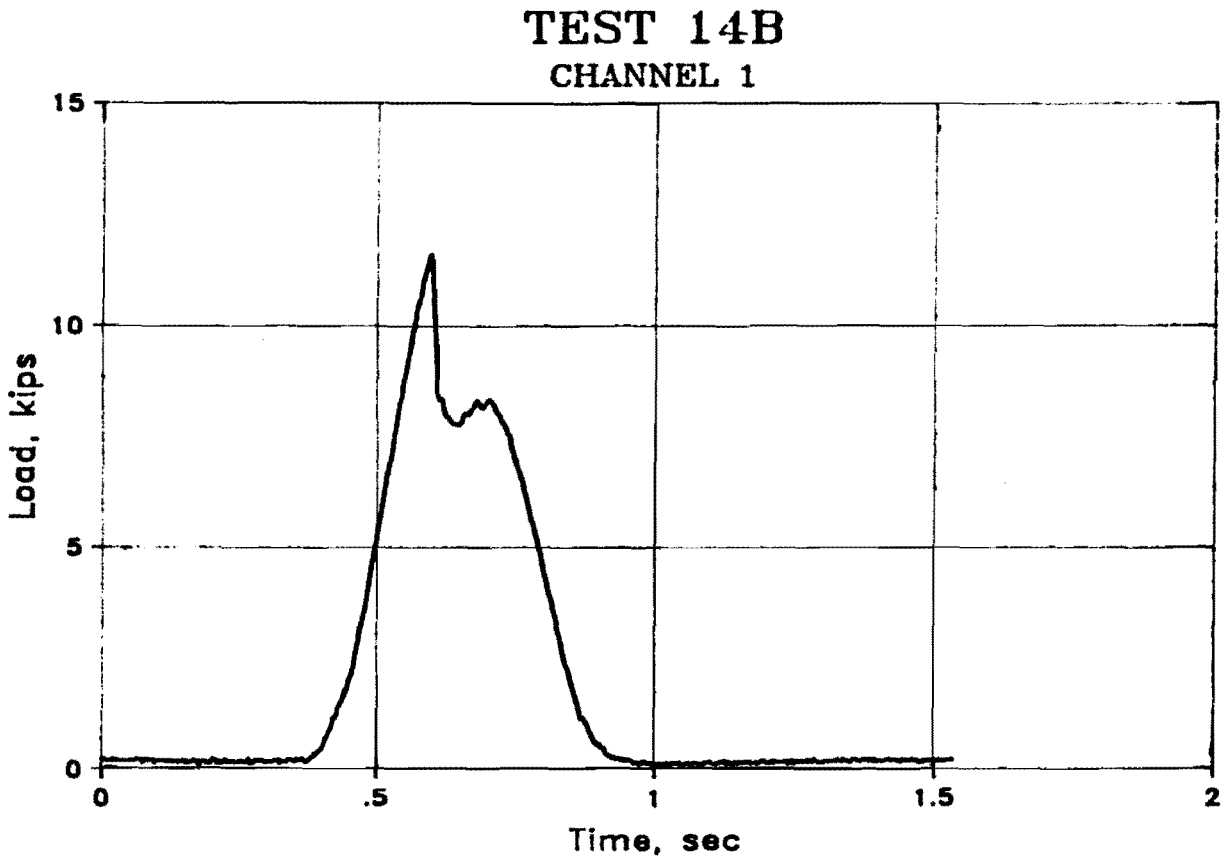

Fig. 5.36 Applied load vs. time, impact test on east-end post (Test 14B)

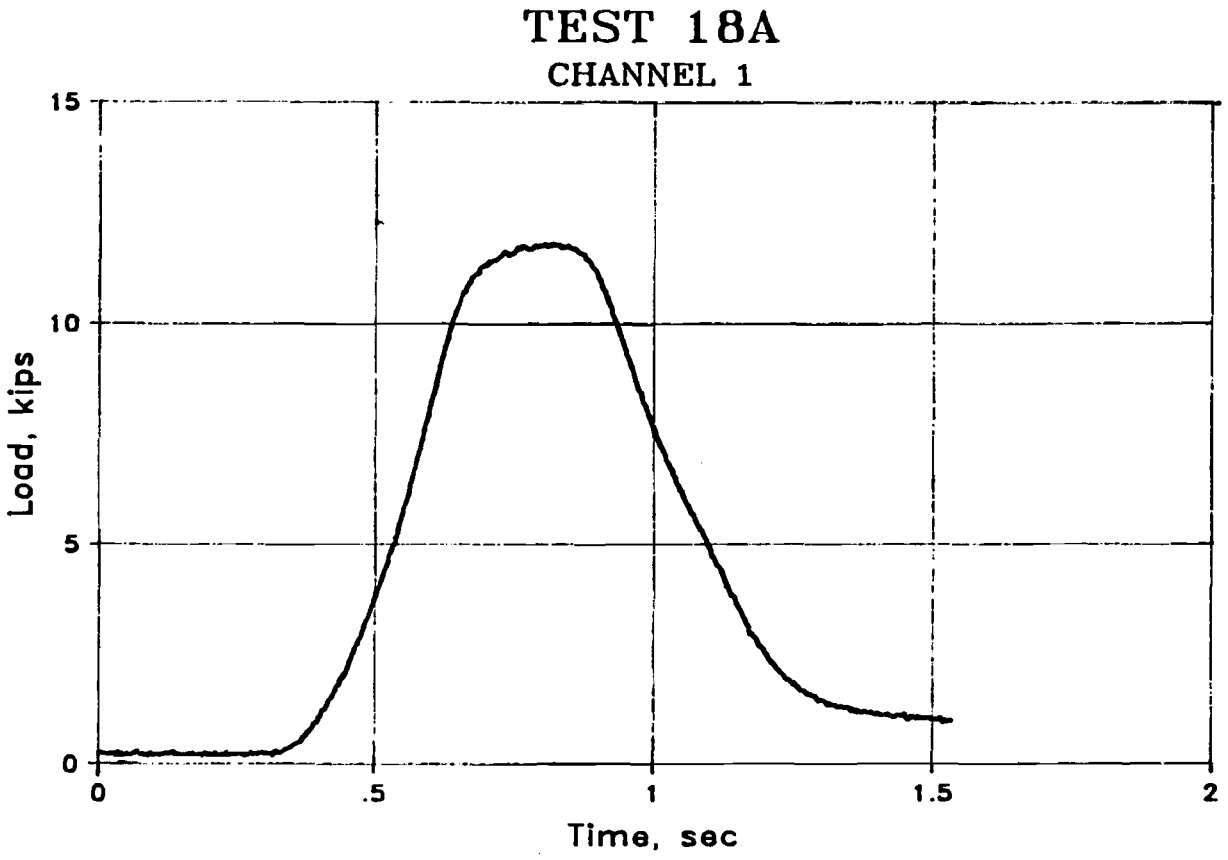

Fig. 5.37 Applied load vs. time, impact test on east-end post (Test 18A)

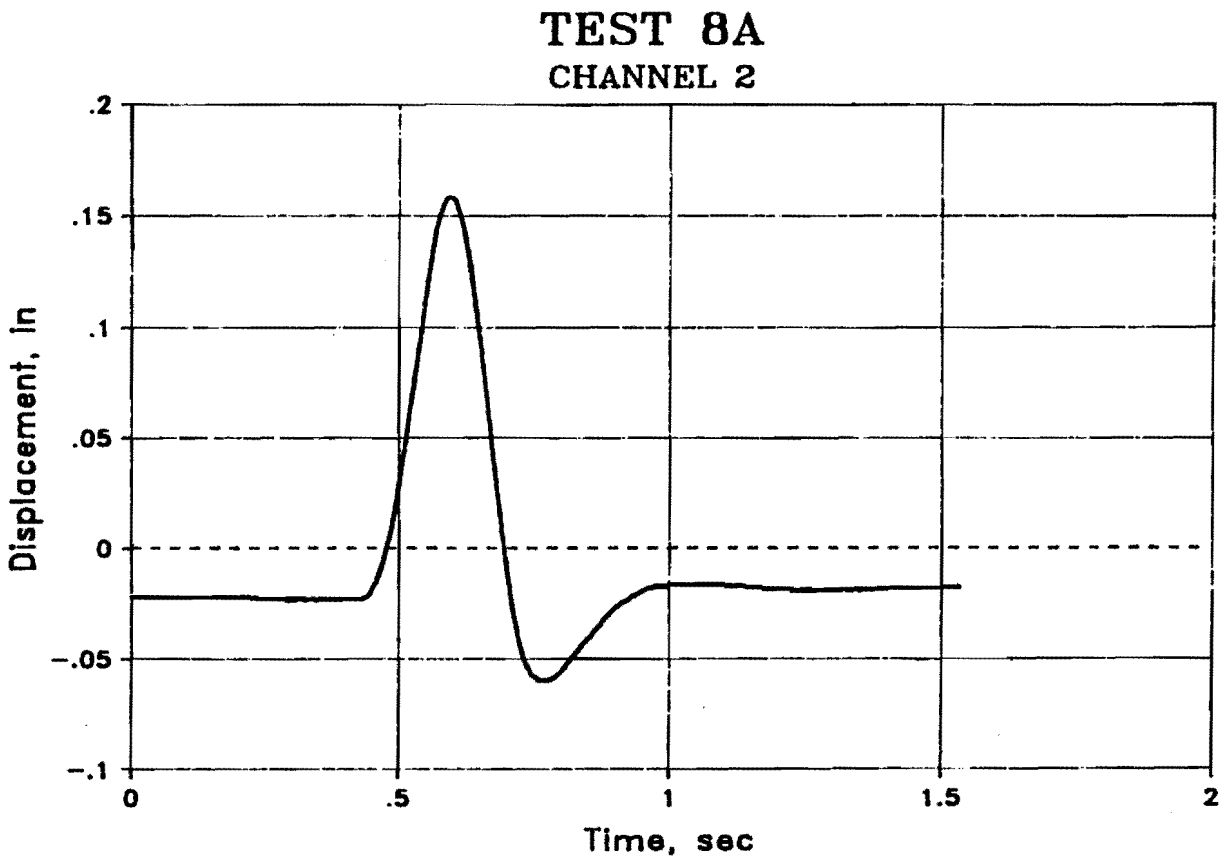

Fig. 5.38 Post displacement vs. time, impact test on east-end post (Test 8A)

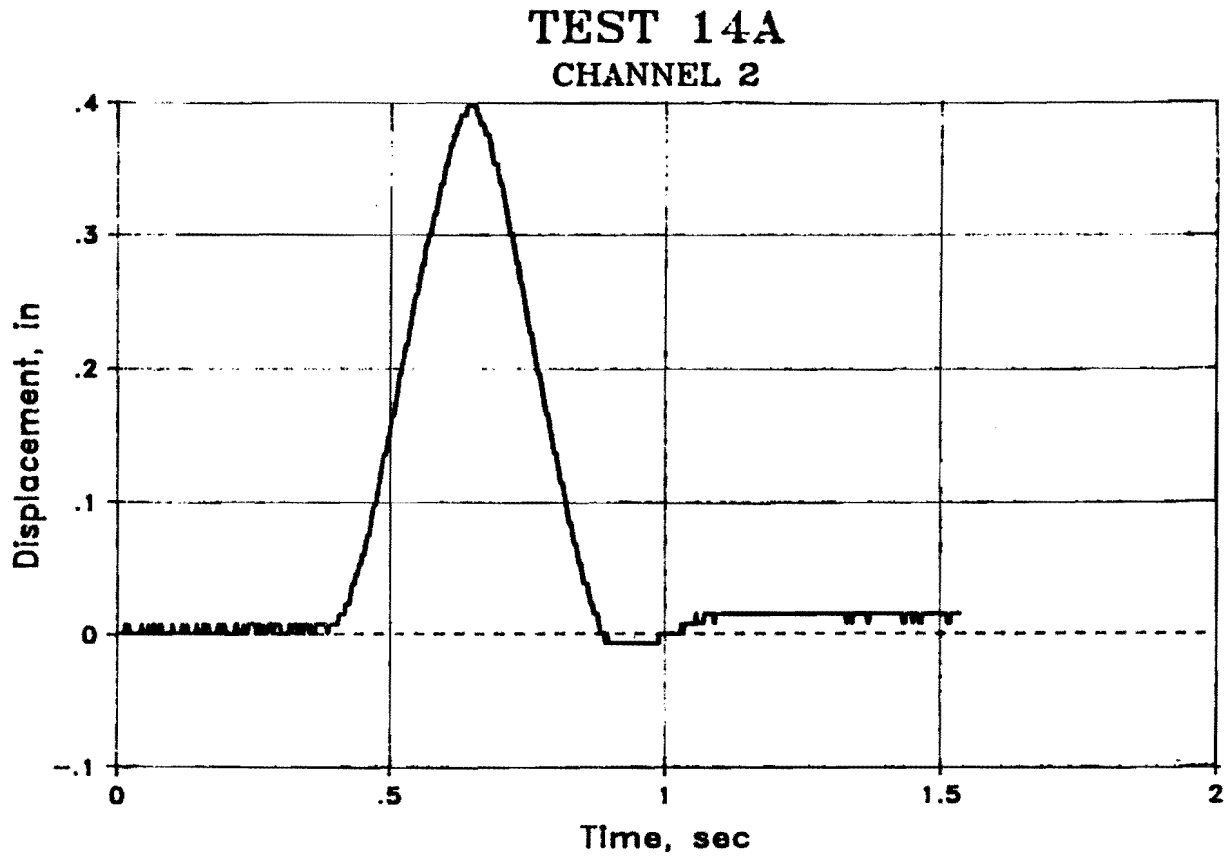

Fig. 5.39 Post displacement vs. time, impact test on east-end post (Test 14A)

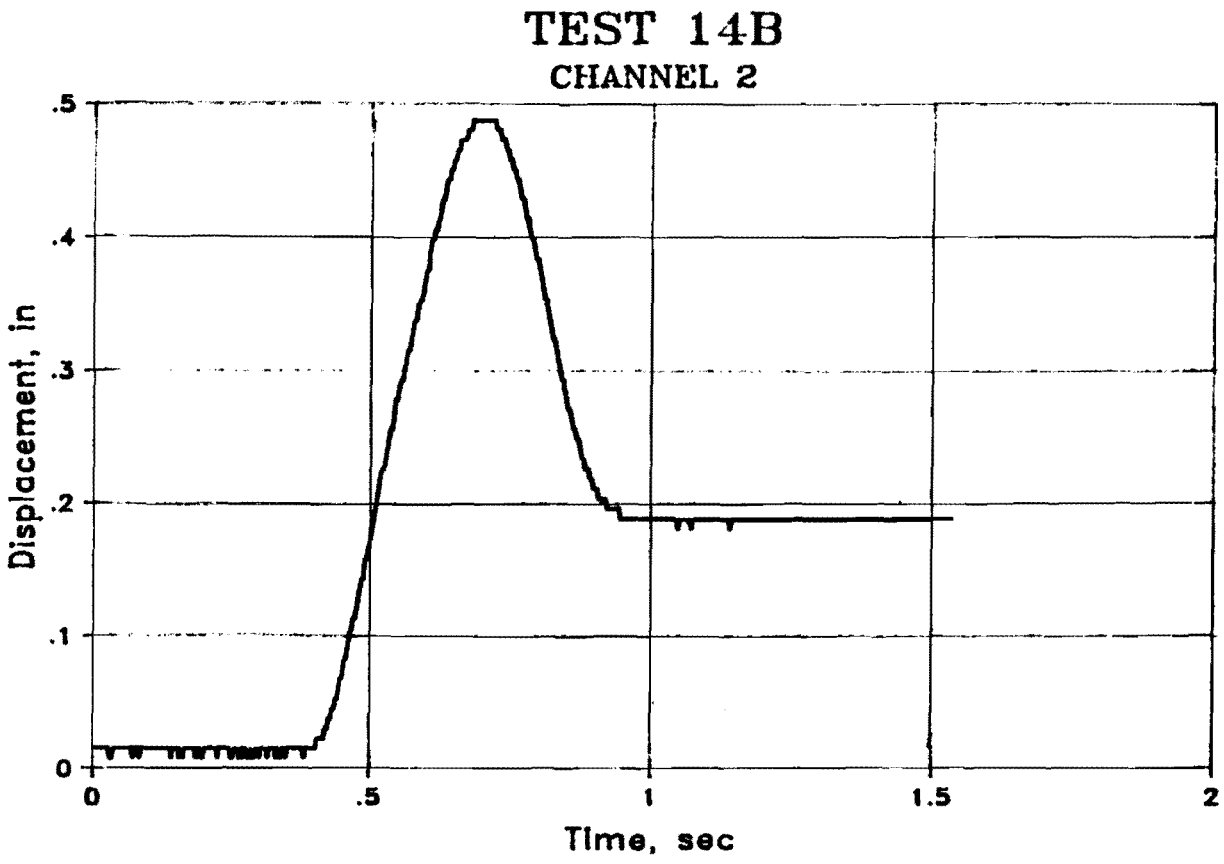

Fig. 5.40 Post displacement vs. time, impact test on east-end post (Test 14B)

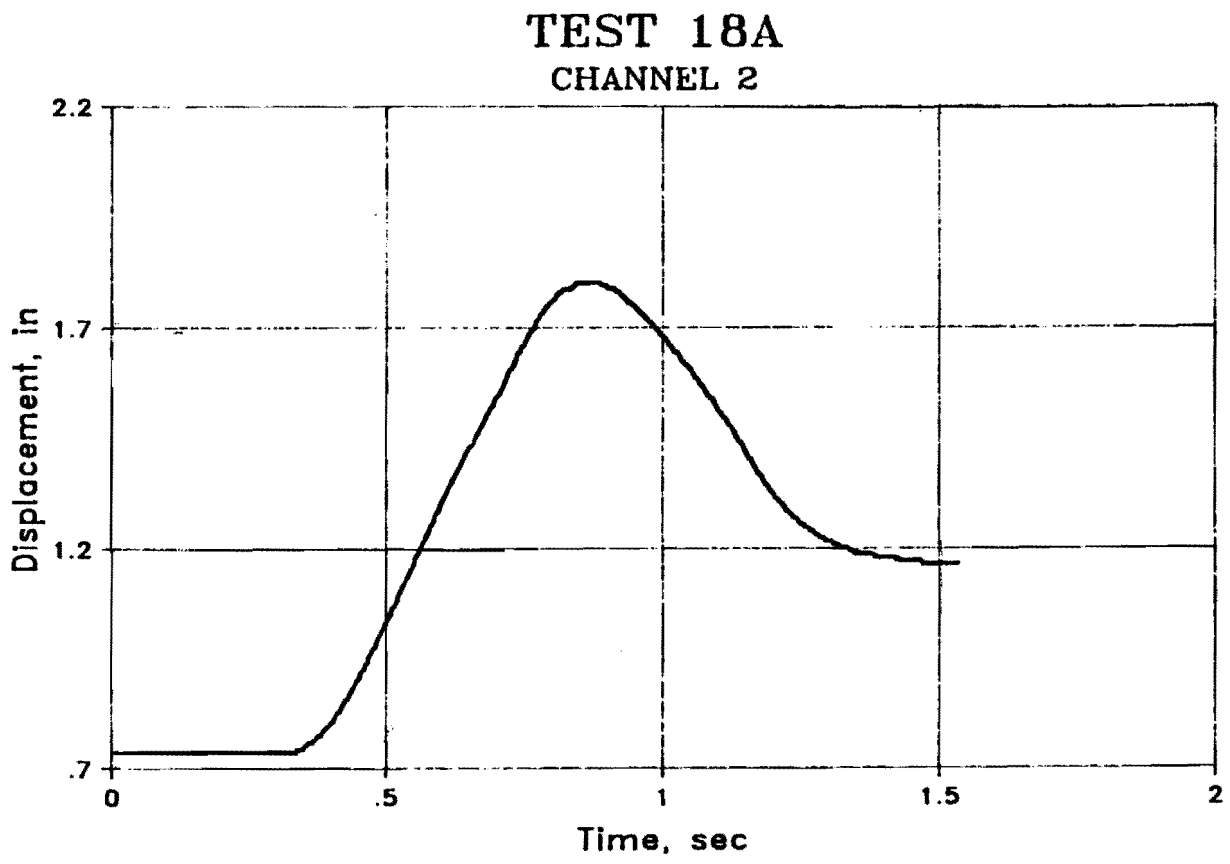

Fig. 5.41 Post displacement vs. time, impact test on east-end post (Test 18A)

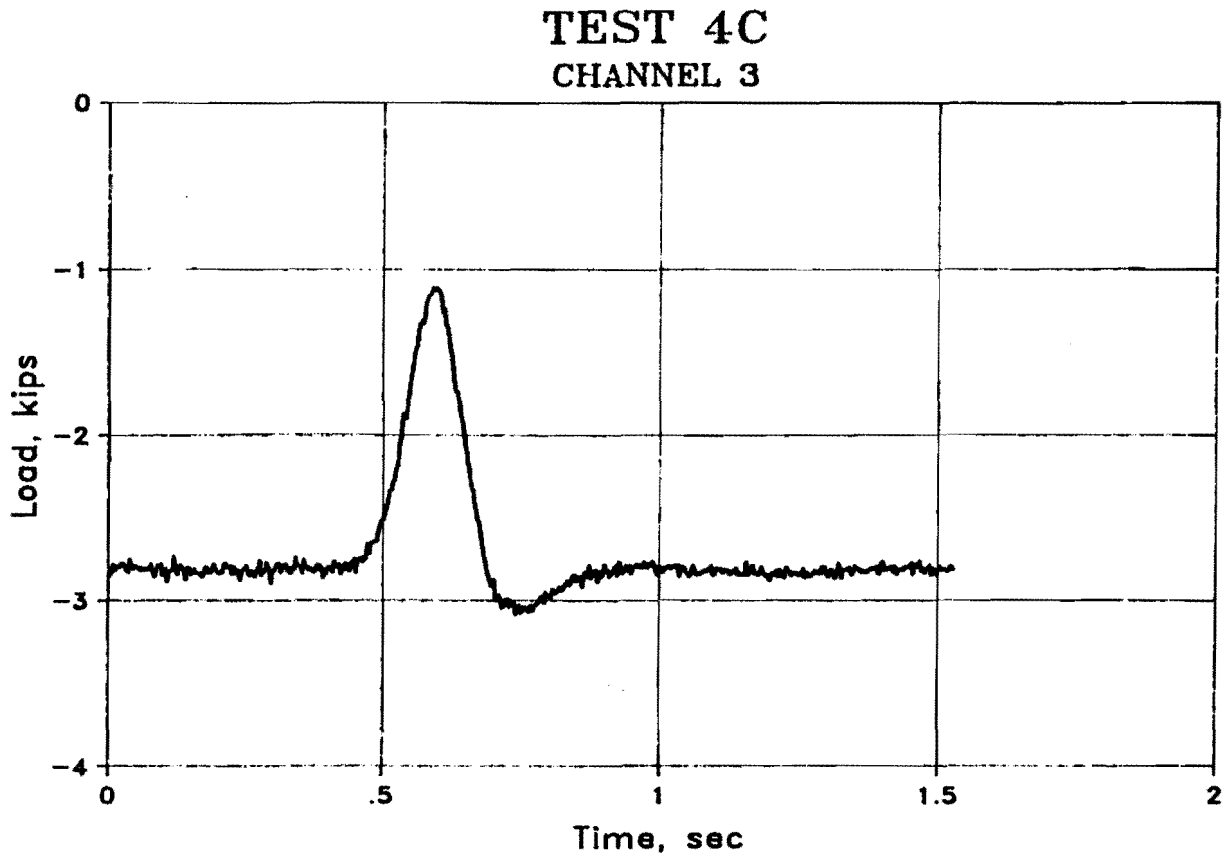

Fig. 5.42 Load in east tension anchor vs. time, impact test on east-end post (Test 4C)

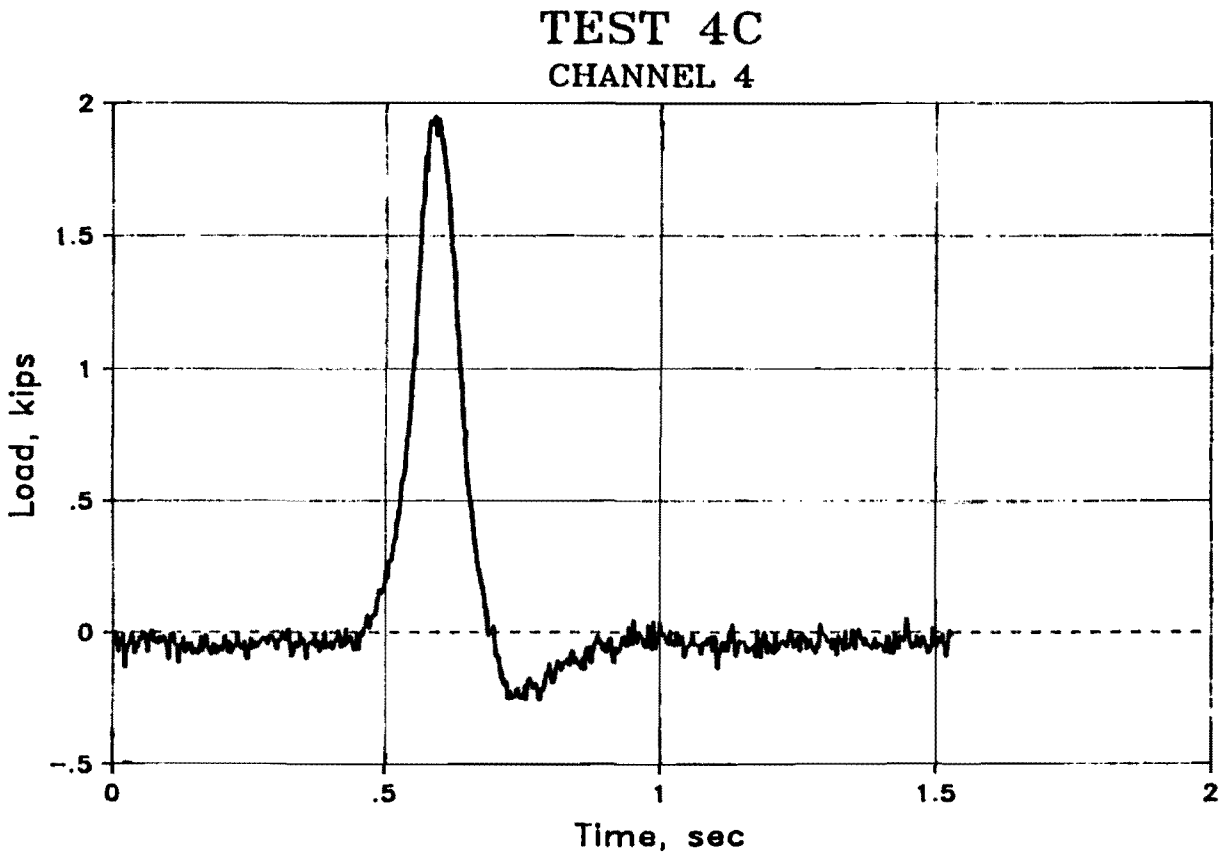

Fig. 5.43 Load in west tension anchor vs. time, impact test on east-end post (Test 4C)

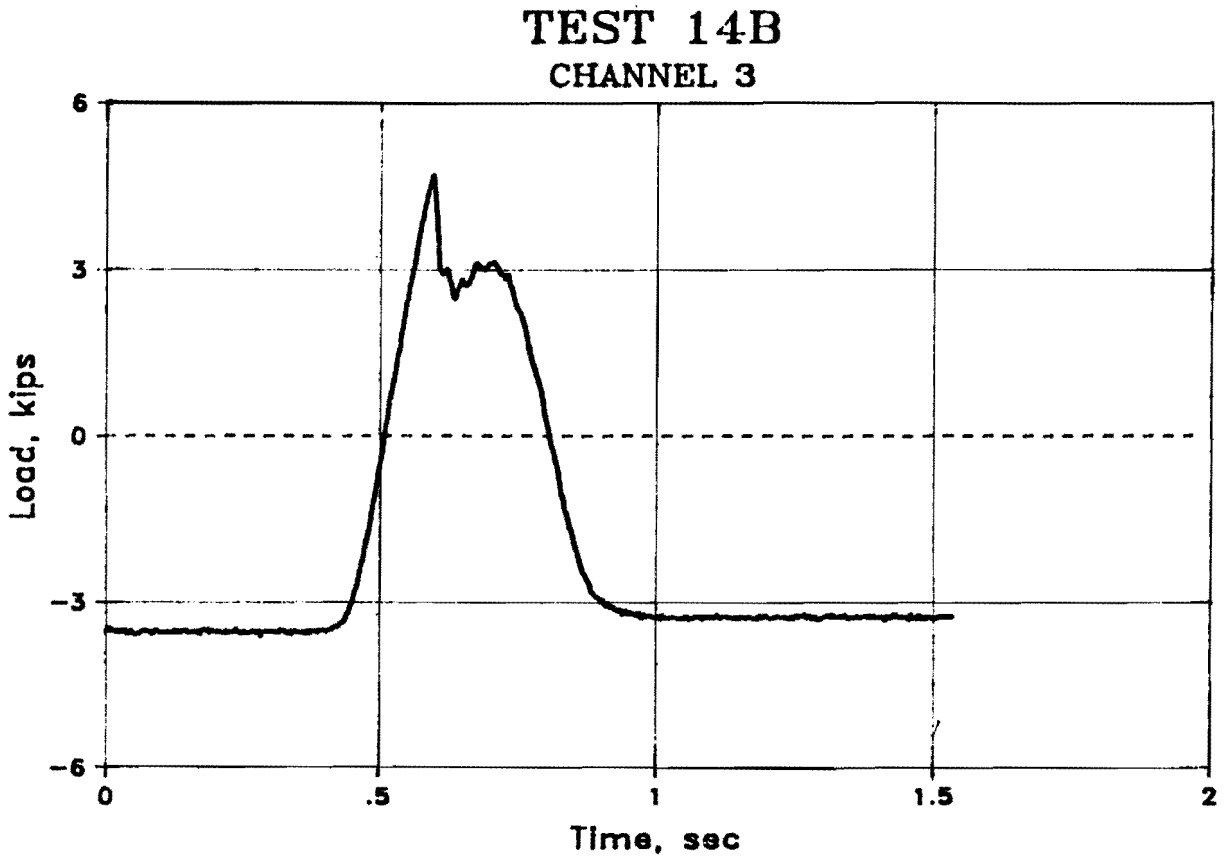

Fig. 5.44 Load in east tension anchor vs. time, impact test on east-end post (Test 14B)

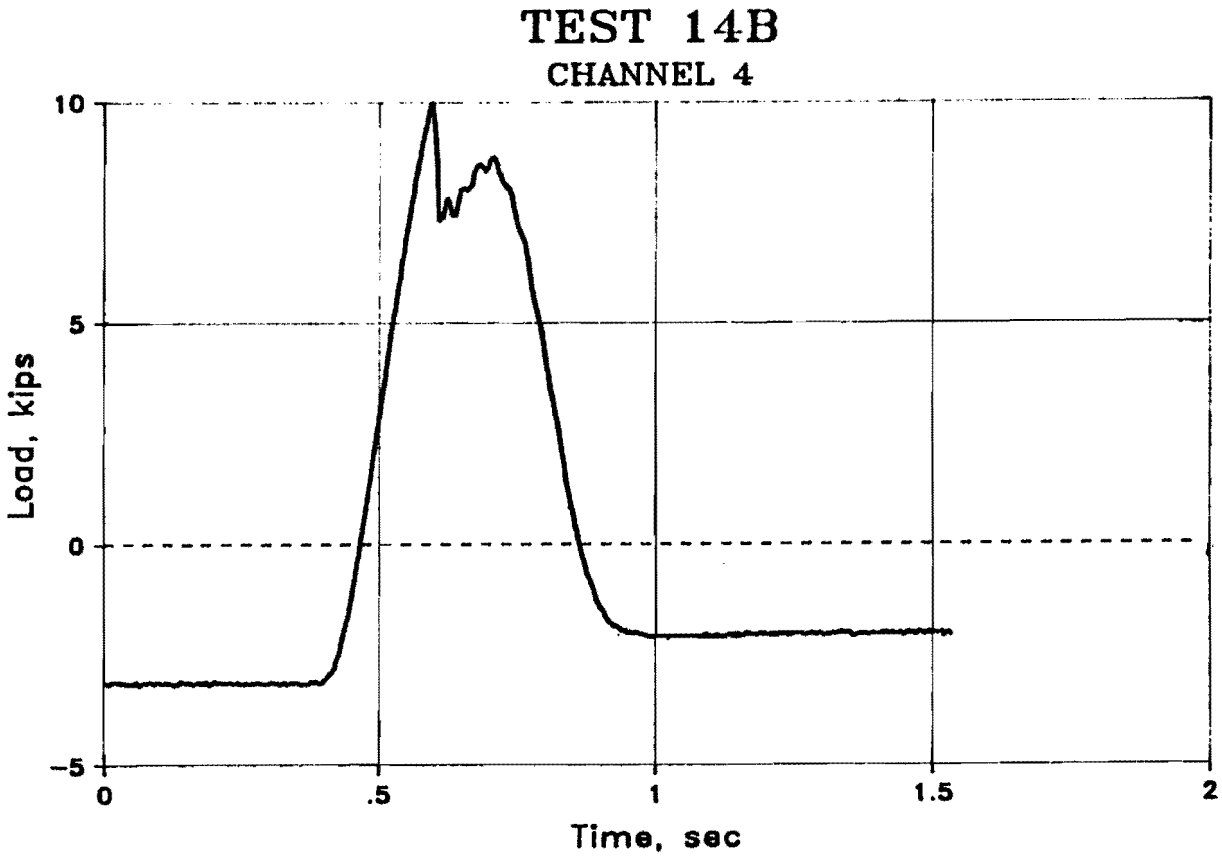

Fig. 5.45 Load in west tension anchor vs. time, impact test on east-end post (Test 14B)

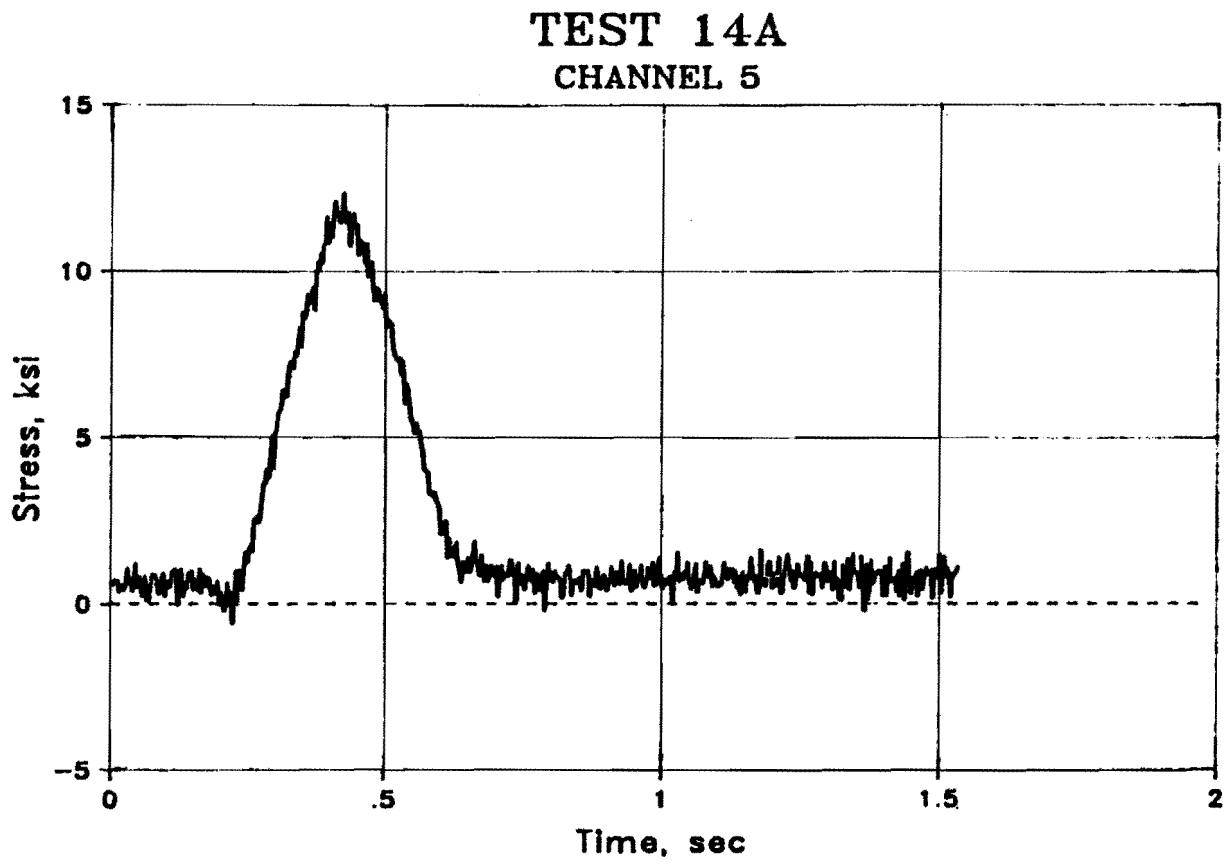

Fig. 5.46 Stress in top horizontal leg of west inside bar vs. time, impact test on east-end post (Test 14A)

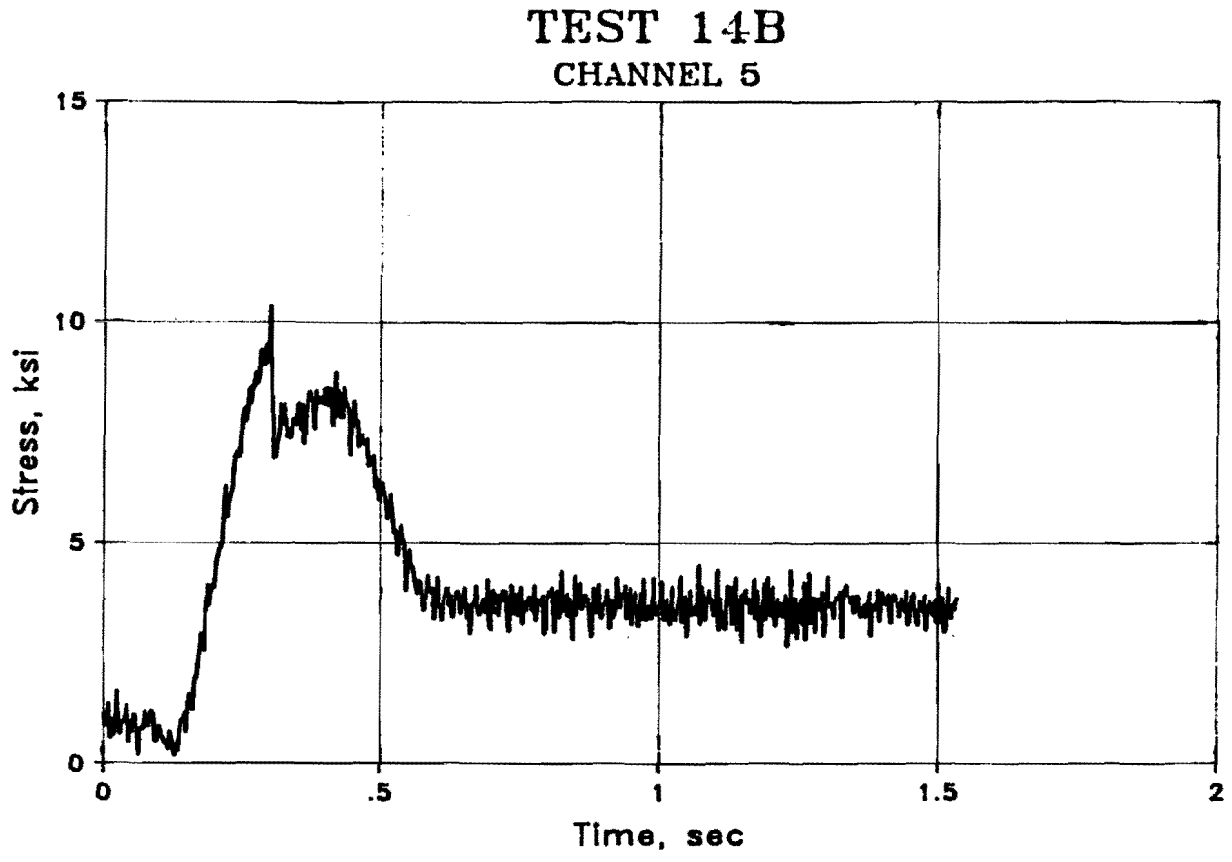

Fig. 5.47 Stress in top horizontal leg of west inside bar vs. time, impact test on east-end post (Test 14B)

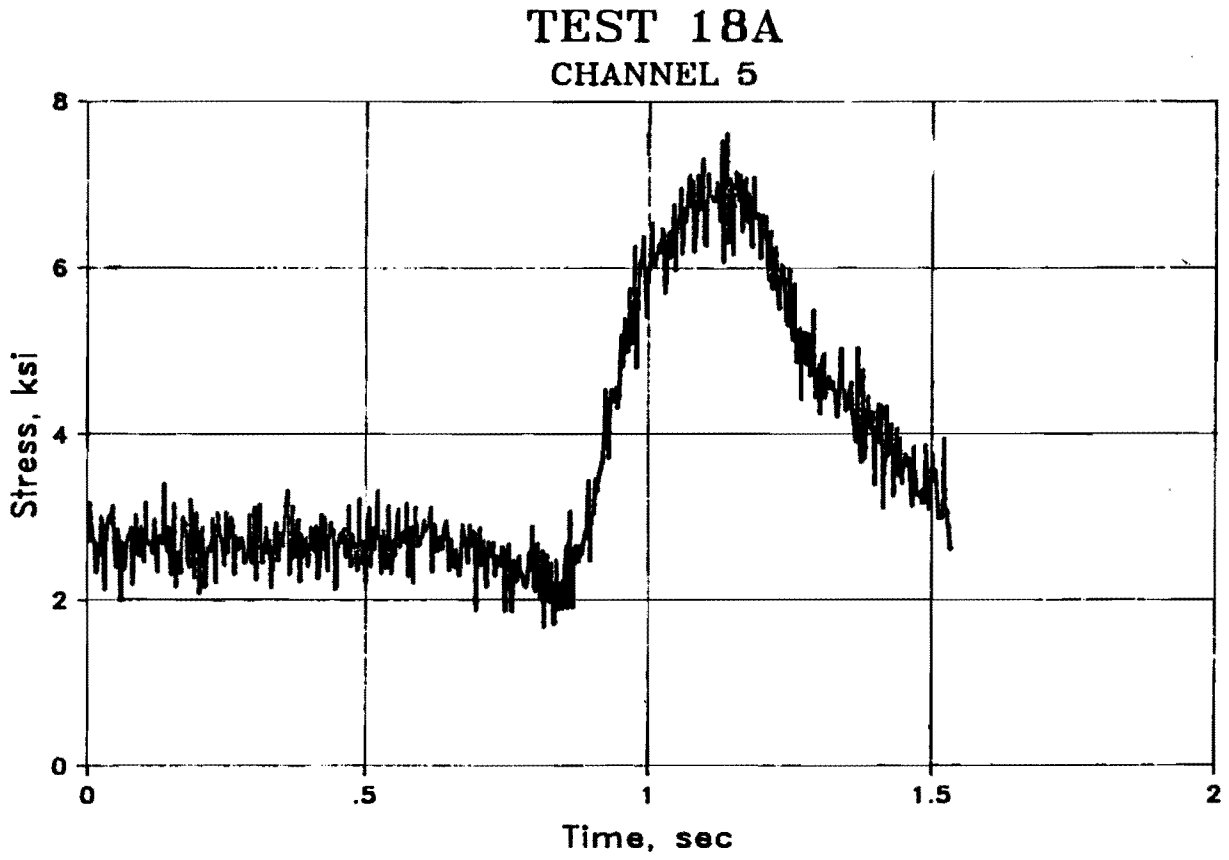

Fig. 5.48 Stress in top horizontal leg of west inside bar vs. time, impact test on east-end post (Test 18A)

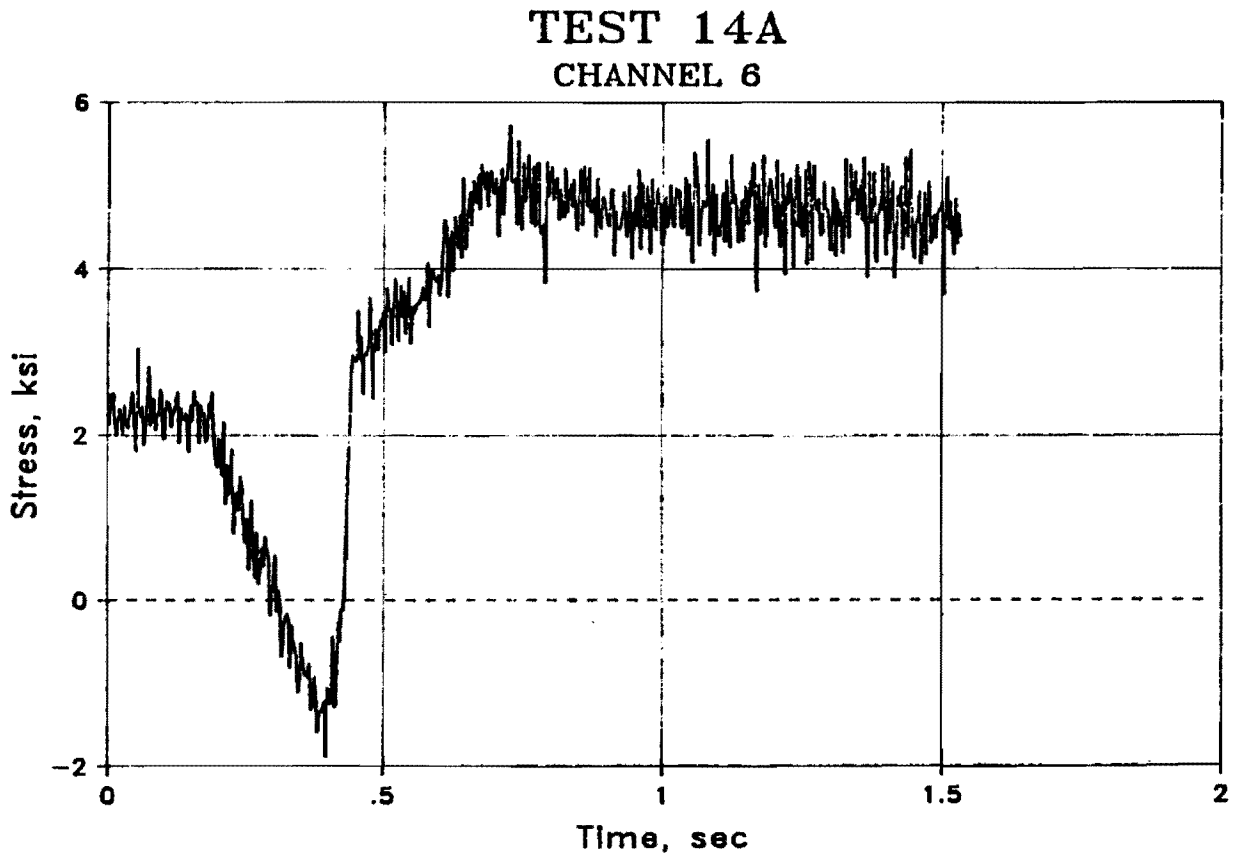

Fig. 5.49 Stress in vertical leg of west inside bar vs. time, impact test on east-end post (Test 14A)

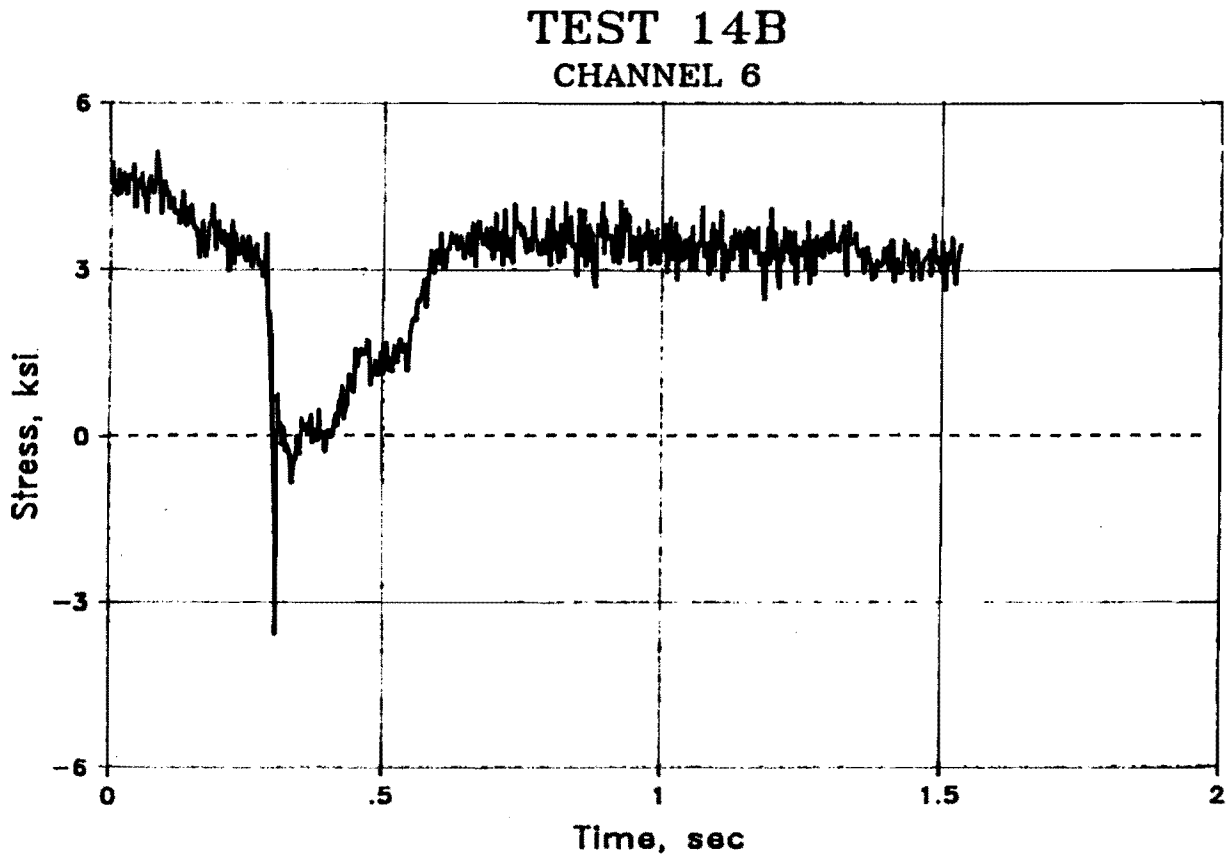

Fig. 5.50 Stress in vertical leg of west inside bar vs. time, impact test on east-end post (Test 14B)

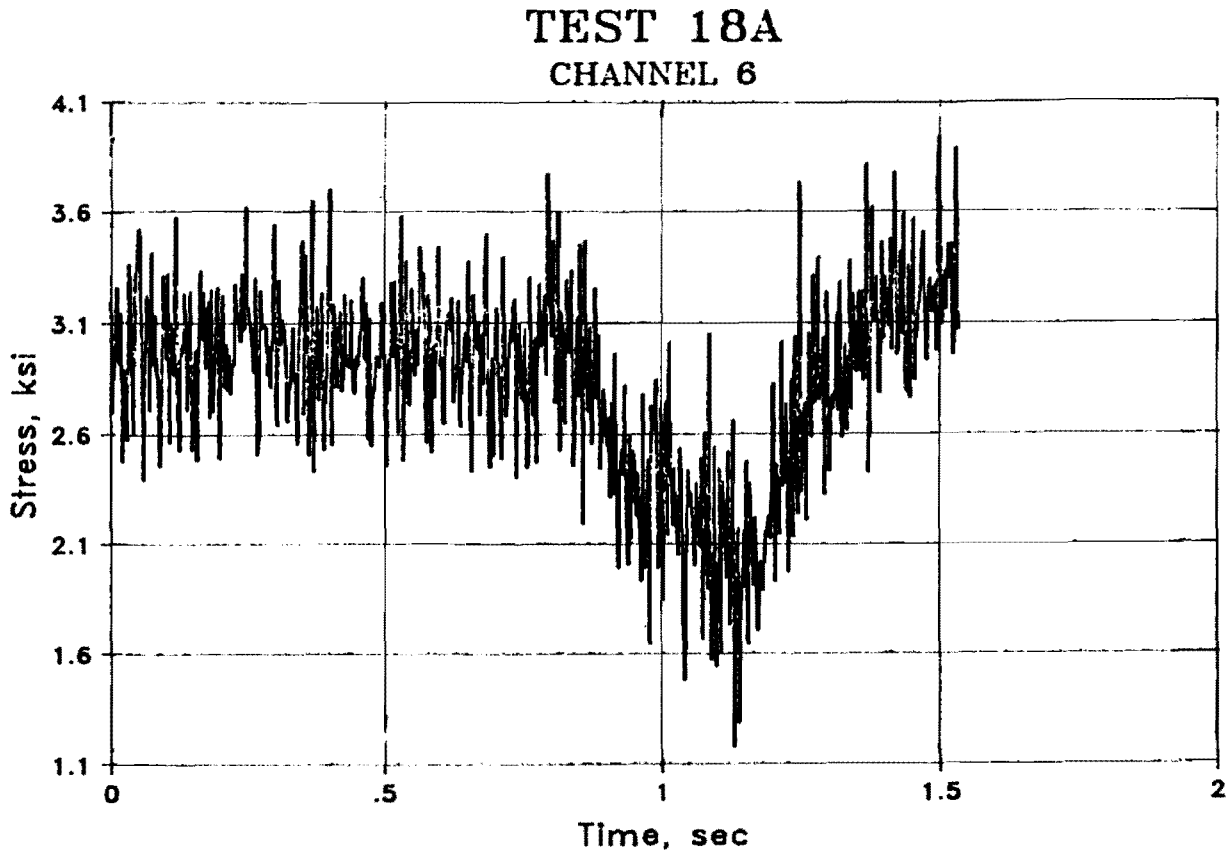

Fig. 5.51 Stress in vertical leg of west inside bar vs. time, impact test on east-end post (Test 18A)

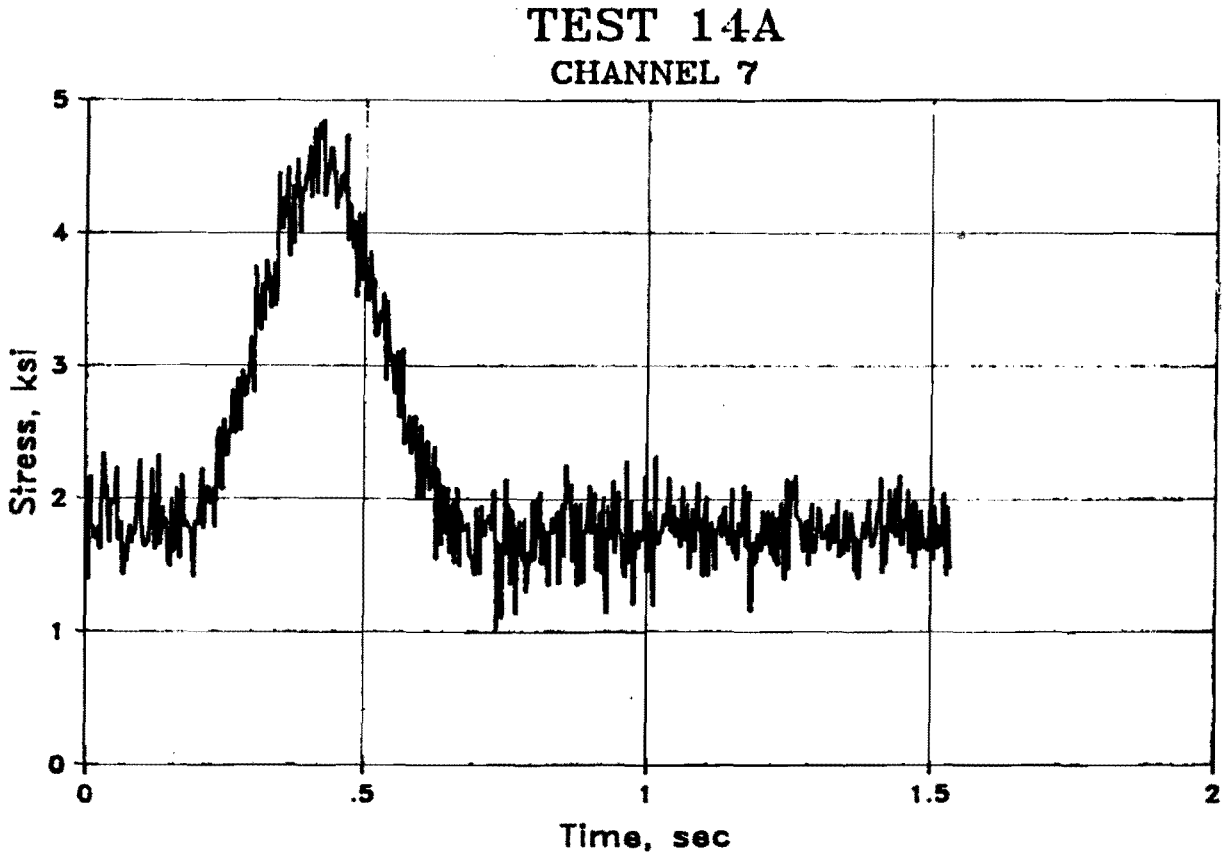

Fig. 5.52 Stress in top horizontal leg of east outside bar vs. time, impact test on east-end post (Test 14A)

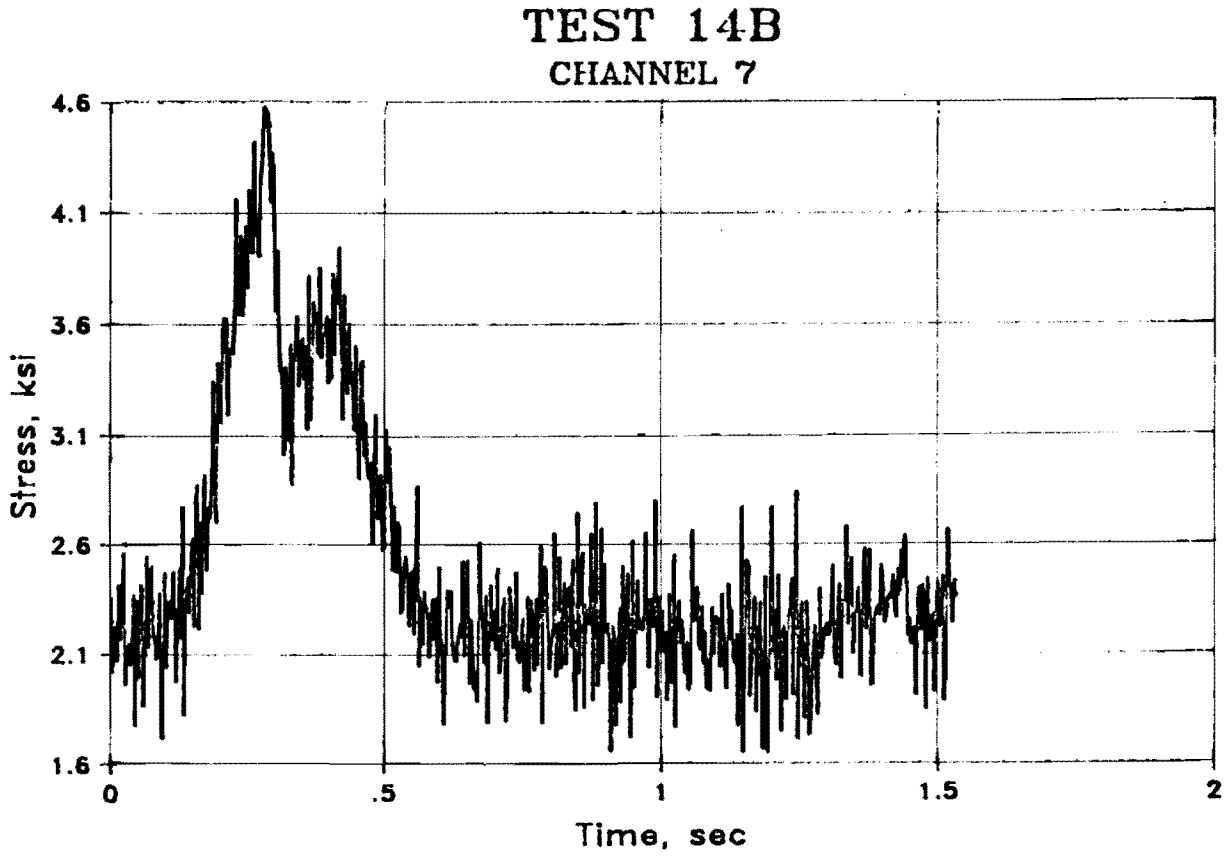

Fig. 5.53 Stress in top horizontal leg of east outside bar vs. time, impact test on east-end post (Test 14B)

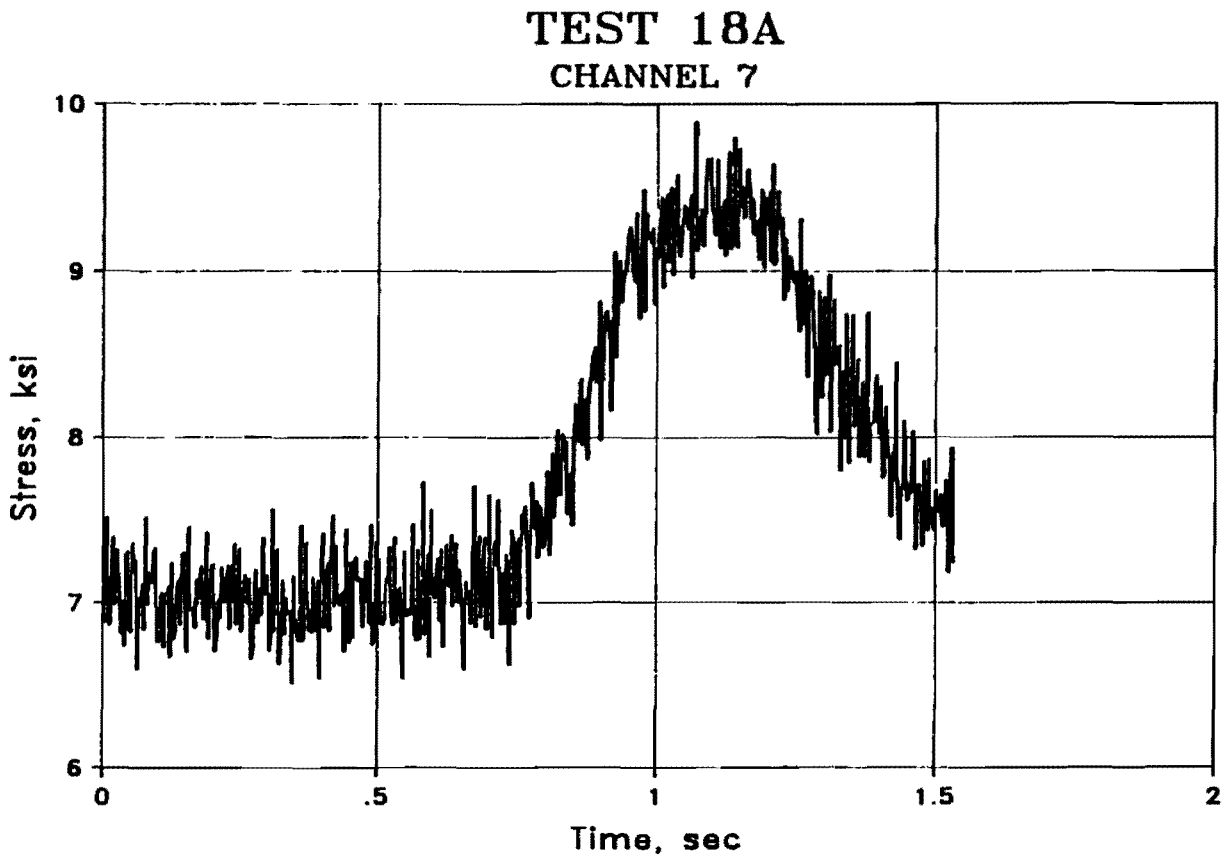

Fig. 5.54 Stress in top horizontal leg of east outside bar vs. time, impact test on east-end post (Test 18A)

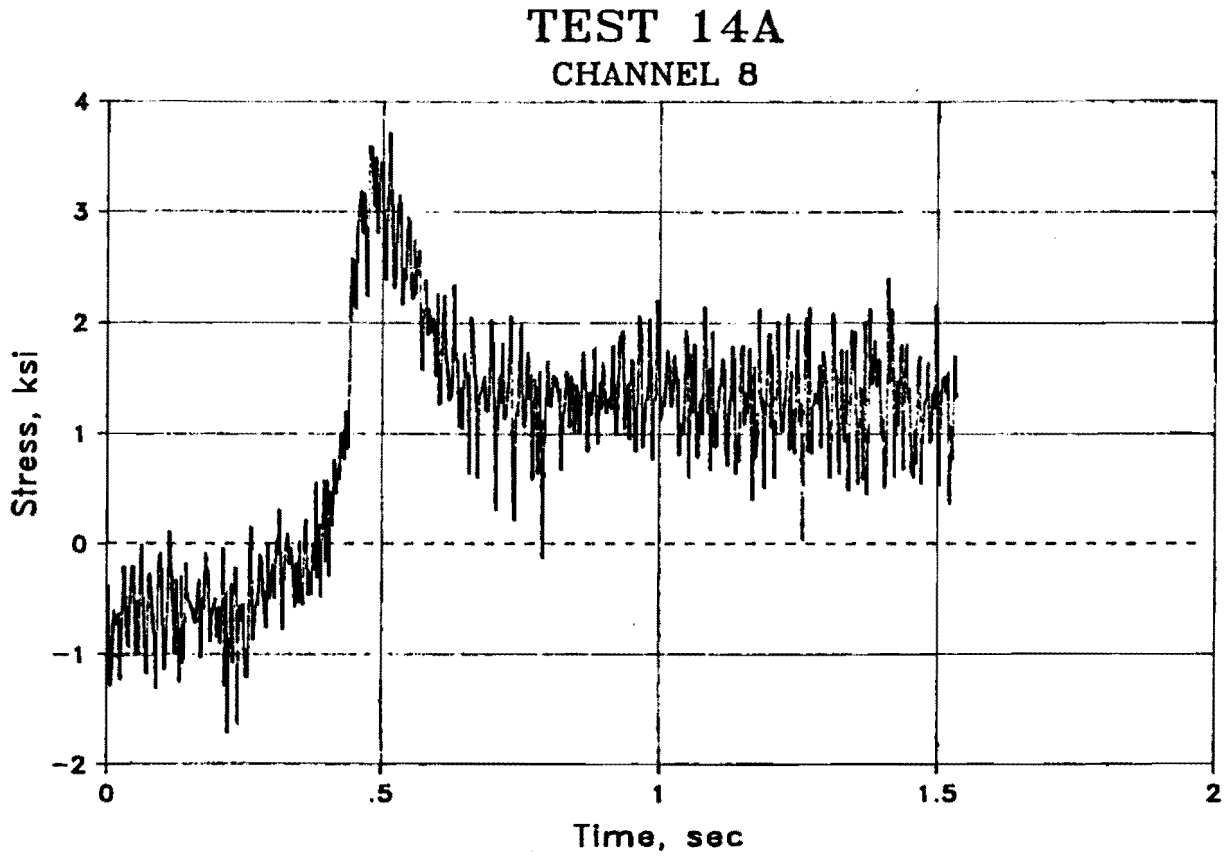

Fig. 5.55 Stress in vertical leg of west outside bar vs. time, impact test on east-end post (Test 14A)

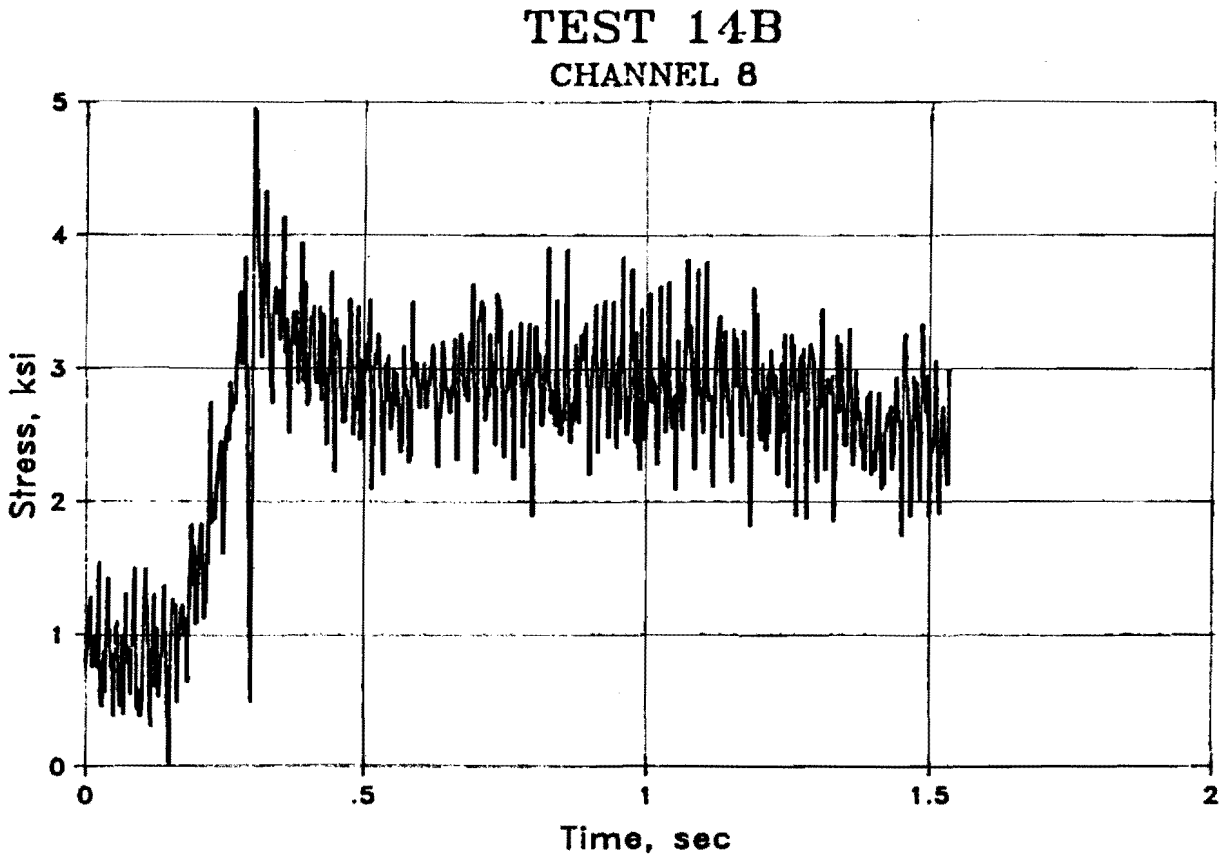

Fig. 5.56 Stress in vertical leg of west outside bar vs. time, impact test on east-end post (Test 14B)

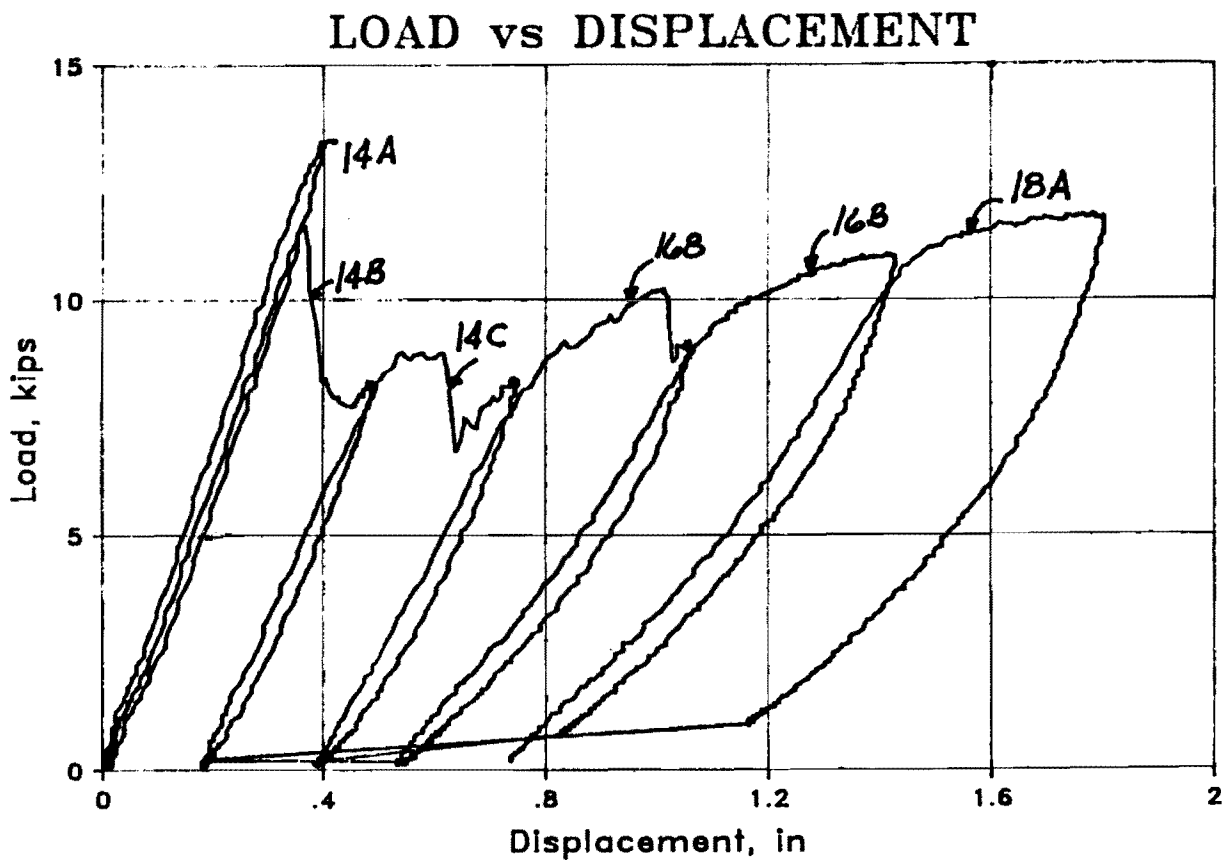

Fig. 5.57 Applied load vs. post displacement, impact tests on east-end post (Tests 14A, 14B, 14C, 16A, 16B, 18A)

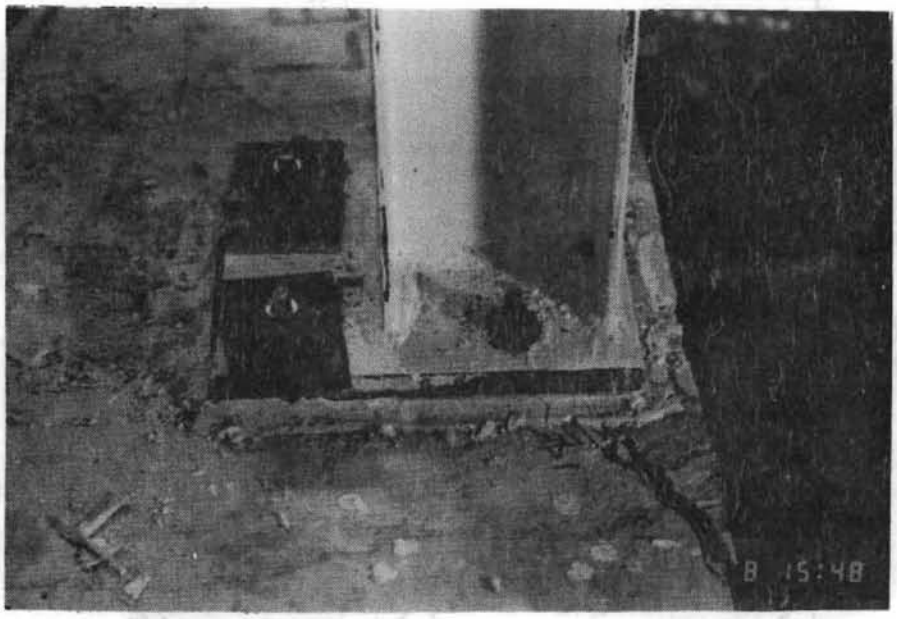

Fig. 5.58 Initial cracking at east-end post location

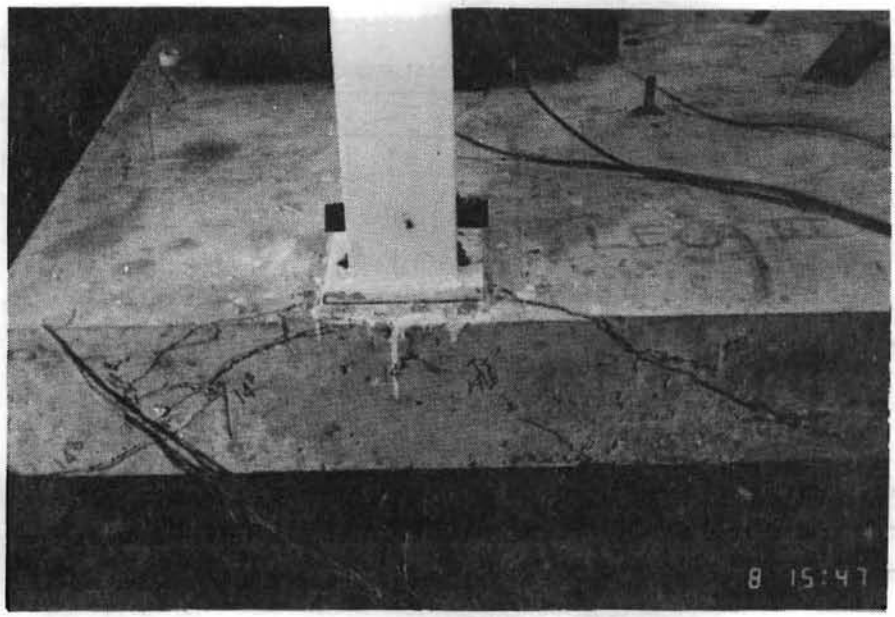

Fig. 5.59 Diagonal cracking at east-end post location

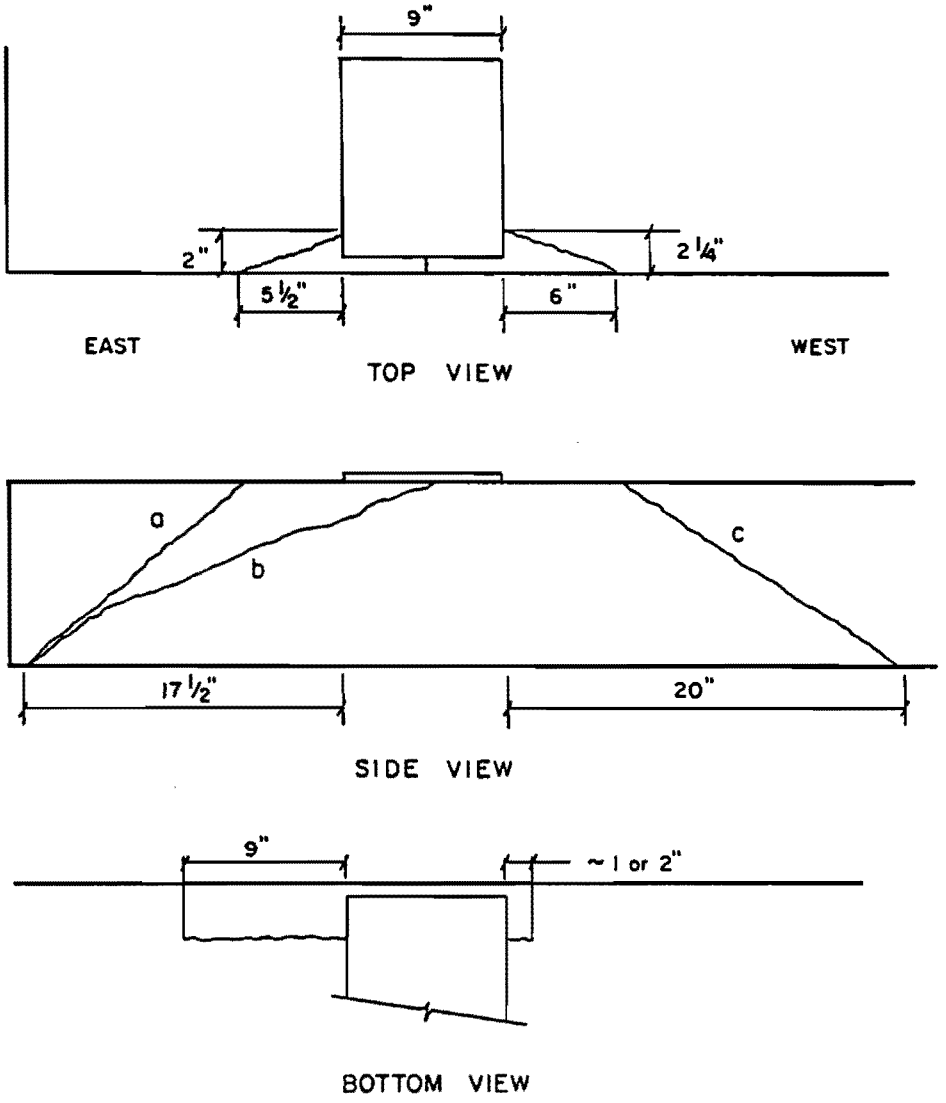

Fig. 5.60 Cracking pattern at east-end post

Fig. 5.61 East-end post location at failure

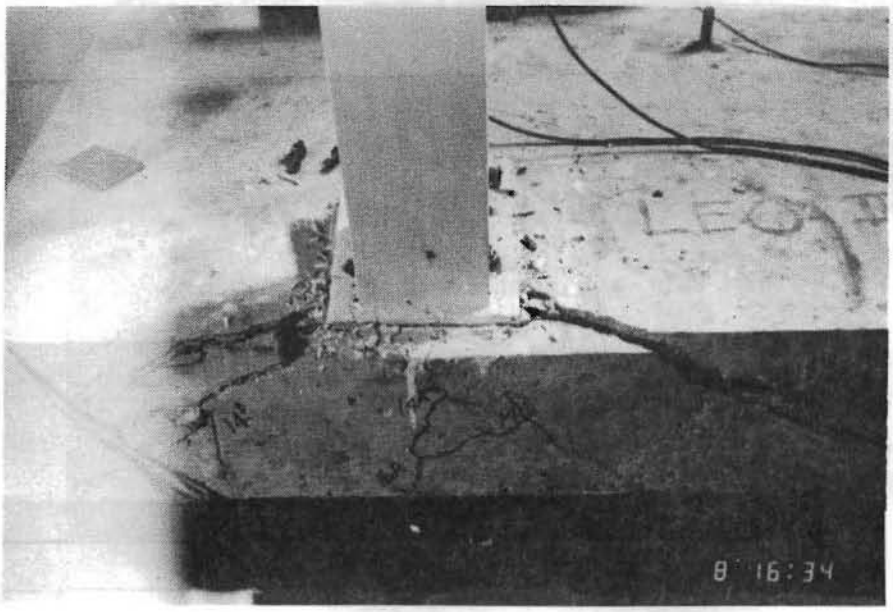

Fig. 5.62 East-end post location at failure

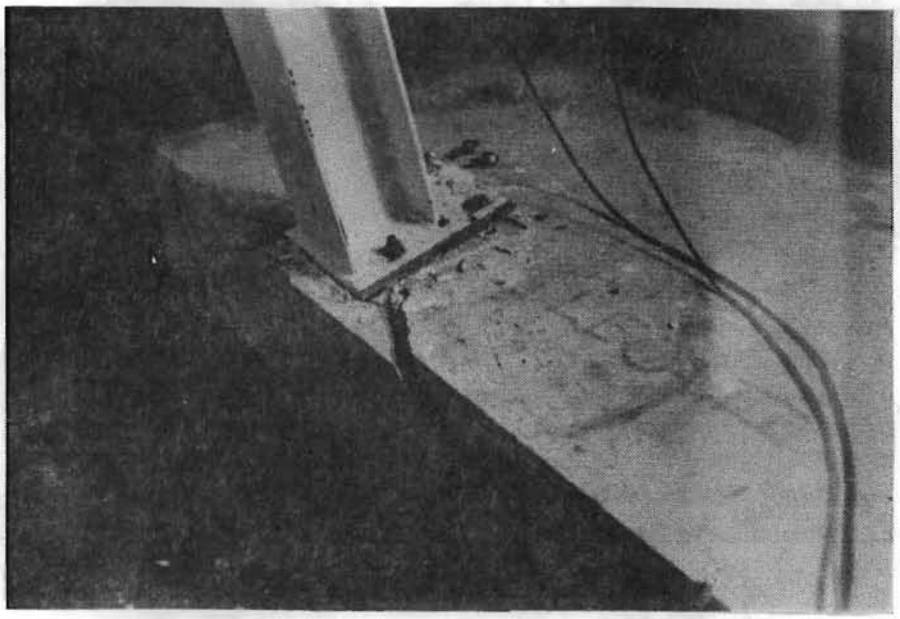

Fig. 5.63 East-end post location at failure

CHAPTER 6

DISCUSSION OF RESULTS

6.1 Review of Observed Behavior

As discussed in Chapters 2 and 3, the specimen was designed to fail by fracture of the tension anchors. Such a failure was in fact observed, but only after the area of the tension anchors was decreased to less than half the currently specified value, and only after extensive damage to the deck. The other failure modes which had been considered, such as tensile cone pullout or yielding of the slab in flexure, were prevented. Although failure of the weld connecting the post to the base plate caused premature failure in the center post test, the problem was corrected by improved welding techniques, and this failure mode did not occur in any of the subsequent tests.

Although the observed crack patterns generally resembled the expected pattern for flexural-torsional failure, this failure mode did not fully develop. Stress measurements indicate that the U-shaped reinforcing bars did not yield in any of the tests. For the west-end post test, the recorded stresses in the slab reinforcement are quite low even near failure. It is hypothesized that the full development of this failure mechanism was prevented by a local failure at the slab edge. Due to high compressive stresses near the back (outside edge) of the base plate, a narrow strip at the deck edge was pushed down and away from the remainder of the deck. This failure mode is discussed in the following section.

One of the objectives of this research program was to obtain information on the behavior of the system under repeated impact loads. Load vs. deflection curves for the two impact test series indicate that, for low-level impacts, the behavior is very stable. The occurrence of a brittle failure, however, prevented investigation of the system's energy dissipation capabilities at high loads.

6.2 Diagonal Tension Failure Mode

In the flexural-torsional failure model, the failure surface was assumed to slope away from the top of the slab at an angle of 45°. The failure surface was actually much steeper, and was located much closer to the free edge of the slab. Figure 6.1 shows the shape of the failure surface at the east-end post location, based on measurements of the crack pattern of Fig. 5.60. Note that at Section AA of the figure, the failure surface extends almost vertically from the compression zone. Thus, the failure is restricted to a thin strip at the edge of the deck.

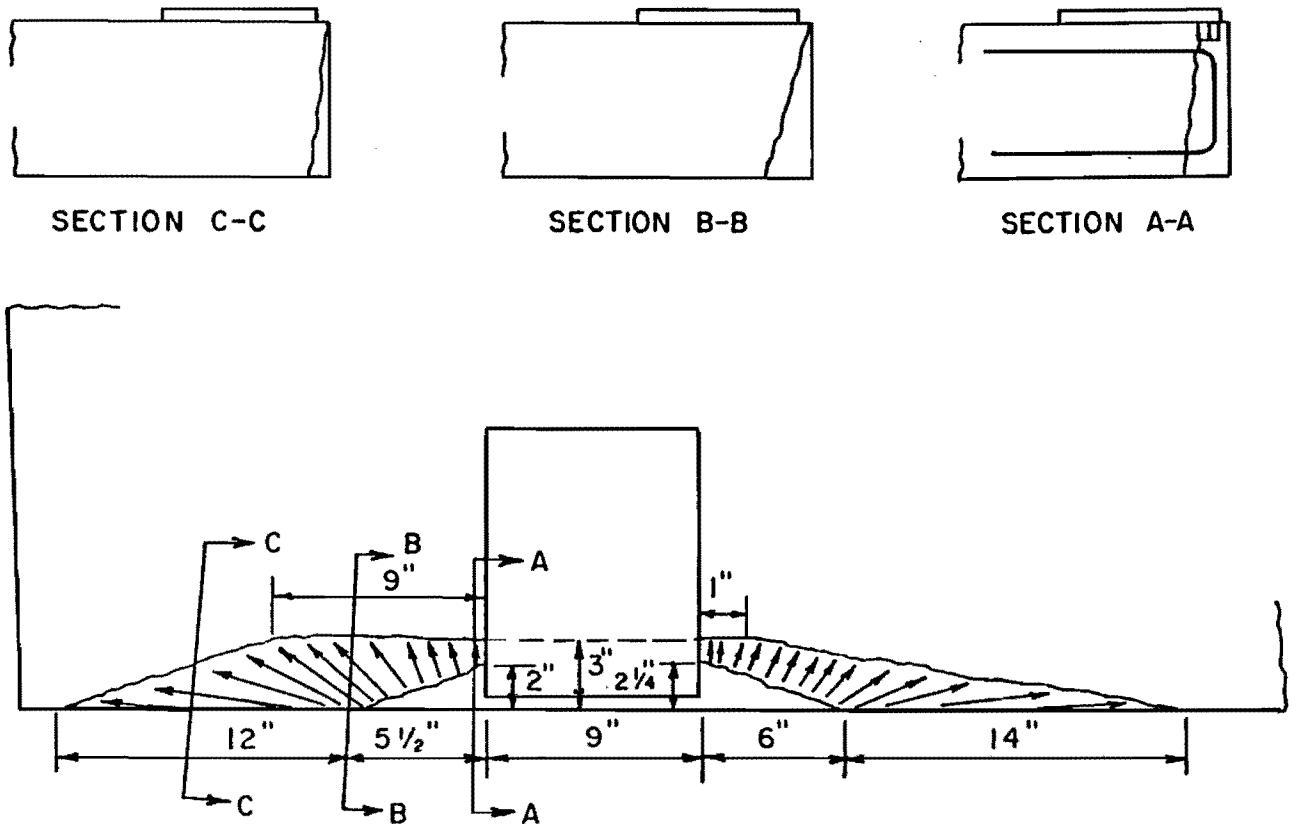

Fig. 6.1 Probable Failure Surface at East-end Post

One of the implications of this failure mode is that the reinforcement, positioned to cross the assumed failure surfaces, does not function in the intended manner. Examination of the strain gage data (Table 5.2) for the first static test (center post) reveals that although stress was highest in the top horizontal leg of the interior U-bar (as would be expected), the vertical leg and top horizontal leg of the outside U-bar reached approximately the same stress level. The horizontal leg picked up more stress than expected, while the vertical leg picked up less. Results from the second static test (west-end post) are even more pronounced. The maximum stress in the top horizontal leg of the outside U-bar was only slightly less than that in the top horizontal leg of the inside bar. On the other hand, stress in the vertical leg was very low for both the inside and outside bars.

These results seem to indicate that most of the U-bars which had been placed so that their vertical legs would cross the assumed failure surface, actually had their vertical leg completely contained inside the block of concrete which broke away from the rest of the slab. In such cases, the top horizontal legs of the bars crossed the actual failure surface.

Behavior during the impact tests is more difficult to interpret. Due to prior damage sustained during the static tests, no strain gage data are available from the west-end post tests. Data for the vertical legs of U-bars at the east-end location are ambiguous. The horizontal leg stresses during the east-end tests, however, show an interesting trend. When stress in the inside bar was maximum (12 ksi for Test 14A), stress in the outside bar was low (4.6 ksi). By Test 18A, stress in the inside bar had dropped to 7 ksi, while stress in the outside bar had risen to 9.3 ksi. Thus, the horizontal leg of the outside bars became effective as the failure surface propagated away from the loading point. This is illustrated in Fig. 6.2, in which the failure surface at a distance of 1-1/2 in. from the free edge of the slab (coinciding with the clear cover) is shown by dashed lines.

Although the top horizontal legs of most of the U-bars resisted flexural-torsional failure of the slab, they were not effective in resisting the diagonal tensile stresses caused by the downward force on the edge strip. Only the strength of the concrete was available to resist this failure mode.

6.3. Analytical Model for Diagonal Tension Failure Mode

A model for this type of failure is described in Section 3.2. It was not considered in the design process for specimens of this study, because the predicted failure loads as governed by this diagonal tension mechanism were considerably lower than the actual failure loads of the tests of Ref. 2. This seemed to indicate that the failure model was incorrect.

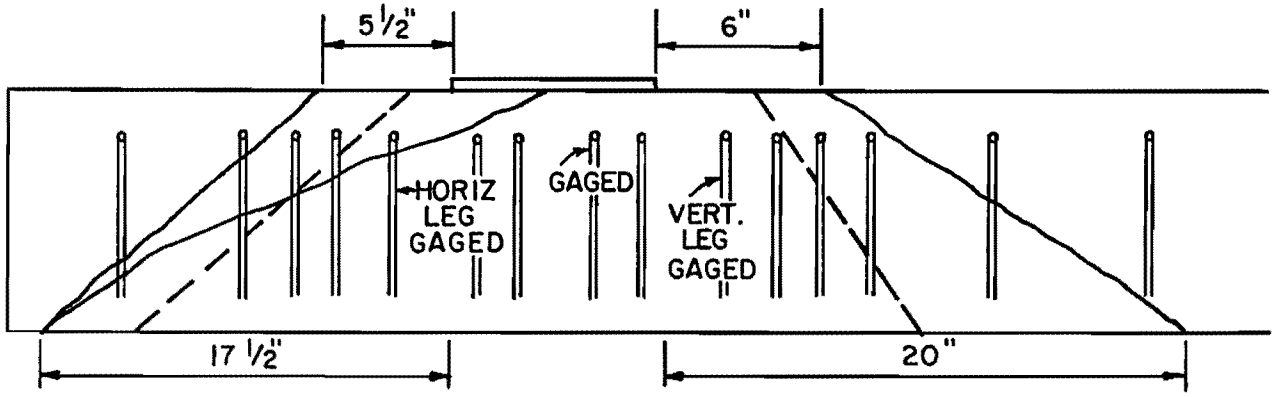

Fig. 6.2 Location of Reinforcement with Respect to Actual Failure Surface

When a uniform tensile strength of $4\sqrt{f'_c}$ is assumed to act over the projected area of the east-end post failure surface (Fig. 6.1), the available resistance is found to be 19.5 kips. To prevent failure, resistance would have to equal or exceed the compressive force applied to the top of the slab by the base plate. That compressive force, equal in magnitude to the tensile force acting on the inner set of anchor bolts, can be calculated based on the rotational equilibrium of the post. The applied load acted at a height of 20.5 in. above the deck surface (Fig. 3.1). Using the analytical model shown in Fig. 3.2, the depth of the compressive stress block was estimated to be about 0.5 in., and the distance between the tensile and compressive reactions on the base plate was about (9.25 - 0.5/2) in., or 9.0 in. Summing moments about the tensile resultant, the magnitude of the compressive force C applied to the concrete is given by V (the lateral load applied to the post) multiplied by the ratio (20.5/9.0), or 2.3. If the available concrete failure resistance is 19.5 kips, the post load required to produce a compressive force just equal to that resistance is (19.5/22), or 8.5 kips. The actual failure load was 11.8 kips.

The failure surfaces at the other two test locations are less well defined. Both the crack patterns and the magnitude of the failure loads seem to indicate that the failure surfaces extended farther into the slab.

Because of the wide variation in possible failure surfaces, prediction of failure load using this model is very difficult. The shape of the projected failure surface is idealized in Fig. 6.3. This idealized shape is close to the observed failure surface, and its area is simple to calculate. The failure load V can be computed from the following equations:

$$V = C\ (d_p - a/2)/H \tag{6.1}$$

$$C = 0.85\ f'_c\ ab \tag{6.2}$$

$$C = 4\sqrt{f'_c}\ A_p \tag{6.3}$$

$$A_p = (s+a)\ [2t - 3(s+a)] + 6\ (s+a)^2$$

$$= 2t\ (s+a) + 3\ (s+a)^2 \tag{6.4}$$

Where b = width of base plate
s = distance from free edge of slab to back edge of base plate, and
H = vertical distance from point of application of post load to top of slab

Equations (6.1) through (6.4) can be solved (for example) by substituting Eq. (6.4) into Eq. (6.3), equating Eqs. (6.2) and (6.3), and solving for a. V is then easily computed.

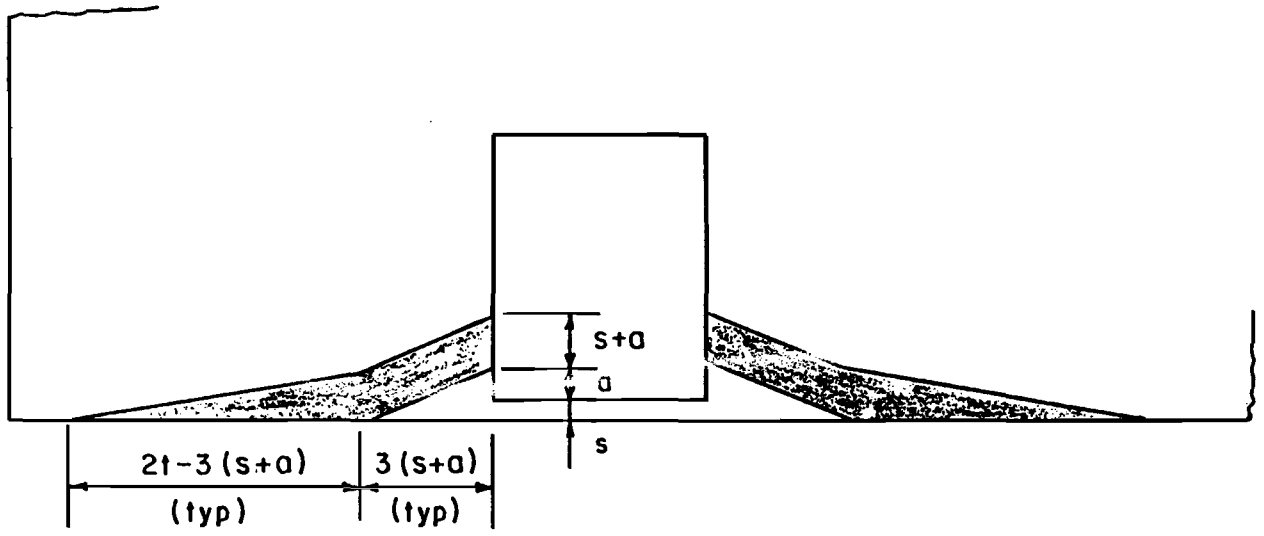

Fig. 6.3 Idealized Projected Failure Surface for Diagonal Tension Model

6.4. Design for Ductile Failure

As explained in Section 3.1, a design load of 27 kips (at top of post) was assumed for the specimen, consistent with the plastic moment capacity of the post. This required the use of two 3/4-in. diameter threaded rods, placed 9-1/4 in. from the back edge of the base plate. The specimen was designed so that failure would be caused by yielding of the tension anchors. The capacity of the section as governed by the other failure modes considered in Chapters 2 and 3 was set to exceed the load corresponding to fracture of the bolts. The diagonal tension mode of the previous section was not considered in the design of the specimen.

The ultimate tensile strength of the two tension anchors is 80.2 kips. To prevent a diagonal tension failure, the deck would have to be able to withstand a compressive force of 80.2 kips applied near its edge. Since all of the resistance is provided by plain concrete, a strength reduction factor of 0.65 would be appropriate. The deck would therefore have to have a nominal diagonal tension resistance of 123 kips. From equations 6.2 and 6.3, the dimension of the compressive stress block measures 4.0 in. perpendicular to the slab edge, and the necessary projected area of the failure surface is therefore 486 in.

Note that f'_c was taken as 4000 psi for this calculation, while the measured strength of 6720 psi was used in the calculations of the previous section.

The required projected area computed from equation 6.4 can be achieved only by using a thicker deck section or a larger post setback. To get the necessary projected area of the failure surface by increasing deck thickness, while keeping the current setback of 1-1/4 in, requires a 49-in. thick deck. This alternative is clearly not feasible. Since the setback occurs as a squared term in Eq. 6.4, its effect is more pronounced. Solving the quadratic equation for the value of (s+a) required to produce the necessary area gives a value of 9.8 in. The required setback is then 5.8 in.

This analysis is probably conservative. It is possible that increasing post setback slightly while maintaining existing side cover requirements would allow the slab reinforcement to cross the failure surface and prevent this type of failure. Different arrangements of reinforcement near the failure surface (an arrangement similar to Fig 2.10a, for example) could also give increased capacity. Due to lack of time, these hypotheses were not explored further.

Another means of achieving ductility is to sacrifice some strength. If 5/8-in. diameter rods are used at the 9-1/4 in. spacing, a 5-in. setback is required (based on Eq. 6.4) and a load of 19 kips can be safely applied to the post. For 1/2-in. diameter bolts, the required setback is 4 in., and a 12.4 kip load can be applied. The strength of the barrier could be increased somewhat by lengthening the

base plate. However, this would require a stronger base plate to resist the increased flexure. Decreased post spacing (more posts) could also offset the loss in strength to some extent.

CHAPTER 7

SUMMARY AND CONCLUSIONS

7.1 Summary

Although much effort has been devoted to the safe design of highway barriers, it is only recently that anchorage of the barrier to the concrete bridge deck has been studied. Tests by Arnold and Hirsch [2] indicate that the standard deck section used by the Texas State Department of Highways and Public Transportation does not possess sufficient strength to develop the full capacity of either the barrier post or the anchor bolts.

In the present study, a series of static and impact tests were carried out on a steel barrier post (T101 type) anchored to a 10-in. thick reinforced concrete deck. Slab reinforcement was modified in an attempt to produce a test specimen which would fail by yielding of the tension anchors with little damage to the deck. Analytical models were developed for various failure modes, including one which was developed by interpreting the results of Ref. 2.

All of the tests resulted in brittle failures. In most cases, this was attributed to a local diagonal tension failure near the slab edge. This type of failure could not be eliminated without changing key elements of the current design, such as the distance the post is set back from the free edge of the slab, the slab thickness, or the overall configuration of transverse slab reinforcement.

The necessary changes would involve one or more of the following fundamental modifications to current bridge deck/barrier design:

1) increased post setback
2) increased deck thickness
3) innovative placement of special transverse reinforcement near the anchor bolts.

Due to lack of time, these fundamental modifications were not explored further.

The primary objective of this research was to study the behavior of the anchorage under repeated impact loading. Repeated impact at low to moderate load levels proved not to be a problem for either the anchorage or concrete deck; the response was very stable.

However, larger loads resulted in brittle failures even when applied statically. Response to repeated impacts at higher load levels

could not be determined, because the brittle failure prevented repetition of the critical load.

7.2 Conclusions

The current Texas SDHPT design detail for anchorage of steel post highway barriers (T101 type) is non-ductile. Most of the brittle failure modes, such as tension or shear cone pullout and the flexural-torsional failure, can be eliminated by relatively simple adjustments to existing details. On the other hand, local failure due to diagonal tension, which was the critical failure mode in these tests, is very difficult to prevent.

7.3 Recommendations

Safety as well as repair considerations require that highway barriers fail in a ductile manner under lateral loads. One way of achieving this is to modify the current anchorage detail by the most practical and economical combination possible of:

1. increased post setback;
2. increased slab thickness;
3. decreased anchor sizes, offset by increased length of base plate or decreased post spacing;
4. innovative placement details for special reinforcement near the anchor bolts; and
5. increased diagonal tensile resistance of concrete near the anchor bolts, achieved by means of fiber reinforcement or a similar technique.

Otherwise, the steel-post barrier system should be replaced with a barrier system which does not present such a severe ductility problem.

7.4 Recommendations for Further Research

Research should be directed toward the development of a ductile steel-post barrier system to replace the current non-ductile design.

APPENDIX A.1

Derivations

A.1.1 Pullout Strength

Pullout strength equals resultant of inclined stresses acting on surface area of truncated cone. Refer to Fig. A.1.

$$S = \text{surface area} = \frac{\pi}{\sin\alpha}\left(l_e D_h + \frac{l_e^2}{\tan\alpha}\right)$$

P' = resultant of tensile stress acting perpendicular to cone

$$= f_t S$$

$$= f_t \frac{\pi}{\sin\alpha}\left(l_e D_h + \frac{l_e^2}{\tan\alpha}\right)$$

where

f_t = uniform tensile stress

P_c = resultant of stresses acting in the direction of the applied load

$$= f_t \cos\alpha \frac{\pi}{\sin\alpha}\left(l_e D_h + \frac{l_e^2}{\tan\alpha}\right)$$

$$= f_t \frac{\pi}{\tan\alpha}\left(l_e D_h + \frac{l_e^2}{\tan\alpha}\right)$$

For $\alpha = 45°$ and $f_t = 4\sqrt{f'_c}$

$$P = 4\pi\sqrt{f'_c}\left(l_e D_h + l_e^2\right) = 4\pi l_e \left(D_h + l_e\right)\sqrt{f'_c}$$

Pullout strength equals resultant of tensile stresses acting on projected area of a truncated cone.

$$A_{pc} = \text{projected area} = \left(r_1^2 - r_2^2\right)$$

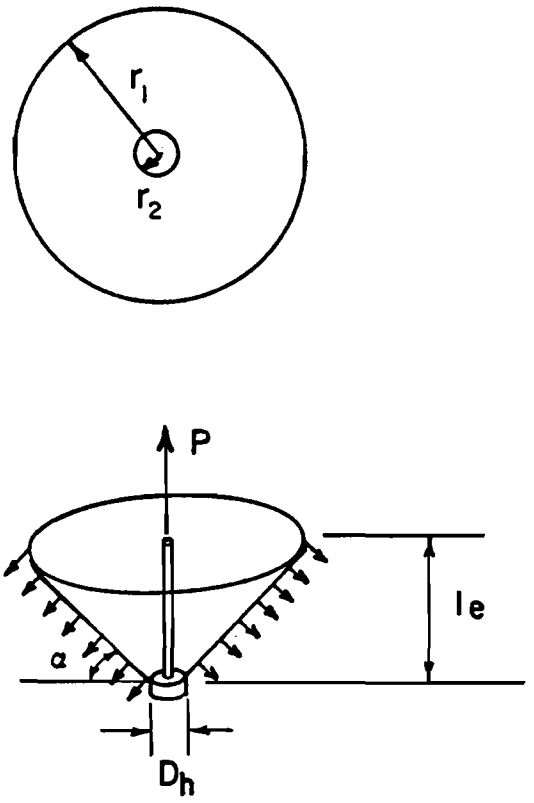

Fig. A.1 Tension pullout cone

$$r_1 = \frac{l_e}{\tan\alpha} + \frac{D_h}{2} \qquad r_2 = \frac{D_h}{2}$$

$$A_{pc} = \pi\left[\left(\frac{l_e}{\tan^2\alpha} + \frac{D_h}{2}\right)^2 - \left(\frac{D_h}{2}\right)^2\right]$$

$$= \pi l_e \left(\frac{l_e}{\tan^2\alpha} + \frac{D_h}{\tan\alpha}\right)$$

P_c = resultant of stresses acting on projected area

$$= f_t \frac{\pi}{\tan\alpha}\left(\frac{l_e^2}{\tan\alpha} + l_e D_h\right)$$

where

f_t = uniform tensile stress

For $\alpha = 45°$ and $f_t = 4\sqrt{f'_c}$,

$$P_c = 4\pi l_e(l_e + D_h)\sqrt{f'_c}$$

For $\alpha = 45°$, pullout strength equals the resultant of tensile stresses acting parallel to a hypothetical cylinder. (Fig. A.1c)

$$S = 2\pi R\, l_e$$

$$R = 1/2\,(l_e + \frac{D_h}{2})$$

$$S = l_e\pi(l_e + \frac{D_h}{2})$$

$$P_c = f_t \pi l_e \left(l_e + \frac{D_h}{2}\right)$$

For $f_t = 4\sqrt{f'_c}$

$$P_c = 4\pi l_e \left(l_e + \frac{D_h}{2}\right) \sqrt{f'_c}$$

A.1.2 Minimum Edge Distance to Prevent Lateral Bursting

Refer to figure A.2.

P_L = lateral bursting force = $1/4\ A_s\ f_{ut}$

$P_L \leq \phi f_t \pi d_e^2 \qquad \phi = 0.65$

$1/4\ A_s f_{ut} \leq (0.65)\ 4\sqrt{f'_c}\ \pi d_e^2$

$$d_{e\ min} = \sqrt{\frac{A_s\ f_{ut}}{32\sqrt{f'_c}}} \qquad \text{(2.5), repeated}$$

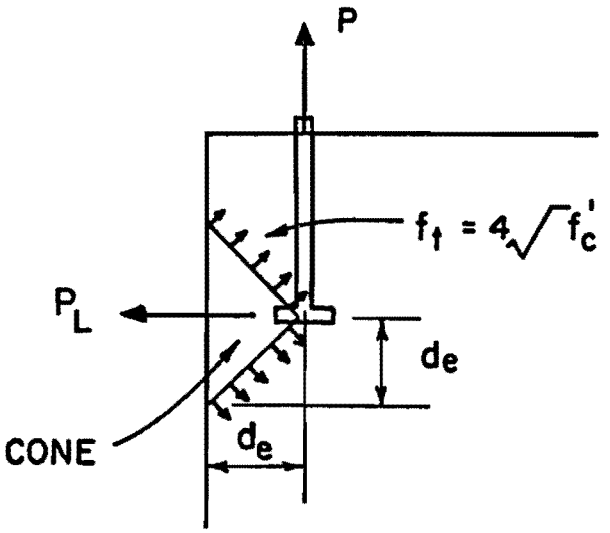

Fig. A.2 Lateral bursting

APPENDIX A.2

Sample Anchorage Calculations

A.2.1 Effective Projected Area

When the projected areas of stress cones for individual anchors in a multiple anchor connection overlap, or when the projected area extends beyond the free edge of the concrete section, the effective area may be calculated by breaking the complex shape into a number of simple shapes -- triangles, rectangles, and sectors of circles.

For example: 4 anchors separated by a distance of 6 in. in one direction, 4 in. in the other; D_h = 1 in.; 1_e = 7-1/2 in.; d_e = 10 in. (Fig. A.3)

$$R = 1_e + D_h/2 = 8 \text{ in.}$$

$$d_e > R$$

$$m = 3 \text{ in.}$$

$$n = 2 \text{ in.}$$

Area 1 is composed of a triangle and a sector.

$$\theta_1 = \sin^{-1}(m/R)$$

$$A_1 = (1/2)\theta_1 R^2 + (1/2)m\sqrt{R^2-m^2}$$

$$A_1 = (1/2)\, R^2 \sin^{-1}(m/R) + (1/2)m\sqrt{R^2-m^2}$$

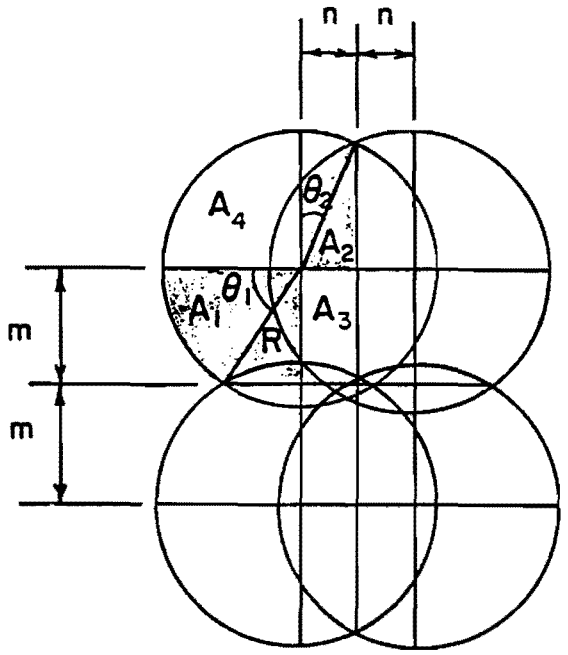

Fig. A.3 Projected area, $d_e > r$

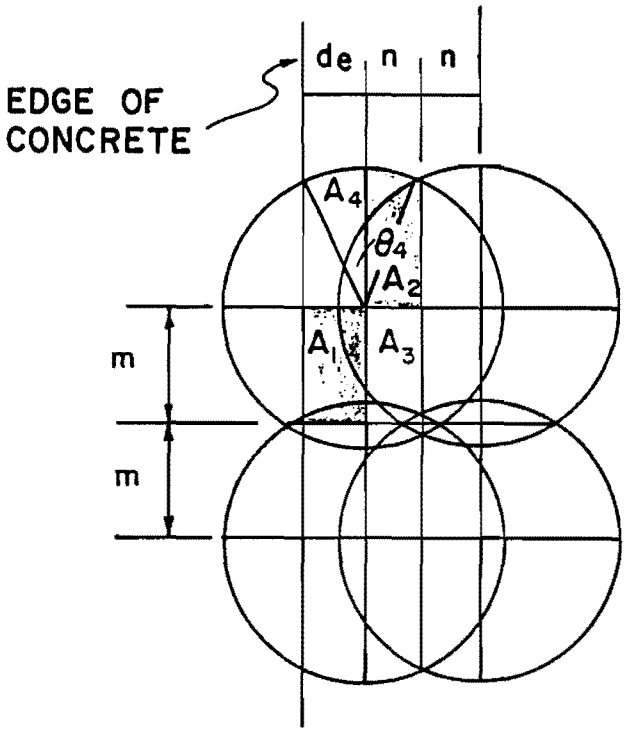

Fig. A.4 Projected area, $d_e < r$

Simlarly,

$$A_2 = (1/2)\theta_2 R^2 + (1/2)n\sqrt{R^2-n^2}$$

$$\theta_2 = \sin^{-1}(n/R)$$

$$A_2 = (1/2)R^2\sin^{-1}(n/R) + (1/2)n\sqrt{R^2-n^2}$$

Area 3 is a rectangle: $A_3 = mn$

Area 4 is a quarter circle: $A_4 = (1/4)\pi R^2$

The area of one quadrant equals the sum of these areas.

$$A_Q = A_1 + A_2 + A_3 + A_4$$

So,

$$A_{pc} = 4A_Q - 4\pi(D_h/2)^2$$

In this case

$$A_1 = 23.4 \text{ in.}^2$$
$$A_2 = 15.8 \text{ in.}^2$$
$$A_3 = 6.0 \text{ in.}^2$$
$$A_4 = 50.3 \text{ in.}^2$$
$$A_Q = 95.5 \text{ in.}^2$$

$$A_{pc} = 4(95.5) - 4\ (1/2)^2$$
$$A_{pc} = 379 \text{ in.}^2$$

If in the above problem the edge distance, d_e, were decreased to 6 in. (Fig. A.4), the area of the two interior quadrants would

remain the same.

$$A_Q = 95.5 \text{ in.}^2$$

The area of the two exterior quadrants can be calculated as follows:

As before, $A_2 = (1/2)R^2\sin^{-1}(n/R) + (1/2)n\sqrt{R^2-n^2}$

and $A_3 = mn$

Now, $A_1 = md_e$

and $A_4 = (1/2)R^2\sin^{-1}(d_e/R) + (1/2)d_e\sqrt{R^2-d_e^2}$

then, $A_1 = 18.0 \text{ in.}^2$

$A_2 = 15.8 \text{ in.}^2$

$A_3 = 6.0 \text{ in.}^2$

$A_4 = 43.0 \text{ in.}^2$

$A_Q = 82.8 \text{ in.}^2$ $\quad A_{pc} = 2(82.8) + 2(95.5) - 4\pi(1/2)^2$

$A_{pc} = 353 \text{ in.}^2$

For the special case when $\sqrt{R^2-m^2} < d_e < R$, the area of the two outer quadrants must be calculated differently.

$$A_1 = m\sqrt{R^2-m^2}$$

$$A_4 = (1/2)R^2\sin^{-1}(\sqrt{R^2-m^2})/R + (1/2)m\sqrt{R^2-m^2}$$

To compute A_5, the area of the circular segment which lies beyond the free edge must be subtracted from that of the larger segment.

$$A_5 = [R^2\sin^{-1}(m/R) - m\sqrt{R^2-m^2}] - [R^2\sin^{-1}(\sqrt{R^2-d_e^2})/R - d_e\sqrt{R^2-d_e^2}]$$

For d_e = 7-1/2 in.,

$$A_1 = 22.2 \text{ in.}^2$$
$$A_2 = 15.8 \text{ in.}^2$$
$$A_3 = 6.0 \text{ in.}^2$$
$$A_4 = 49.1 \text{ in.}^2$$
$$A_5 = 0.5 \text{ in.}^2 \qquad A_Q = 93.6 \text{ in.}^2$$

$$A_{pc} = (2)(93.6) + (2)(95.5) - 4\pi(1/2)^2$$
$$A_{pc} = 375 \text{ in.}^2$$

In some cases, it is easier to subtract the overlapping areas from the total of individual areas. This is true when only two anchors are used or when $\sqrt{m^2+n^2} > R$ (Fig. A.5).

Example:

l_e = 7-1/2 in., $d_e > R$

D_h = 1 in.

R = 8 in.

m = n = 6 in.

$$A_1 = A_2 = 2[R^2\cos^{-1}(n/R) - n\sqrt{R^2-n^2}]$$
$$= 29.0 \text{ in}^2$$
$$A_{pc} = 4\pi(8)^2 - 4(29.0) - 4\pi(1/2)^2 \qquad = 685 \text{ in.}^2$$

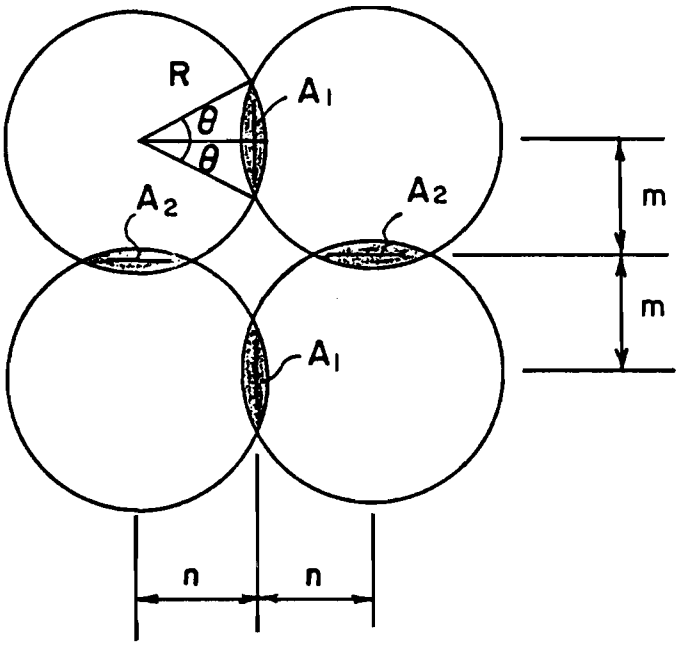

Fig. A.5 Projected area, $\sqrt{\overline{m^2 + n^2}}r$

A.2.2 Design Examples

Example #1

Assume a 4-bolt configuration subjected to a 10-kip load (Fig. A.6), $f'_c = 4000$ psi

$M = 270$ kip-in.

Try a 6 in. bolt spacing in the direction of the load; 5 in. spacing other direction; plate width = 8 in.; (Fig. A.7a)

$d = 9$ in.

$M = T(d - a/2) = Tz$ (2.16), repeated

Assume $z = 8$ in., then $T = 33.75$ kips

$T = C = 0.85f'_c ab$ (2.15), repeated

$a = (0.85)(4)(8) = 1.24$ in.

$z = d - (a/2) = 8.38$ in.

$T = 32.1$ kips

$P_u = 1.7T = 54.6$ kips

Design Tension Bolts

$P_u \leq \phi_s P_s$ (2.1), repeated

$P_s = A_s f_y$ (2.2), repeated

$\phi_s = 0.90$ $f_y = 92$ ksi for A325 Bolts

$$A_{s\ min} = \frac{54.6}{(0.90)(92)} = 0.66 \text{ in.}^2$$ (Tensile stress area must be used.)

Use two 3/4-in. diameter A325 bolts $A_{ts} = 0.67$ in.^{2} o.k.

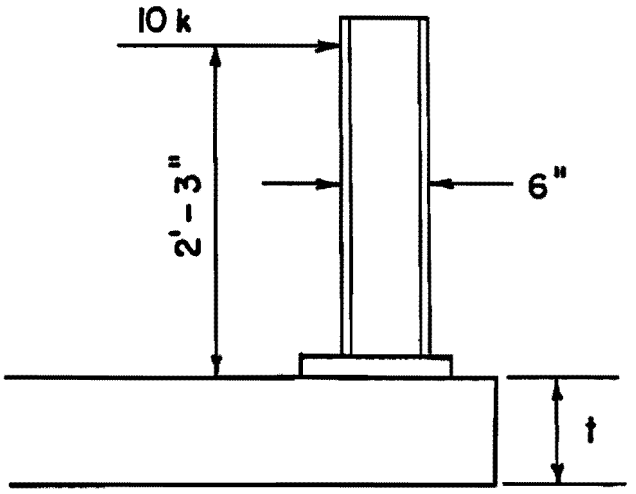

Fig. A.6 Design example No. 1

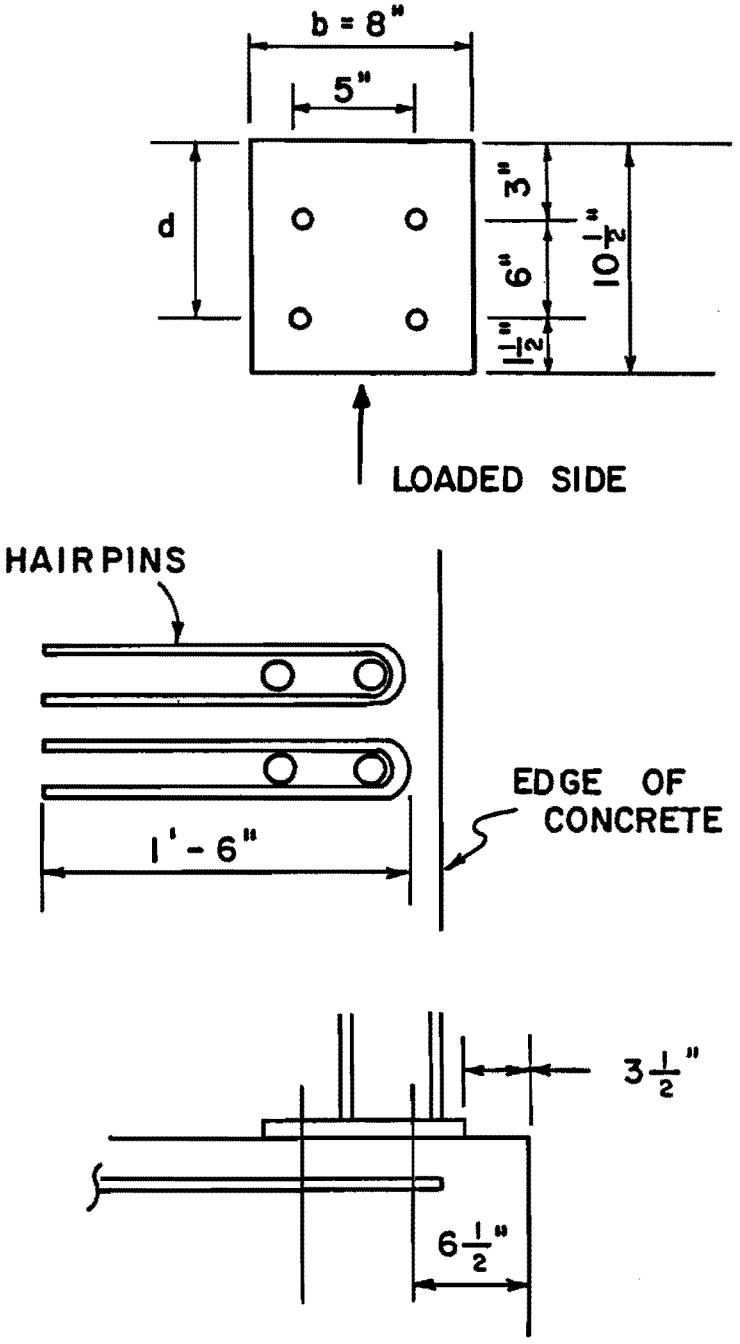

Fig. A.7 Design example No. 1, details

Design Bolts for Shear

$$f_{yv} = 0.67\ f_{ut} \qquad \text{(2.9), repeated}$$

$$f_{ut} = 120 \text{ ksi}$$

$$f_{yv} = 81 \text{ ksi}$$

$$V_u \leq \phi_s V_s \qquad \text{(2.7), repeated}$$

$$\phi_s = 0.90$$

$$V_s = A_s f_{yv} \qquad \text{(2.8), repeated}$$

$$V_u = 1.7(10) = 17 \text{ kips}$$

$$A_{s\ min} = \frac{17}{0.9(81)} = 0.23 \text{ in.}^2$$

In this case, the shear load can be easily taken by the two back bolts -- redistribution of shear load to the tension bolts is not necessary.

Use two 1/2-in. diameter A325 bolts $\quad A_{ts} = 0.28 \text{ in.}^2 \quad$ o.k.

Determine Required Embedment Length

$$\phi_c P_c \geq A_s f_{ut} \qquad \text{(2.17), repeated}$$

$$\phi_c = 0.65$$

$$P_c = 4\sqrt{f'_c}\, A_{pc} \qquad \text{(2.4), repeated}$$

$$f_{ut} = 120 \text{ ksi}$$

$$P_c \geq \frac{(0.67 \text{ in.}^2)(120 \text{ ksi})}{0.65} = 123.7 \text{ kips}$$

$$A_{pc\ min} = \frac{123{,}700}{4\sqrt{4000}} = 489 \text{ in.}^2$$

A_{pc} = projected area of tension anchors minus overlapping areas minus area of anchor heads

Try l_e = 10 in.

$$R = l_e + D_h/2 \qquad D_h = 1\text{-}1/4 \text{ in.}$$

$$R = 10.63 \text{ in}$$

$$A_{pc} = 2\,(10.63)^2 - 2[(10.63)^2\cos^{-1}(2.5/10.63)] - 2.5\sqrt{(10.63)^2 - (2.5)^2} - 2\pi(0.63)^2$$

$$A_{pc} = 457 \text{ in.}^2$$

For l_e = 11 in. A_{pc} = 537 in.^{2}

l_e = 10-1/2 in. A_{pc} = 497 in.^{2}

For 1-1/2 in. cover, slab thickness = t = 12 in.

Alternatively, the bolts could be extended through the slab, requiring only a 10-1/2-in. thick slab.

Another possibility is to tie the tension bolts together on the bottom side of the slab using a steel plate. A trapezoidal failure surface results.

For a 3 in. x 8 in. A36 plate,

$$A_{pc} = (21_e + 8)(21_e + 3) - (3)(8) \geq 489 \text{ in.}^2$$

$$l_{e\ min} = 8.6 \text{ in.}$$

Use a 9-in. thick slab.

Choose plate thickness to prevent punching shear:

$$A = 2\pi D_h t_p$$

$$t_{p\ min} = \frac{80.4 \text{ kips}}{2\pi(1.25 \text{ in.})(14.5 \text{ ksi})} = 0.71 \text{ in.}$$

Use 3/4-in thick plate.

Which of the three possibilities can best prevent pullout failure depends on what thickness of slab is required for flexural strength.

Determine Edge Distance

$$\phi_c V_c \geq A_s f_{ut} \qquad \text{(2.18), repeated}$$

$$V_c = 4\sqrt{f'_c} A_{vc} \qquad \text{(2.11), repeated}$$

$$\phi_c = 0.65$$

$$A_{vc\ min} = \frac{80{,}400}{(0.65)(4)(\sqrt{4000})} = 489 \text{ in.}^2$$

$$R = d_e$$

$$A_{vc} = (1/2)\ d_e^2$$

$$d_{e\ min} = 17.6 \text{ in.}$$

Since the entire shear load is being taken by the back bolts, which are 3 in. from the edge of the base plate, the plate would have to be set 15 in. from the slab edge to give d_e = 18 in. This would not be practical, especially since the slab thickness would have to be increased to 18 in. to develop the full shear cone.

$$\phi_s V_s' \geq A_s f_{ut} \qquad \text{(2.19), repeated}$$

$$V_s' = A_h f_{yh} \qquad \text{(2.12), repeated}$$

$$\phi_s A_h f_{yh} \geq A_s f_{ut} = 80.4 \text{ kips}$$

For f_{yh} = 60 ksi,

$$A_{h\ min} = \frac{80.4}{(0.9)(60)} = 1.49 \text{ in.}^2$$

Area of each leg = 0.37 in.^{2}

Use 2#6 hairpin bars (Fig. A.7b)

$$l_d = 0.04(0.44)(60{,}000)/\sqrt{4000} = 16.7 \text{ in.} \quad \text{Say 18 in.}$$

Check lateral bursting criterion.

$$d_{e\ min} = \sqrt{\frac{A_s f_{ut}}{32\sqrt{f'_c}}} \qquad \text{(2.5), repeated}$$

$$= \sqrt{\frac{80{,}400}{32\sqrt{4000}}}$$

$$d_{e\ min} = 6.3 \text{ in.}$$

Tension bolts are 9 in. from back of base plate, so any setback of the post from the slab edge will work, provided the tension cone surface can fully develop. (Fig. A.7c)

Example #2

Assume a 4-bolt configuration subjected to a 15-kip load (Fig. A.8)

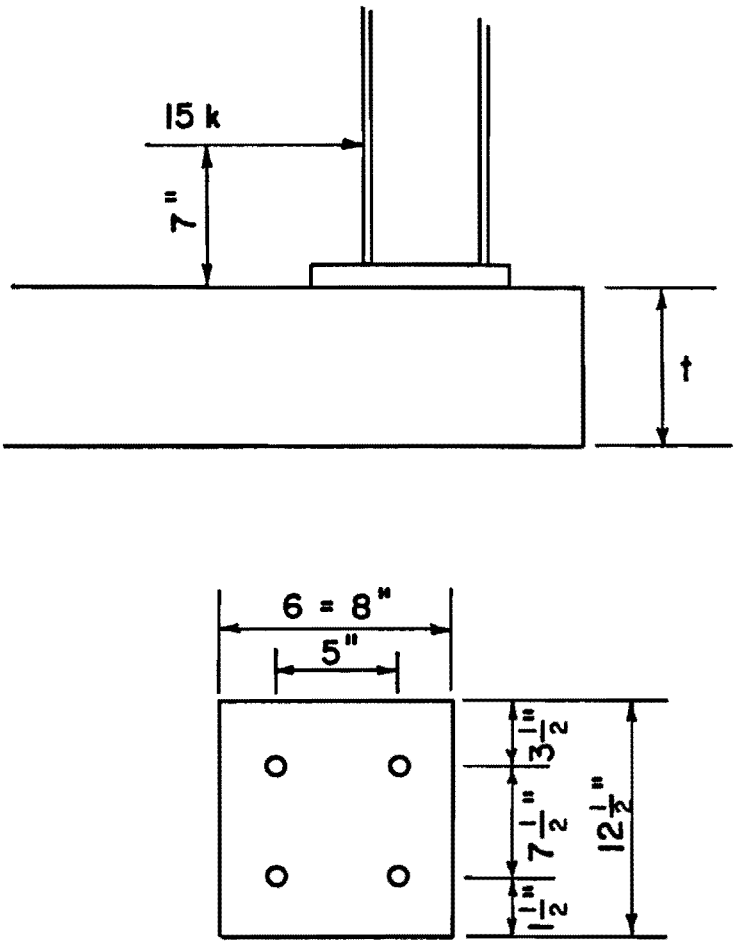

Fig. A.8 Design example No. 2

$f'_c = 4000$ psi

$d = 11$ in.

$M = 105$ kip-in.

$M = T(d - a/2) = Tz$ (2.16), repeated

Assume $z = 10\text{-}1/2$ in., then $T = 10$ kips

$T = C = 0.85f'_c ab$ (2.15), repeated

$$a = \frac{10.0}{(0.85)(4)(8)} = 0.37 \text{ in.}$$

$z = d - (a/2) = 10.8$ in.

$T = 9.7$ kips

$P_u = 1.7\ (9.7) = 16.5$ kips

Design Tension Bolts

$P_u \leq \phi_s P_s$ (2.1), repeated

$P_s = A_s f_y$ (2.2), repeated

$\phi_s = 0.90$ $f_y = 92$ ksi for A325 bolts

$$A_{s\ min} = \frac{16.5}{(0.90)(92)} = 0.20 \text{ in.}^2$$

Use two 1/2-in. diameter A325 bolts. $A_{ts} = 0.28$ in.^{2}

Design Bolts for Shear

$f_{yv} = 0.67\ f_{ut}$ (2.9), repeated

$f_{ut} = 120$ ksi $f_{yv} = 81$ ksi

$V_u \leq \phi_s V_s$ (2.7), repeated

$\phi_s = 0.90$

$$V_s = A_s f_{yv} \qquad \text{(2.8), repeated}$$

$$V_u = (1.7)(15 \text{ kips}) = 25.5 \text{ kips}$$

$$A_s = \frac{25.5}{(0.90)(81)} = 0.35 \text{ in.}^2$$

Try two 1/2-in. diameter bolts $\quad A_{ts} = 0.28 \text{ in.}^2$

$$\phi_s V_s = (0.90)(0.28)(81) = 20.4 \text{ kips}$$

The remaining 5.1 kips must then be redistributed to the front bolts.

Check

$$\frac{P_u}{\phi_s P_s} + \frac{V_u}{\phi_s V_s} \leq 1.0 \qquad \text{(2.14), repeated}$$

$$\frac{16.5}{(0.90)(0.28)(92)} + \frac{5.1}{(0.90)(0.28)(81)} = 0.96 \leq 1.0 \quad \text{o.k.}$$

Use two 1/2-in. dia. A325 bolts in front

two 1/2-in. dia. A325 bolts in back

The rest of the design proceeds as in Example #1.

APPENDIX B

Additional Results from Impact Tests on West-end Post

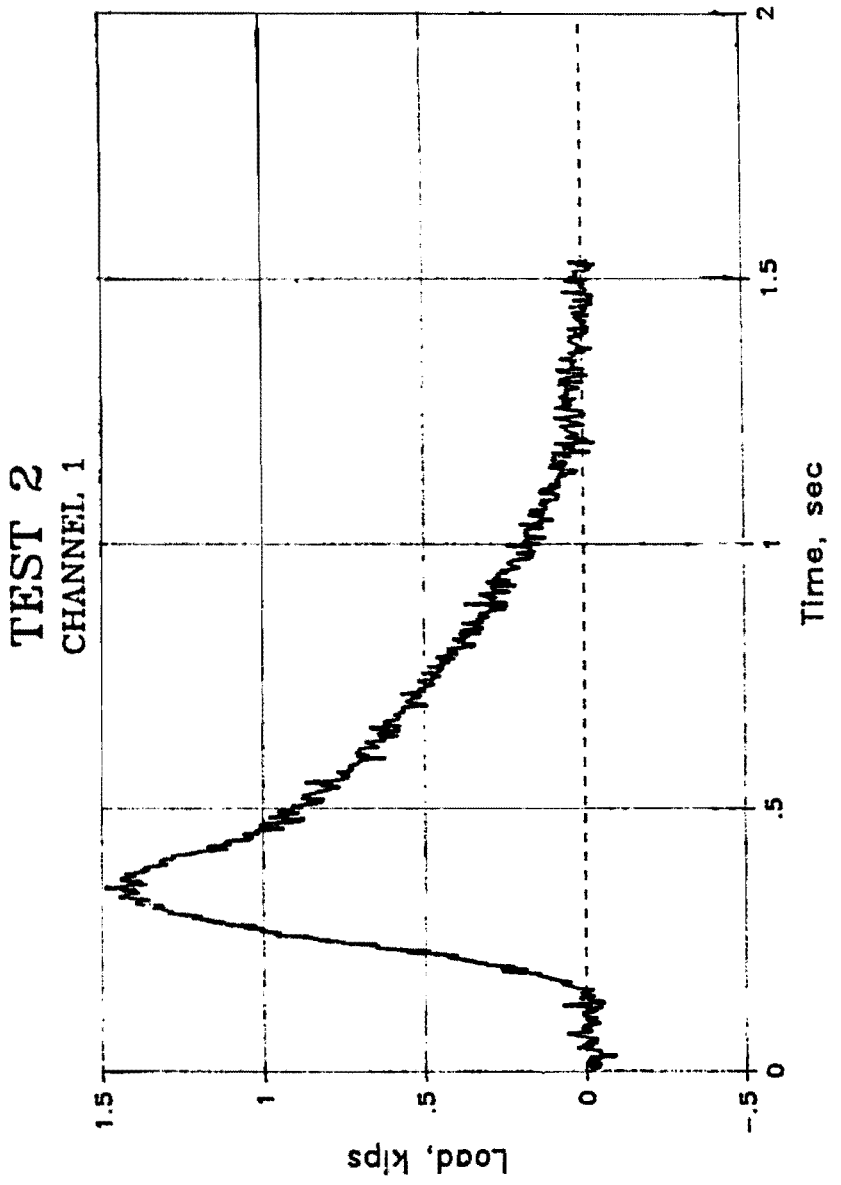
TEST 2
CHANNEL 1
Load, kips
1.5
1
.5
0
-.5
Time, sec
0
.5
1
1.5
2

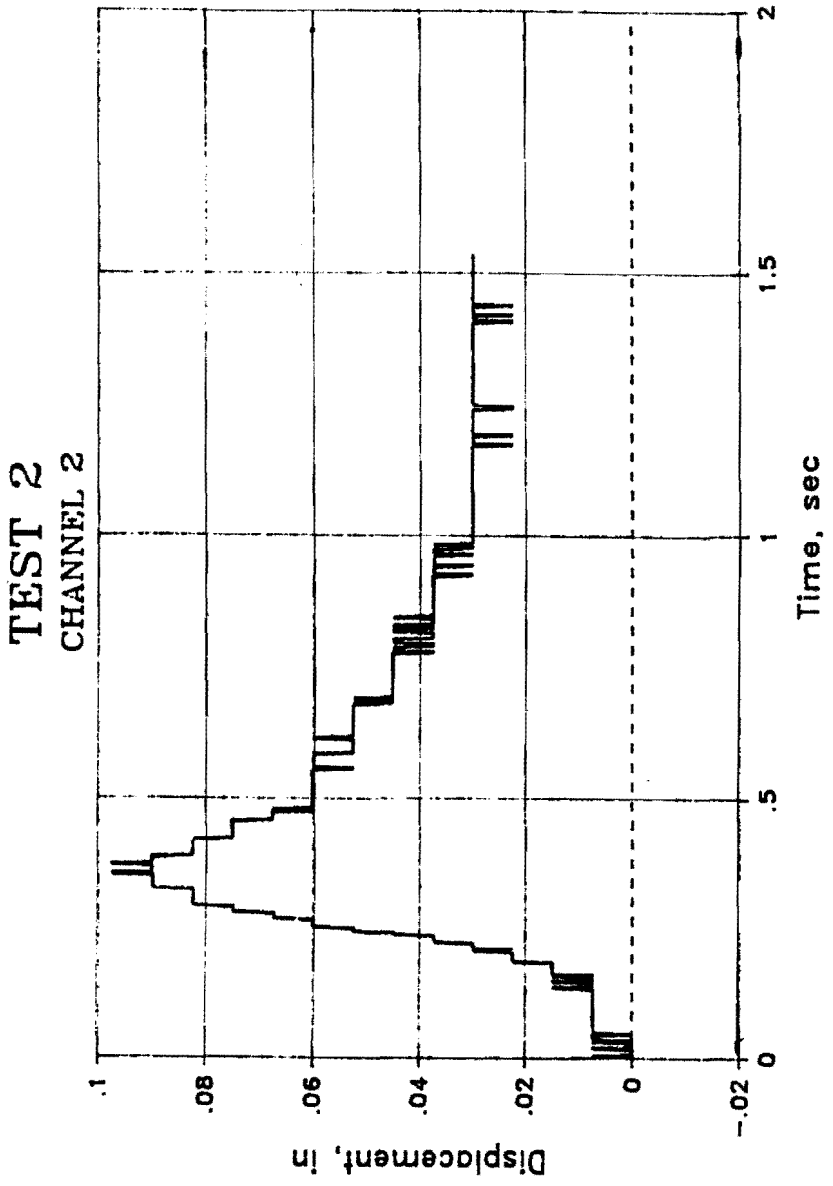
TEST 2
CHANNEL 2
Displacement, in
.1
.08
.06
.04
.02
0
-.02
0
.5
1
1.5
2
Time, sec

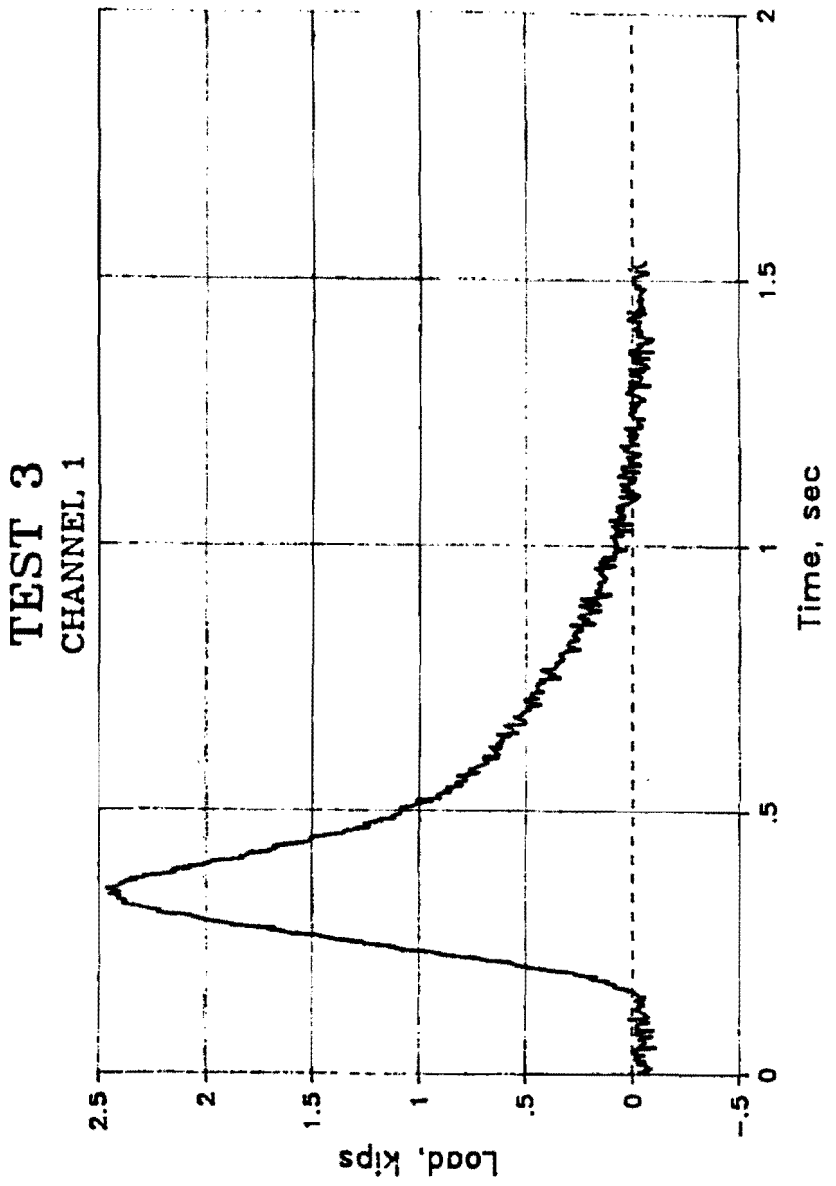
TEST 3
CHANNEL 1
Load, kips
2.5
2
1.5
1
.5
0
-.5
Time, sec
0
.5
1
1.5
2

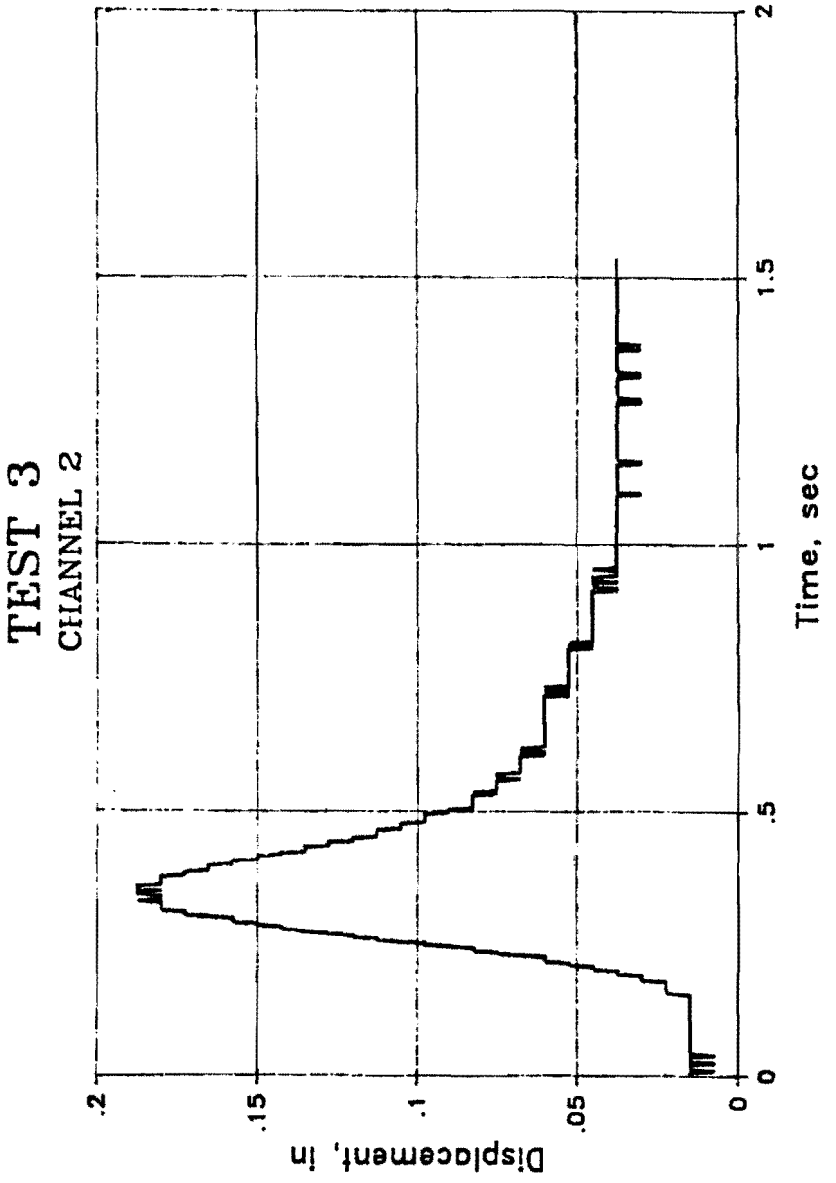
TEST 3
CHANNEL 2
Displacement, in
.2
.15
.1
.05
0
0
.5
1
1.5
2
Time, sec

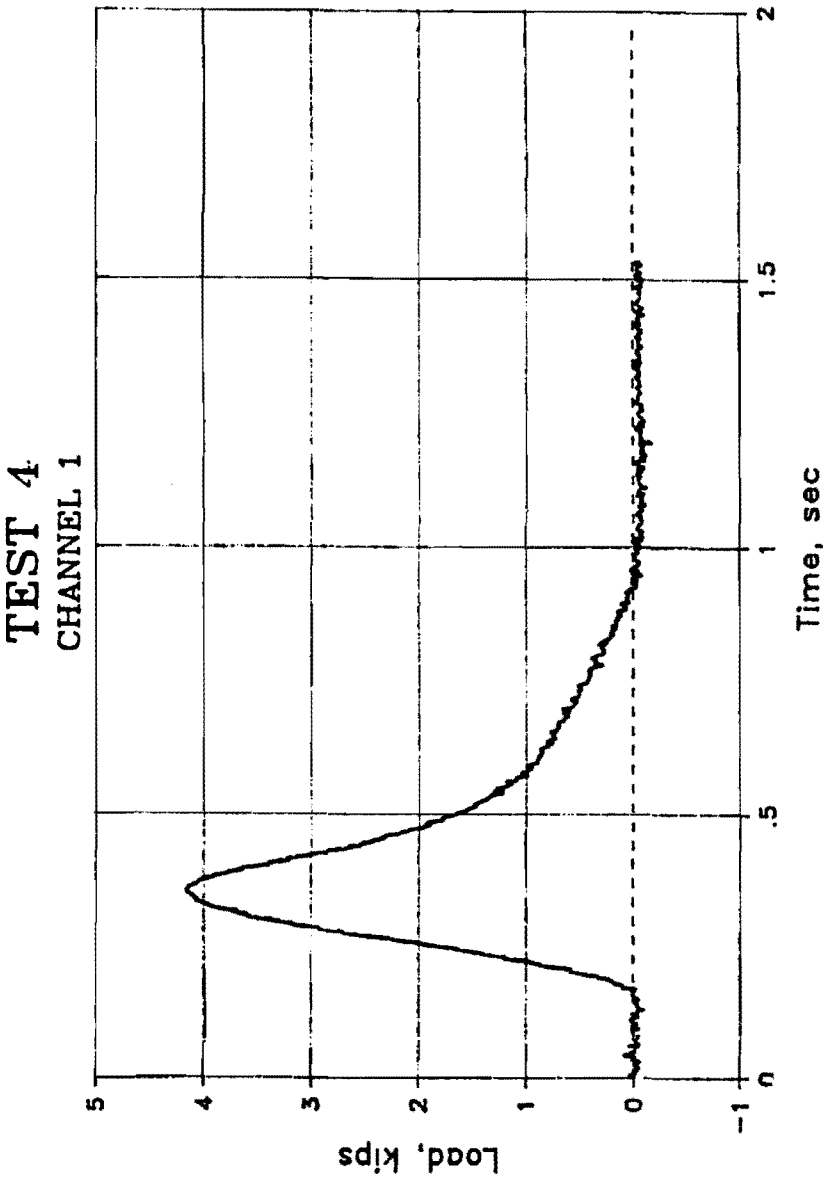
TEST 4
CHANNEL 1
Load, kips
5
4
3
2
1
0
-1
0
.5
1
1.5
2
Time, sec

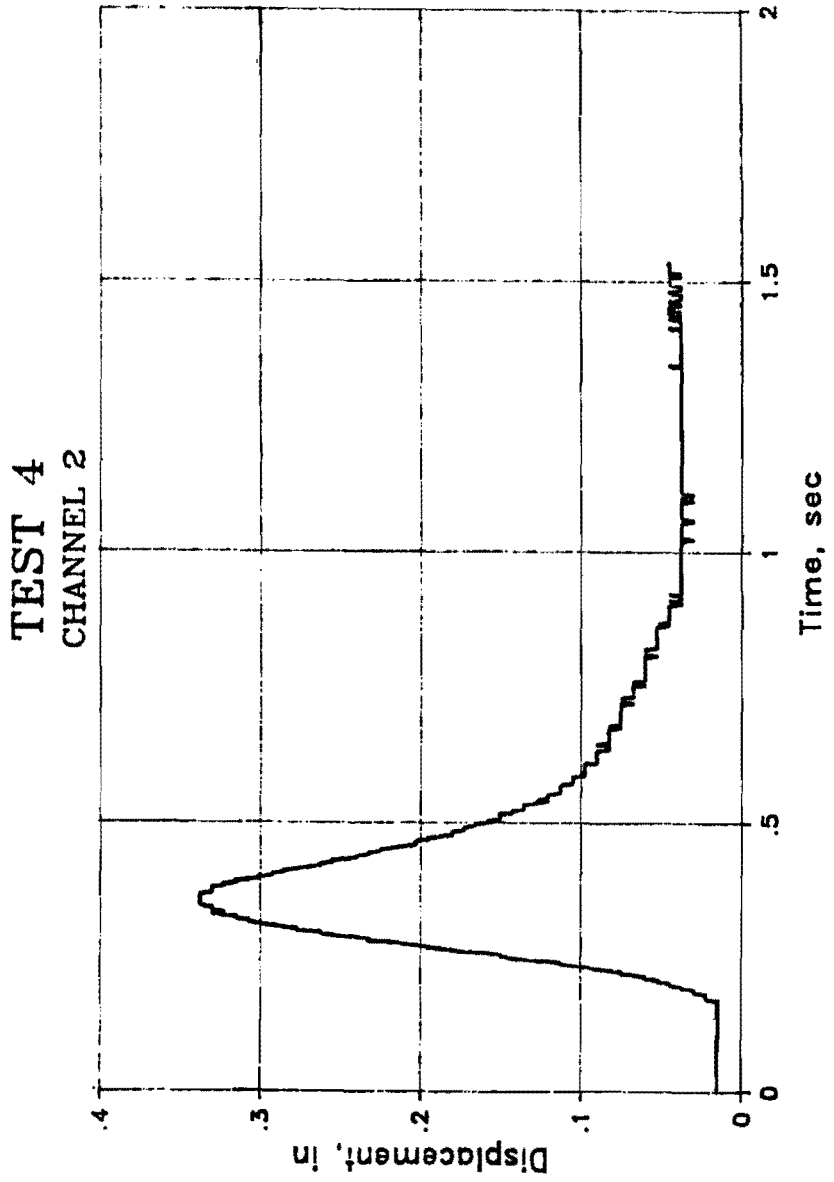
TEST 4
CHANNEL 2
Displacement, in
.4
.3
.2
.1
0
0
.5
1
1.5
2
Time, sec

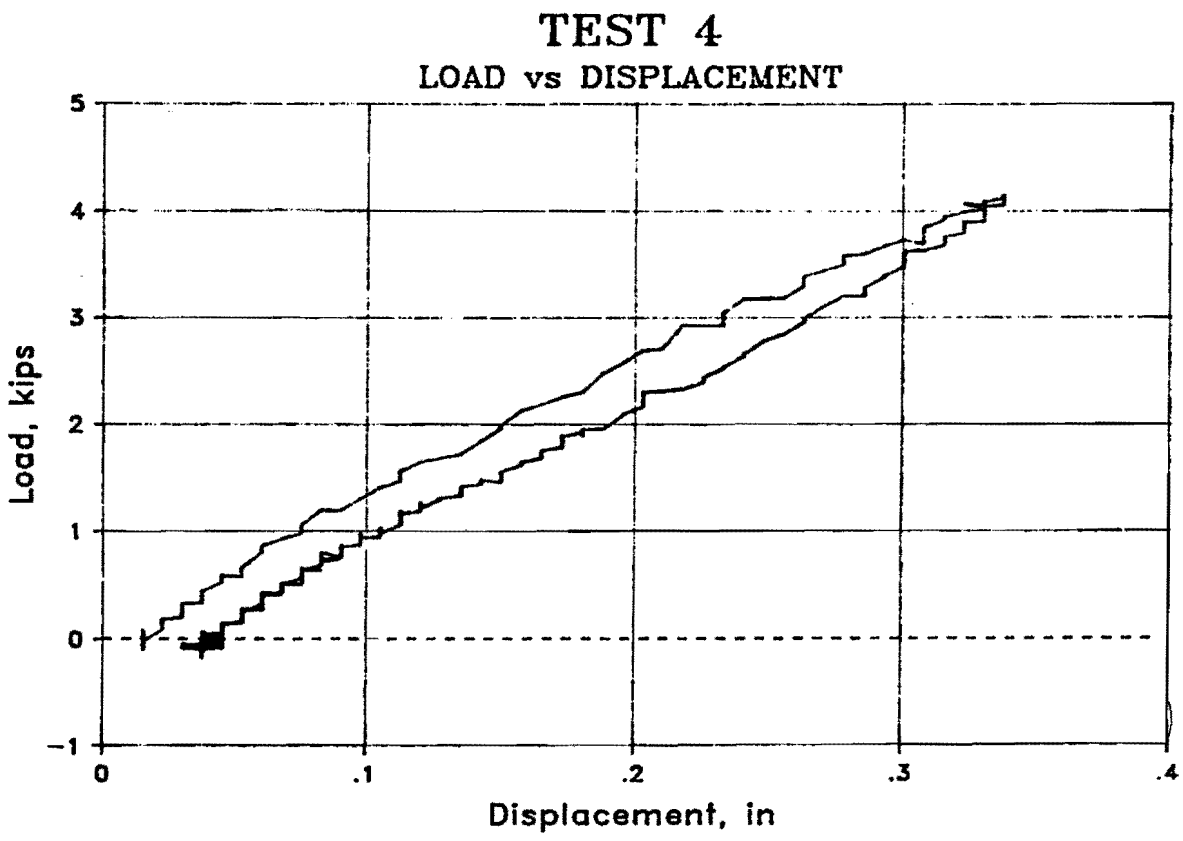
TEST 4
LOAD vs DISPLACEMENT
Load, kips
5
4
3
2
1
0
−1
0
.1
.2
.3
.4
Displacement, in

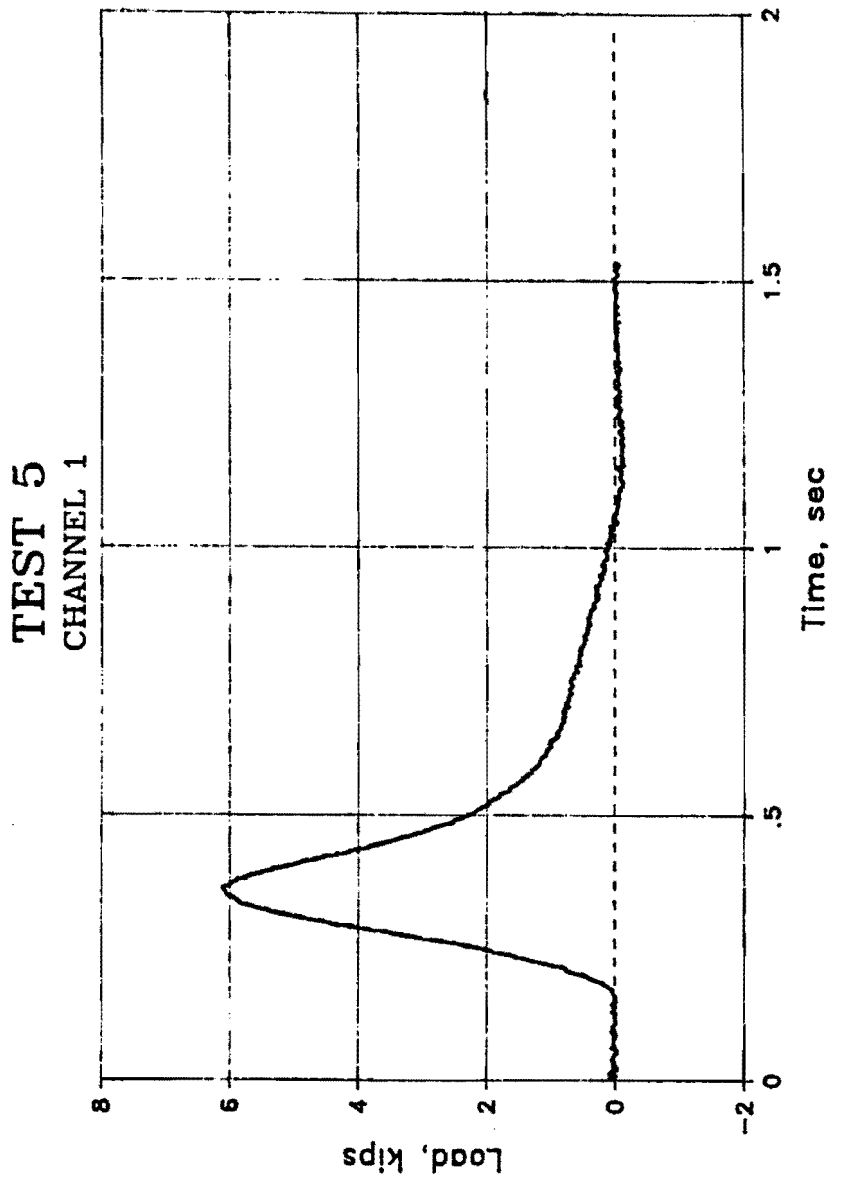
TEST 5
CHANNEL 1
Load, kips
8
6
4
2
0
-2
0
.5
1
1.5
2
Time, sec

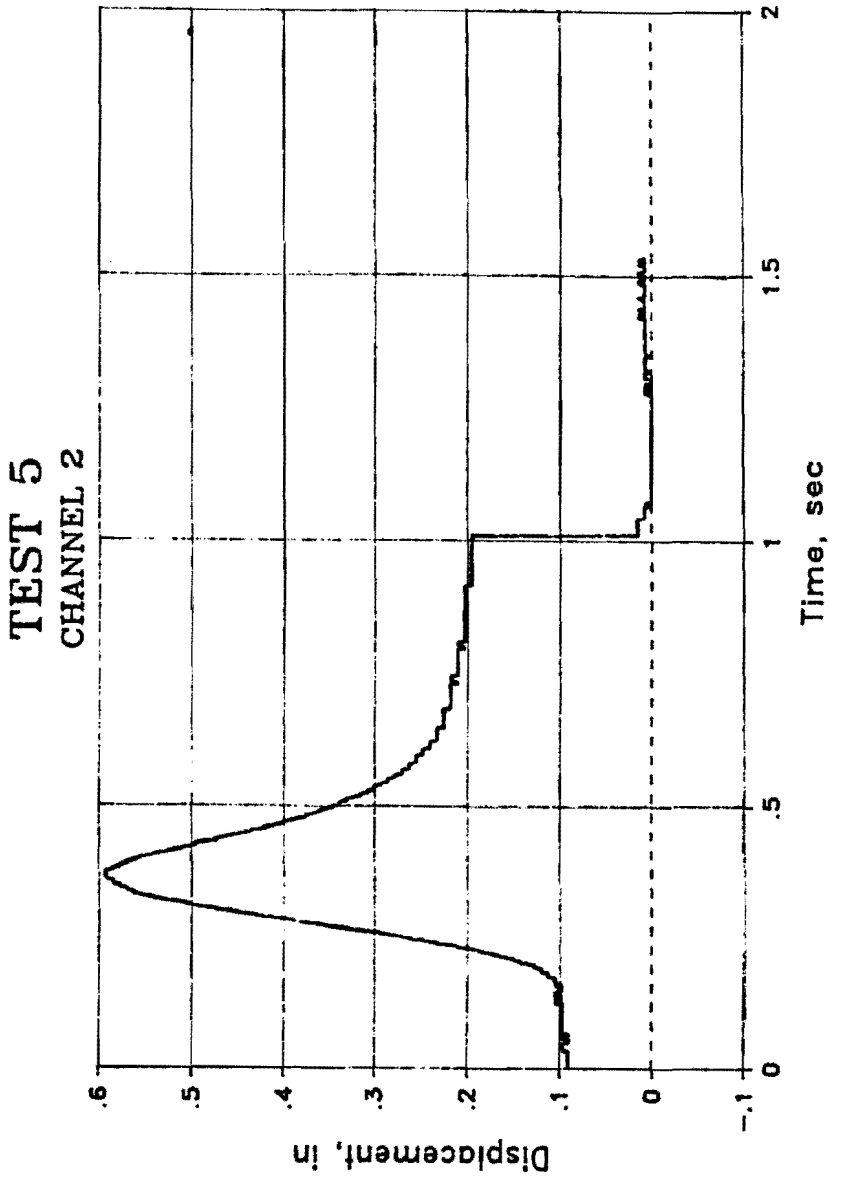
TEST 5
CHANNEL 2
Displacement, in
.6
.5
.4
.3
.2
.1
0
-.1
0
.5
1
1.5
2
Time, sec

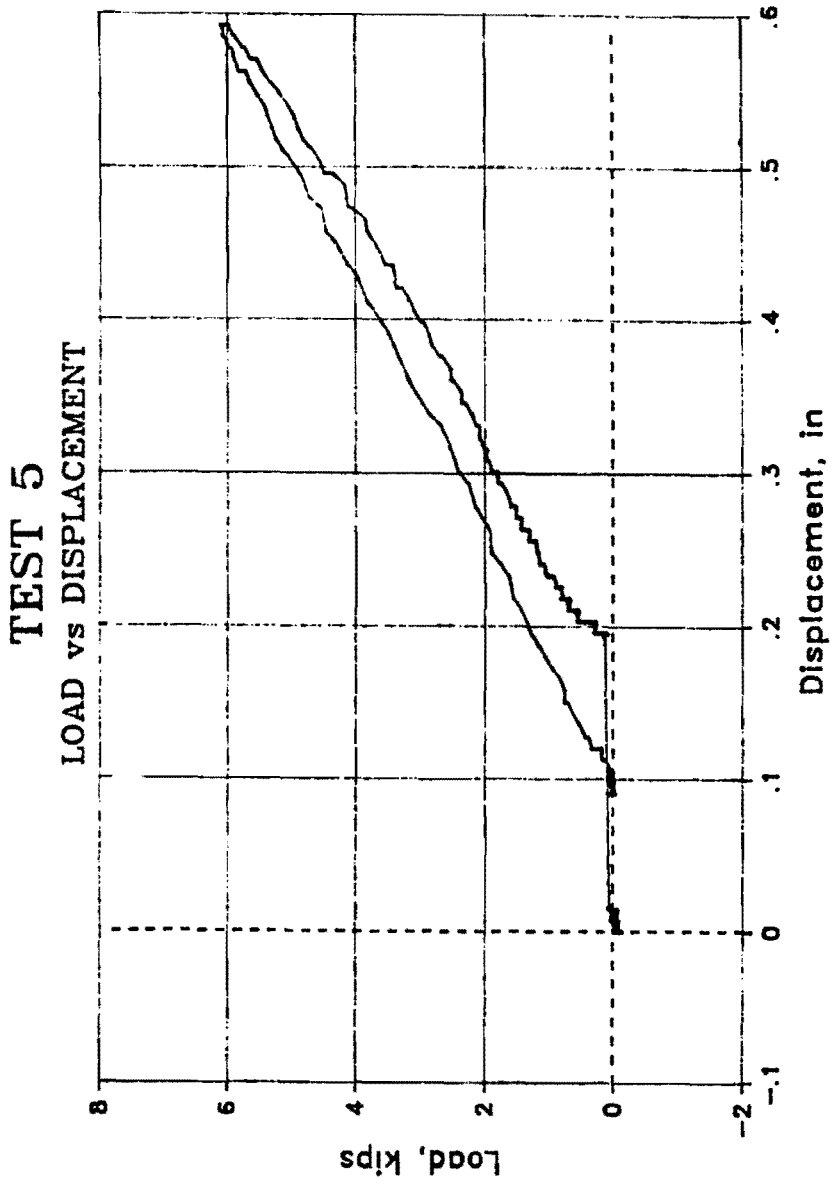
TEST 5
LOAD vs DISPLACEMENT
Load, kips
8
6
4
2
0
-2
.6
.5
.4
.3
.2
.1
0
-.1
Displacement, in

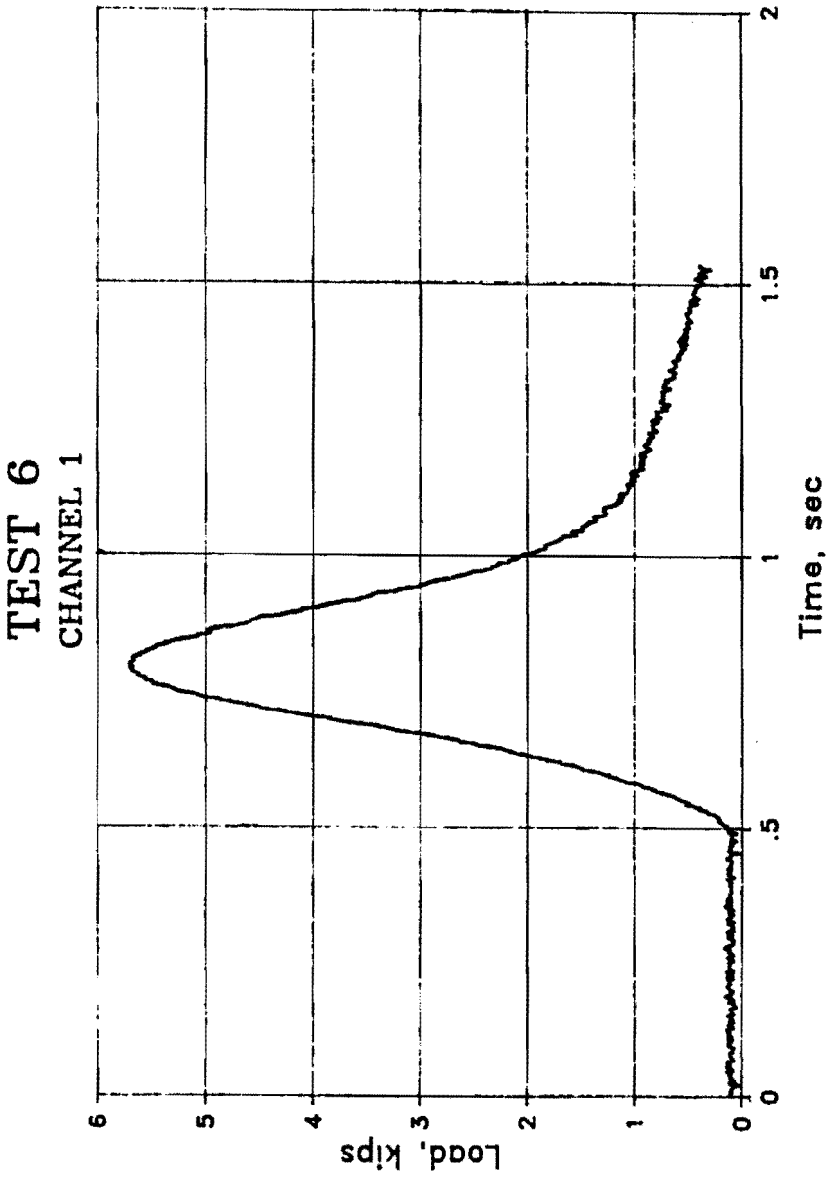
TEST 6
CHANNEL 1
Load, kips
0
1
2
3
4
5
6
Time, sec
0
.5
1
1.5
2

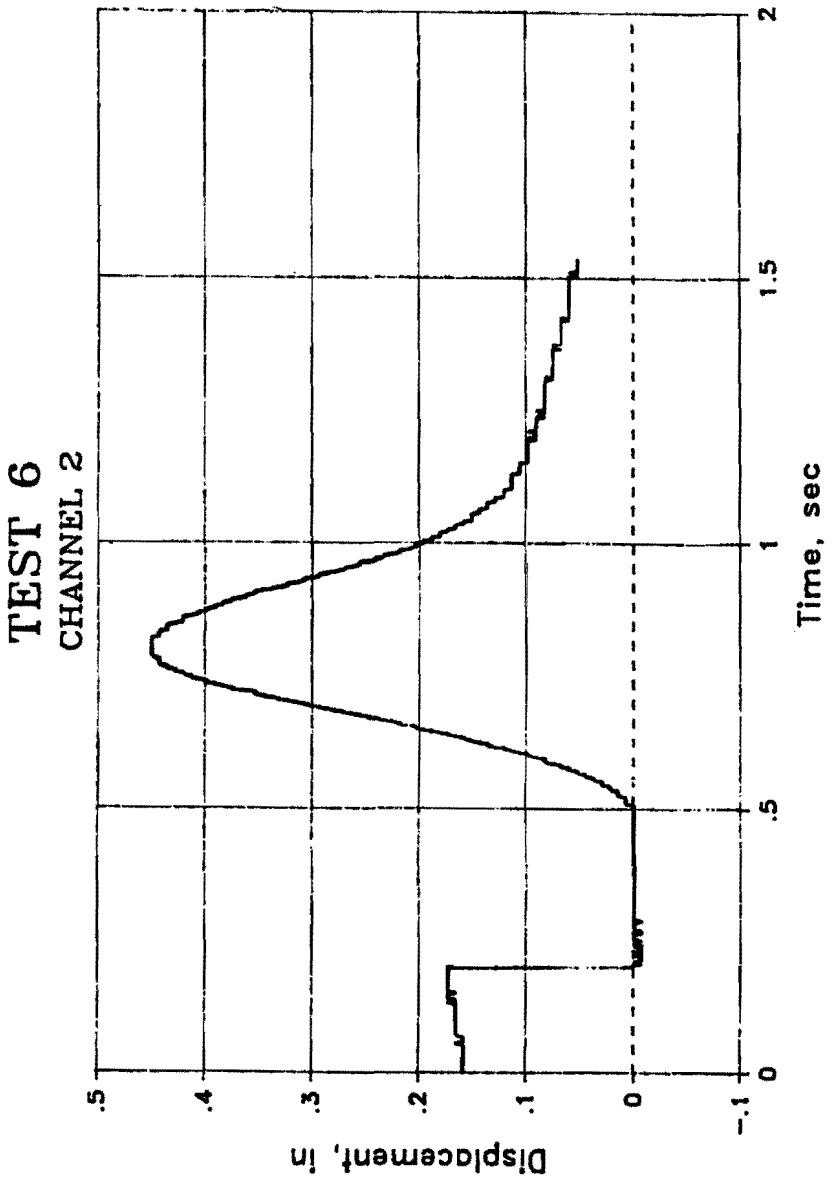
TEST 6
CHANNEL 2
Displacement, in
.5
.4
.3
.2
.1
0
-.1
0
.5
1
1.5
2
Time, sec

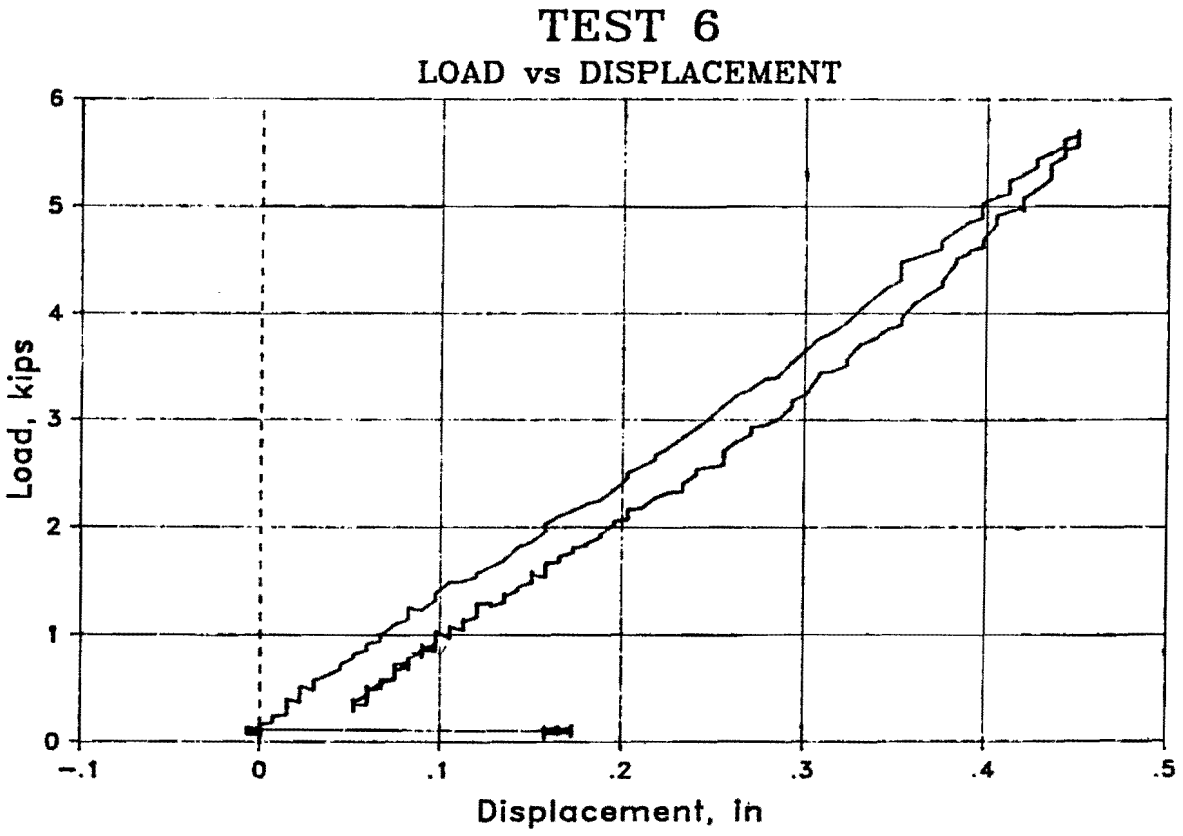
TEST 6
LOAD vs DISPLACEMENT
Load, kips
Displacement, in
6
5
4
3
2
1
0
-.1
0
.1
.2
.3
.4
.5

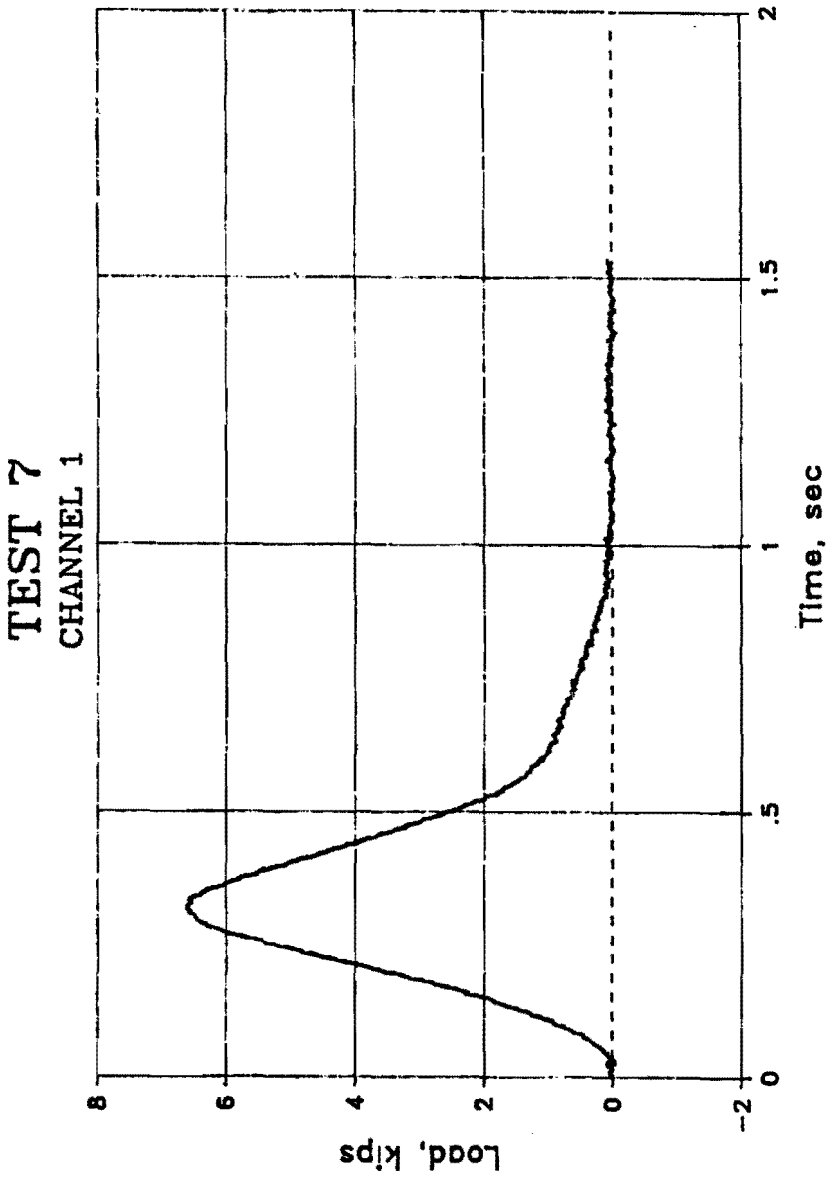
TEST 7
CHANNEL 1
Load, kips
8
6
4
2
0
-2
0
.5
1
1.5
2
Time, sec

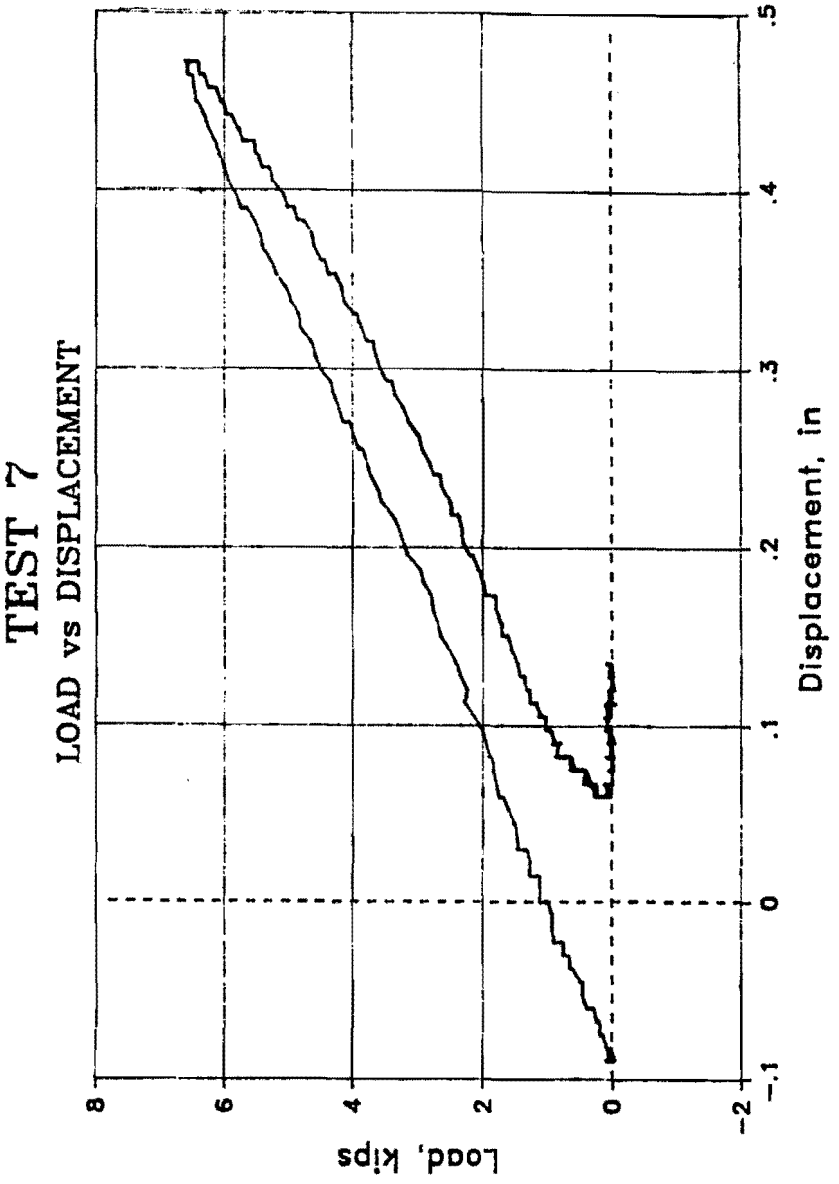
TEST 7
LOAD vs DISPLACEMENT
Load, kips
8
6
4
2
0
-2
Displacement, in
.5
.4
.3
.2
.1
0
-.1

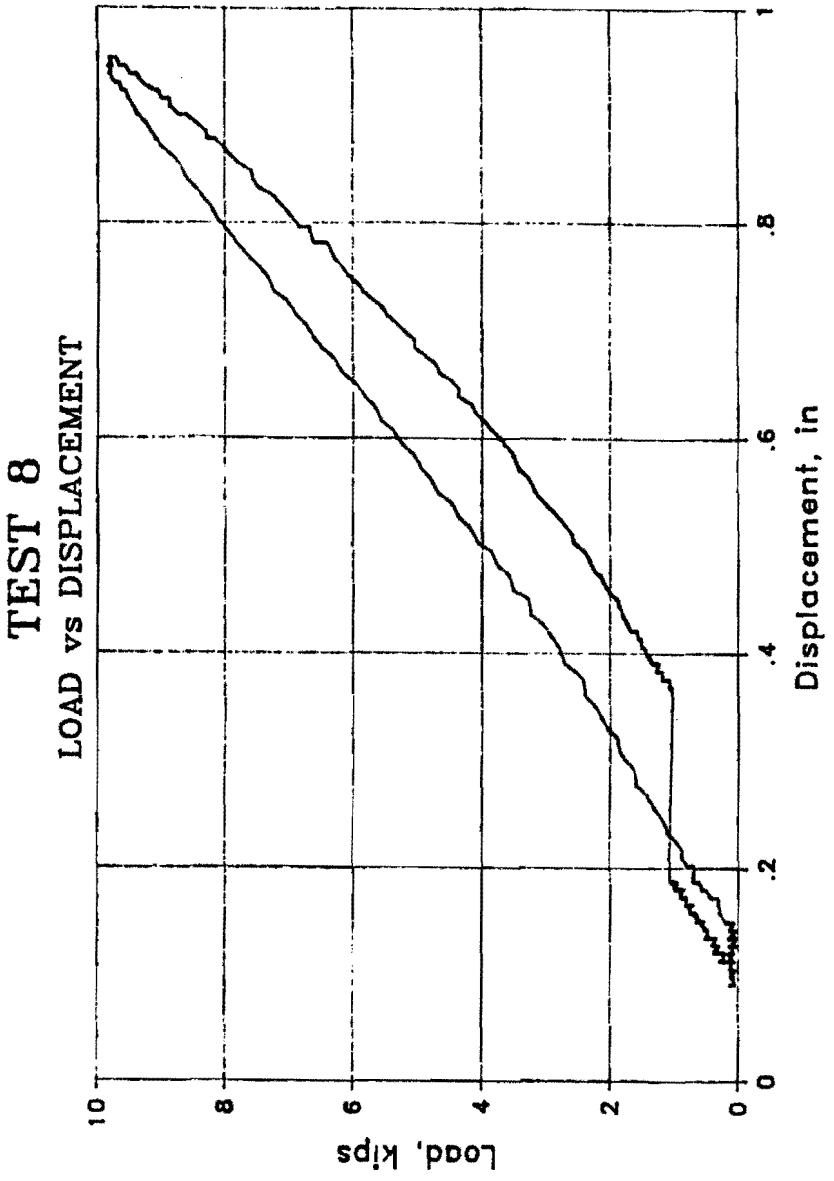
TEST 8
LOAD vs DISPLACEMENT
Load, kips
0
2
4
6
8
10
Displacement, in
0
.2
.4
.6
.8
1

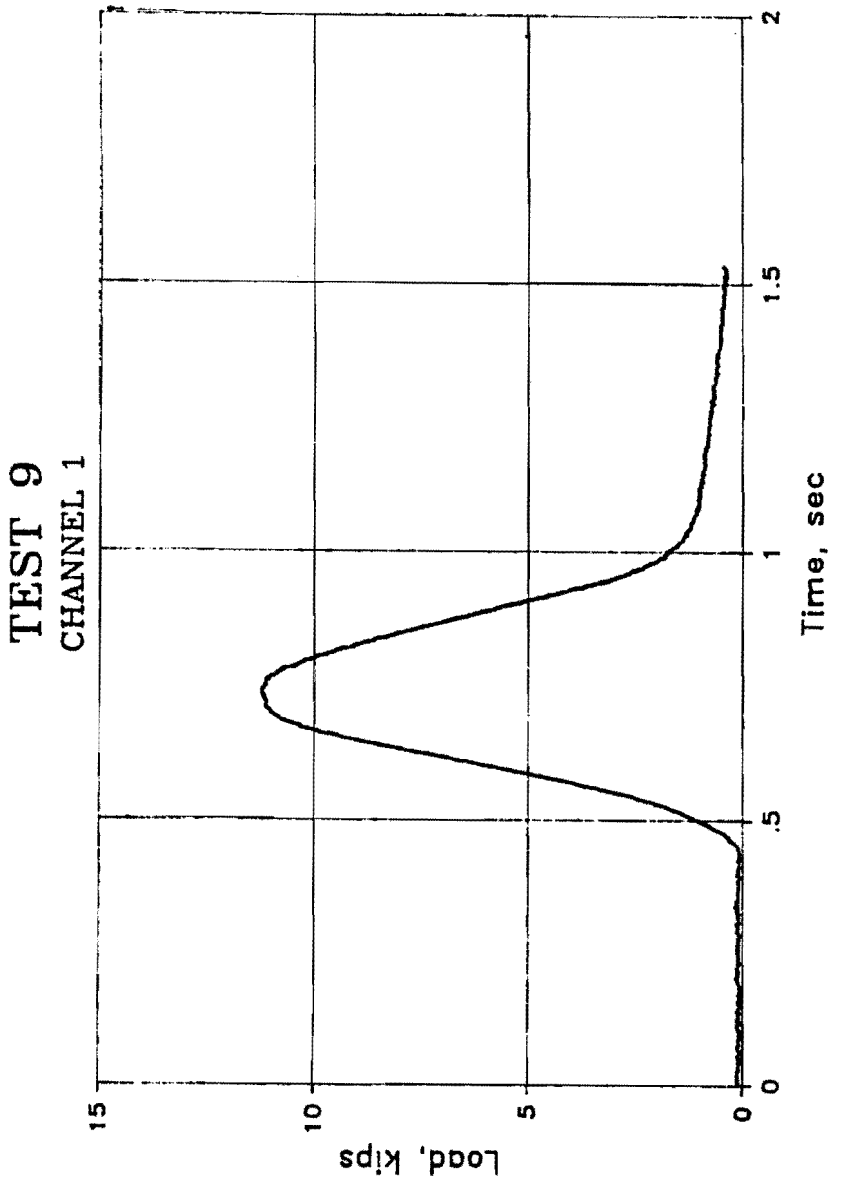
TEST 9
CHANNEL 1
Load, kips
15
10
5
0
0
.5
1
1.5
2
Time, sec

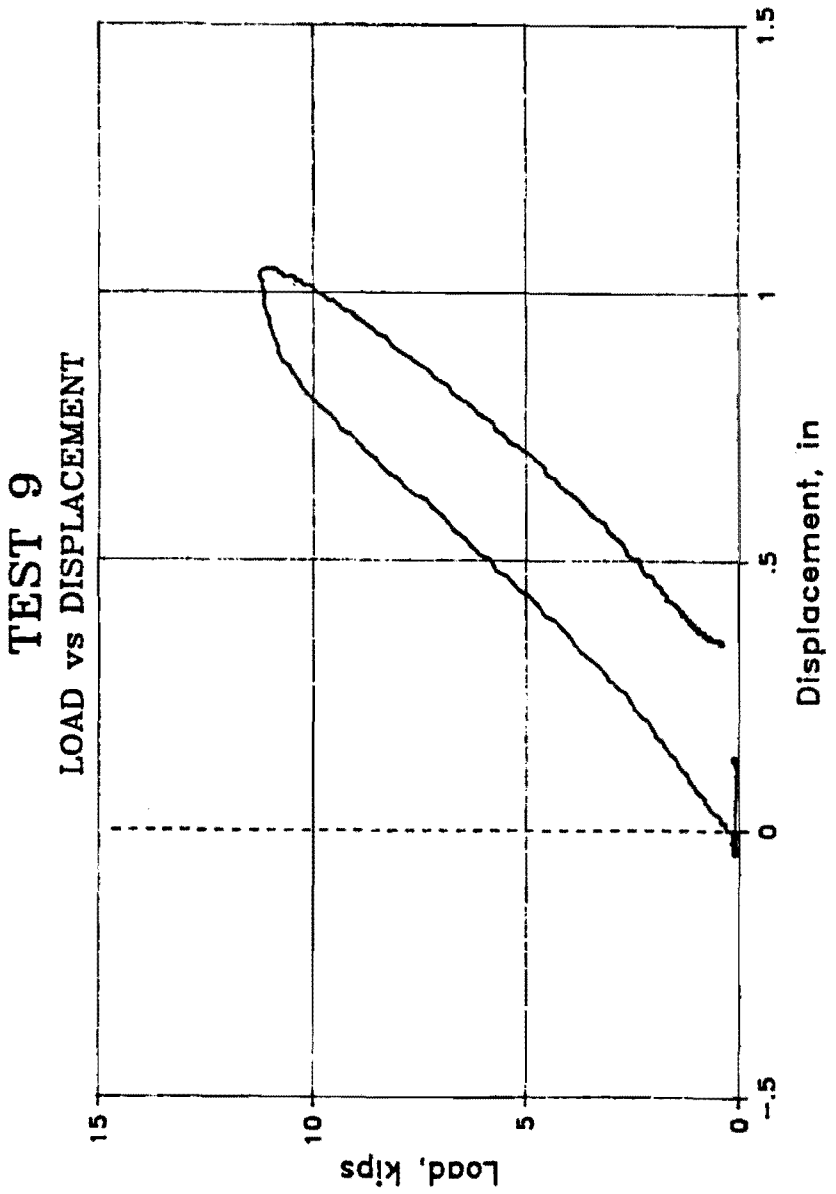
TEST 9
LOAD vs DISPLACEMENT
Load, kips
15
10
5
0
-.5
0
.5
1
1.5
Displacement, in

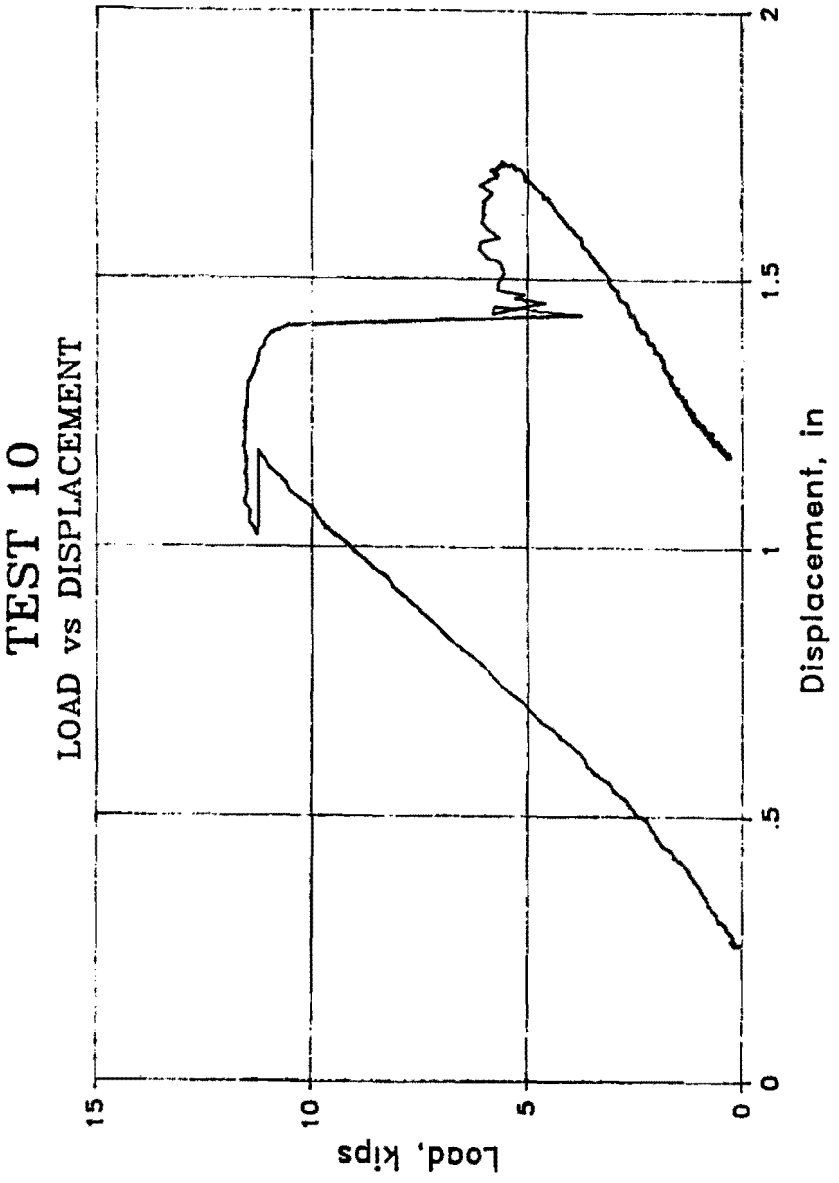
TEST 10
LOAD vs DISPLACEMENT
Load, kips
15
10
5
0
0
.5
1
1.5
2
Displacement, in

APPENDIX C

Additional Results from Impact Tests on East-end Post

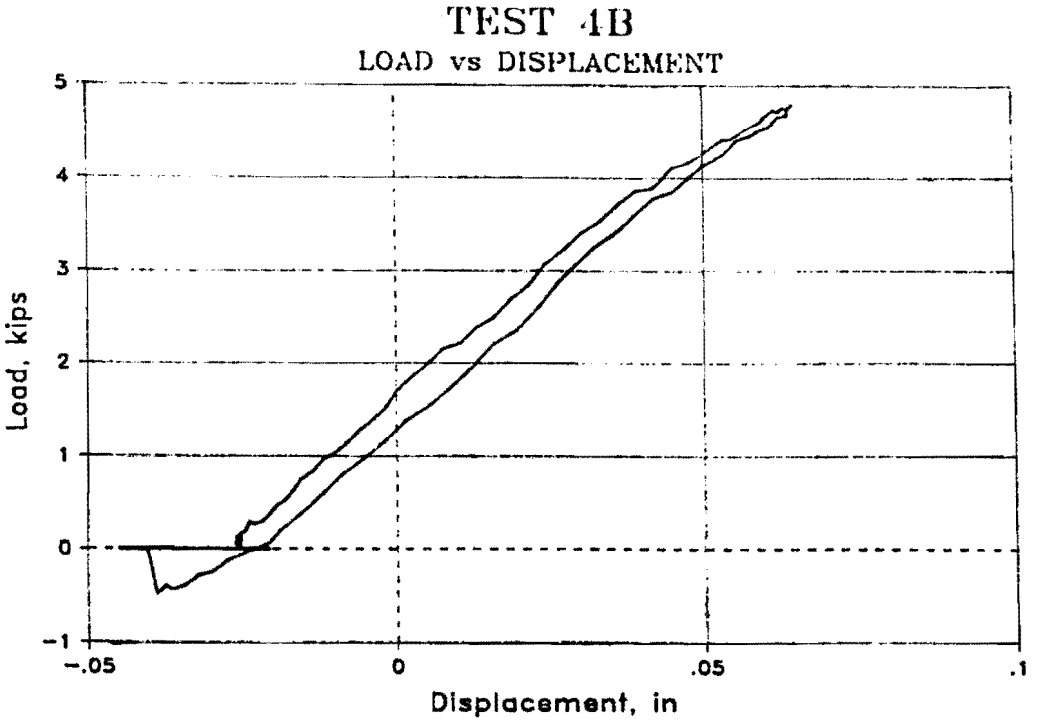
TEST 4B
LOAD vs DISPLACEMENT
Load, kips
5
4
3
2
1
0
-1
-.05
0
.05
.1
Displacement, in

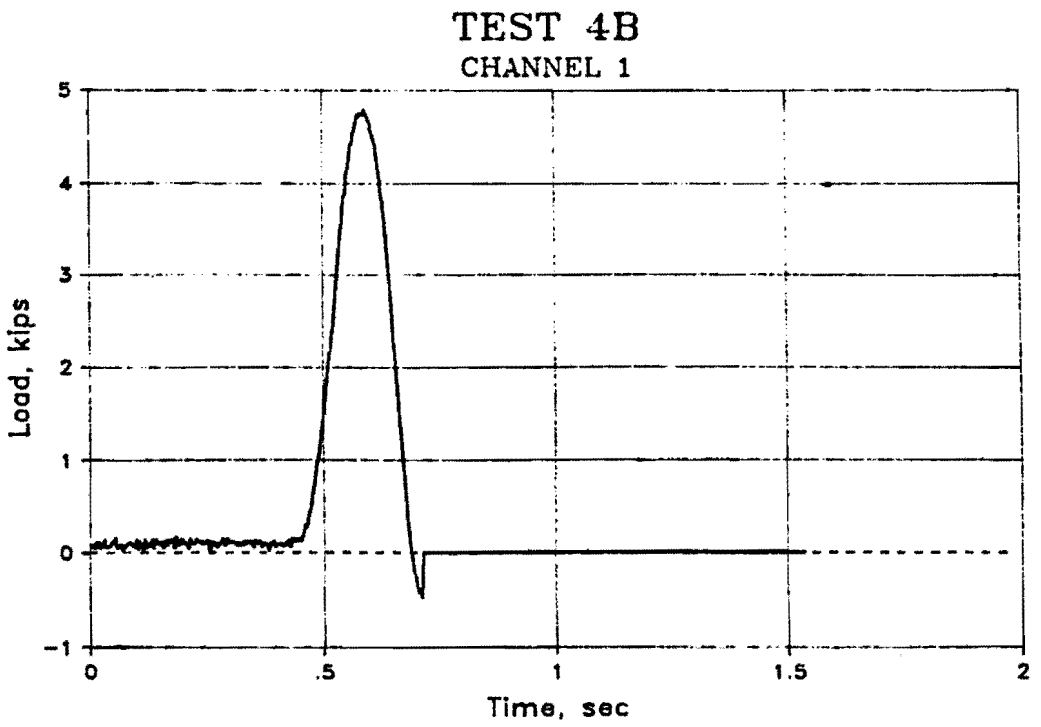
TEST 4B
CHANNEL 1
Load, kips
5
4
3
2
1
0
-1
0
.5
1
1.5
2
Time, sec

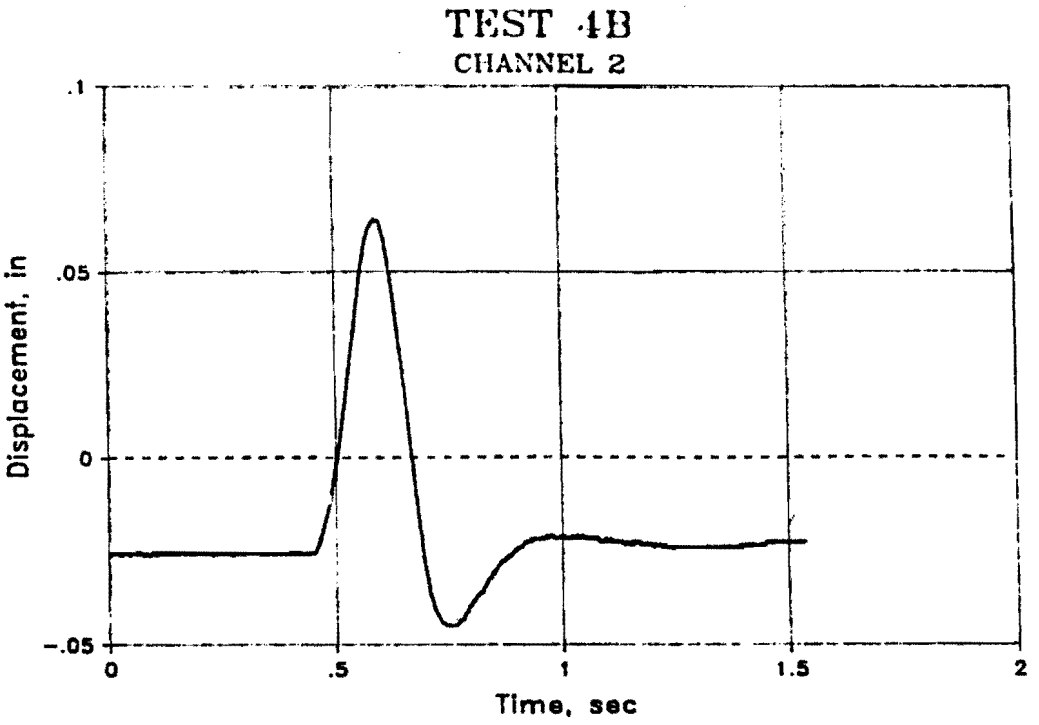
TEST 4B
CHANNEL 2
.1
.05
0
-.05
Displacement, in
0
.5
1
1.5
2
Time, sec

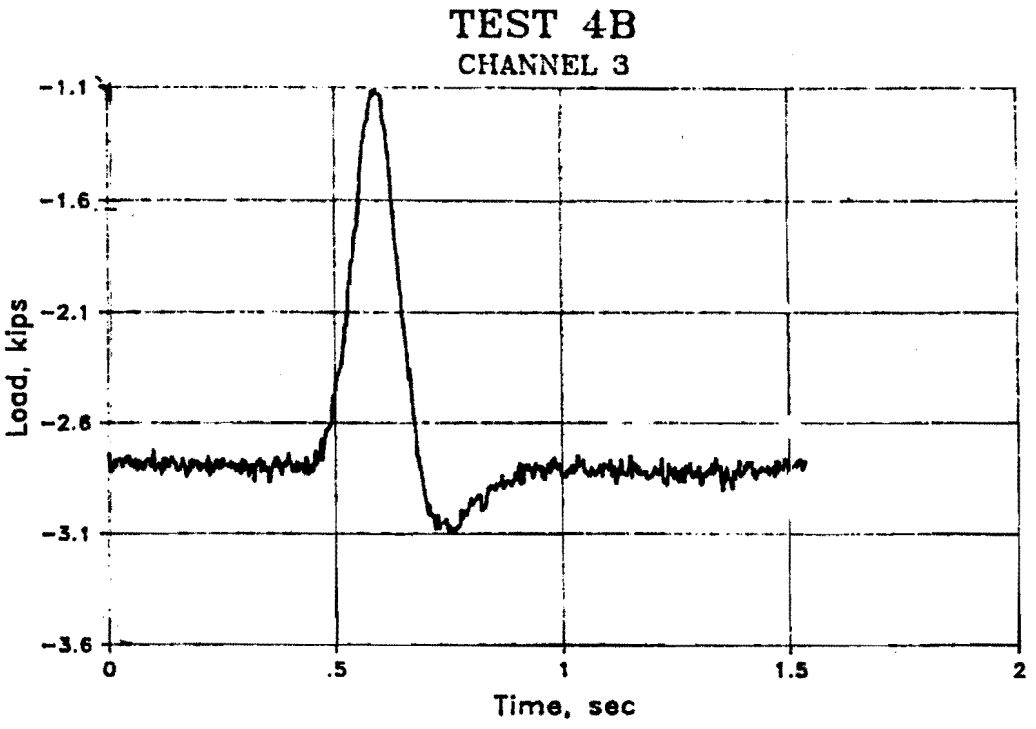
TEST 4B
CHANNEL 3
-1.1
-1.6
-2.1
-2.6
-3.1
-3.6
Load, kips
0
.5
1
1.5
2
Time, sec

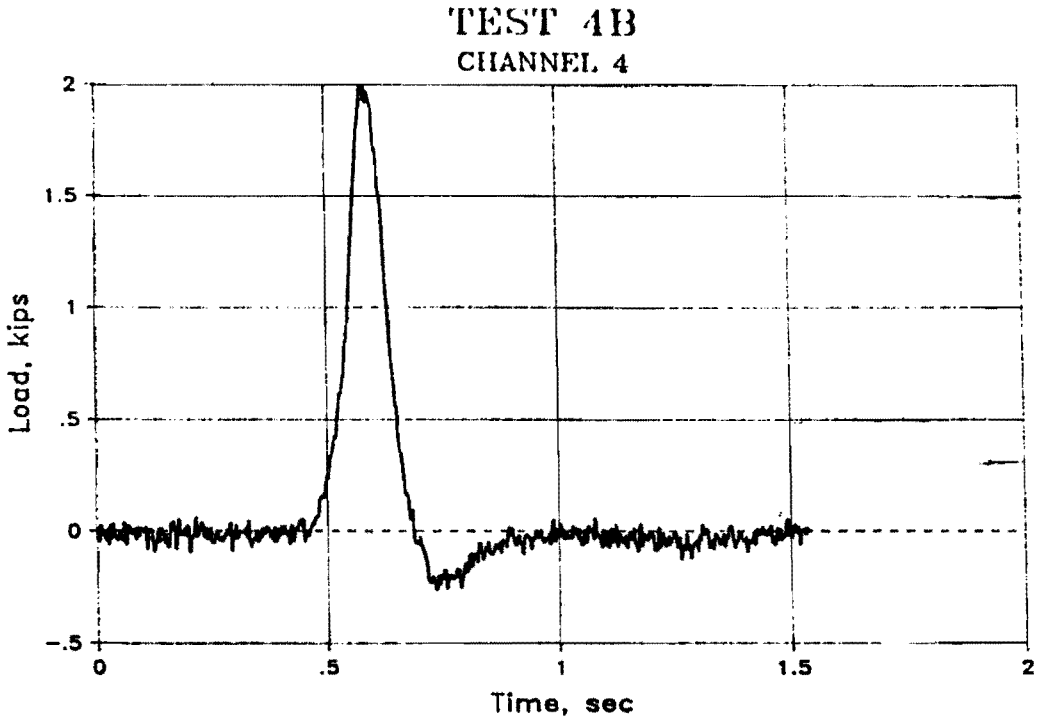
TEST 4B
CHANNEL 4
Load, kips
2
1.5
1
.5
0
-.5
0
.5
1
1.5
2
Time, sec

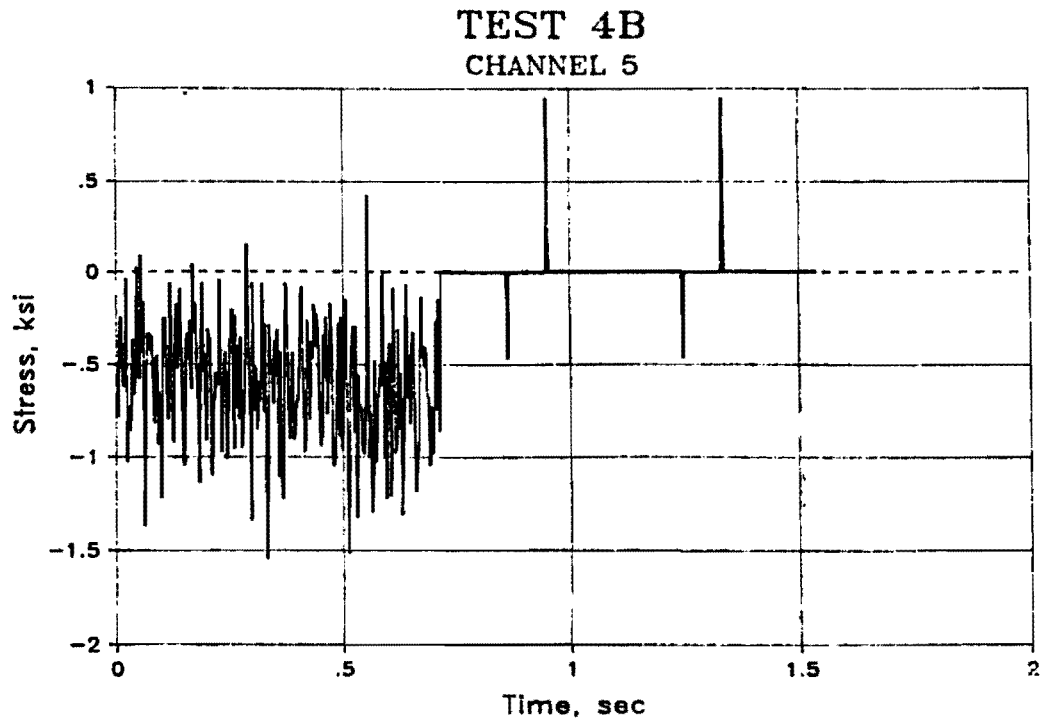
TEST 4B
CHANNEL 5
Stress, ksi
1
.5
0
-.5
-1
-1.5
-2
0
.5
1
1.5
2
Time, sec

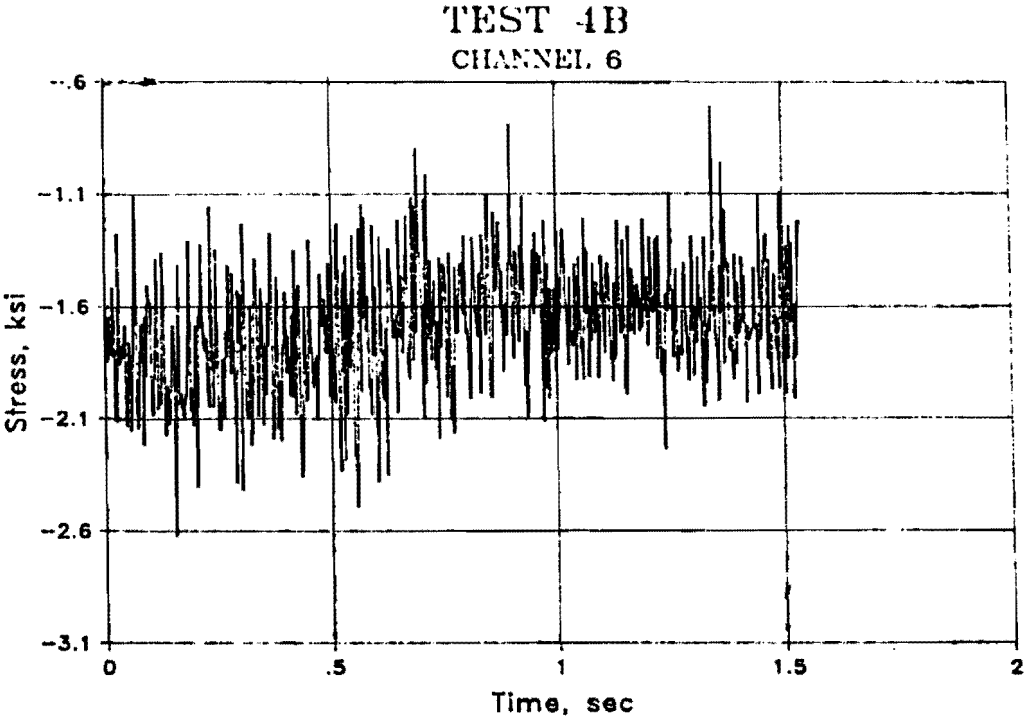
TEST 4B
CHANNEL 6
-.6
-1.1
-1.6
-2.1
-2.6
-3.1
Stress, ksi
0
.5
1
1.5
2
Time, sec

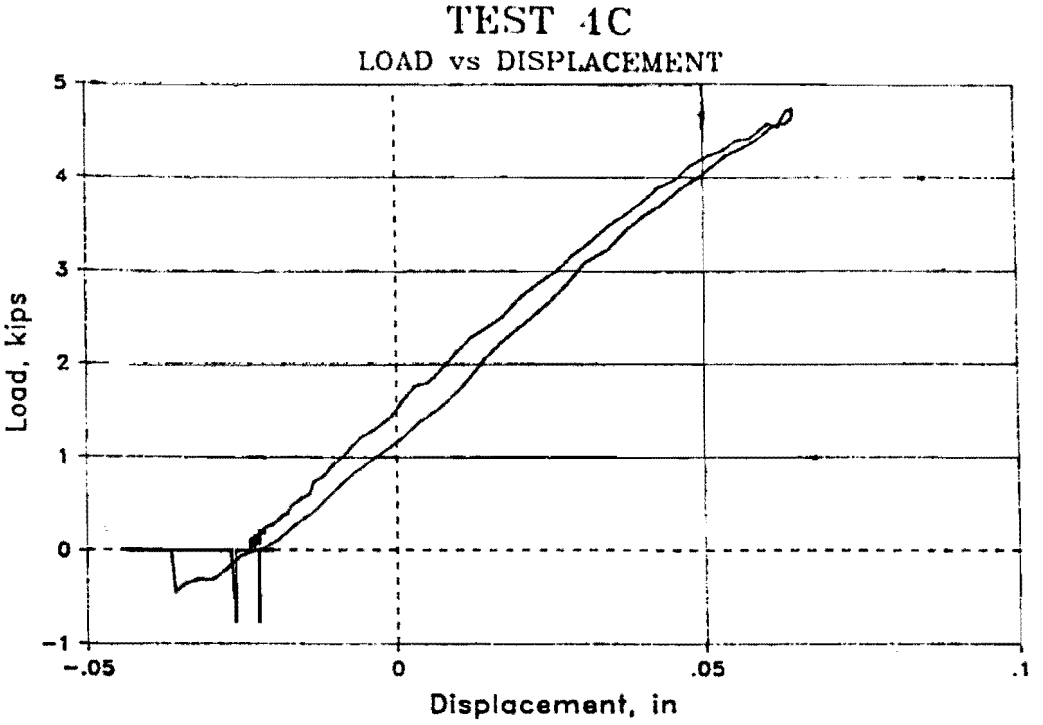
TEST 4C
LOAD vs DISPLACEMENT
Load, kips
5
4
3
2
1
0
-1
-.05
0
.05
.1
Displacement, in

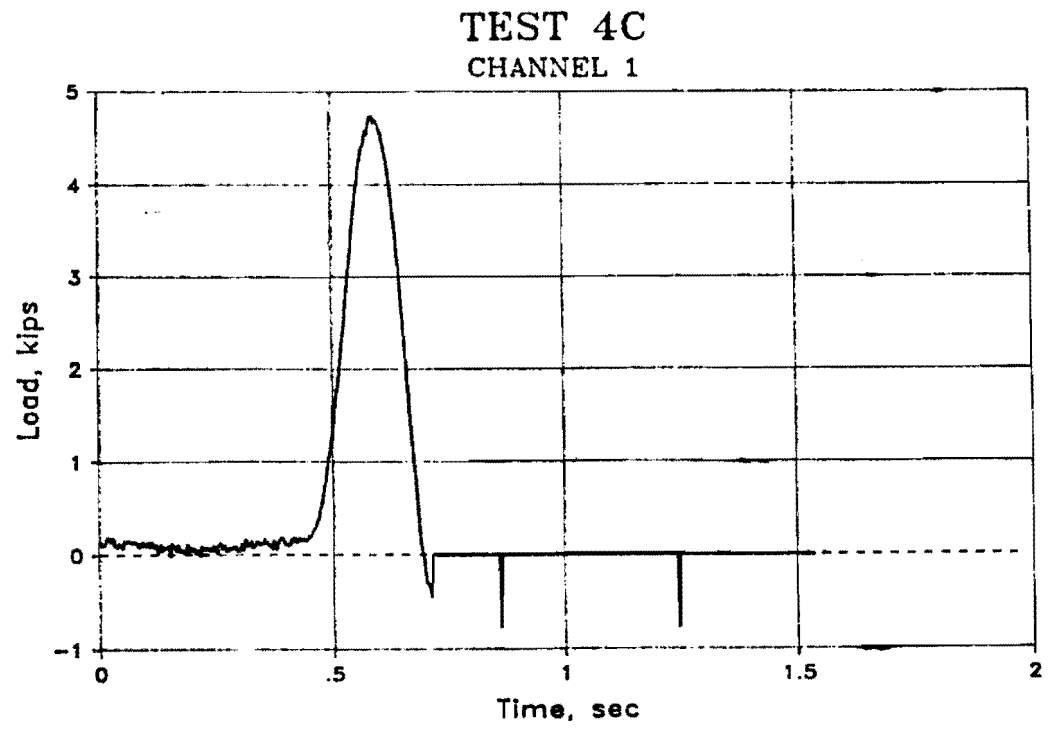
TEST 4C
CHANNEL 1
Load, kips
5
4
3
2
1
0
-1
0
.5
1
1.5
2
Time, sec

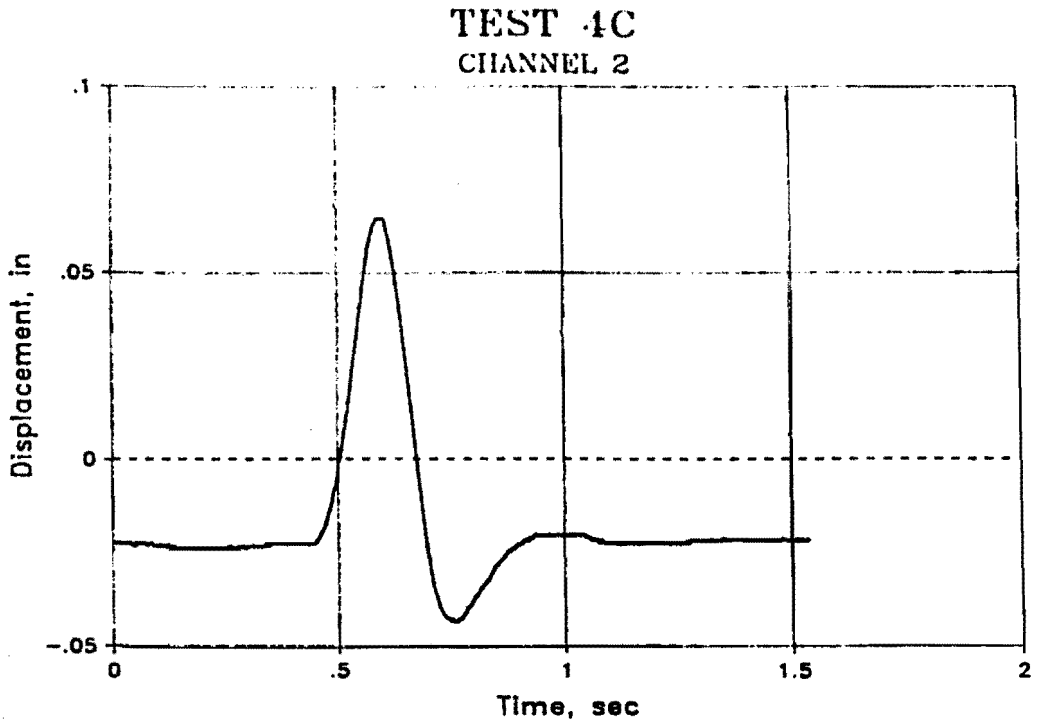
TEST 4C
CHANNEL 2
.1
.05
0
-.05
Displacement, in
0
.5
1
1.5
2
Time, sec

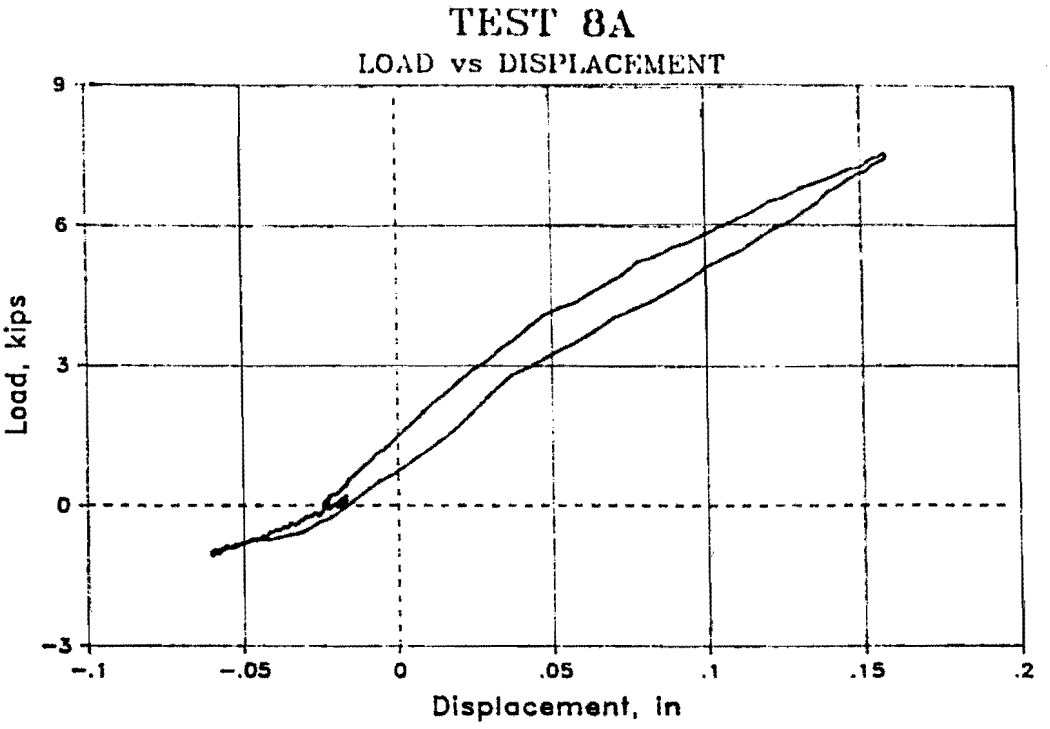
TEST 8A
LOAD vs DISPLACEMENT
Load, kips
9
6
3
0
-3
-.1
-.05
0
.05
.1
.15
.2
Displacement, in

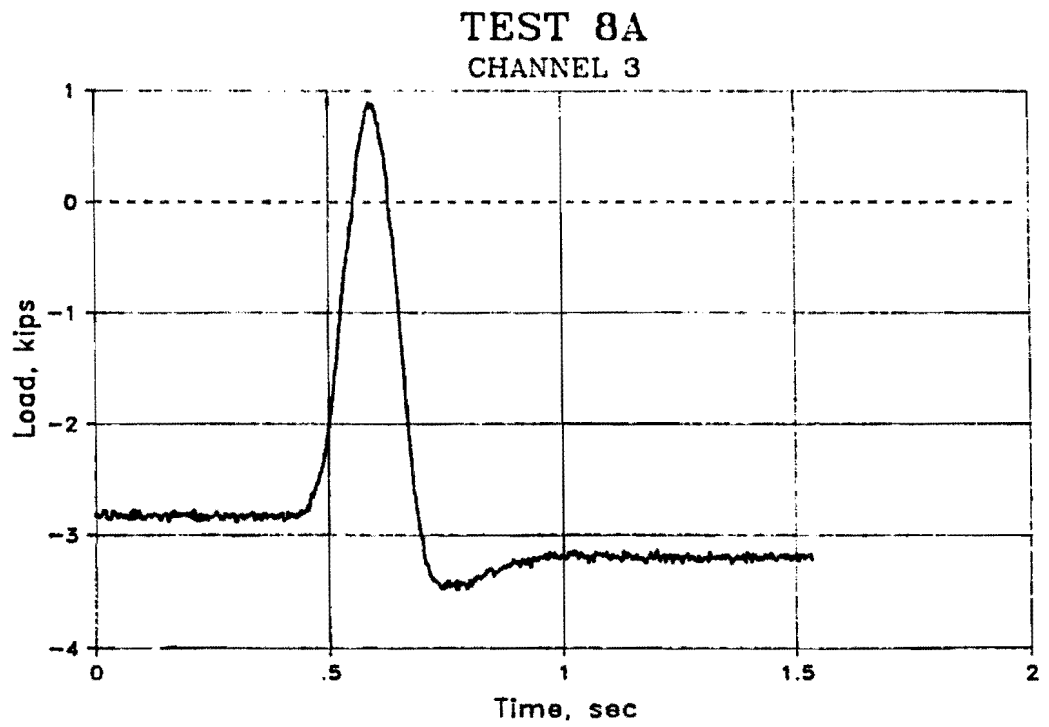
TEST 8A
CHANNEL 3
Load, kips
1
0
-1
-2
-3
-4
0
.5
1
1.5
2
Time, sec

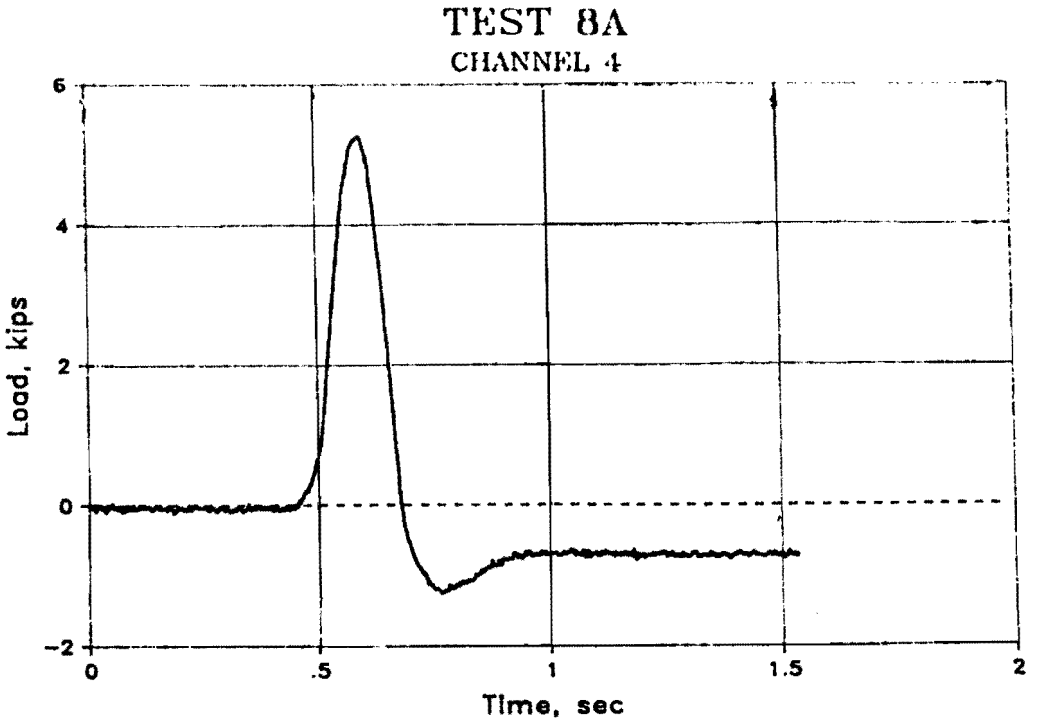
TEST 8A
CHANNEL 4
Load, kips
6
4
2
0
-2
0
.5
1
1.5
2
Time, sec

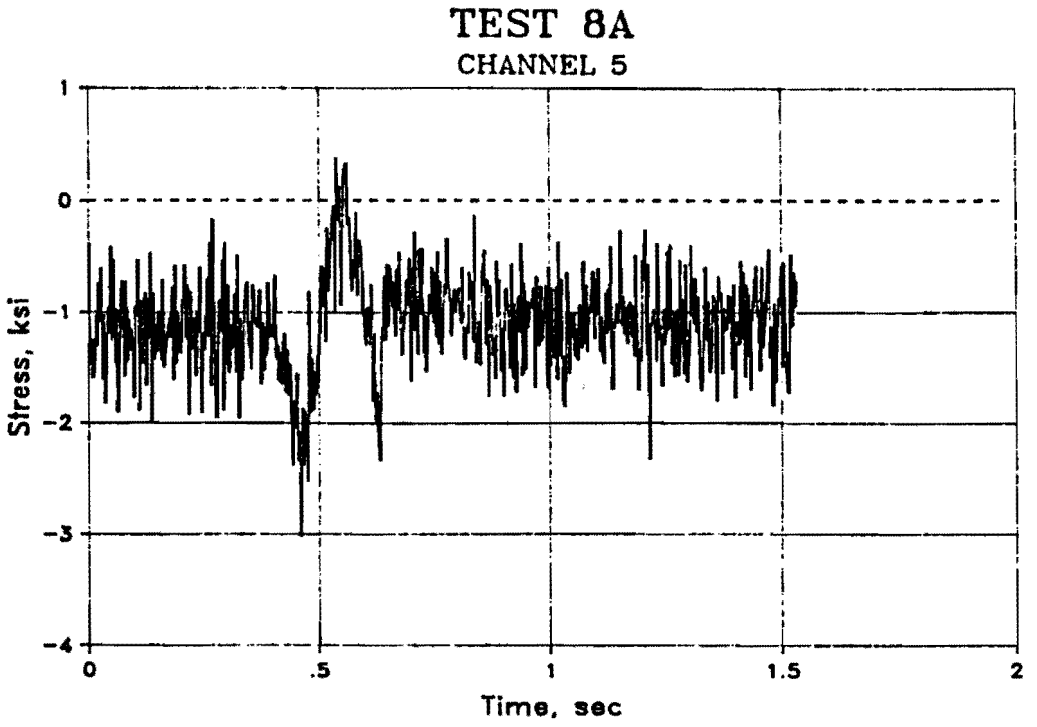
TEST 8A
CHANNEL 5
Stress, ksi
1
0
-1
-2
-3
-4
0
.5
1
1.5
2
Time, sec

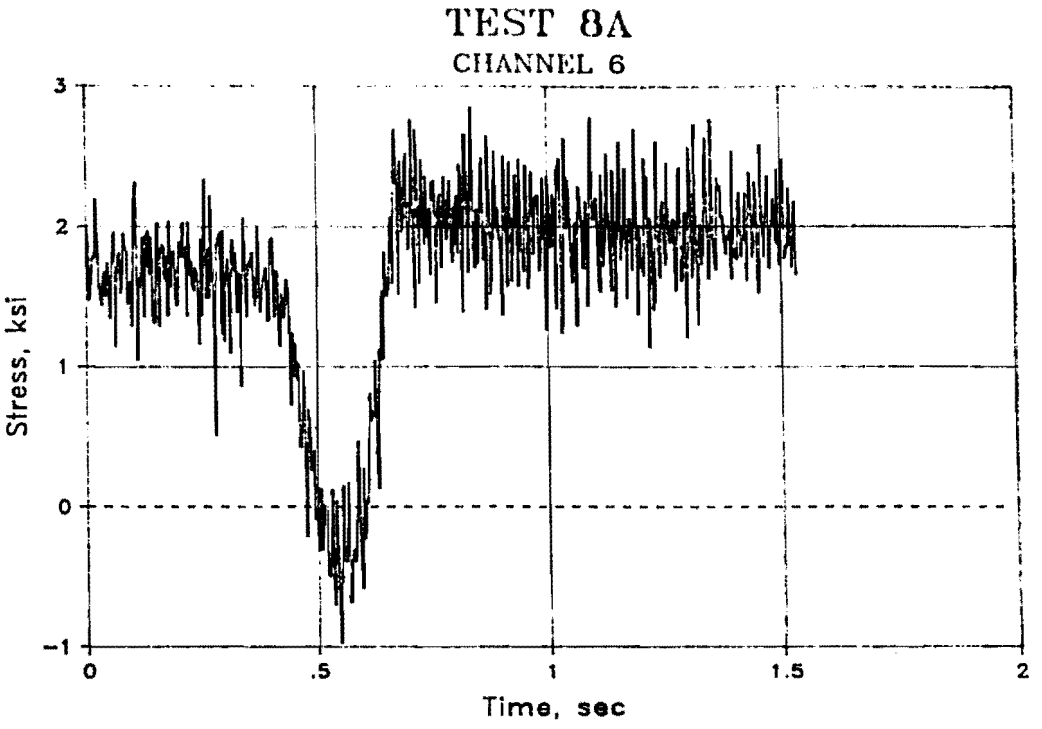
TEST 8A
CHANNEL 6
Stress, ksi
3
2
1
0
-1
0
.5
1
1.5
2
Time, sec

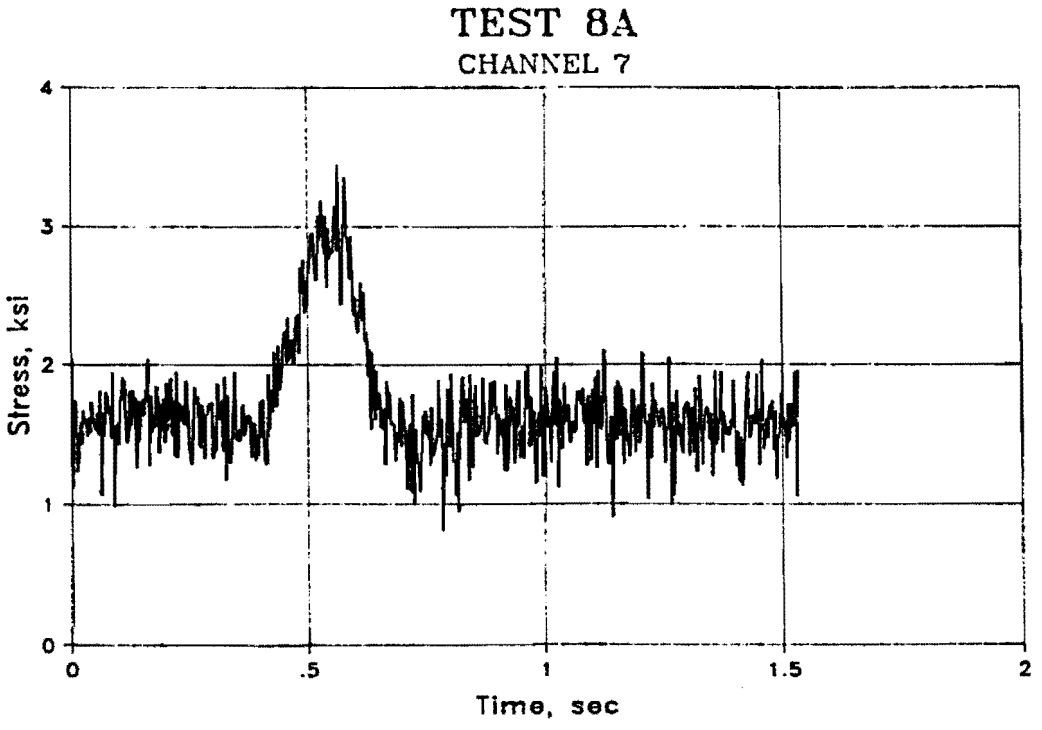
TEST 8A
CHANNEL 7
Stress, ksi
4
3
2
1
0
0
.5
1
1.5
2
Time, sec

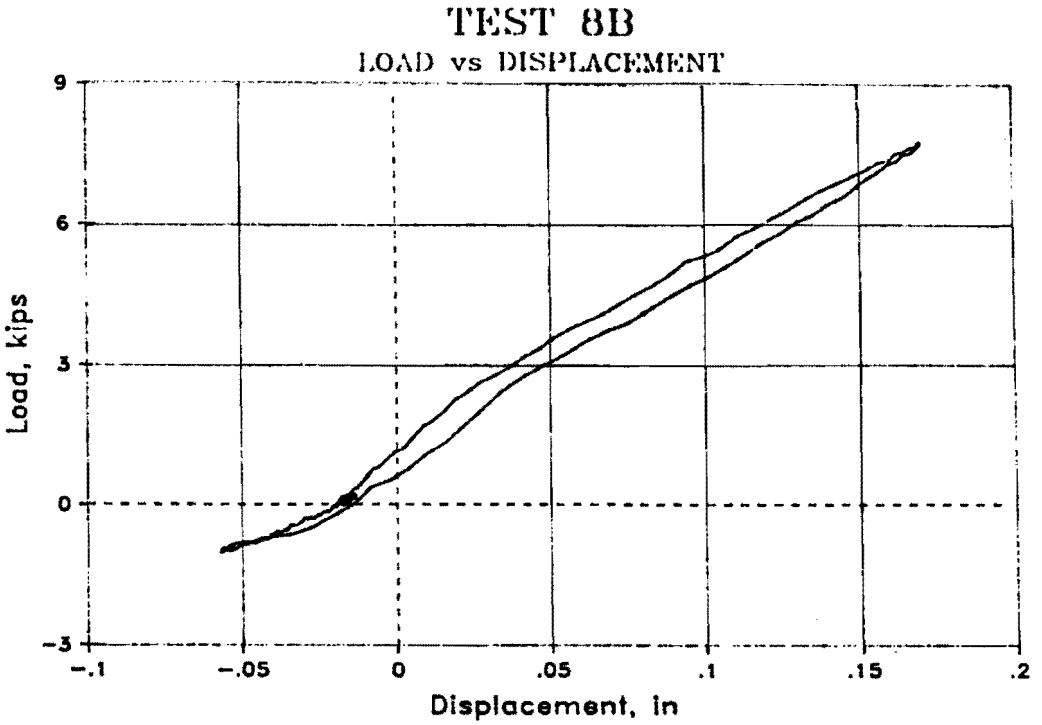
TEST 8B
LOAD vs DISPLACEMENT
Load, kips
9
6
3
0
-3
-.1
-.05
0
.05
.1
.15
.2
Displacement, in

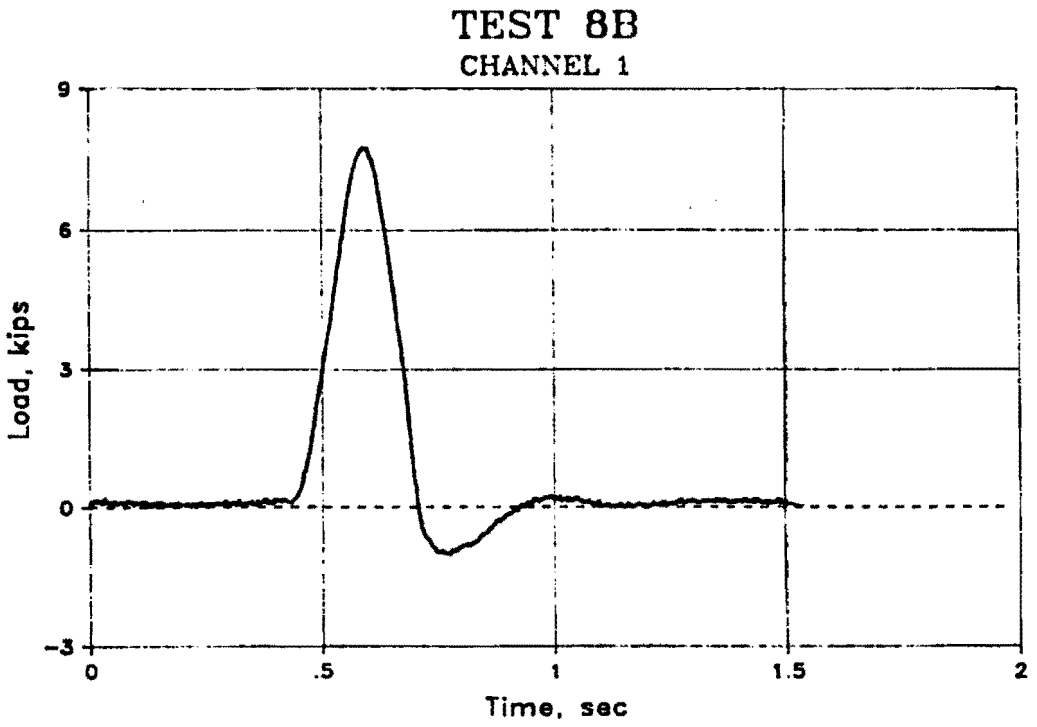
TEST 8B
CHANNEL 1
Load, kips
9
6
3
0
-3
0
.5
1
1.5
2
Time, sec

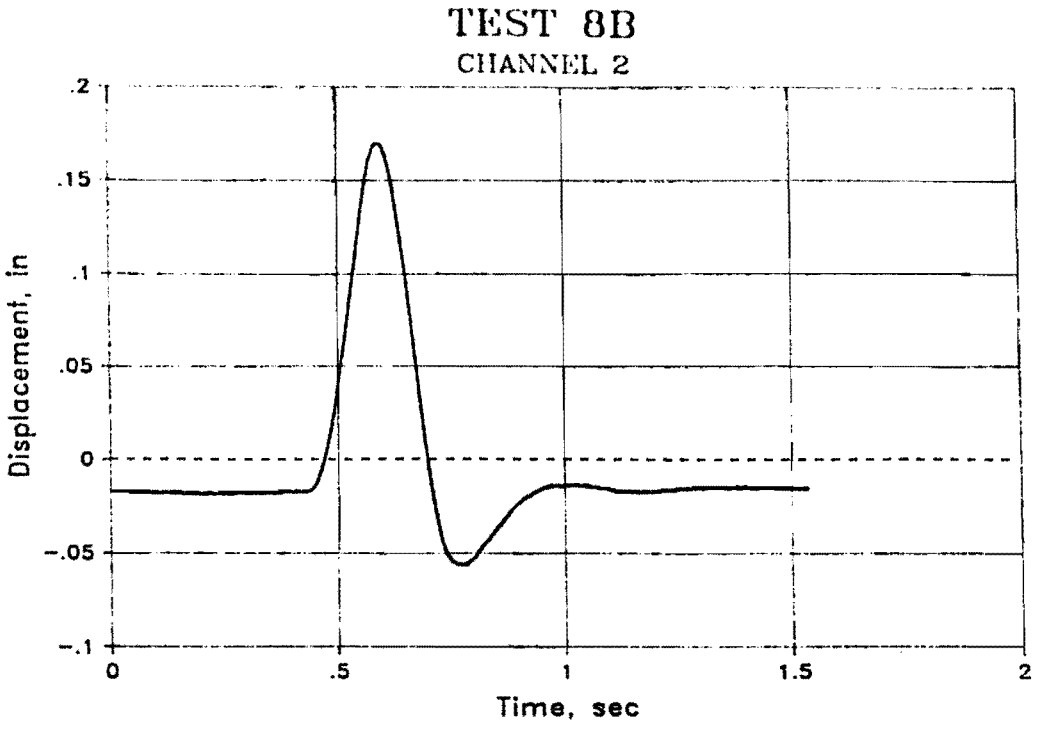
TEST 8B
CHANNEL 2
Displacement, in
.2
.15
.1
.05
0
-.05
-.1
0
.5
1
1.5
2
Time, sec

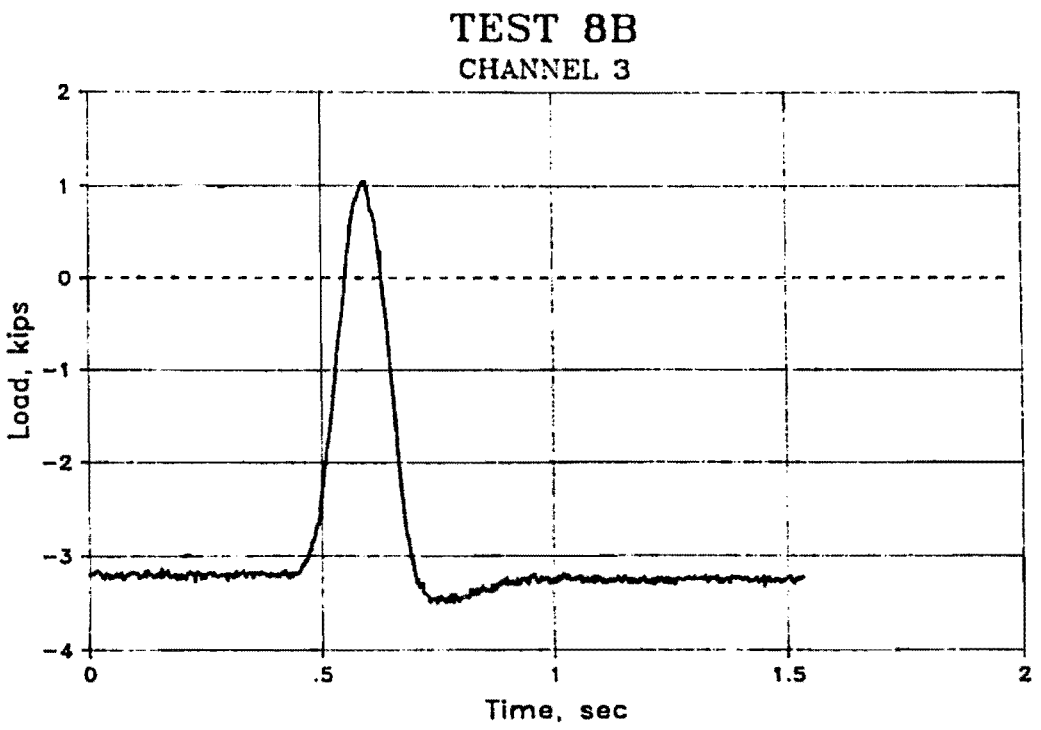
TEST 8B
CHANNEL 3
Load, kips
2
1
0
-1
-2
-3
-4
0
.5
1
1.5
2
Time, sec

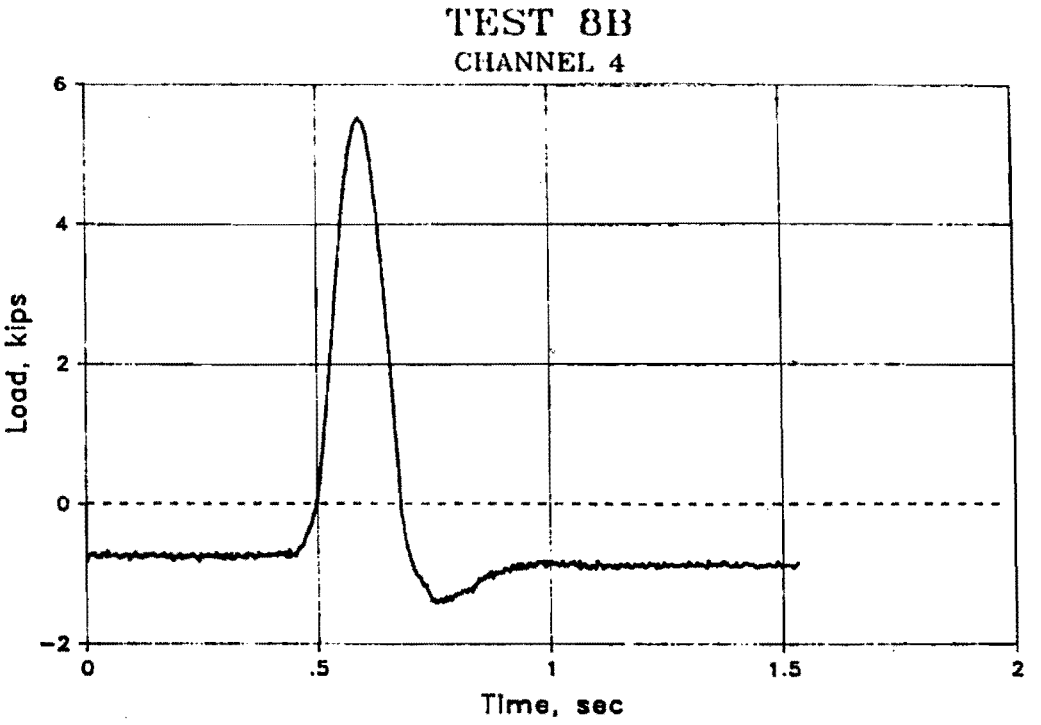
TEST 8B
CHANNEL 4
Load, kips
6
4
2
0
−2
0
.5
1
1.5
2
Time, sec

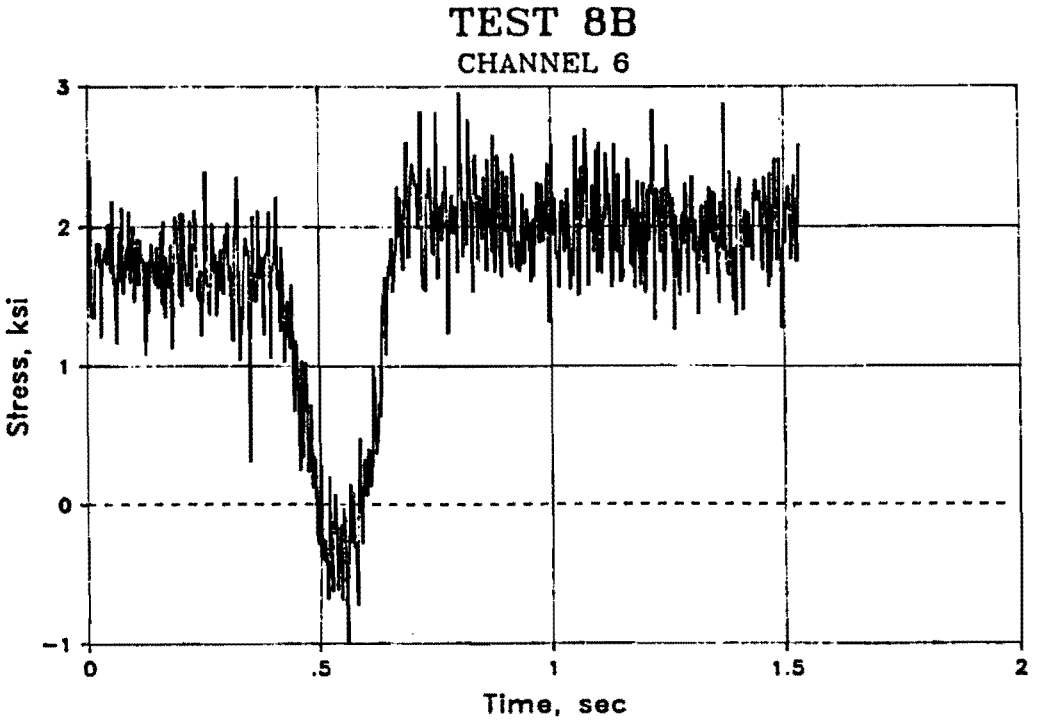
TEST 8B
CHANNEL 6
Stress, ksi
3
2
1
0
−1
0
.5
1
1.5
2
Time, sec

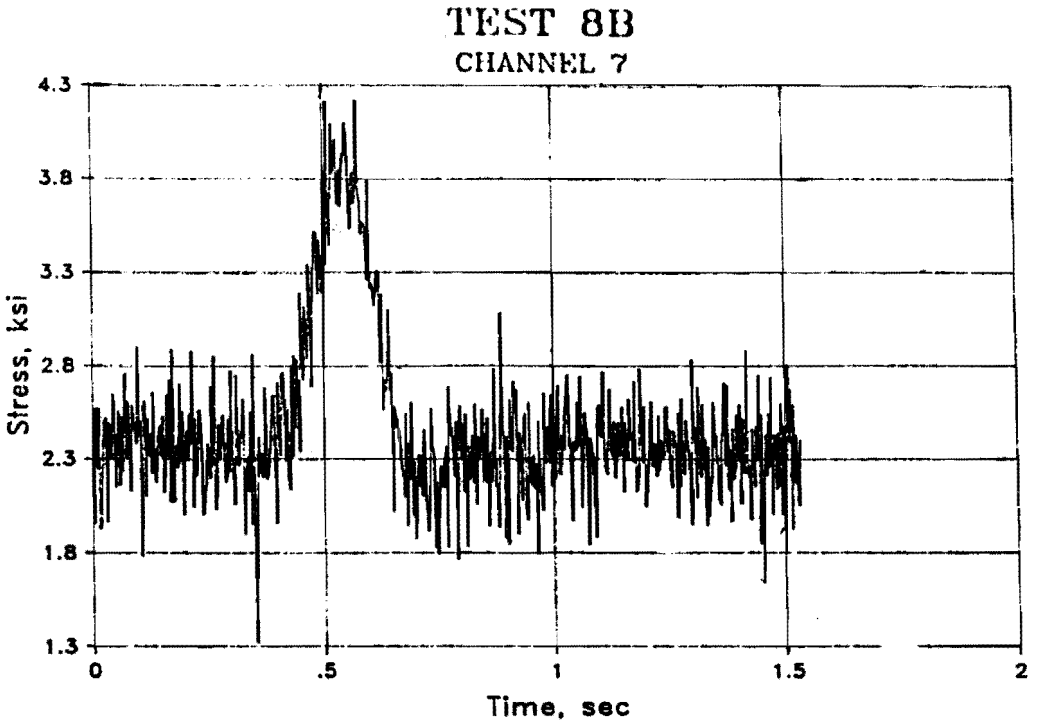
TEST 8B
CHANNEL 7
4.3
3.8
3.3
2.8
2.3
1.8
1.3
Stress, ksi
0
.5
1
1.5
2
Time, sec

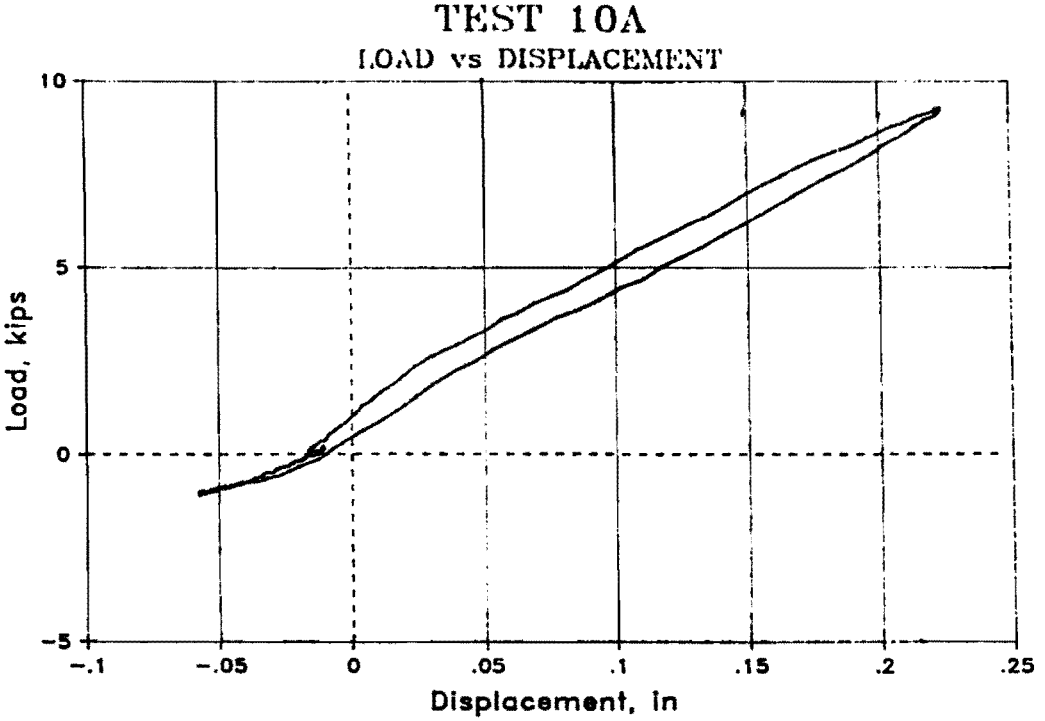
TEST 10A
LOAD vs DISPLACEMENT
Load, kips
10
5
0
-5
-.1
-.05
0
.05
.1
.15
.2
.25
Displacement, in

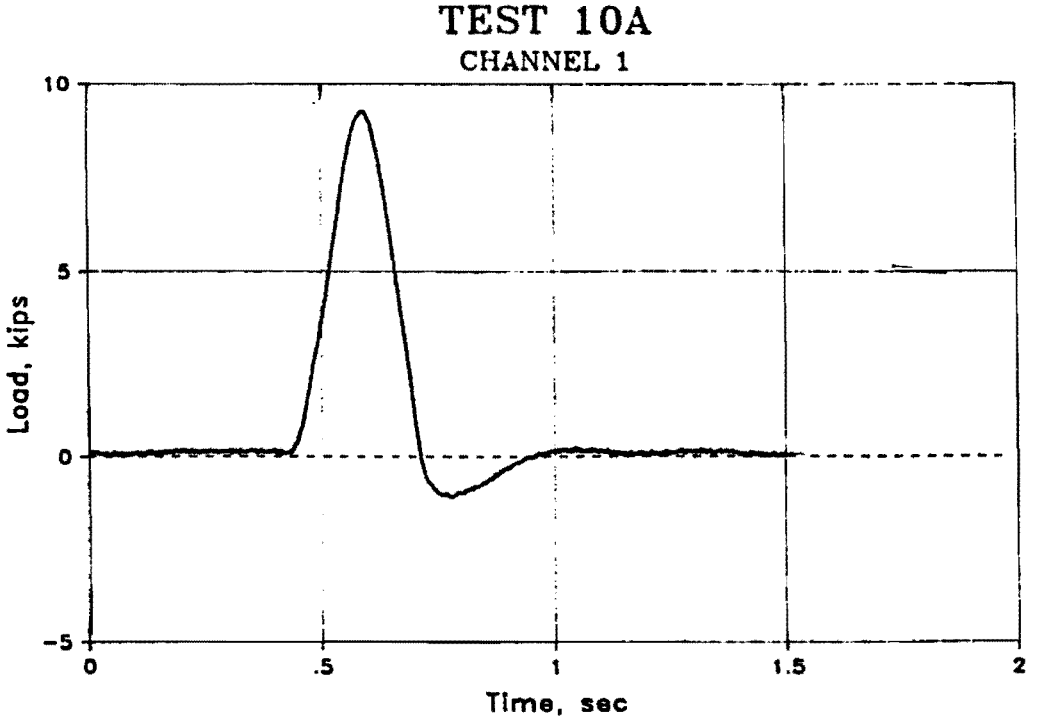
TEST 10A
CHANNEL 1
Load, kips
10
5
0
-5
0
.5
1
1.5
2
Time, sec

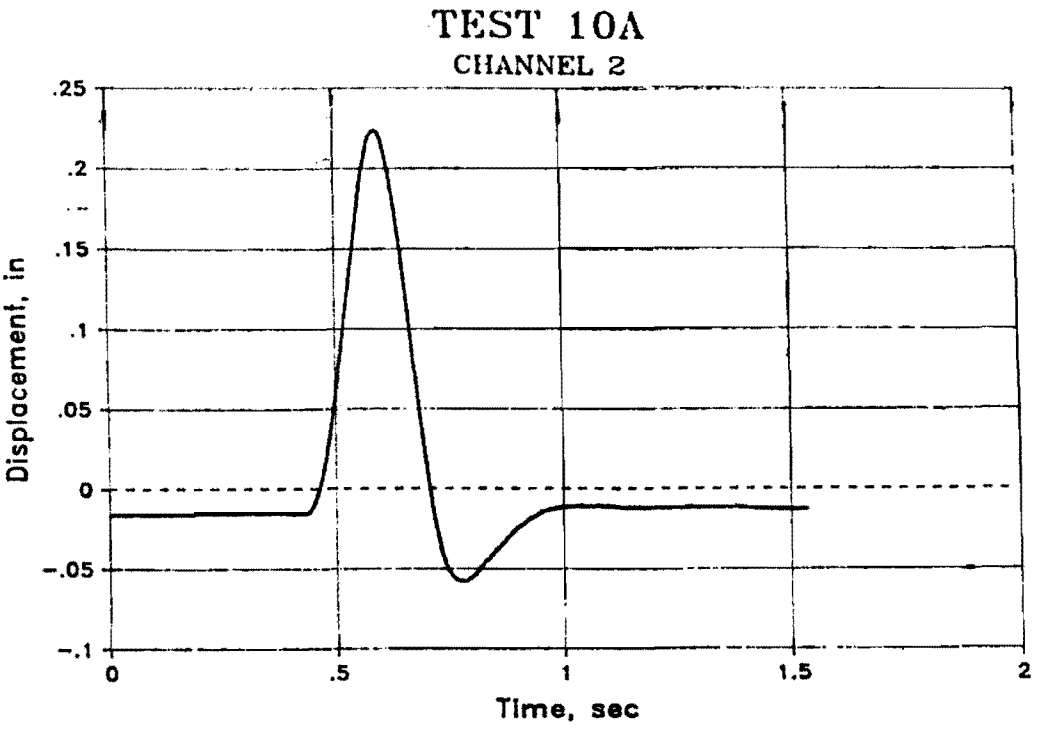
TEST 10A
CHANNEL 2
Displacement, in
.25
.2
.15
.1
.05
0
-.05
-.1
0
.5
1
1.5
2
Time, sec

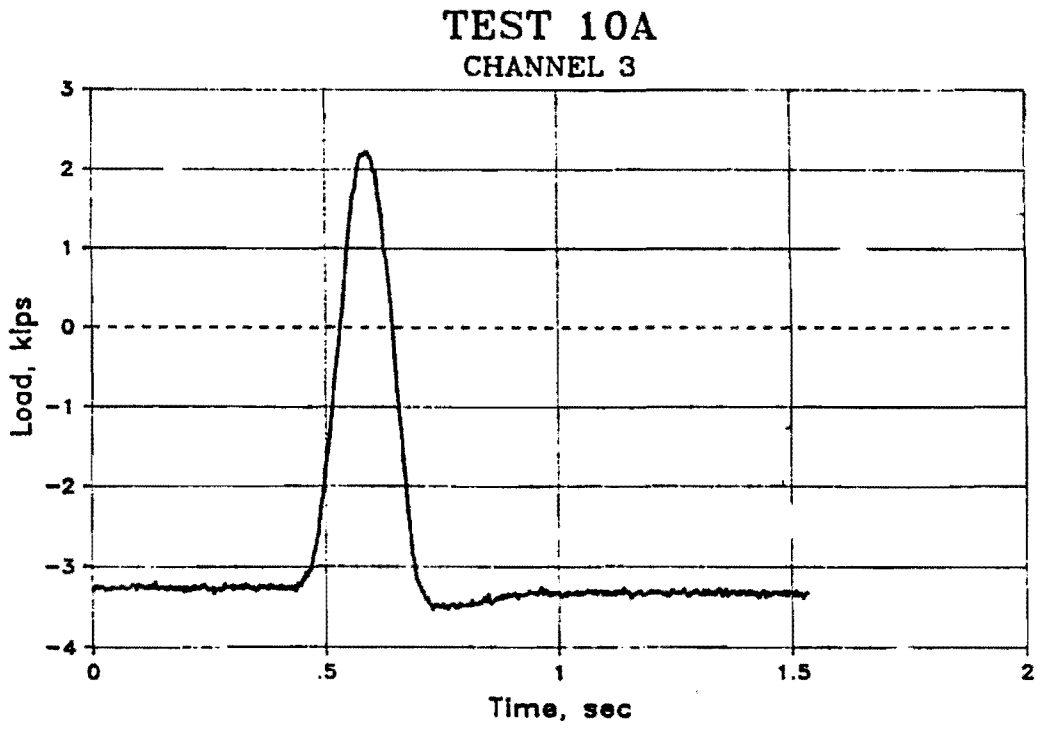
TEST 10A
CHANNEL 3
Load, kips
3
2
1
0
-1
-2
-3
-4
0
.5
1
1.5
2
Time, sec

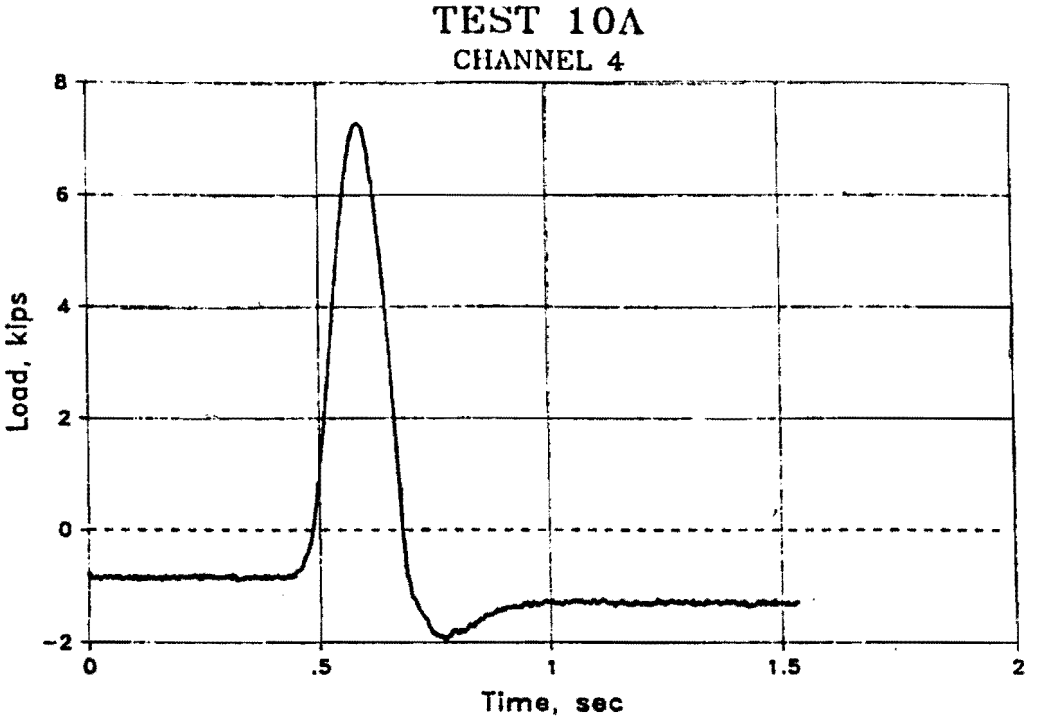
TEST 10A
CHANNEL 4
Load, kips
8
6
4
2
0
-2
0
.5
1
1.5
2
Time, sec

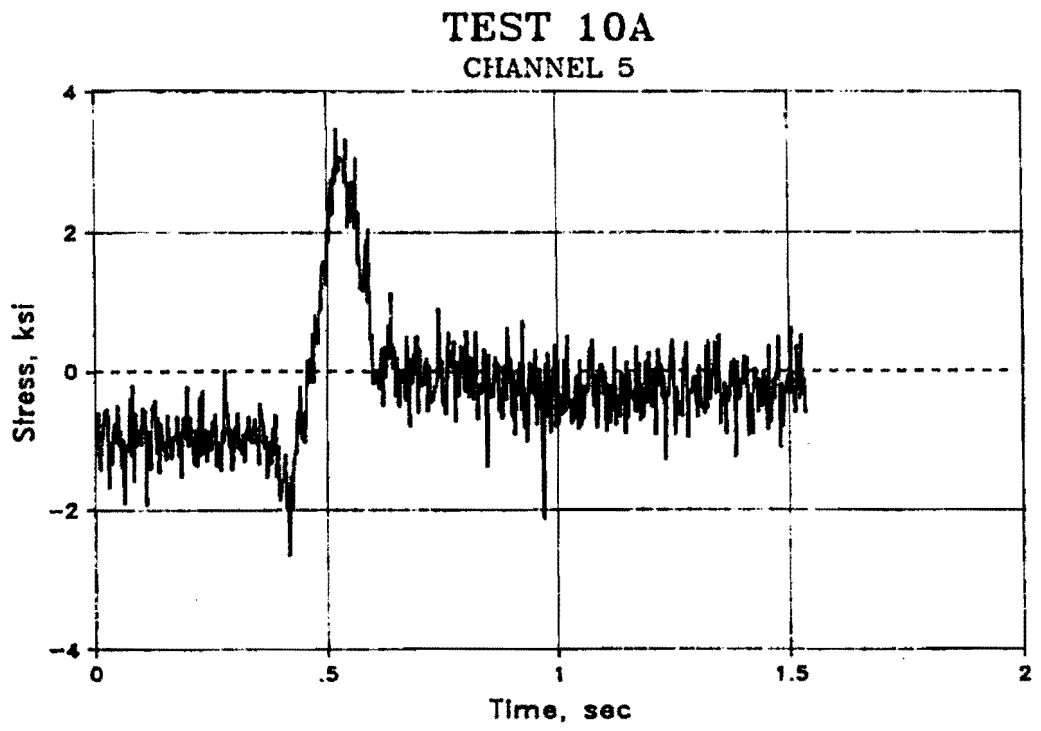
TEST 10A
CHANNEL 5
Stress, ksi
4
2
0
-2
-4
0
.5
1
1.5
2
Time, sec

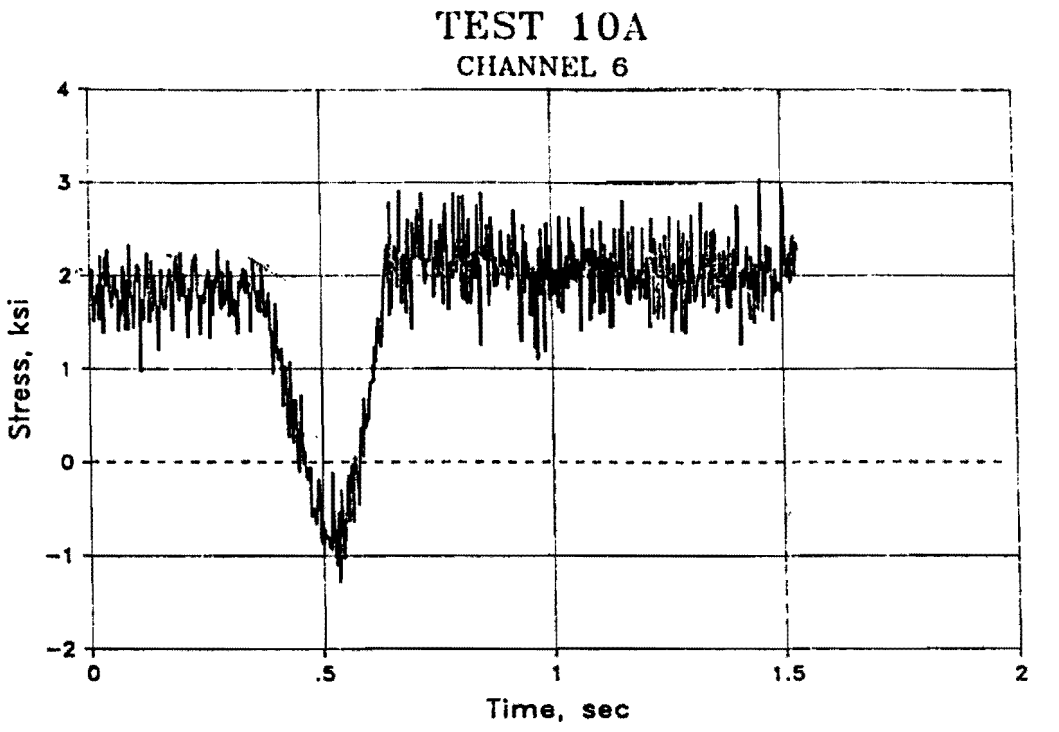
TEST 10A
CHANNEL 6
Stress, ksi
4
3
2
1
0
-1
-2
0
.5
1
1.5
2
Time, sec

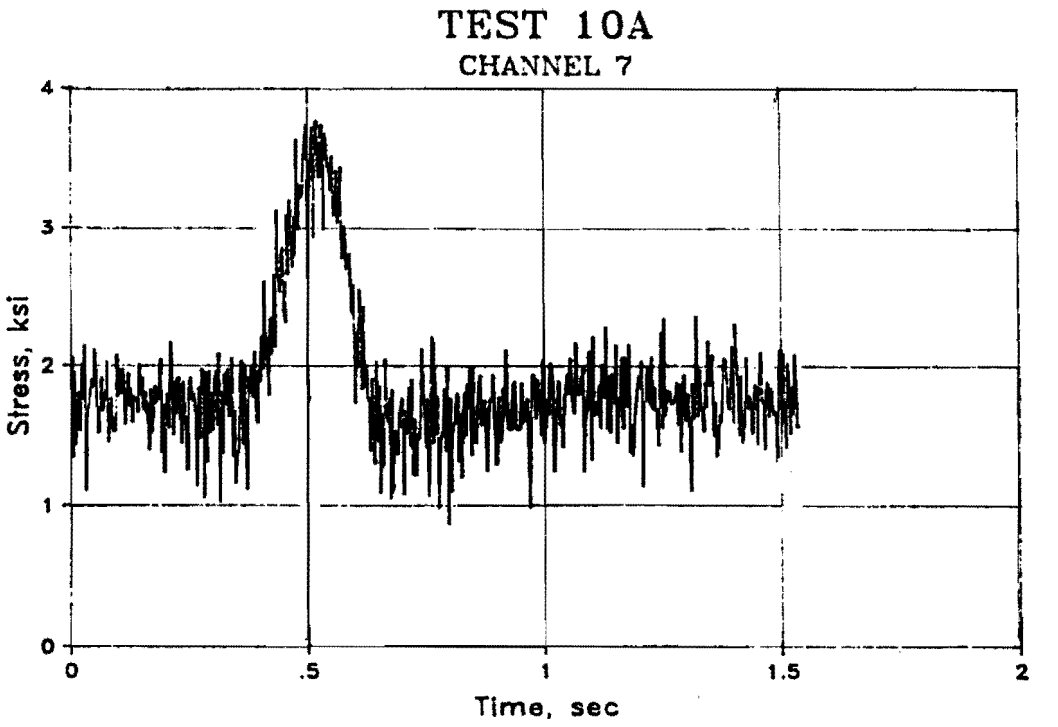
TEST 10A
CHANNEL 7
Stress, ksi
4
3
2
1
0
0
.5
1
1.5
2
Time, sec

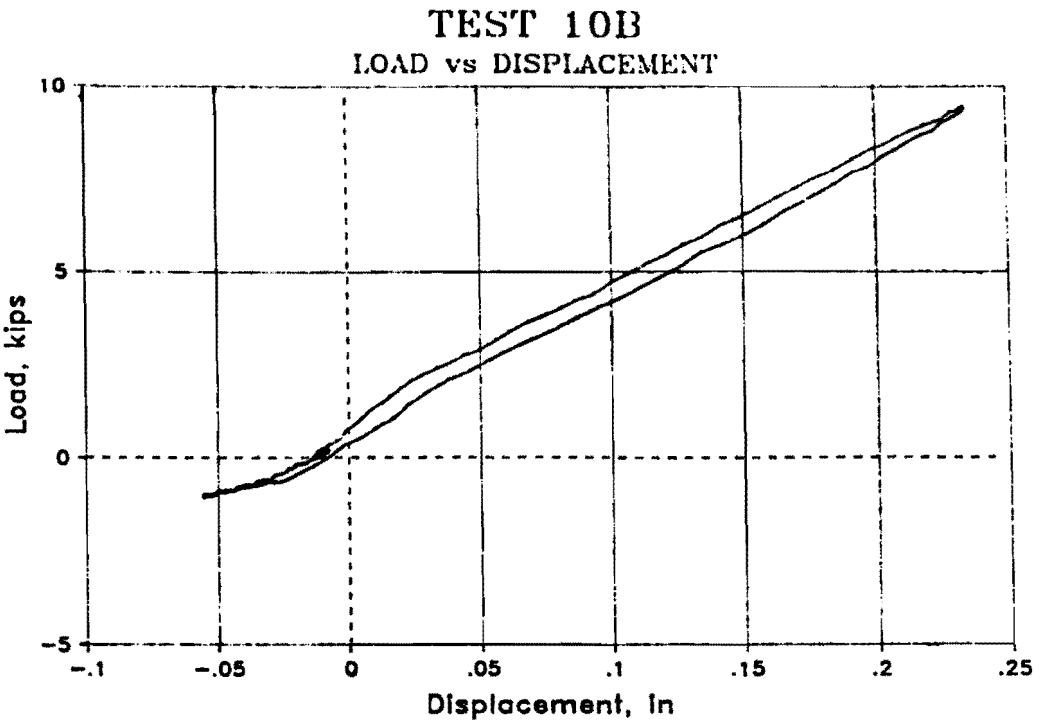
TEST 10B
LOAD vs DISPLACEMENT
10
5
0
-5
Load, kips
-.1
-.05
0
.05
.1
.15
.2
.25
Displacement, in

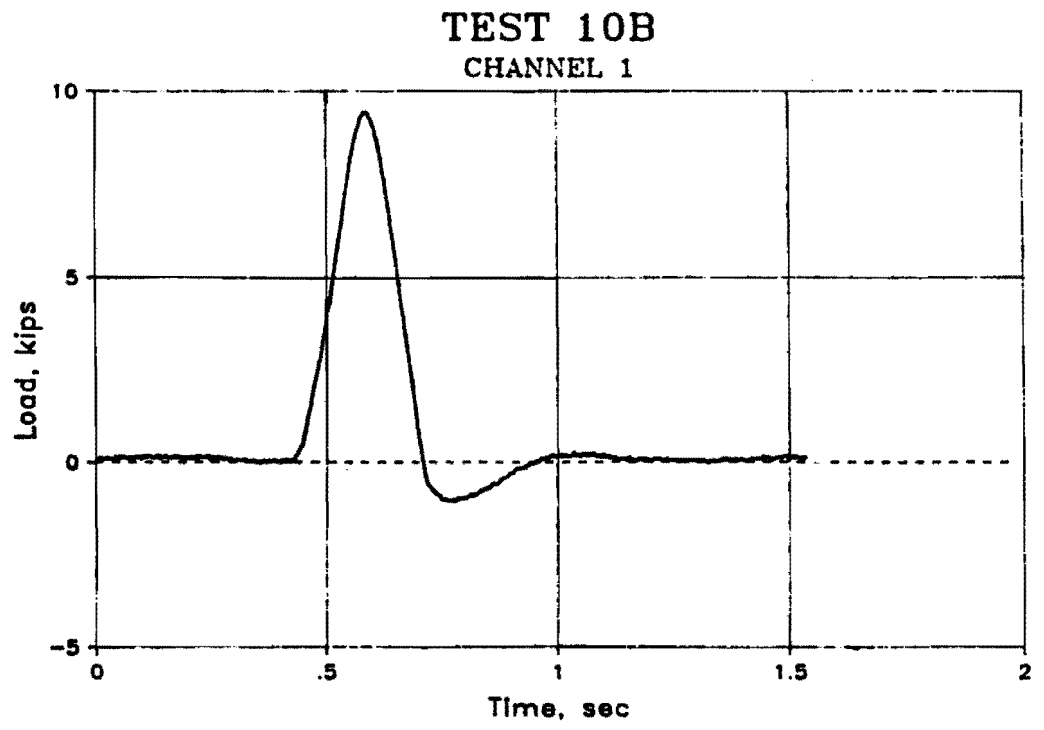
TEST 10B
CHANNEL 1
10
5
0
-5
Load, kips
0
.5
1
1.5
2
Time, sec

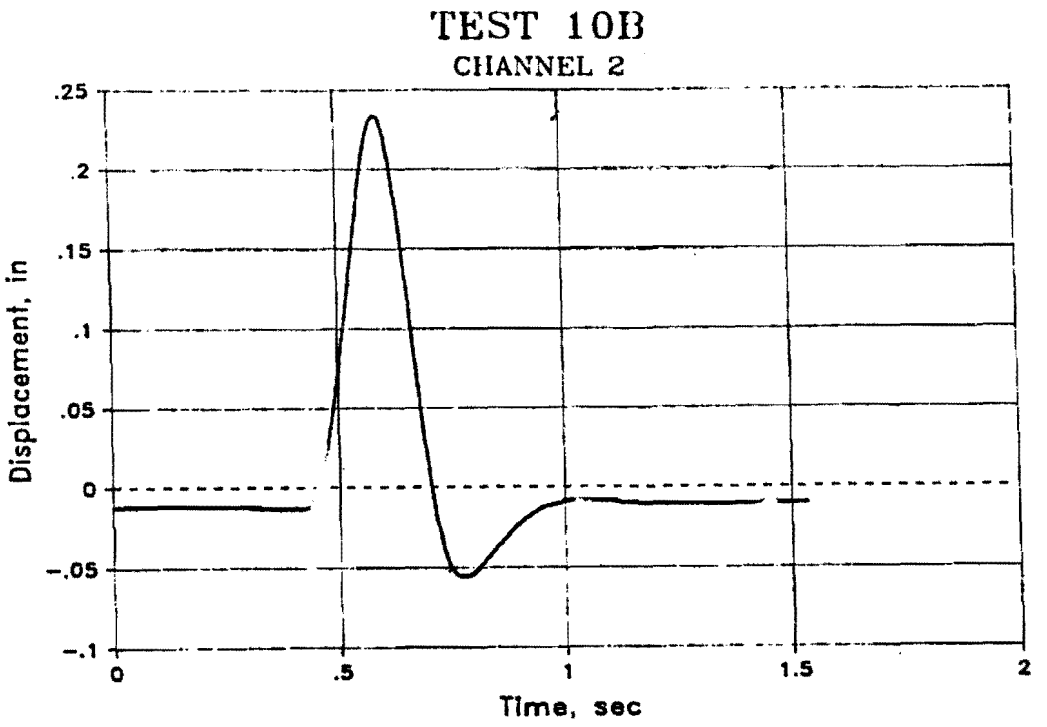
TEST 10B
CHANNEL 2
Displacement, in
.25
.2
.15
.1
.05
0
-.05
-.1
0
.5
1
1.5
2
Time, sec

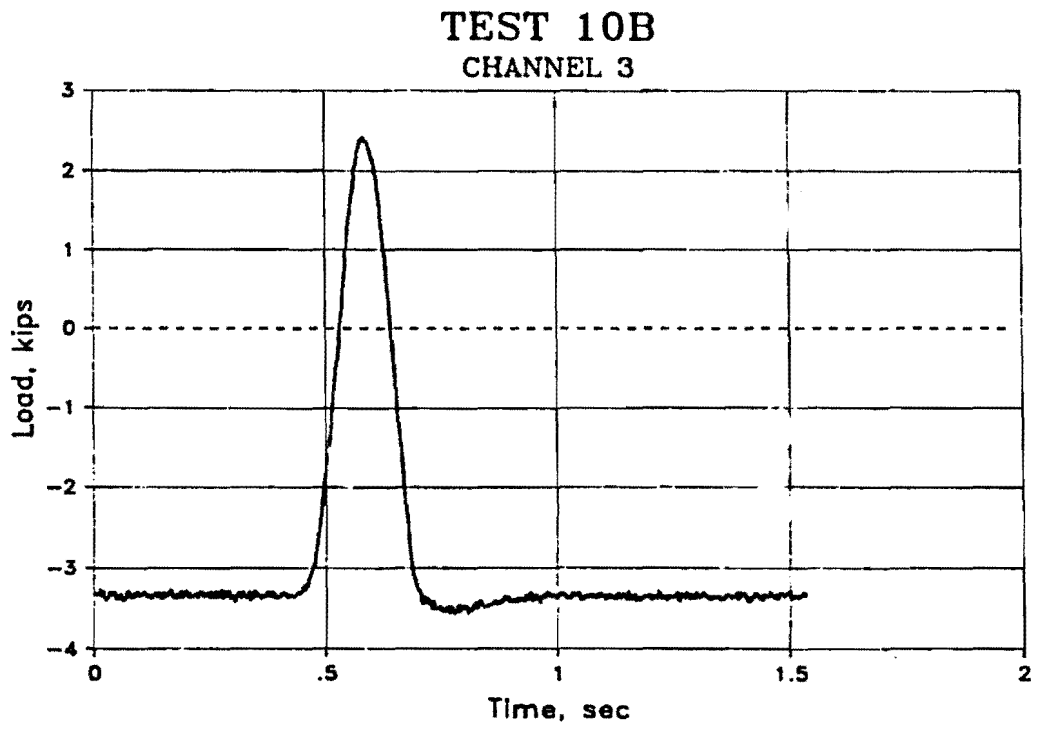
TEST 10B
CHANNEL 3
Load, kips
3
2
1
0
-1
-2
-3
-4
0
.5
1
1.5
2
Time, sec

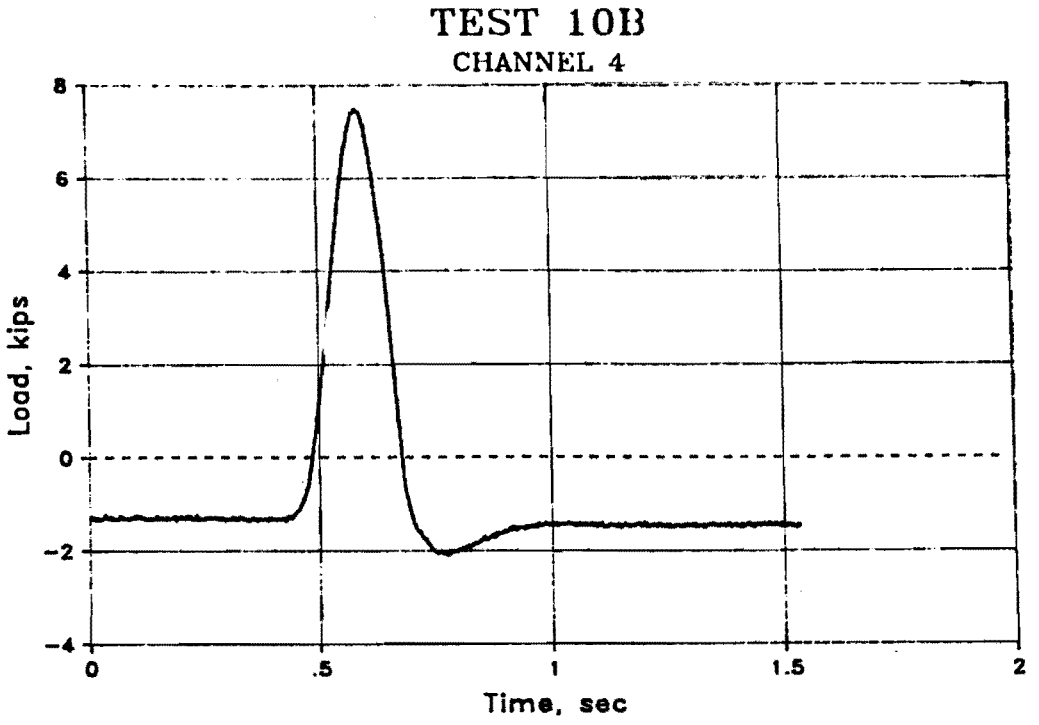
TEST 10B
CHANNEL 4
Load, kips
8
6
4
2
0
-2
-4
0
.5
1
1.5
2
Time, sec

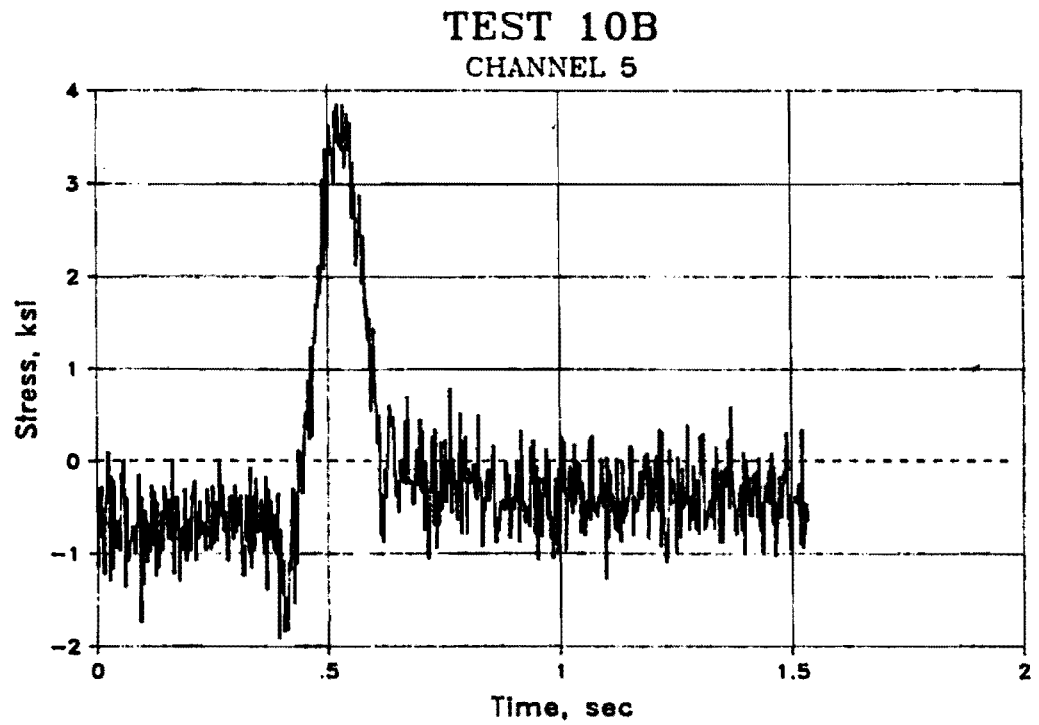
TEST 10B
CHANNEL 5
Stress, ksi
4
3
2
1
0
-1
-2
0
.5
1
1.5
2
Time, sec

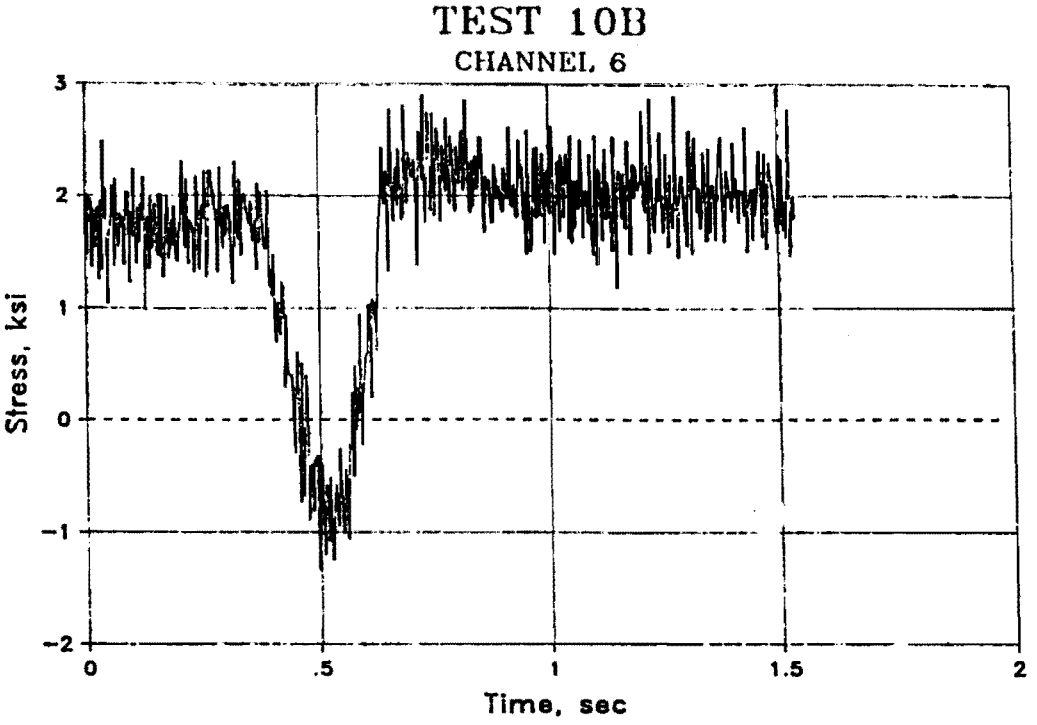
TEST 10B
CHANNEL 6
Stress, ksi
3
2
1
0
-1
-2
0
.5
1
1.5
2
Time, sec

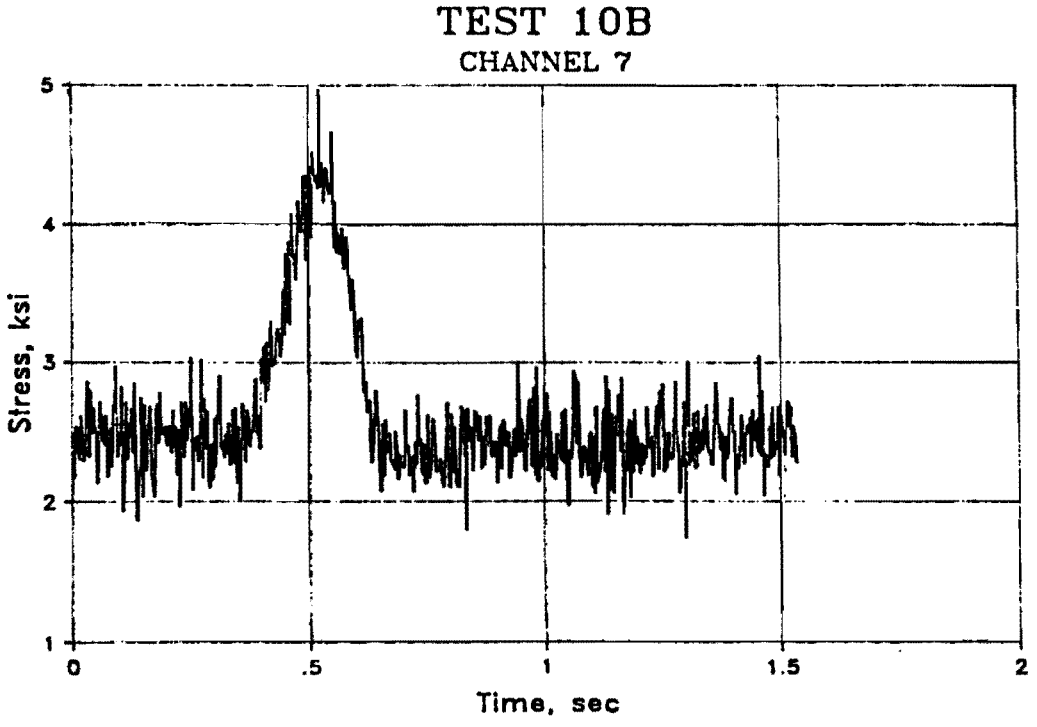
TEST 10B
CHANNEL 7
Stress, ksi
5
4
3
2
1
0
.5
1
1.5
2
Time, sec

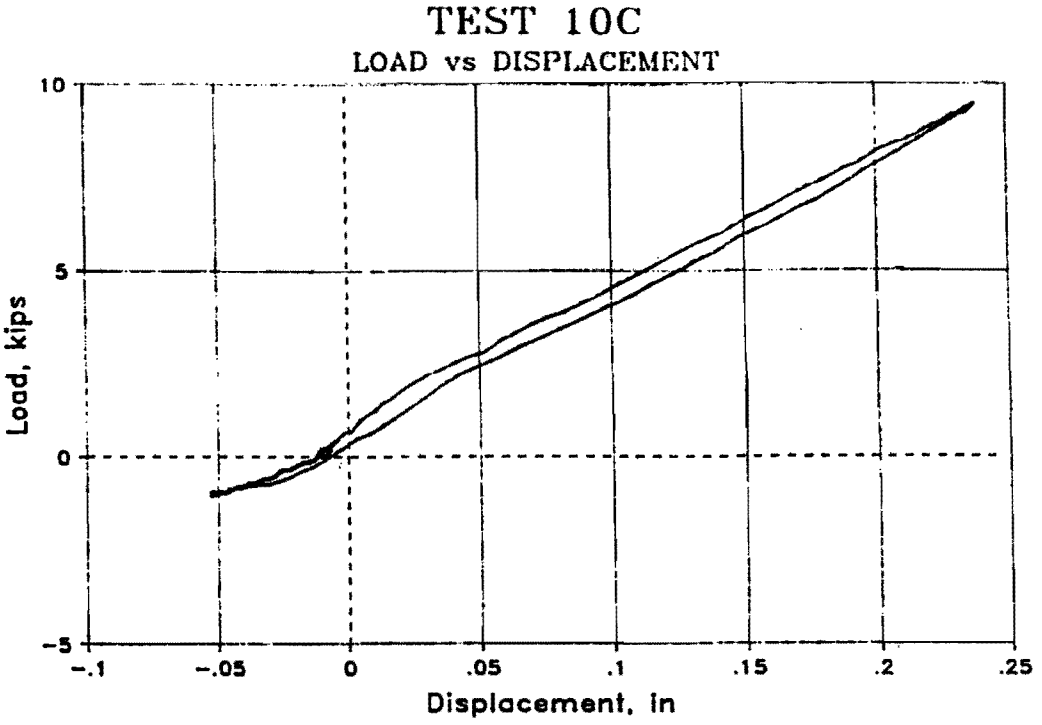
TEST 10C
LOAD vs DISPLACEMENT
Load, kips
10
5
0
-5
-.1
-.05
0
.05
.1
.15
.2
.25
Displacement, in

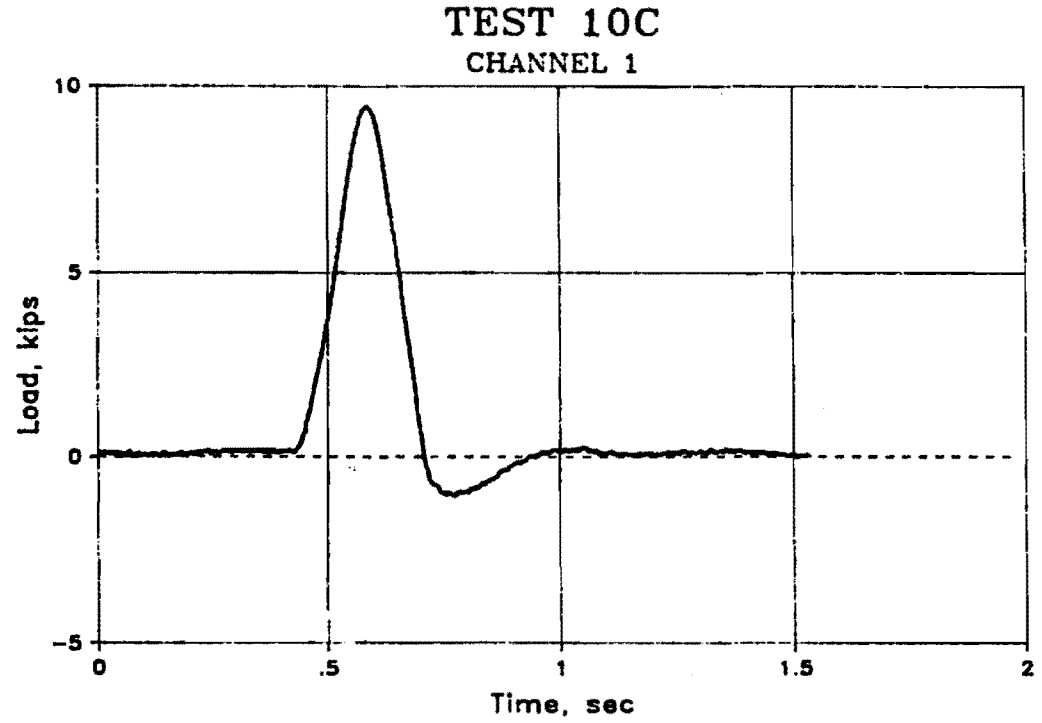
TEST 10C
CHANNEL 1
Load, kips
10
5
0
-5
0
.5
1
1.5
2
Time, sec

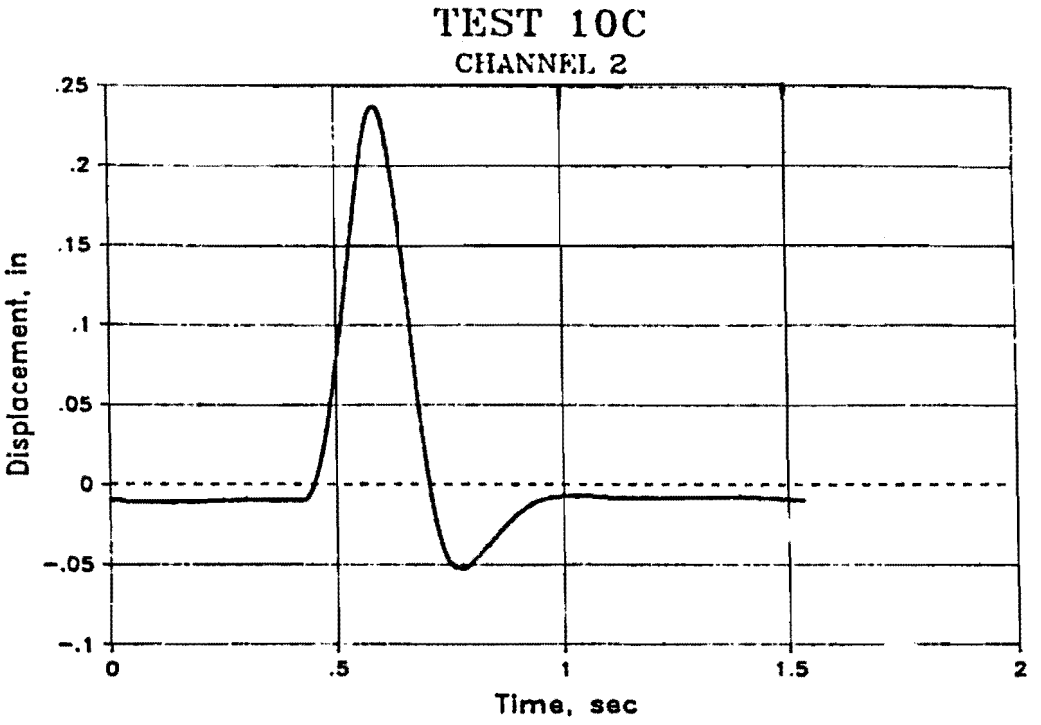
TEST 10C
CHANNEL 2
Displacement, in
.25
.2
.15
.1
.05
0
-.05
-.1
0
.5
1
1.5
2
Time, sec

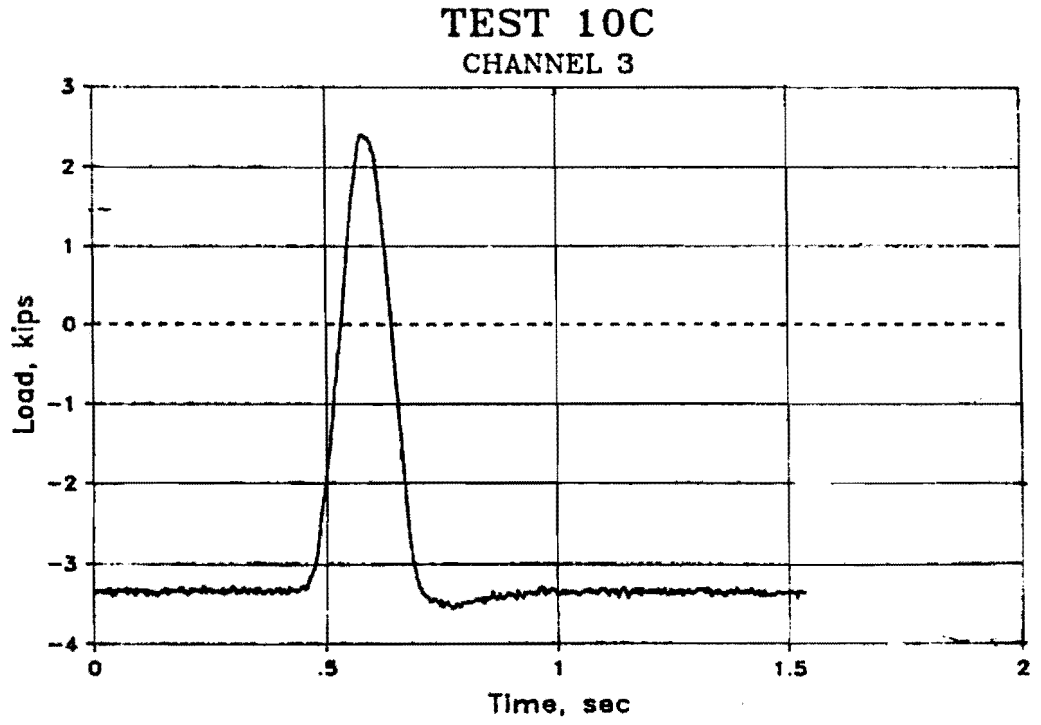
TEST 10C
CHANNEL 3
Load, kips
3
2
1
0
-1
-2
-3
-4
0
.5
1
1.5
2
Time, sec

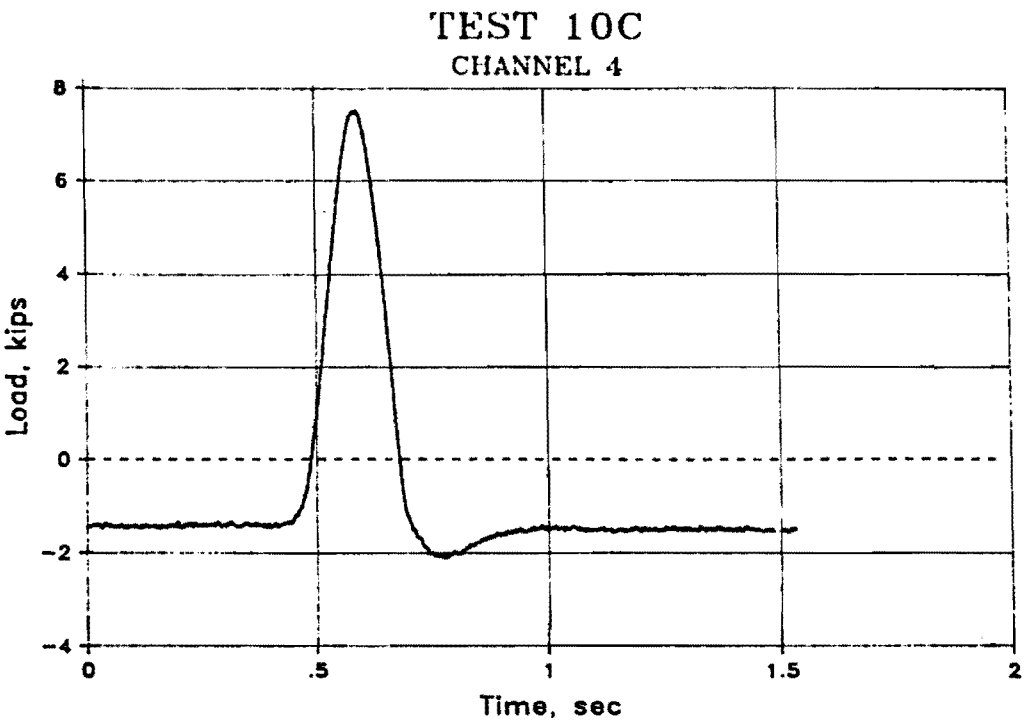
TEST 10C
CHANNEL 4
Load, kips
8
6
4
2
0
-2
-4
0
.5
1
1.5
2
Time, sec

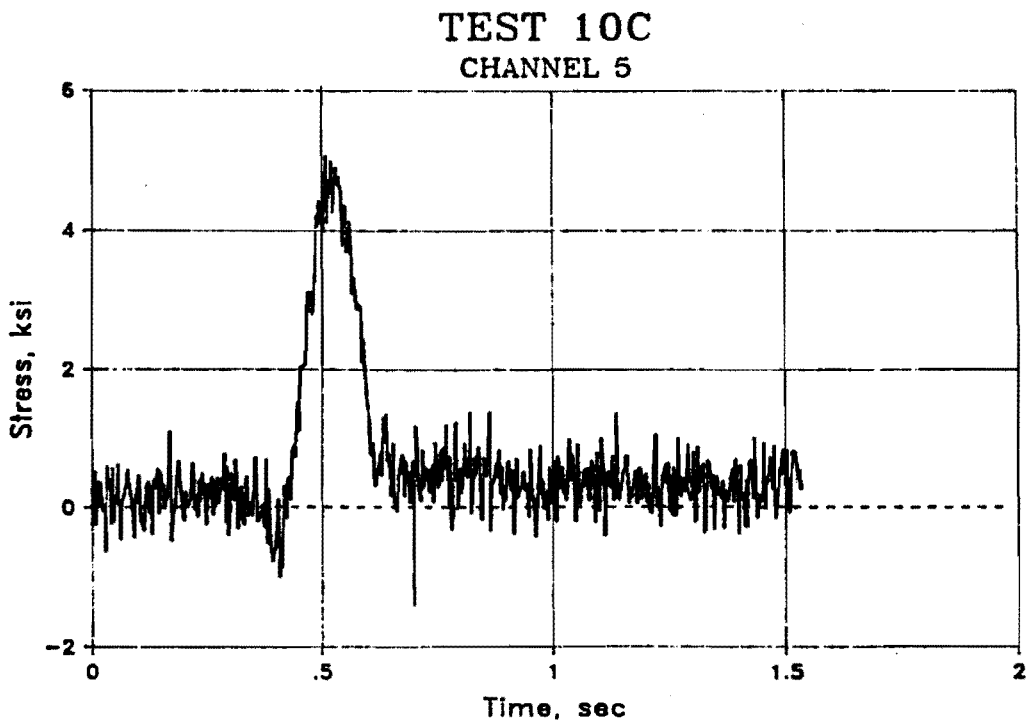
TEST 10C
CHANNEL 5
Stress, ksi
6
4
2
0
-2
0
.5
1
1.5
2
Time, sec

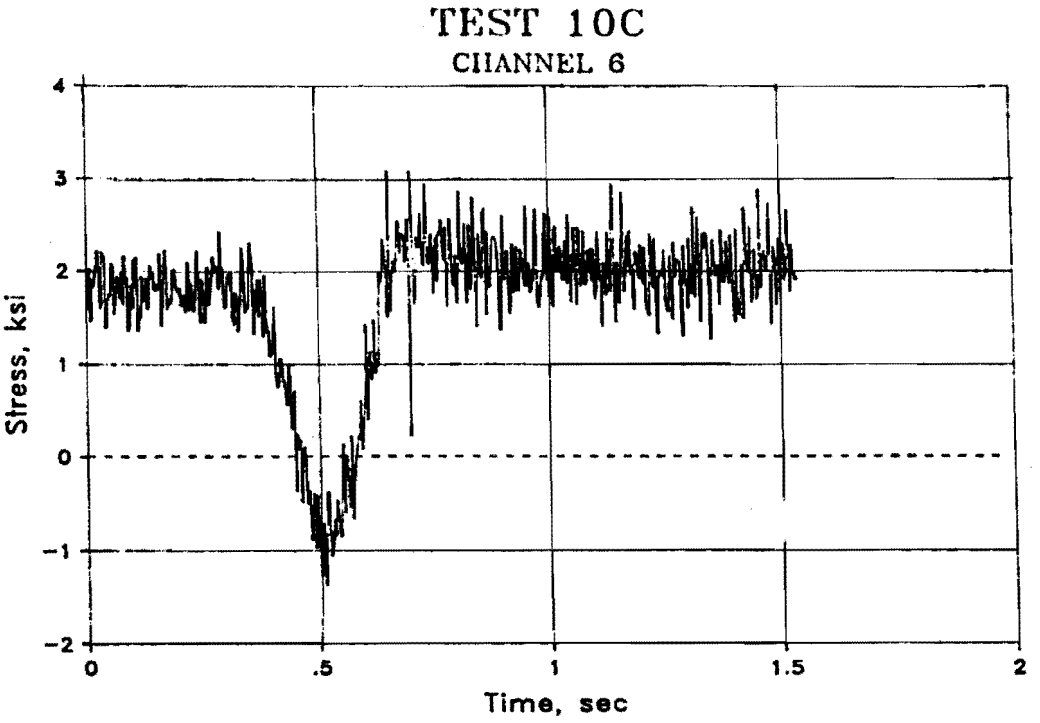
TEST 10C
CHANNEL 6
Stress, ksi
4
3
2
1
0
-1
-2
0
.5
1
1.5
2
Time, sec

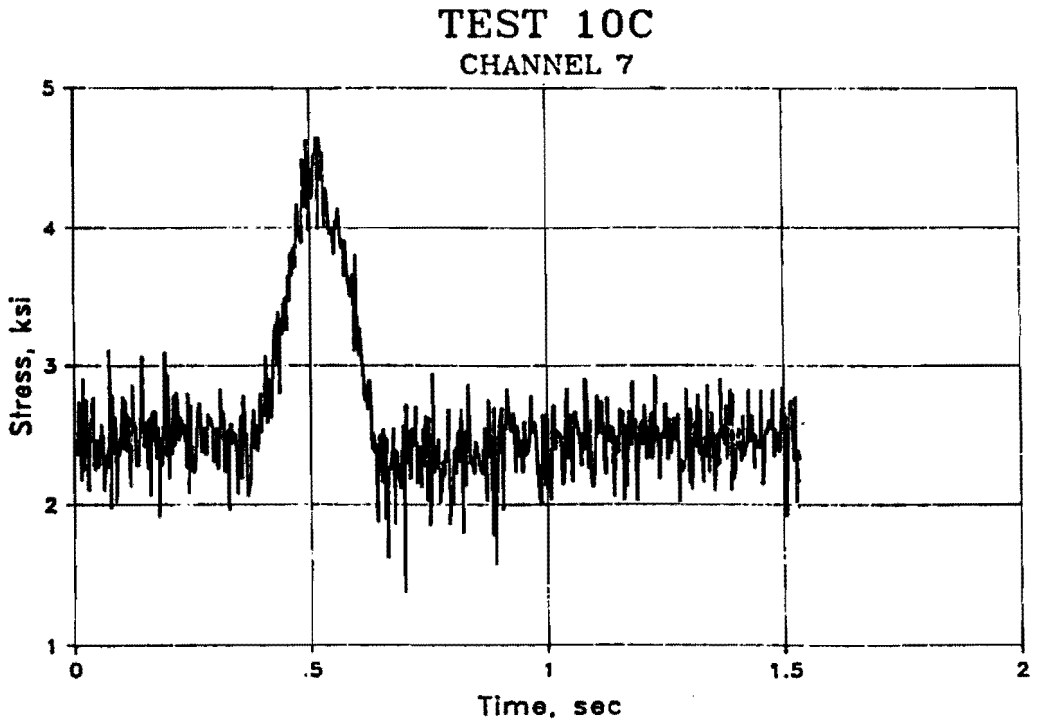
TEST 10C
CHANNEL 7
Stress, ksi
5
4
3
2
1
0
.5
1
1.5
2
Time, sec

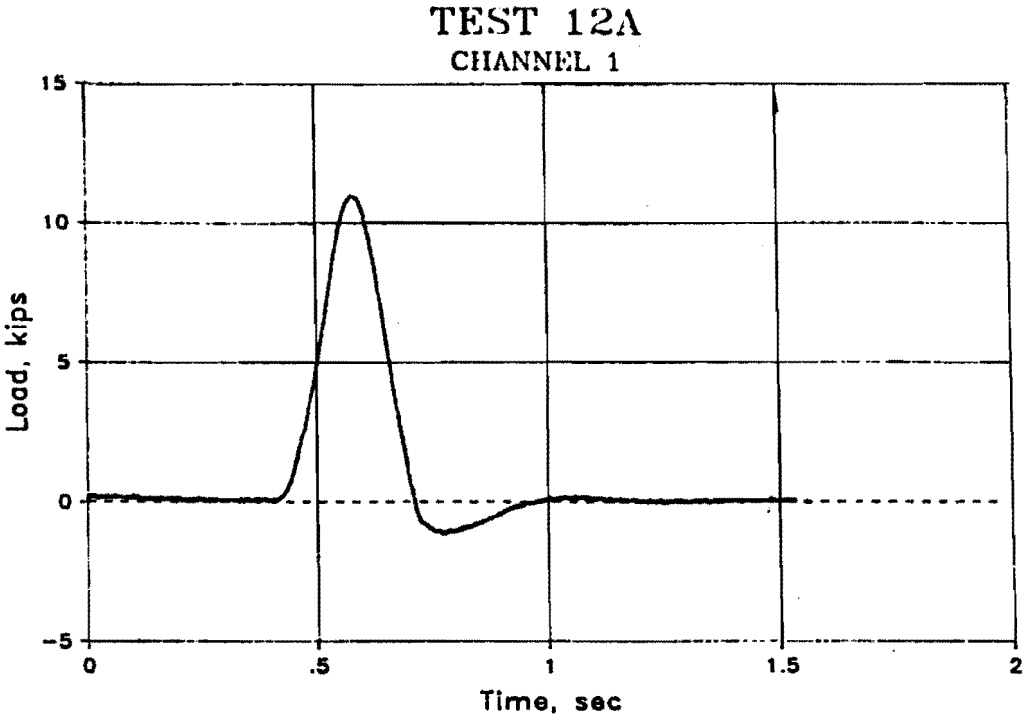
TEST 12A
CHANNEL 1
15
10
5
0
-5
Load, kips
0
.5
1
1.5
2
Time, sec

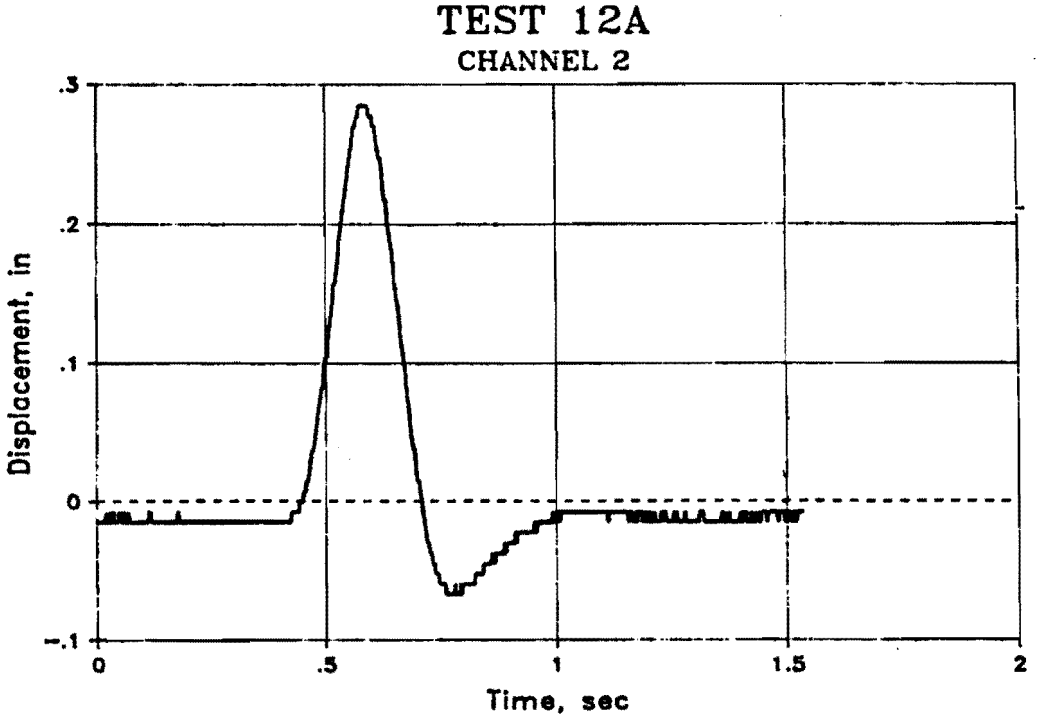
TEST 12A
CHANNEL 2
.3
.2
.1
0
-.1
Displacement, in
0
.5
1
1.5
2
Time, sec

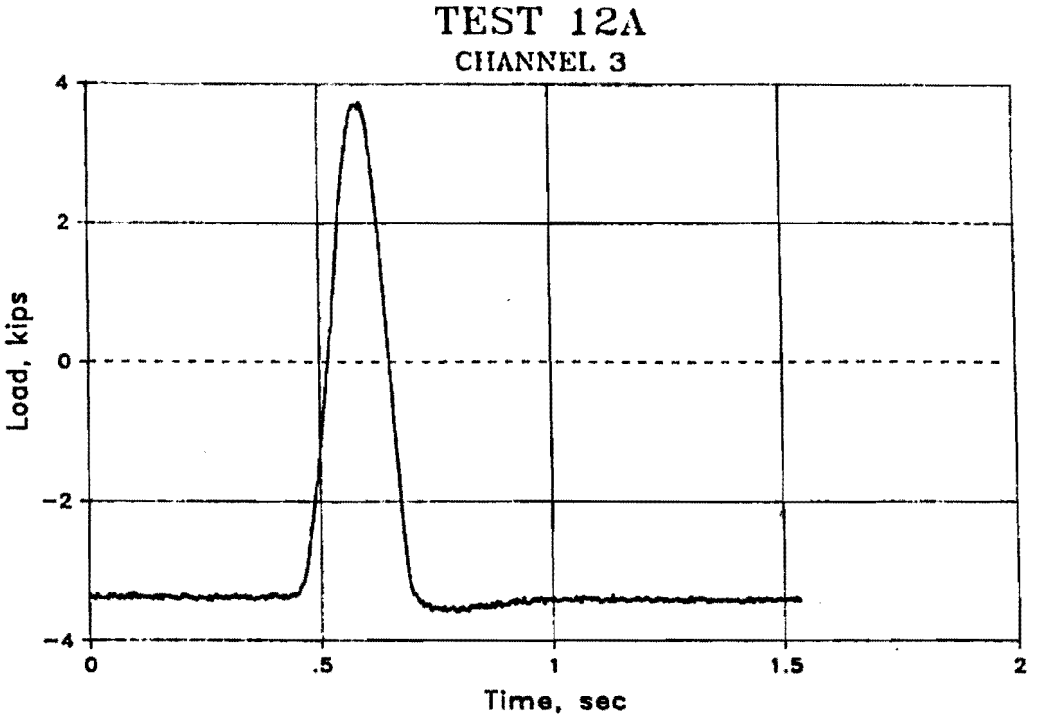
TEST 12A
CHANNEL 3
Load, kips
4
2
0
-2
-4
0
.5
1
1.5
2
Time, sec

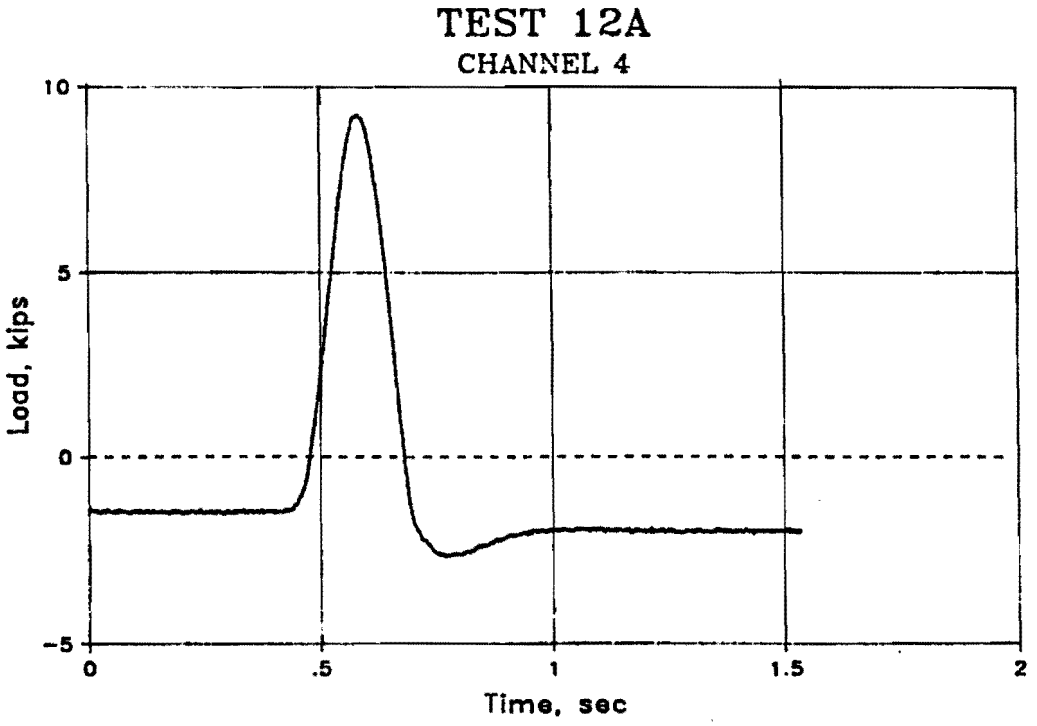
TEST 12A
CHANNEL 4
Load, kips
10
5
0
-5
0
.5
1
1.5
2
Time, sec

TEST 12A
CHANNEL 5

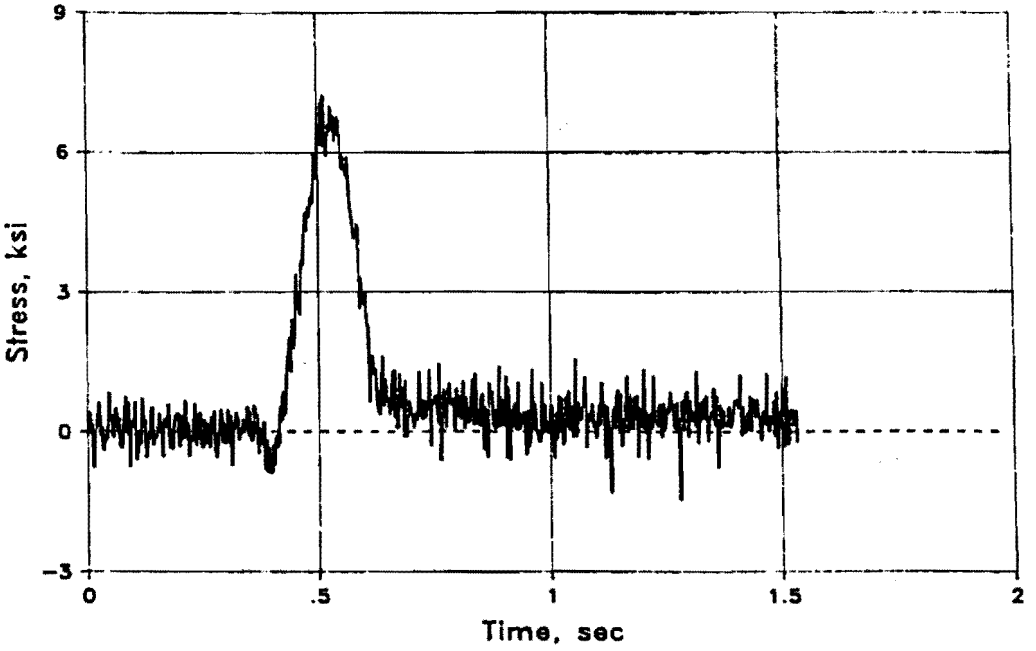

TEST 12A
CHANNEL 6

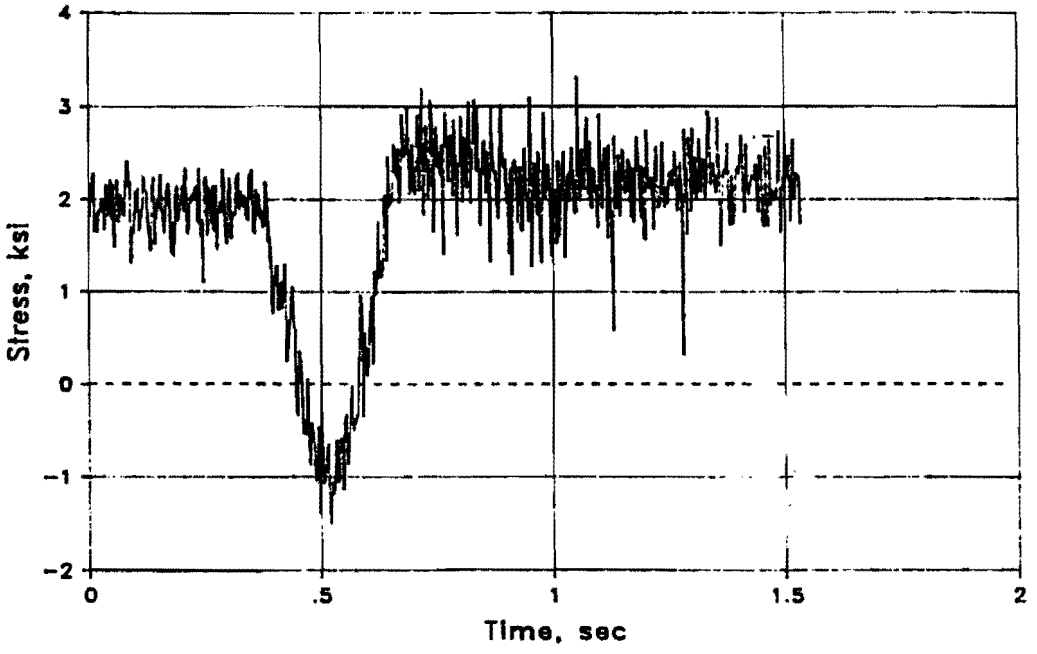

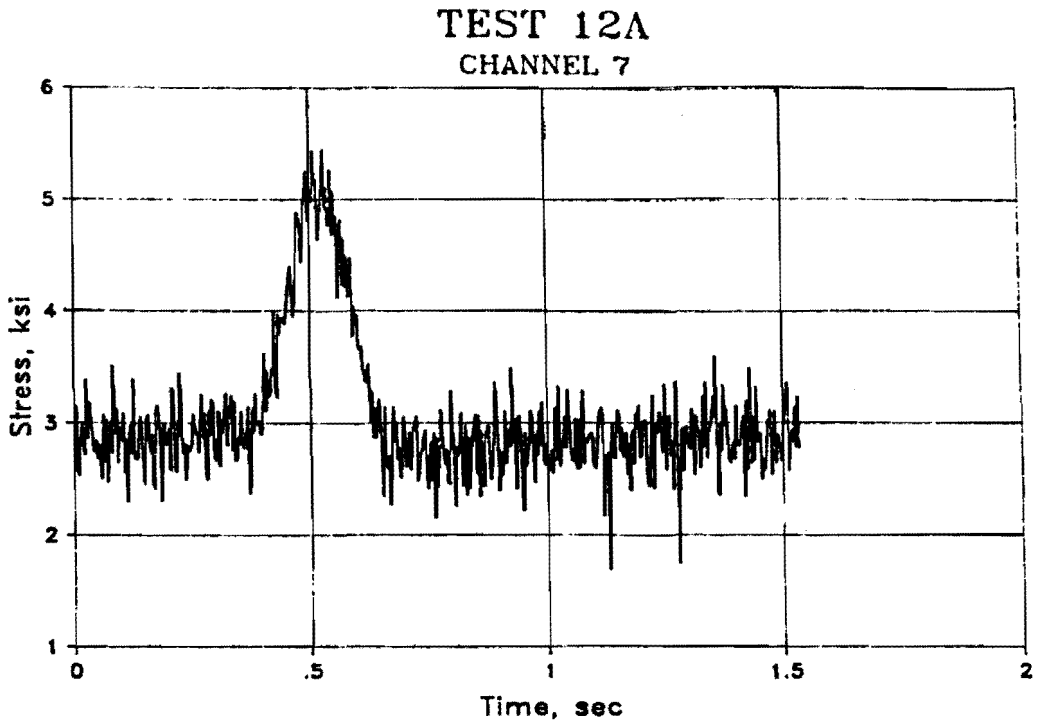
TEST 12A
CHANNEL 7
Stress, ksi
6
5
4
3
2
1
0
.5
1
1.5
2
Time, sec

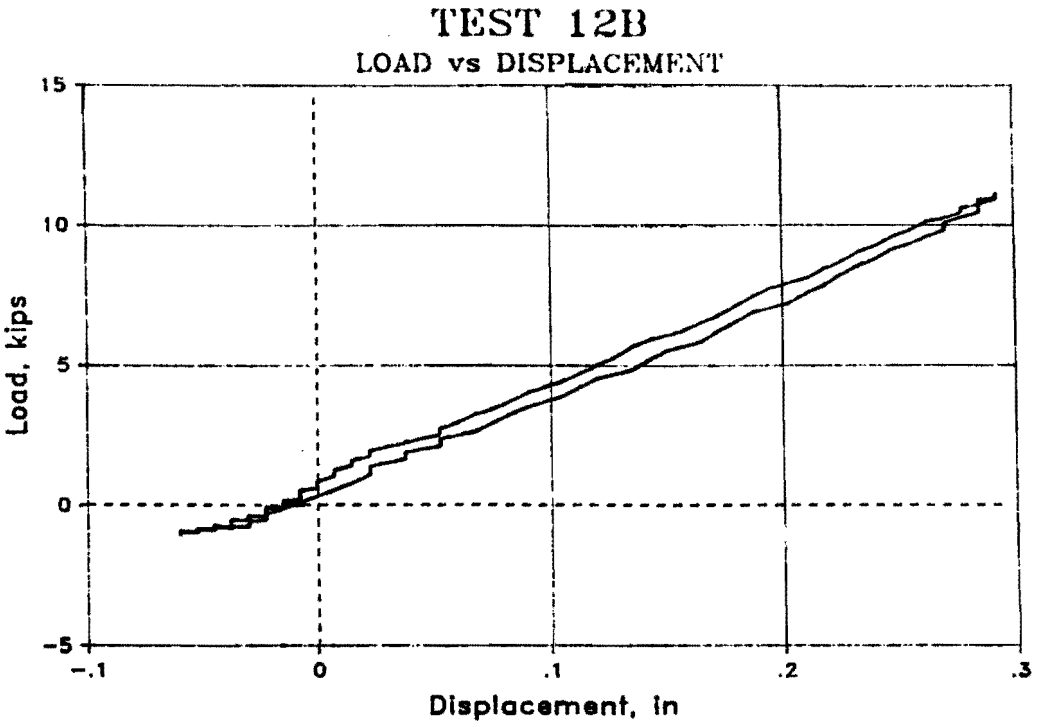
TEST 12B
LOAD vs DISPLACEMENT
15
10
5
0
-5
Load, kips
-.1
0
.1
.2
.3
Displacement, in

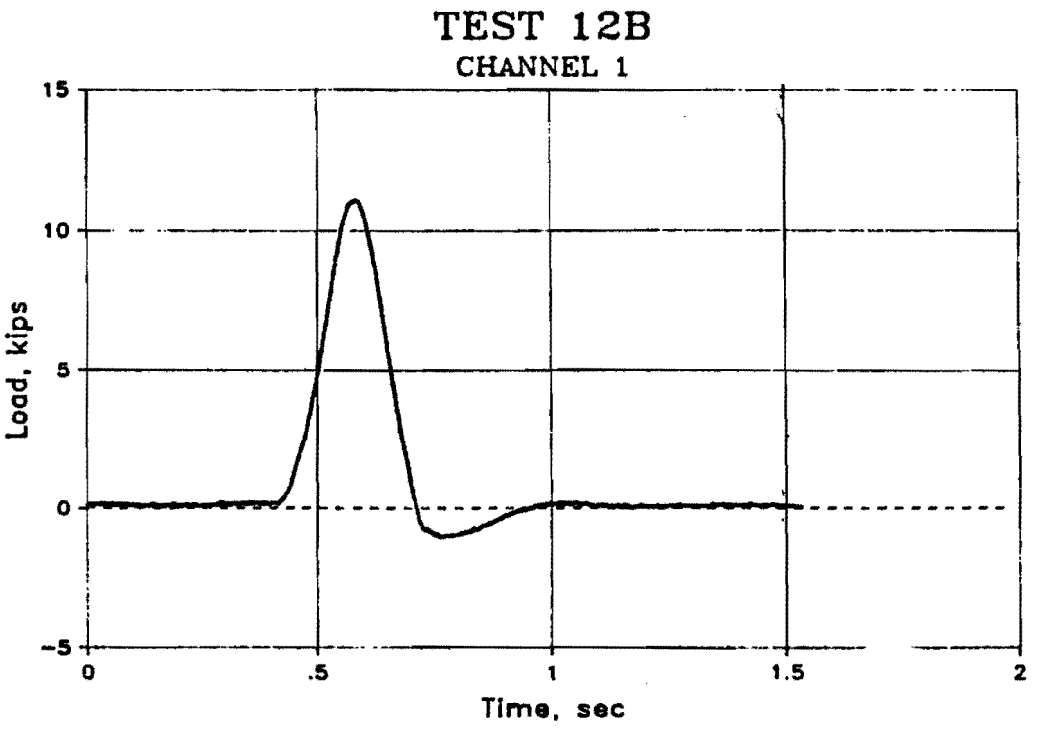
TEST 12B
CHANNEL 1
15
10
5
0
-5
Load, kips
0
.5
1
1.5
2
Time, sec

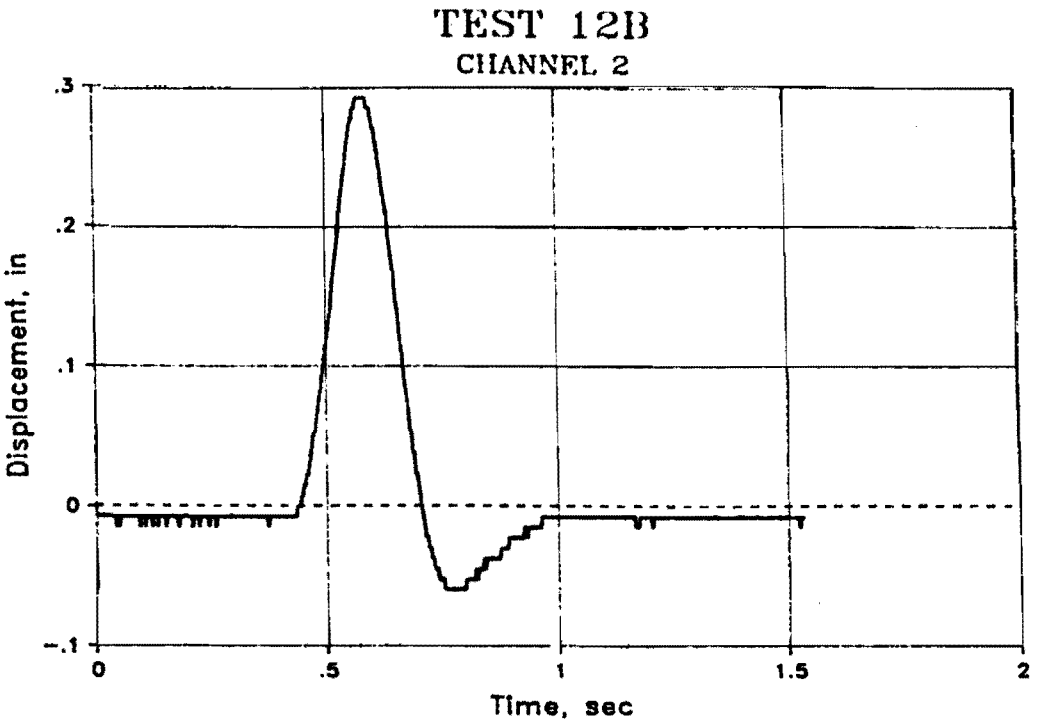
TEST 12B
CHANNEL 2
Displacement, in
.3
.2
.1
0
-.1
0
.5
1
1.5
2
Time, sec

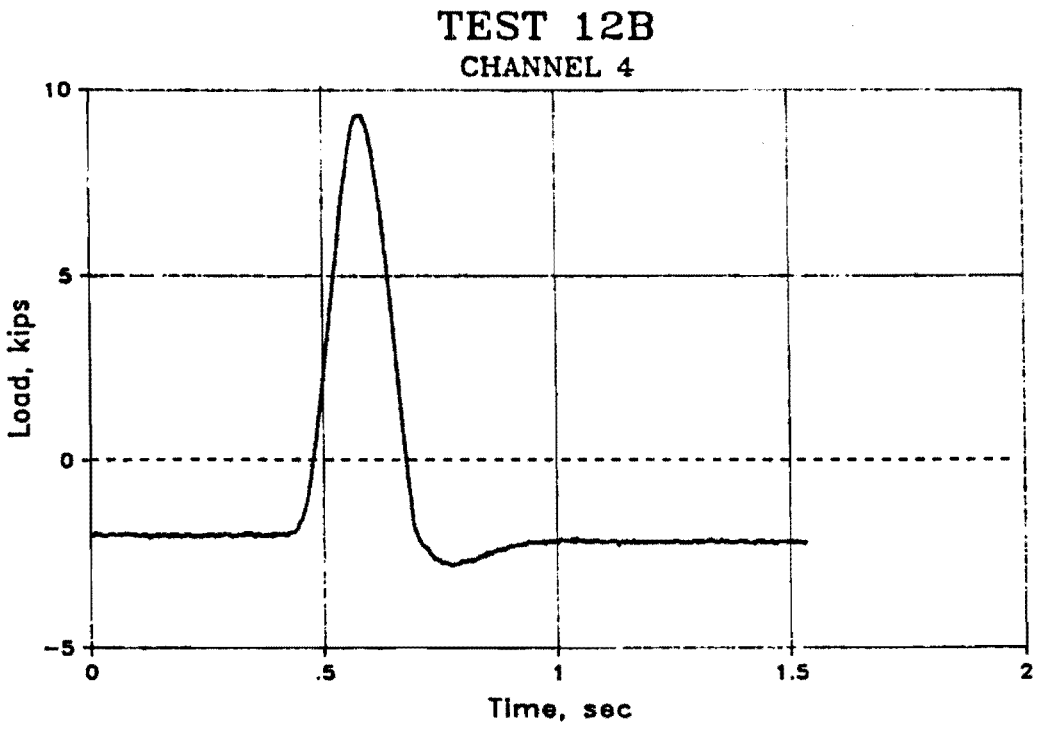
TEST 12B
CHANNEL 4
Load, kips
10
5
0
-5
0
.5
1
1.5
2
Time, sec

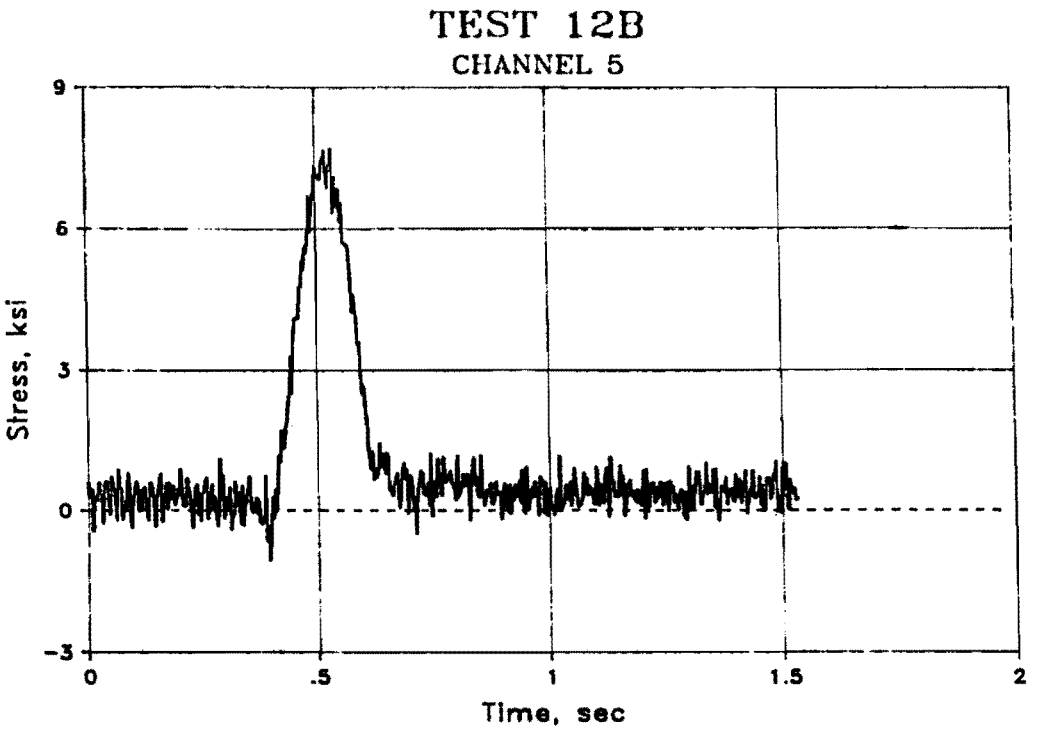
TEST 12B
CHANNEL 5
Stress, ksi
9
6
3
0
-3
0
.5
1
1.5
2
Time, sec

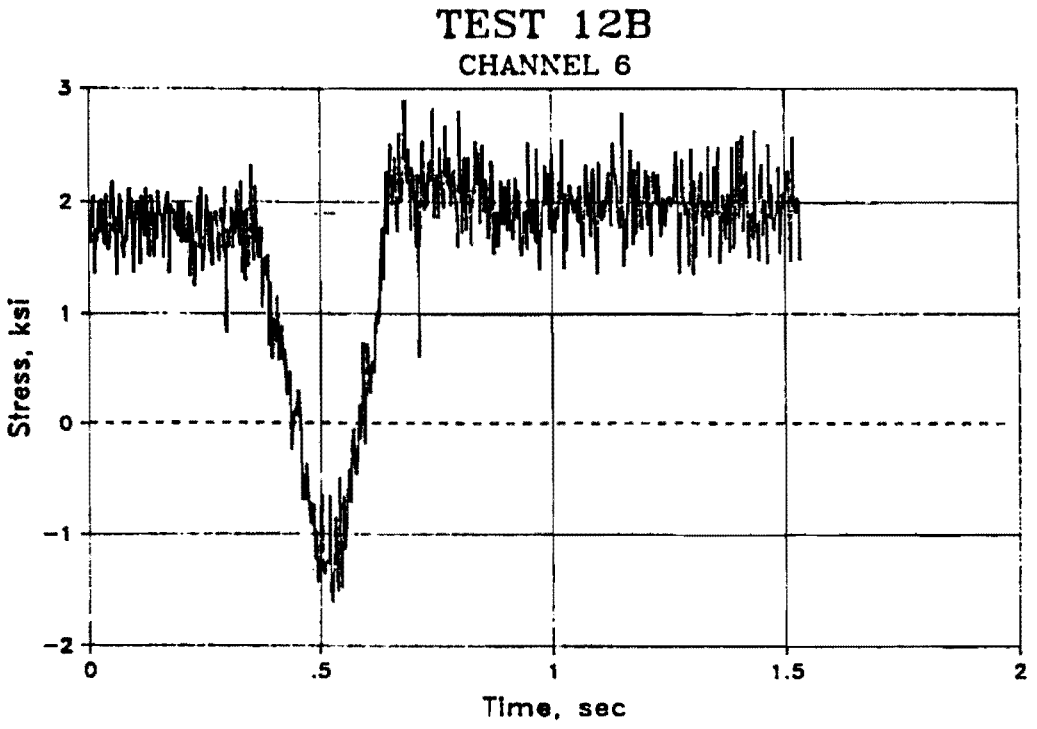
TEST 12B
CHANNEL 6
Stress, ksi
3
2
1
0
-1
-2
0
.5
1
1.5
2
Time, sec

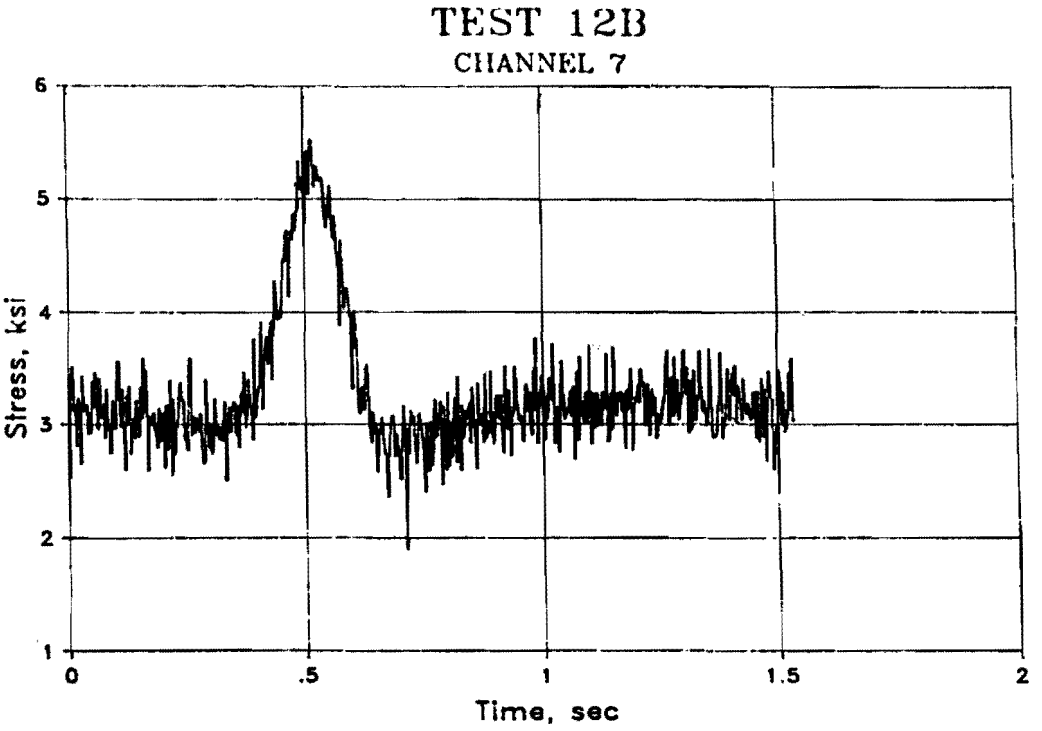
TEST 12B
CHANNEL 7
Stress, ksi
6
5
4
3
2
1
0
.5
1
1.5
2
Time, sec

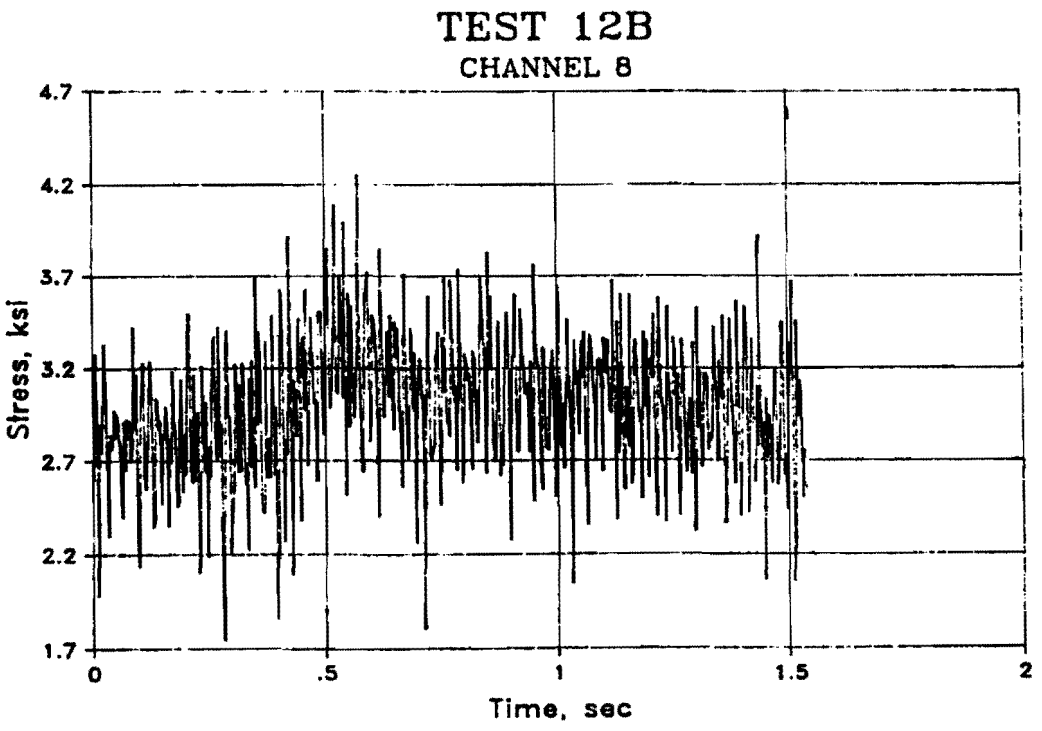
TEST 12B
CHANNEL 8
Stress, ksi
4.7
4.2
3.7
3.2
2.7
2.2
1.7
0
.5
1
1.5
2
Time, sec

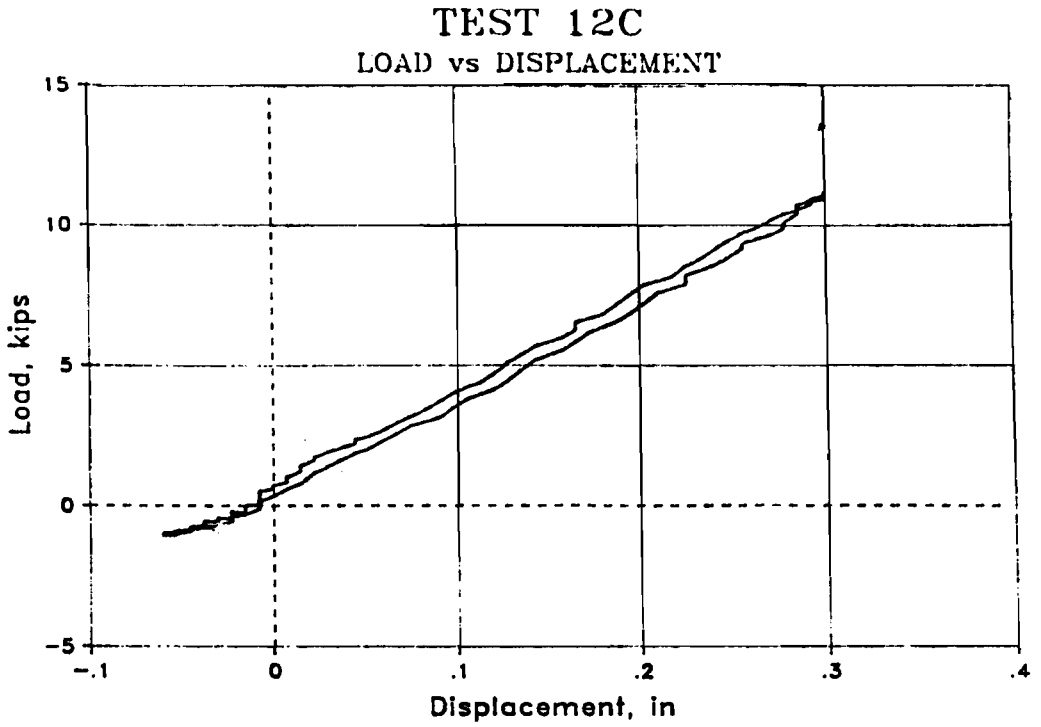
TEST 12C
LOAD vs DISPLACEMENT
15
10
5
0
-5
Load, kips
-.1
0
.1
.2
.3
.4
Displacement, in

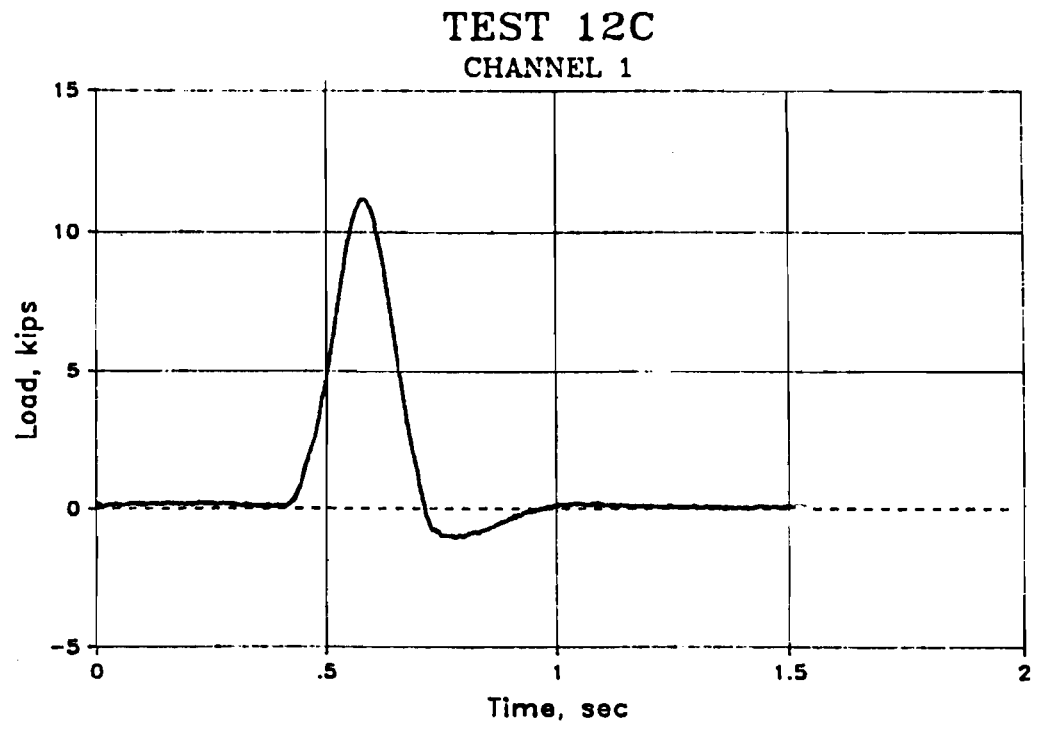
TEST 12C
CHANNEL 1
15
10
5
0
-5
Load, kips
0
.5
1
1.5
2
Time, sec

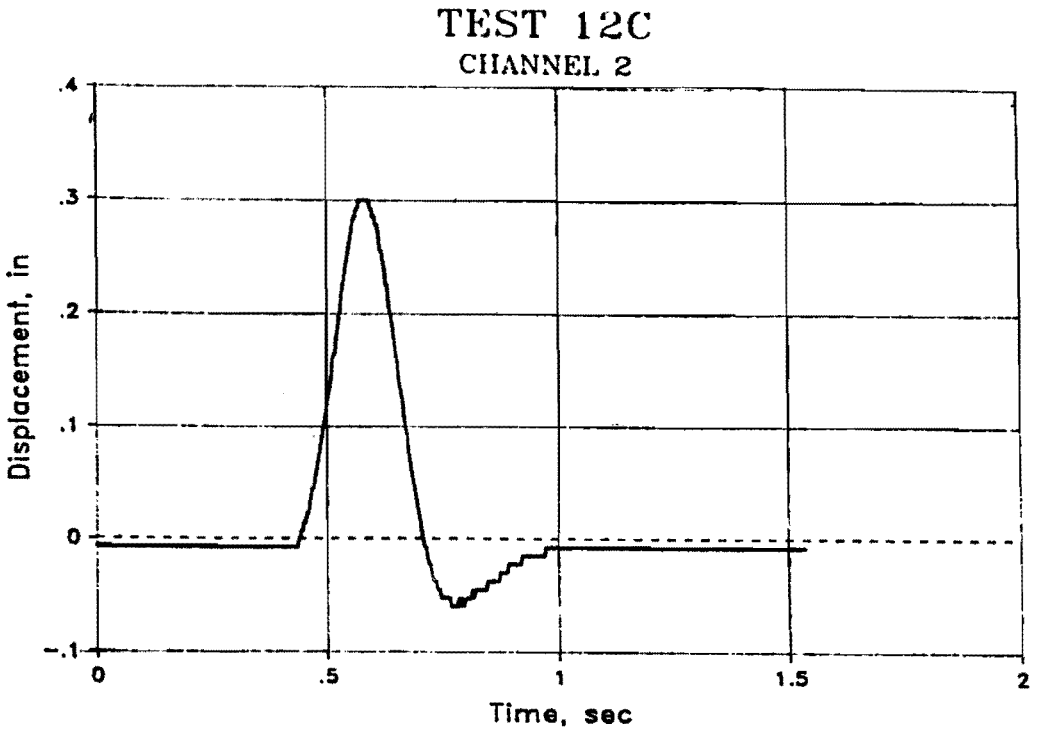
TEST 12C
CHANNEL 2
Displacement, in
.4
.3
.2
.1
0
-.1
0
.5
1
1.5
2
Time, sec

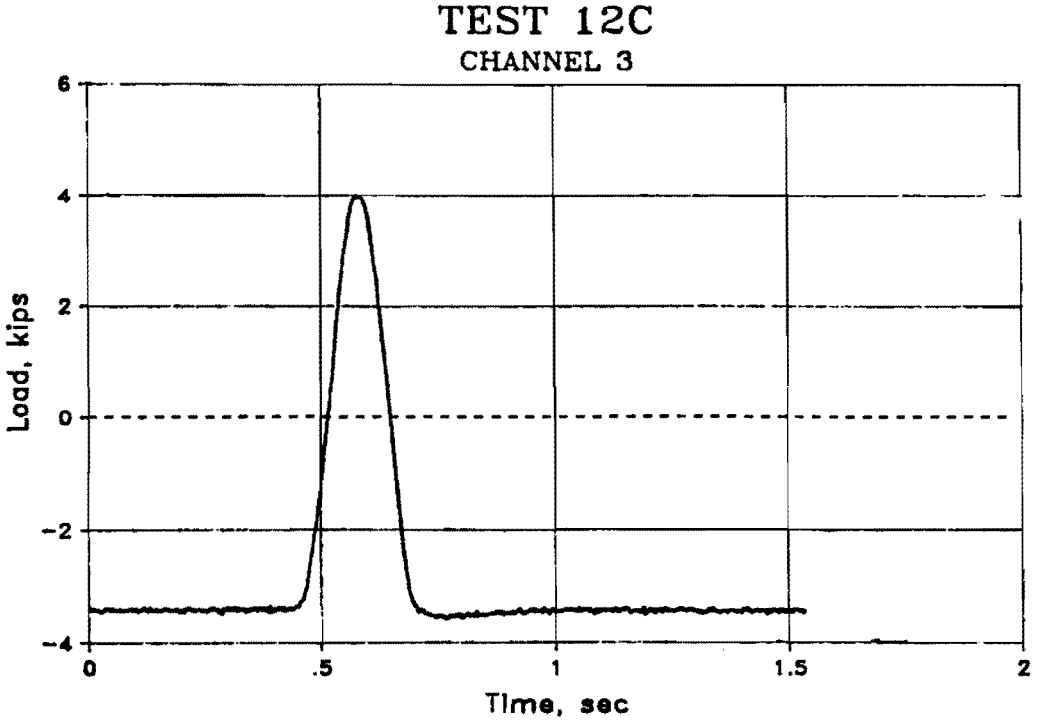
TEST 12C
CHANNEL 3
Load, kips
6
4
2
0
-2
-4
0
.5
1
1.5
2
Time, sec

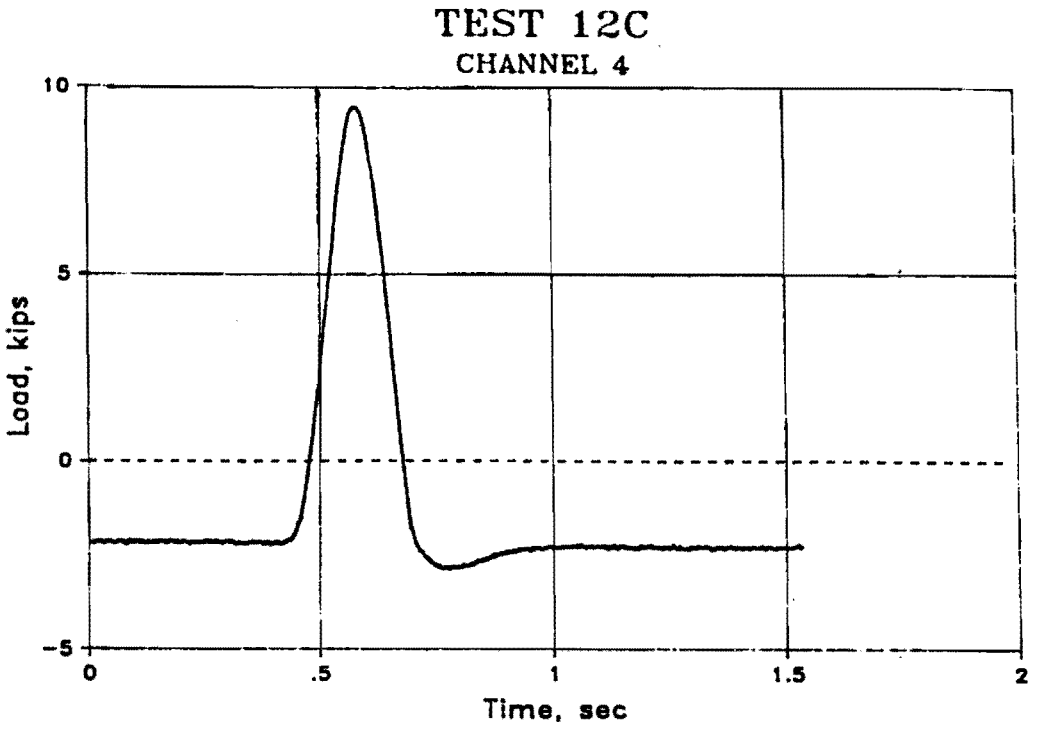
TEST 12C
CHANNEL 4
10
5
0
-5
Load, kips
0
.5
1
1.5
2
Time, sec

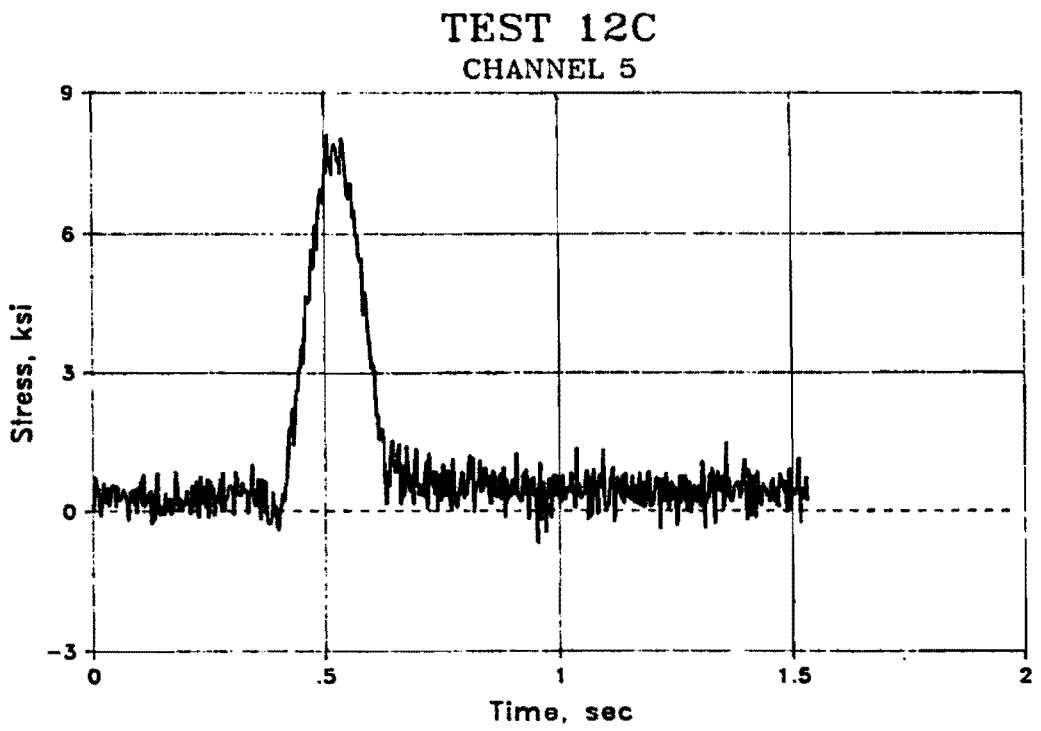
TEST 12C
CHANNEL 5
9
6
3
0
-3
Stress, ksi
0
.5
1
1.5
2
Time, sec

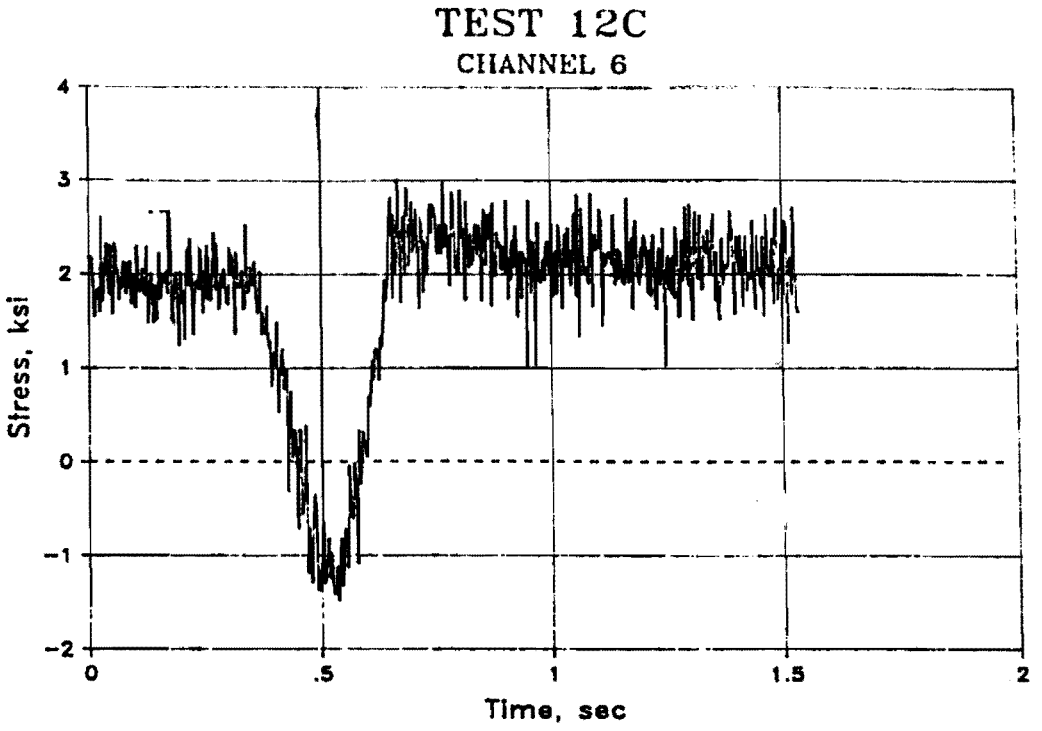
TEST 12C
CHANNEL 6
Stress, ksi
4
3
2
1
0
-1
-2
0
.5
1
1.5
2
Time, sec

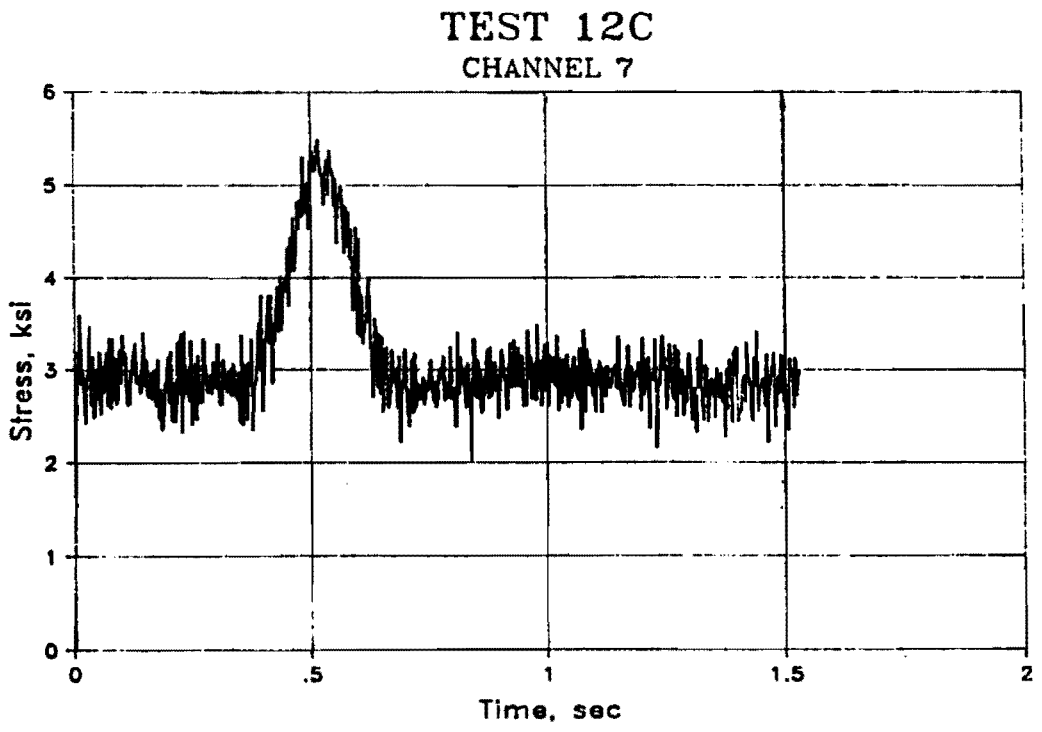
TEST 12C
CHANNEL 7
Stress, ksi
6
5
4
3
2
1
0
0
.5
1
1.5
2
Time, sec

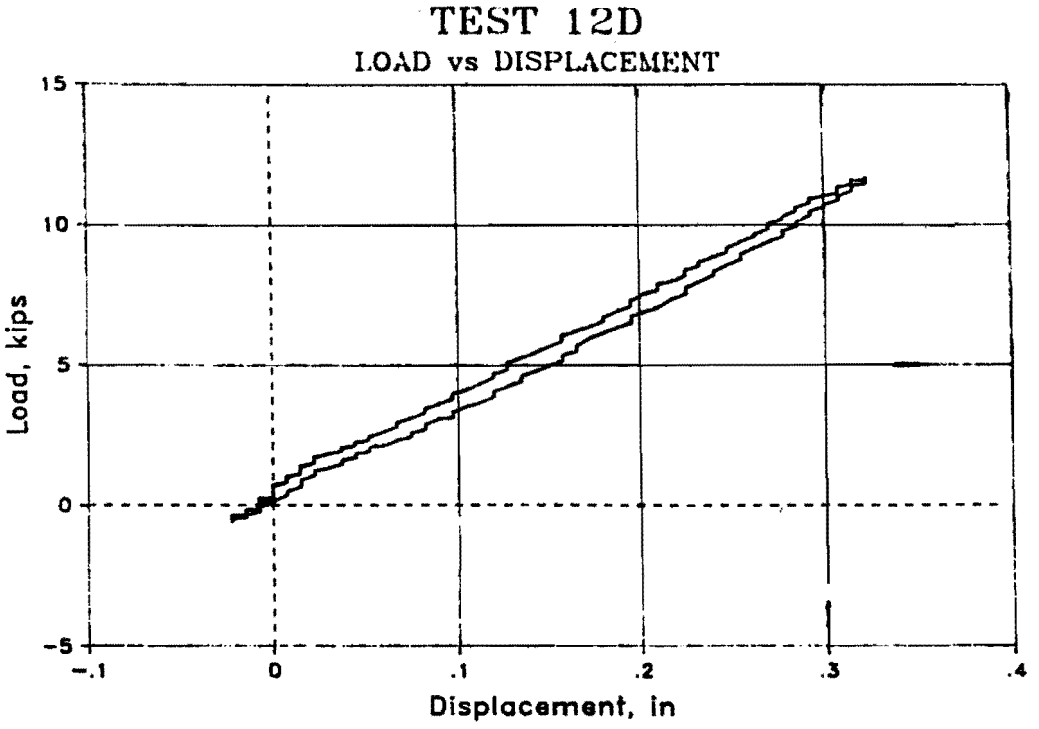
TEST 12D
LOAD vs DISPLACEMENT
Load, kips
15
10
5
0
-5
-.1
0
.1
.2
.3
.4
Displacement, in

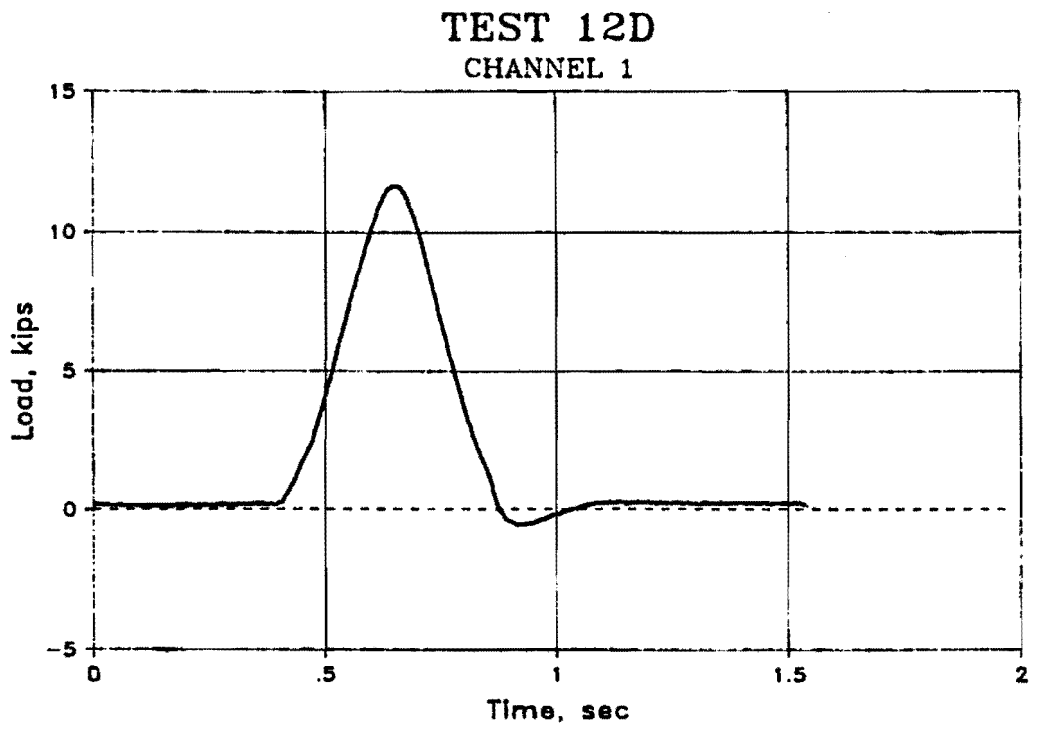
TEST 12D
CHANNEL 1
Load, kips
15
10
5
0
-5
0
.5
1
1.5
2
Time, sec

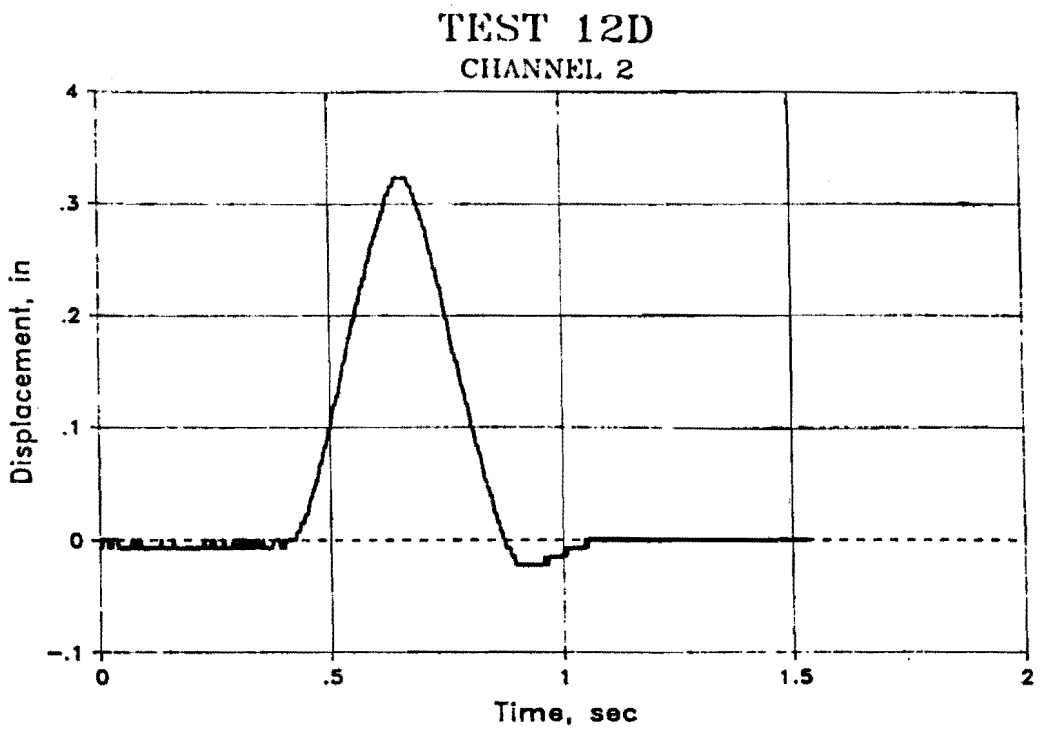
TEST 12D
CHANNEL 2
Displacement, in
4
.3
.2
.1
0
-.1
0
.5
1
1.5
2
Time, sec

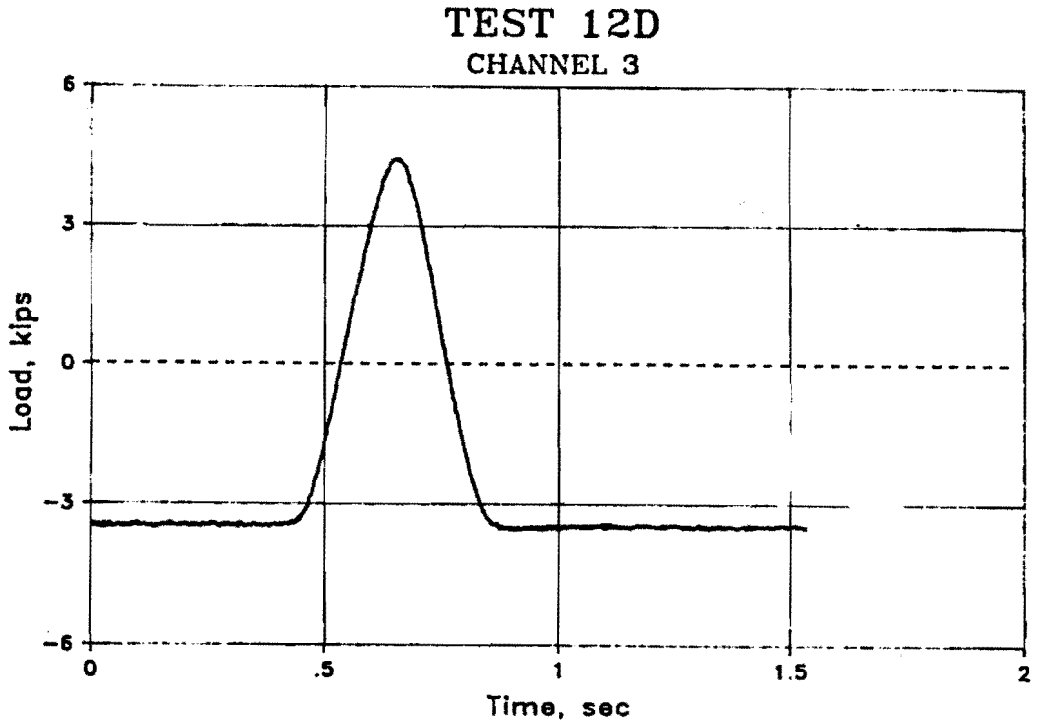
TEST 12D
CHANNEL 3
Load, kips
6
3
0
-3
-6
0
.5
1
1.5
2
Time, sec

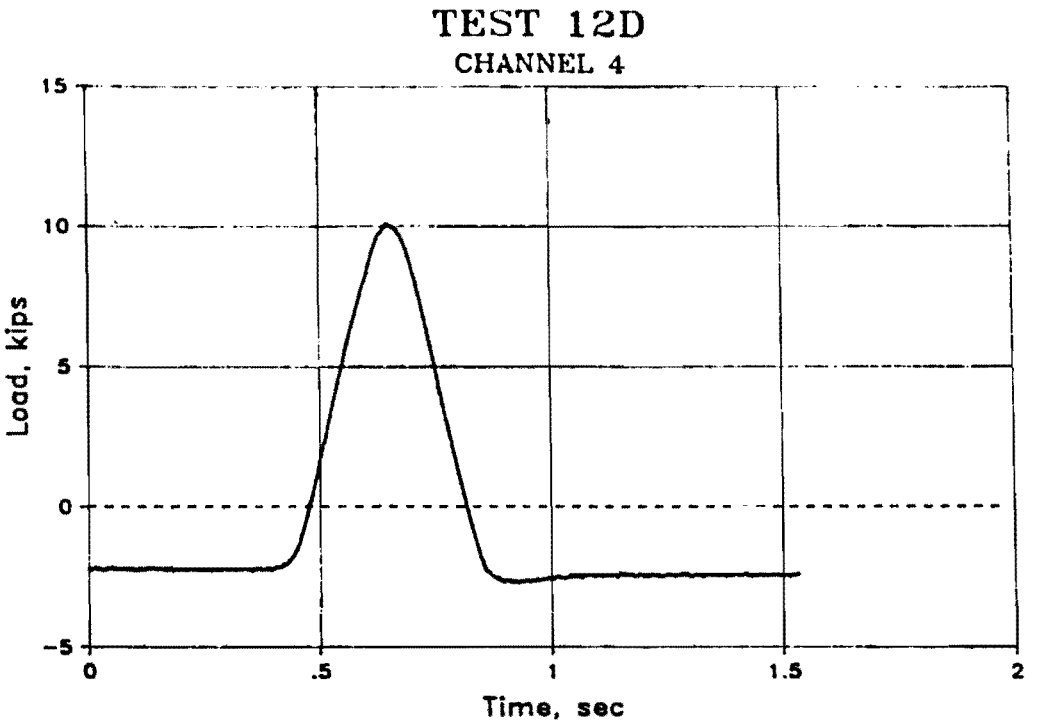
TEST 12D
CHANNEL 4
Load, kips
15
10
5
0
-5
0
.5
1
1.5
2
Time, sec

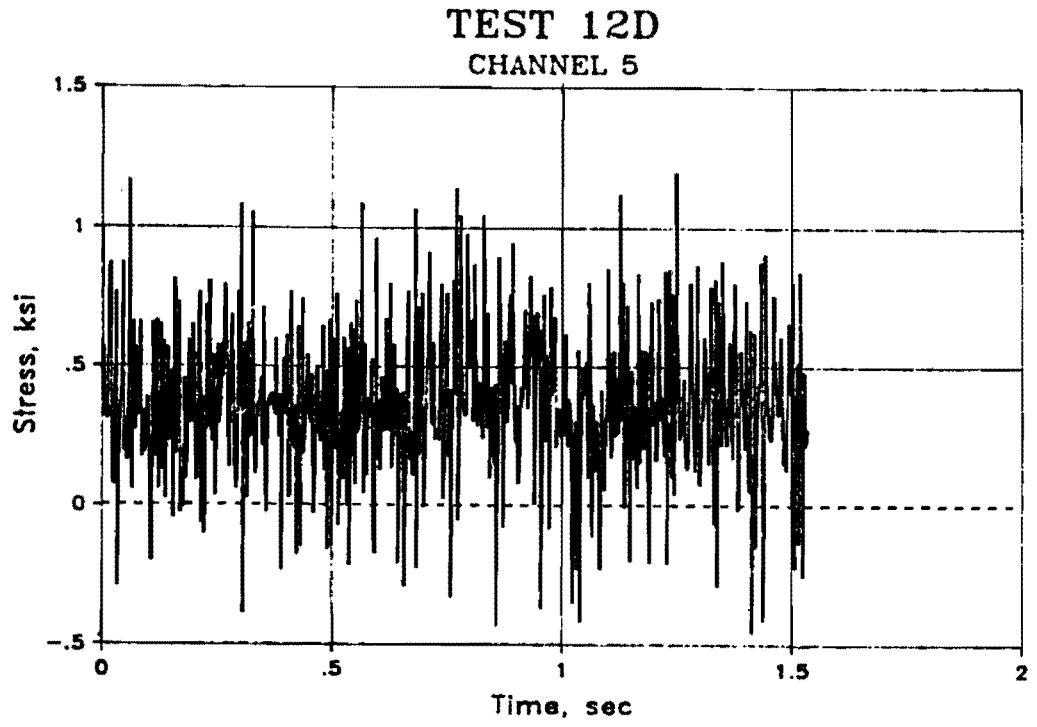
TEST 12D
CHANNEL 5
Stress, ksi
1.5
1
.5
0
-.5
0
.5
1
1.5
2
Time, sec

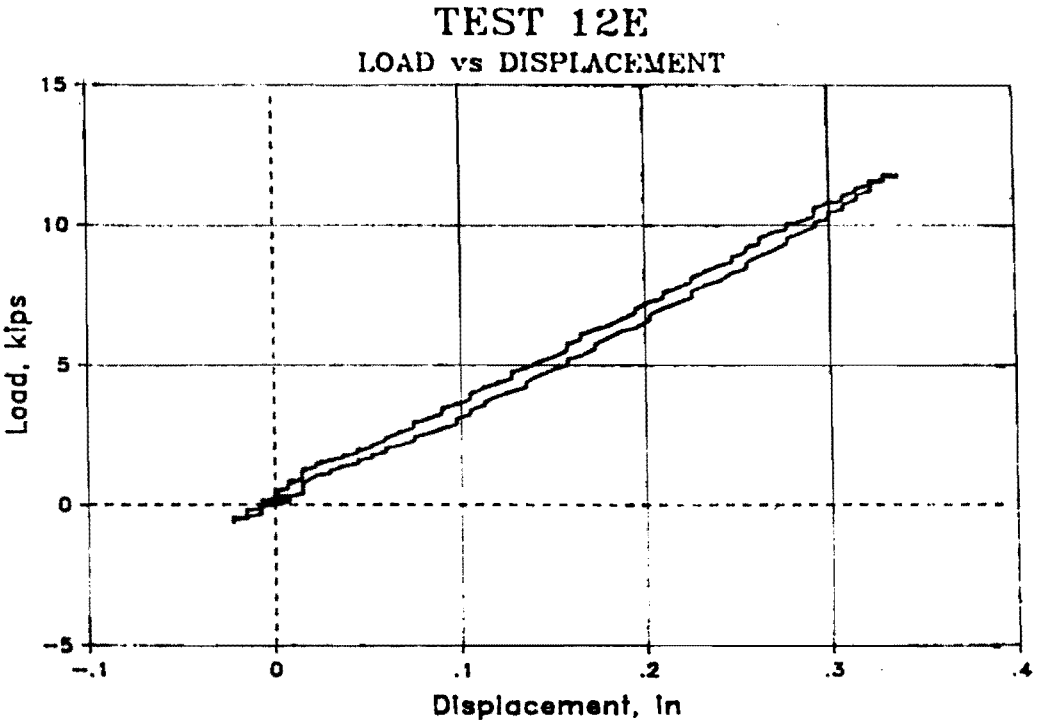
TEST 12E
LOAD vs DISPLACEMENT
Load, kips
15
10
5
0
-5
-.1
0
.1
.2
.3
.4
Displacement, in

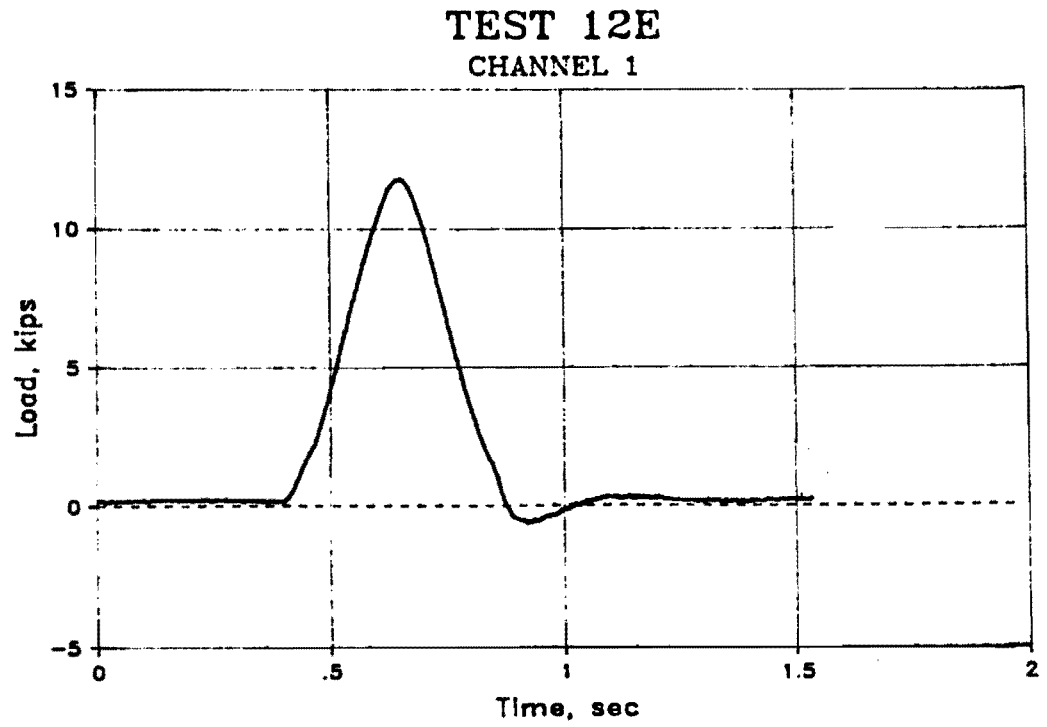
TEST 12E
CHANNEL 1
Load, kips
15
10
5
0
-5
0
.5
1
1.5
2
Time, sec

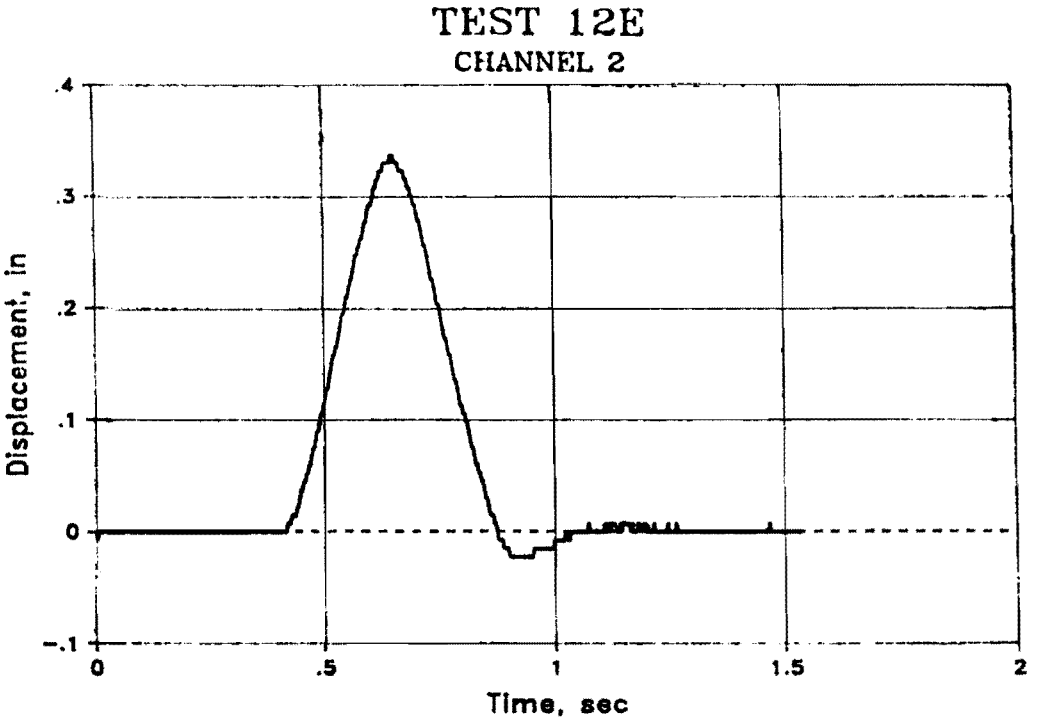
TEST 12E
CHANNEL 2
Displacement, in
.4
.3
.2
.1
0
-.1
0
.5
1
1.5
2
Time, sec

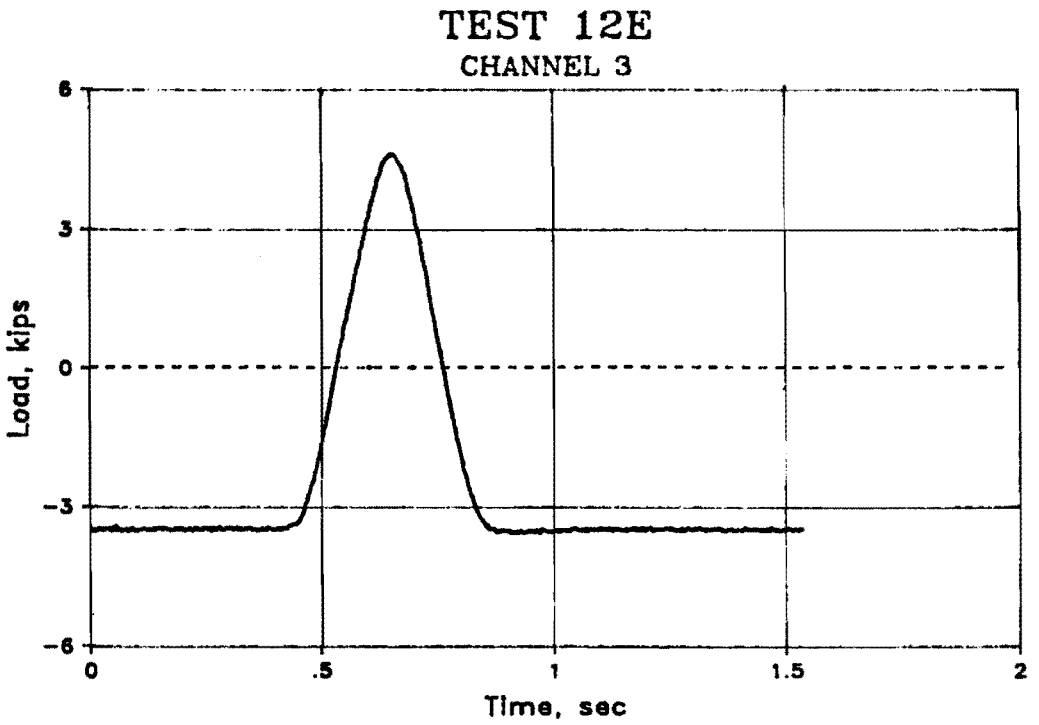
TEST 12E
CHANNEL 3
Load, kips
6
3
0
-3
-6
0
.5
1
1.5
2
Time, sec

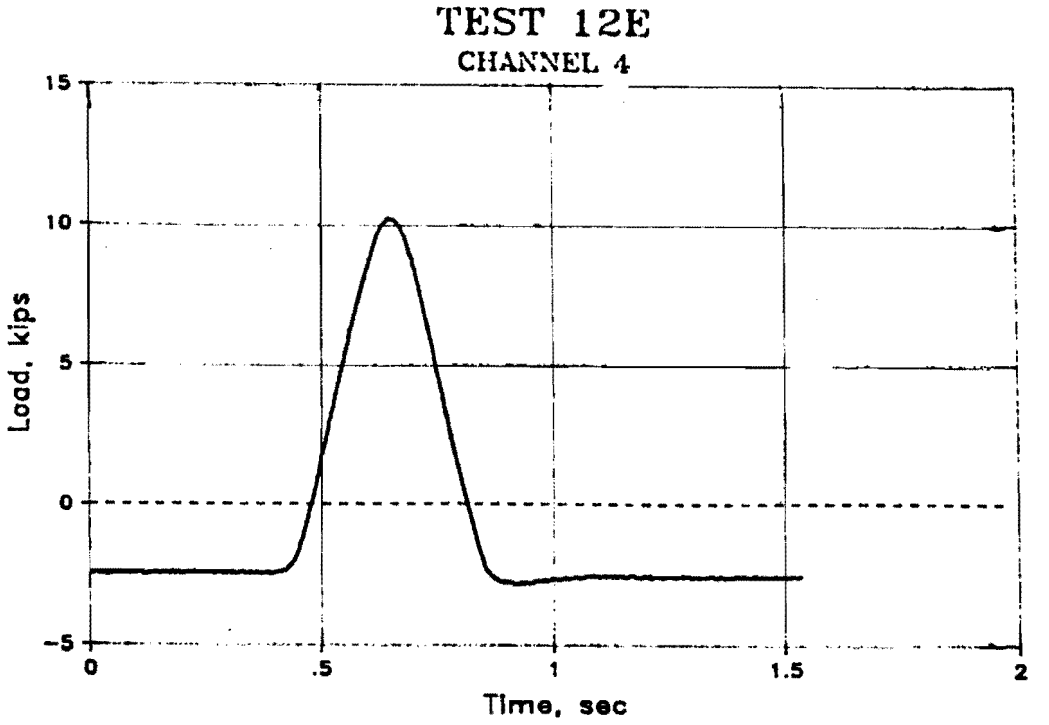
TEST 12E
CHANNEL 4
Load, kips
15
10
5
0
-5
0
.5
1
1.5
2
Time, sec

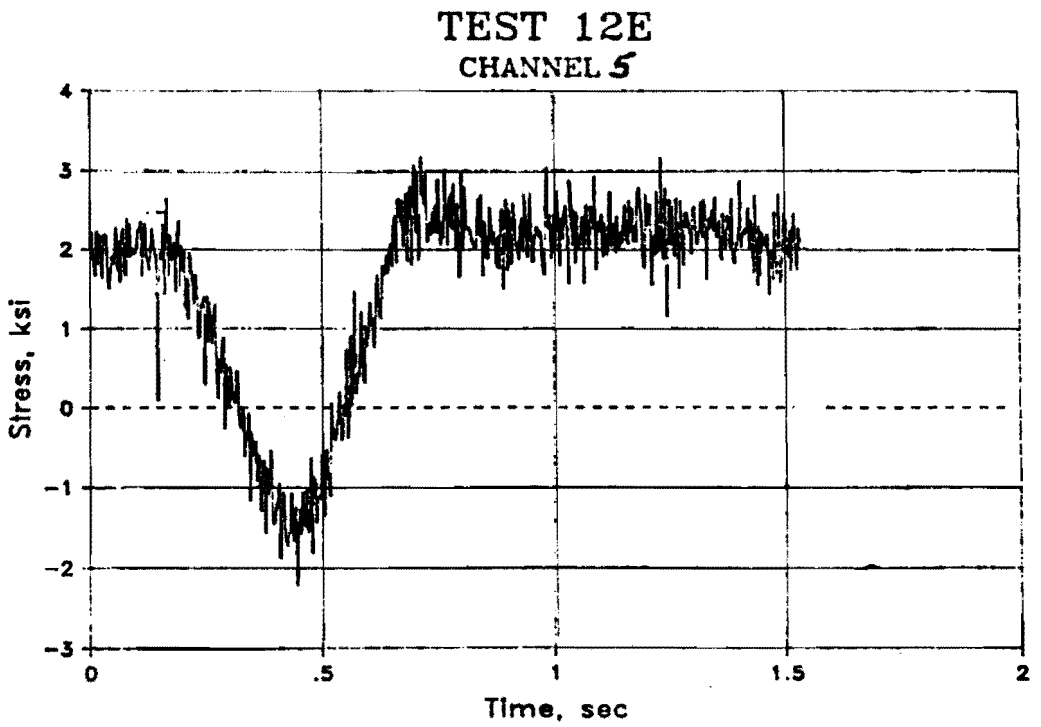
TEST 12E
CHANNEL 5
Stress, ksi
4
3
2
1
0
-1
-2
-3
0
.5
1
1.5
2
Time, sec

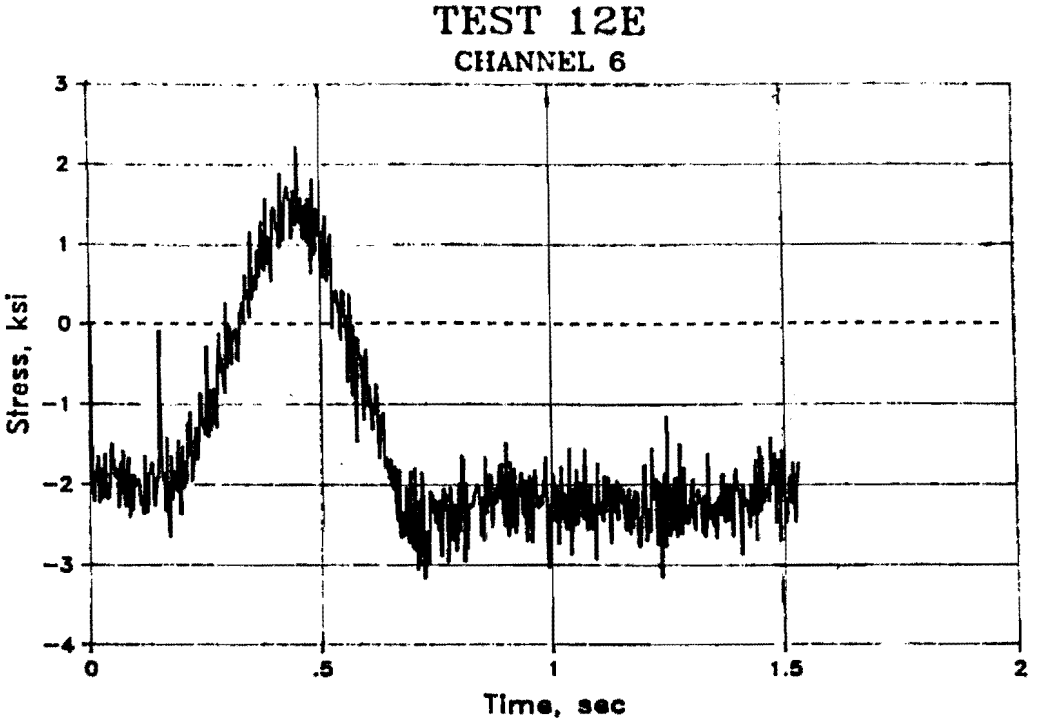
TEST 12E
CHANNEL 6
Stress, ksi
3
2
1
0
-1
-2
-3
-4
0
.5
1
1.5
2
Time, sec

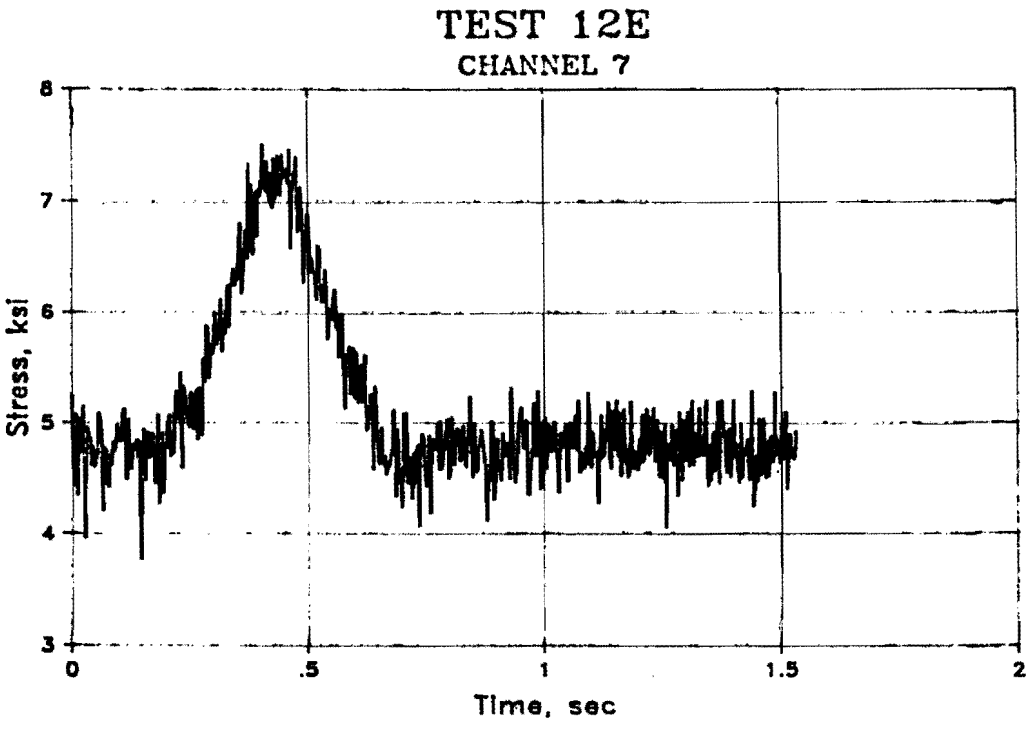
TEST 12E
CHANNEL 7
Stress, ksi
8
7
6
5
4
3
0
.5
1
1.5
2
Time, sec

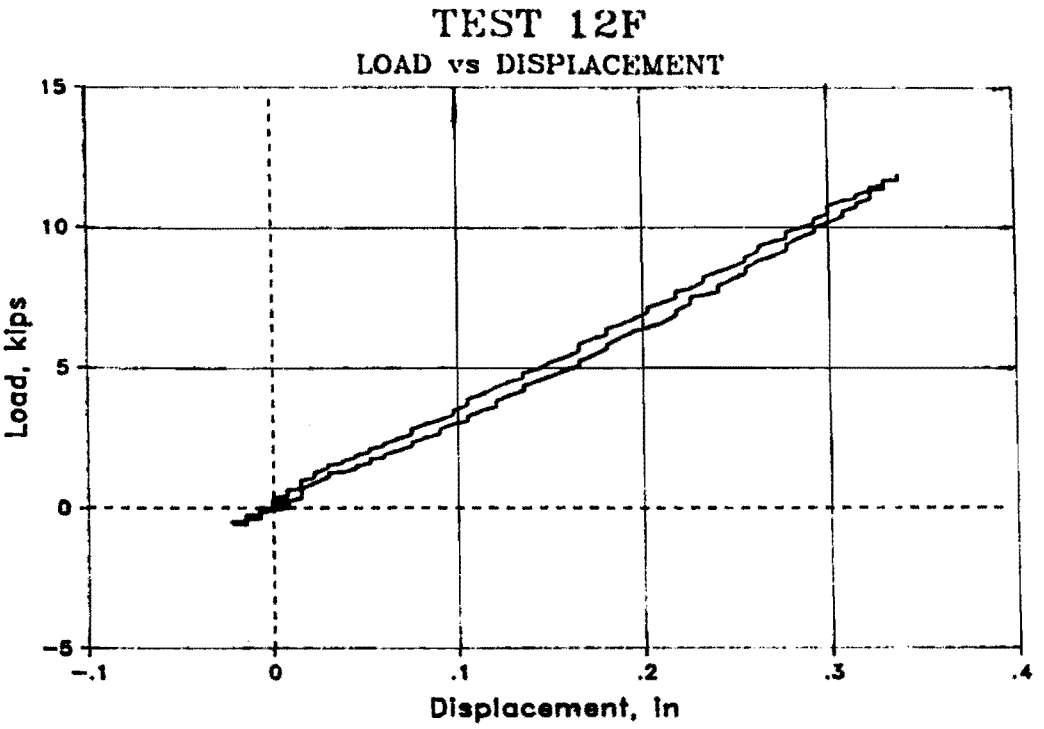
TEST 12F
LOAD vs DISPLACEMENT
Load, kips
15
10
5
0
-5
-.1
0
.1
.2
.3
.4
Displacement, in

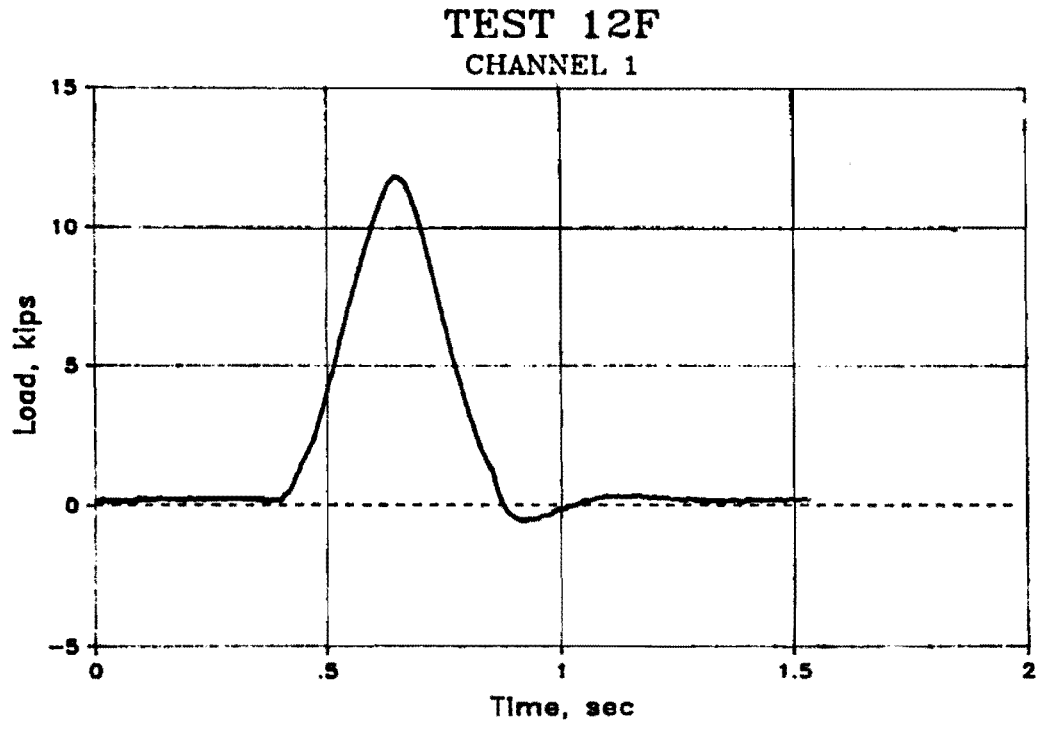
TEST 12F
CHANNEL 1
Load, kips
15
10
5
0
-5
0
.5
1
1.5
2
Time, sec

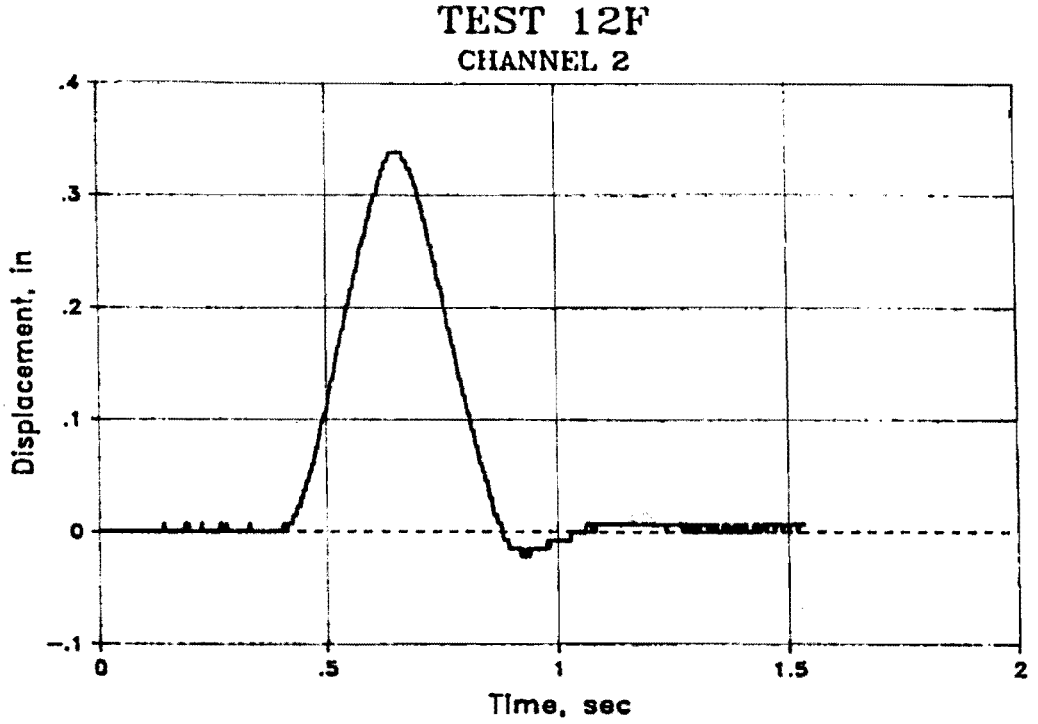
TEST 12F
CHANNEL 2
Displacement, in
.4
.3
.2
.1
0
-.1
0
.5
1
1.5
2
Time, sec

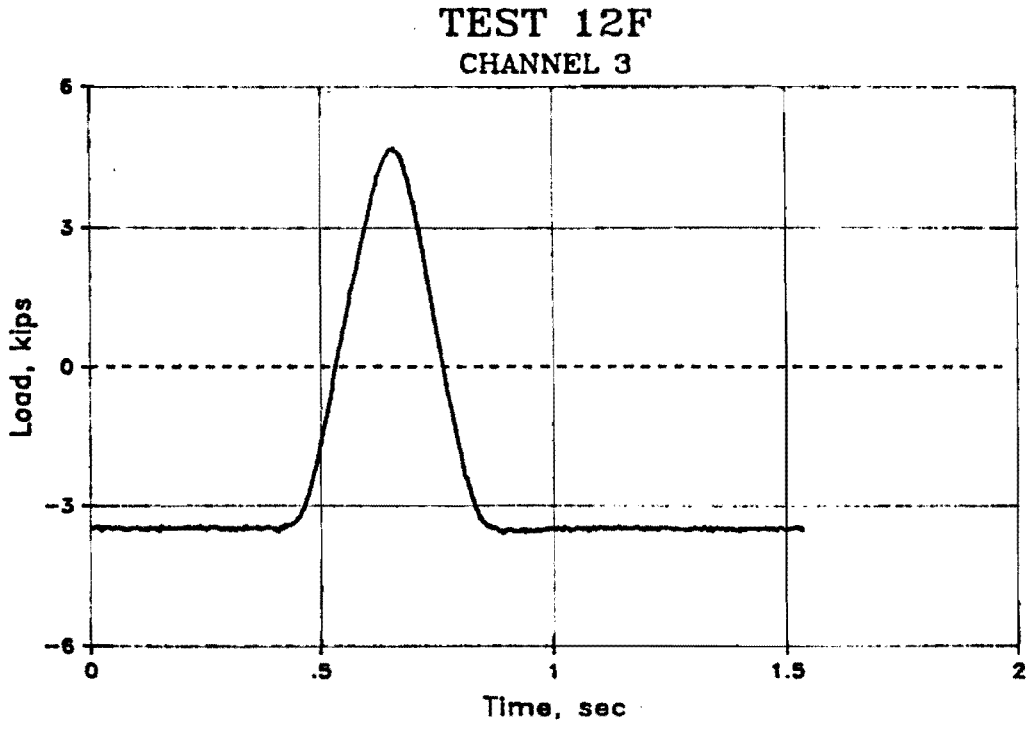
TEST 12F
CHANNEL 3
Load, kips
6
3
0
-3
-6
0
.5
1
1.5
2
Time, sec

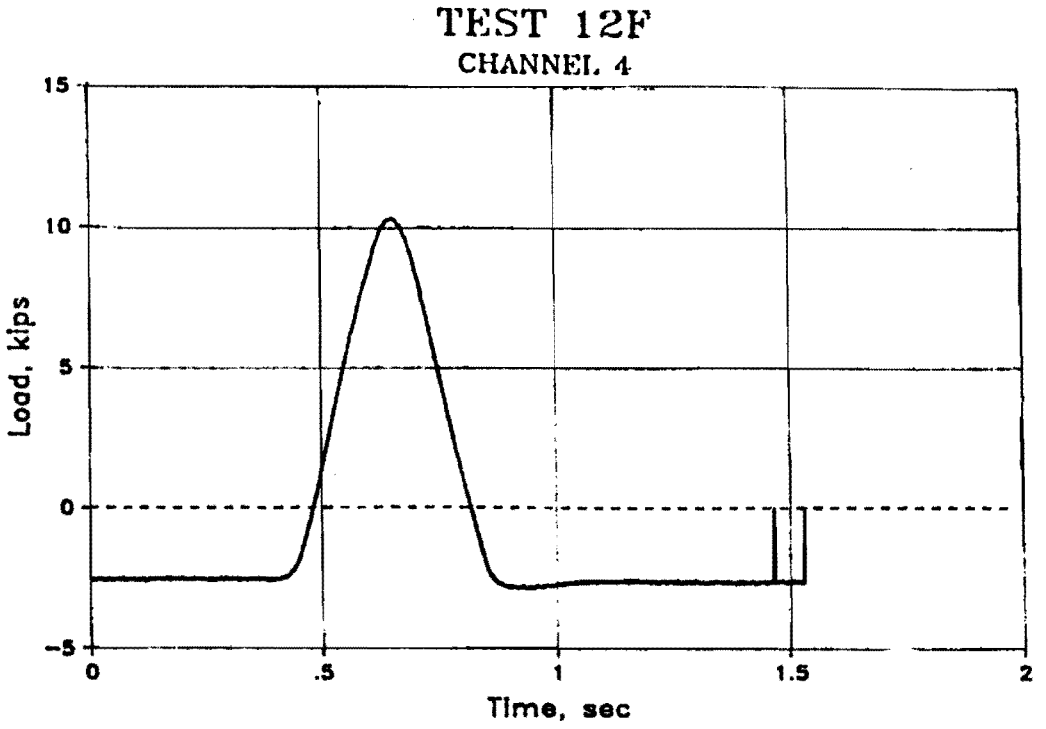
TEST 12F
CHANNEL 4
Load, kips
15
10
5
0
-5
0
.5
1
1.5
2
Time, sec

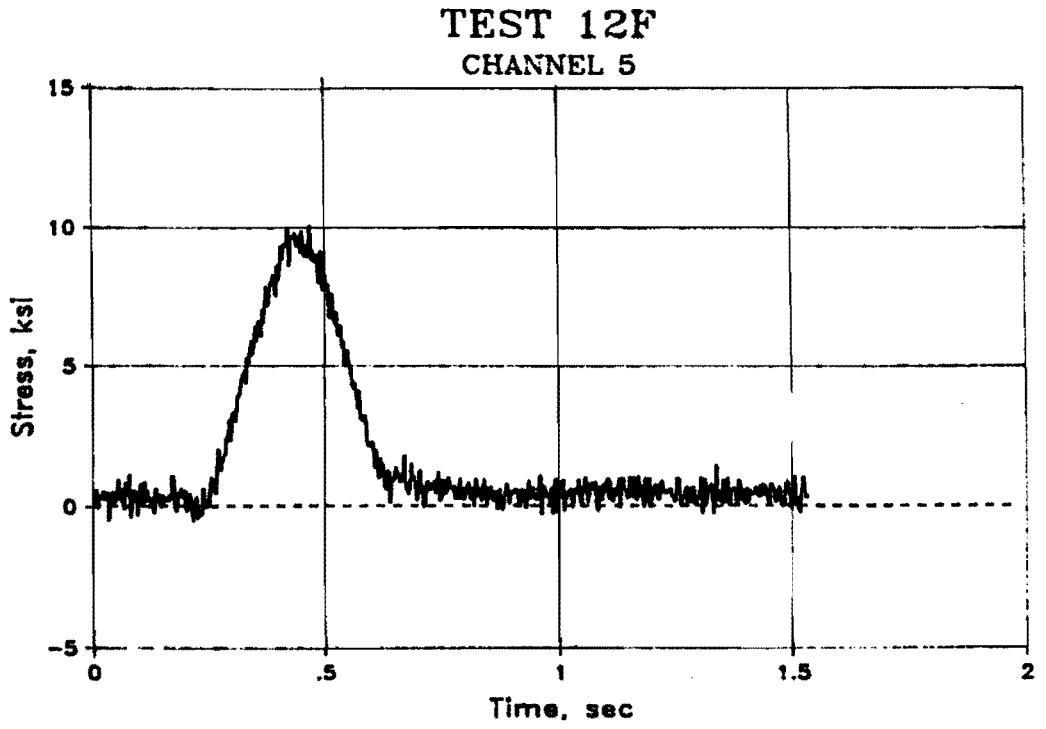
TEST 12F
CHANNEL 5
Stress, ksi
15
10
5
0
-5
0
.5
1
1.5
2
Time, sec

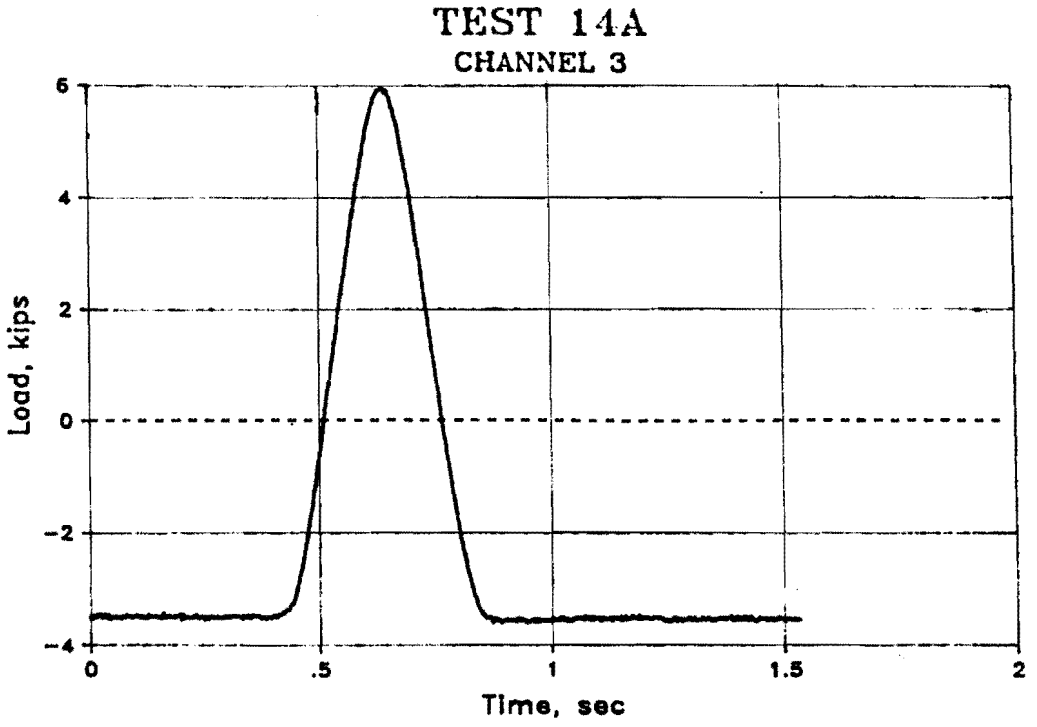
TEST 14A
CHANNEL 3
Load, kips
6
4
2
0
-2
-4
0
.5
1
1.5
2
Time, sec

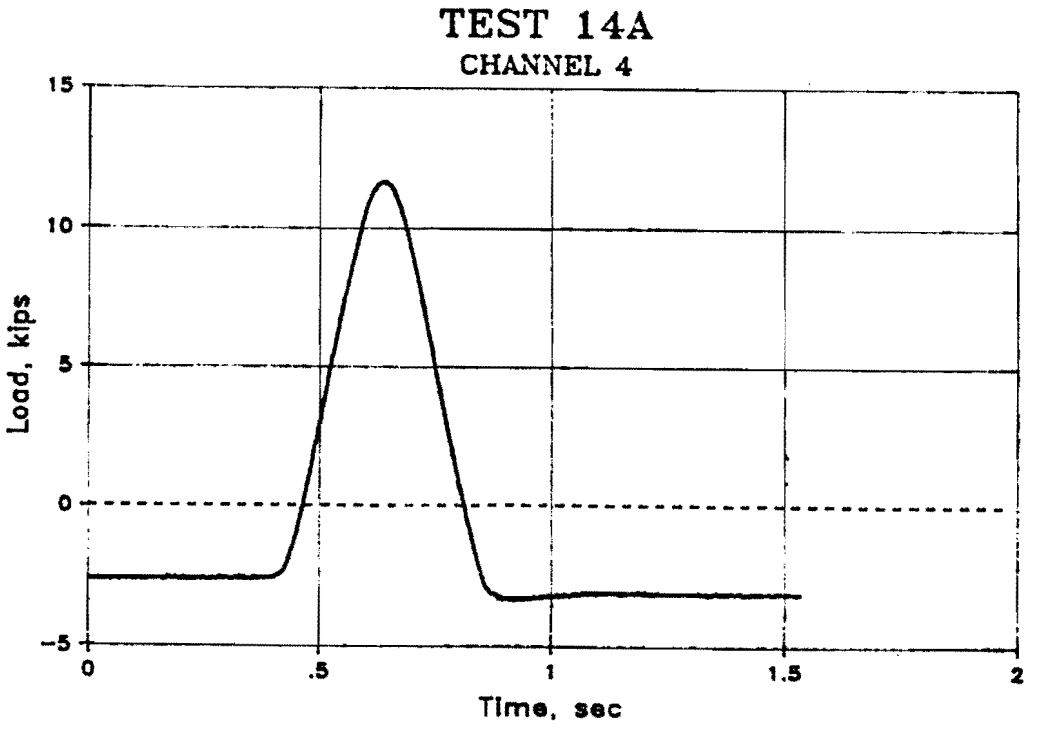
TEST 14A
CHANNEL 4
Load, kips
15
10
5
0
-5
0
.5
1
1.5
2
Time, sec

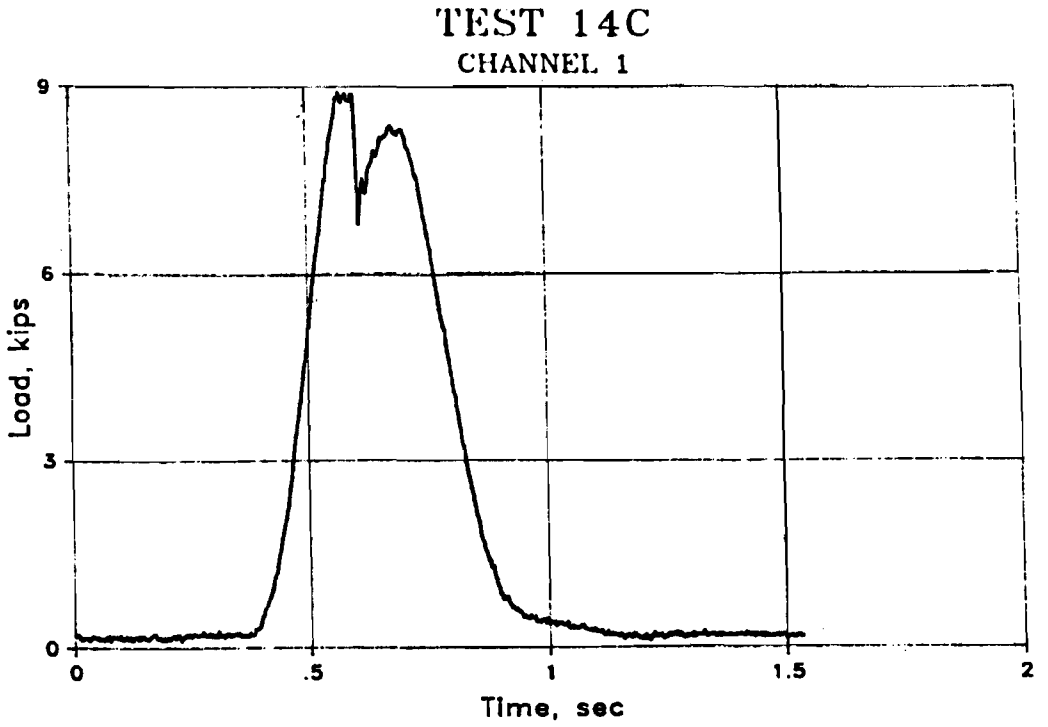
TEST 14C
CHANNEL 1
Load, kips
9
6
3
0
0
.5
1
1.5
2
Time, sec

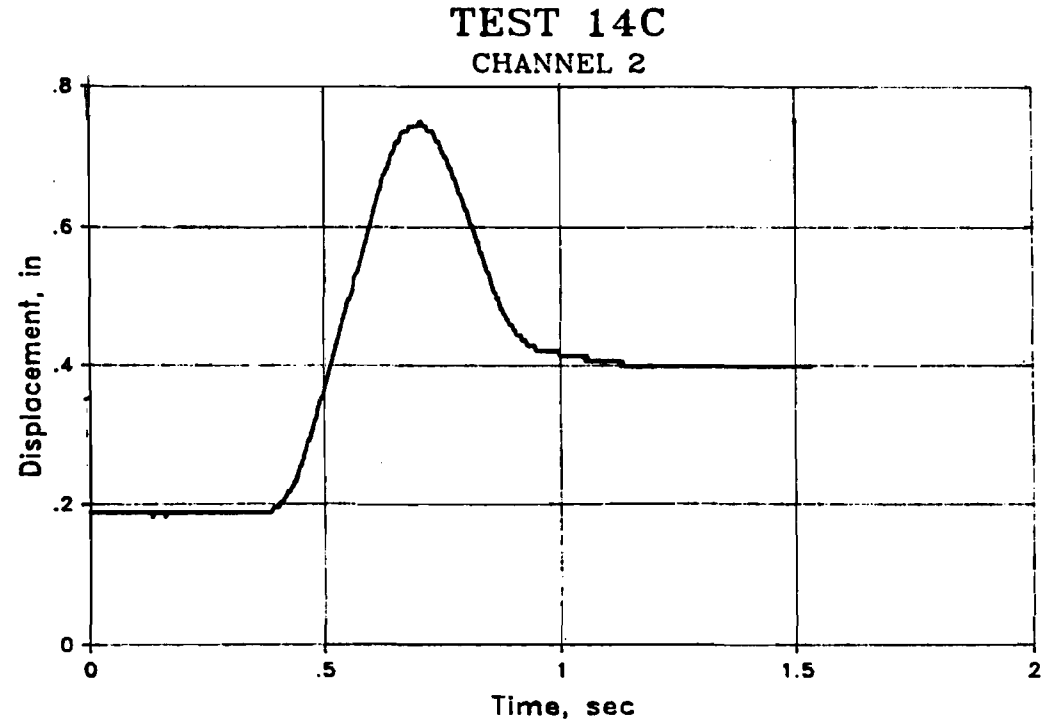
TEST 14C
CHANNEL 2
Displacement, in
.8
.6
.4
.2
0
0
.5
1
1.5
2
Time, sec

TEST 14C
CHANNEL 5

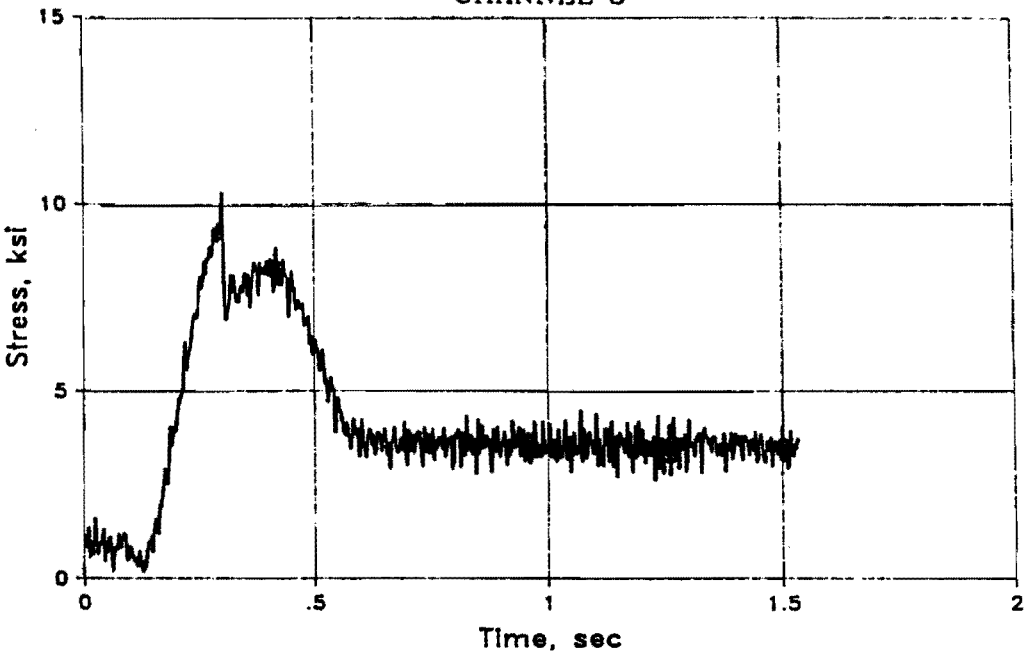

TEST 14C
CHANNEL 6

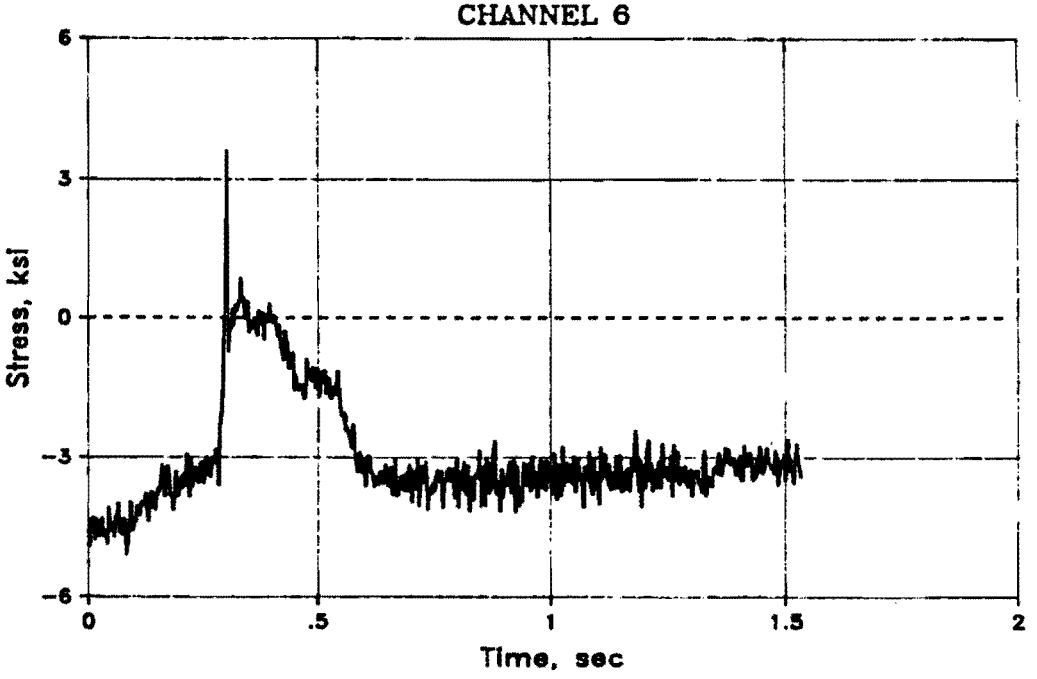

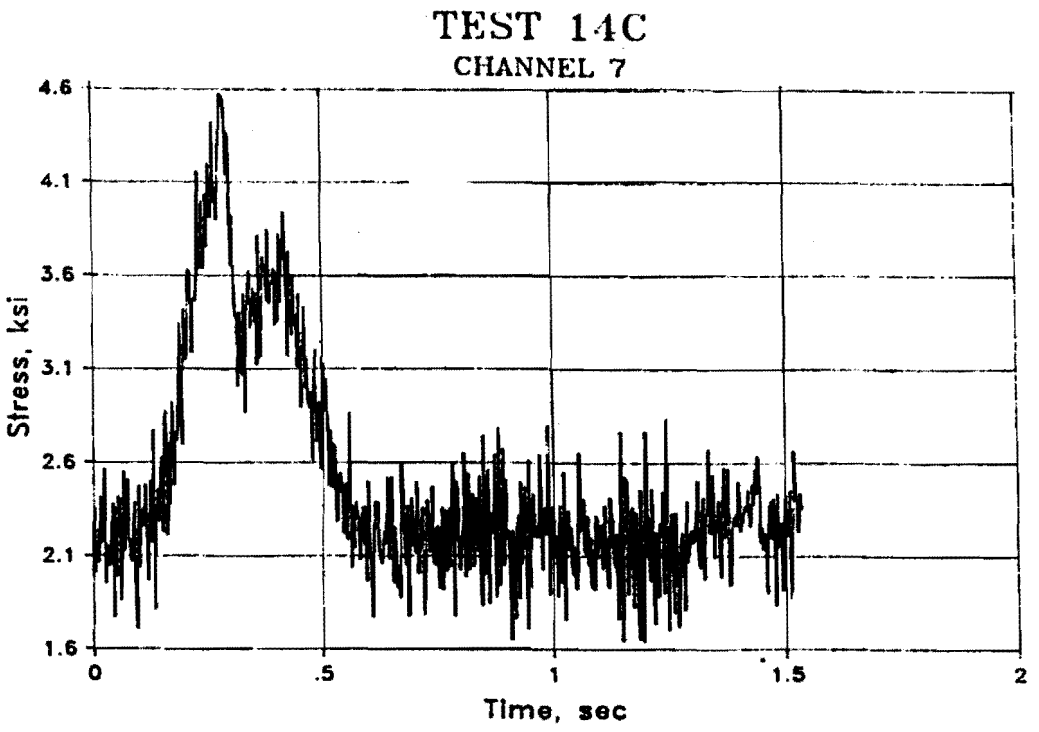
TEST 14C
CHANNEL 7
4.6
4.1
3.6
3.1
2.6
2.1
1.6
Stress, ksi
0
.5
1
1.5
2
Time, sec

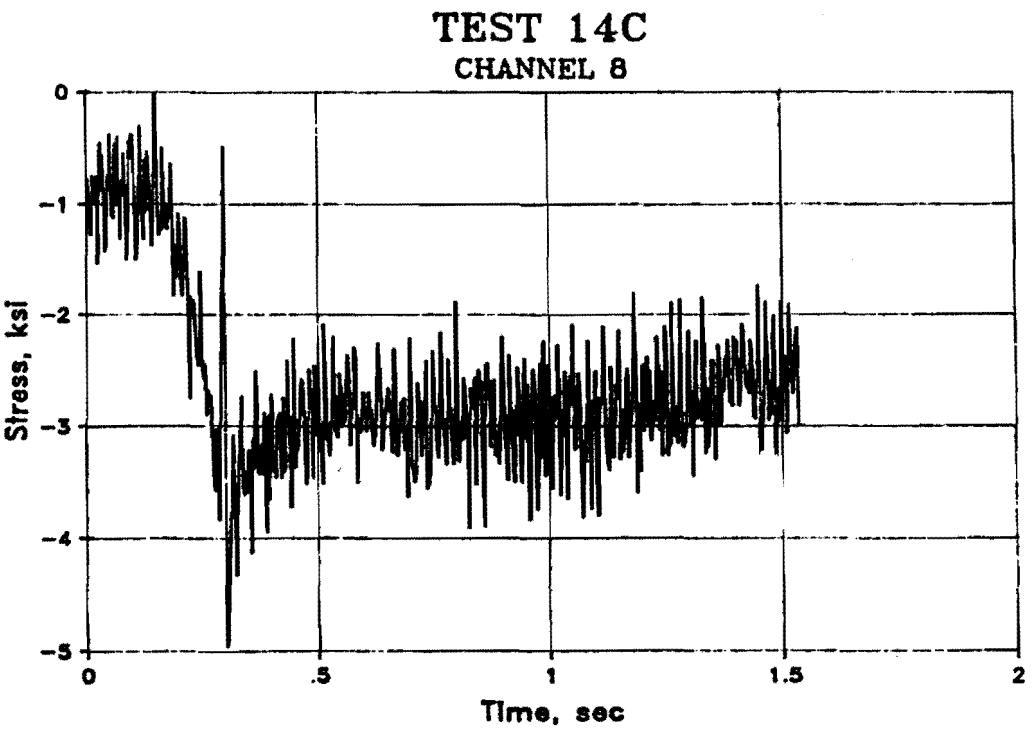
TEST 14C
CHANNEL 8
0
-1
-2
-3
-4
-5
Stress, ksi
0
.5
1
1.5
2
Time, sec

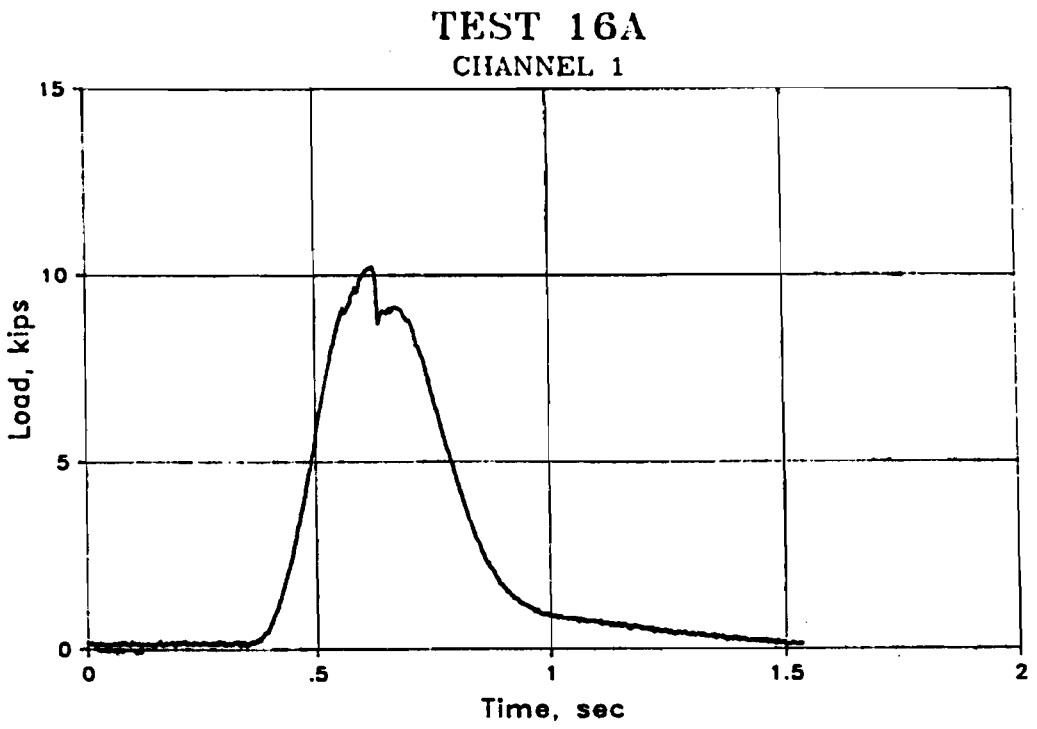
TEST 16A
CHANNEL 1
Load, kips
15
10
5
0
0
.5
1
1.5
2
Time, sec

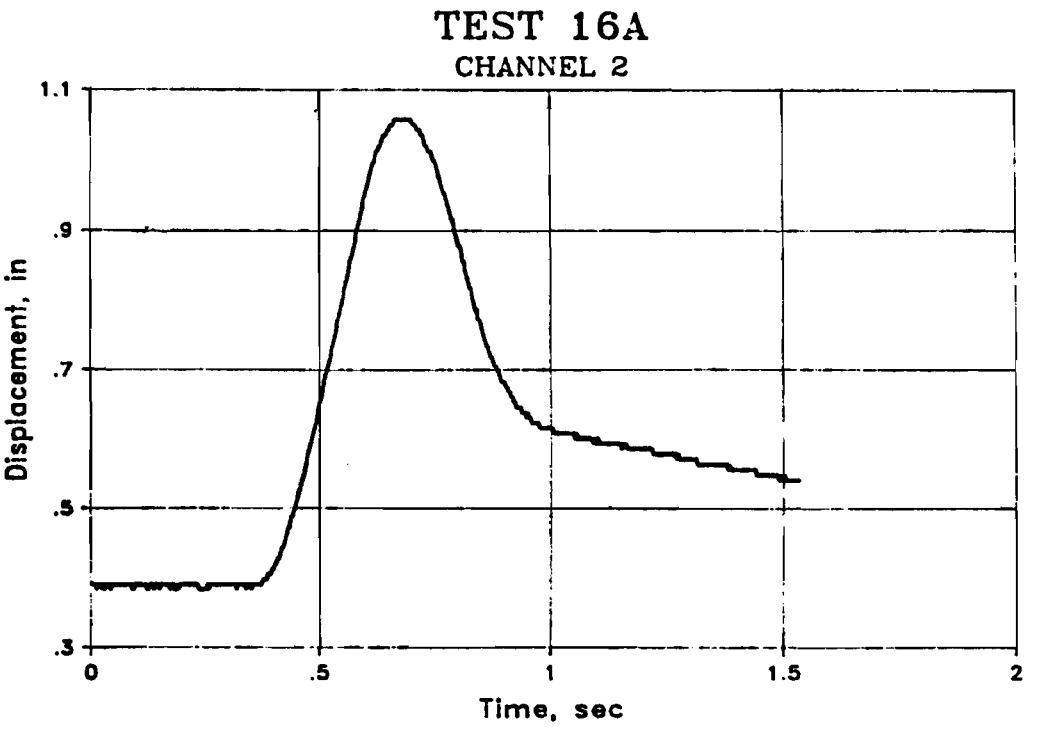
TEST 16A
CHANNEL 2
Displacement, in
1.1
.9
.7
.5
.3
0
.5
1
1.5
2
Time, sec

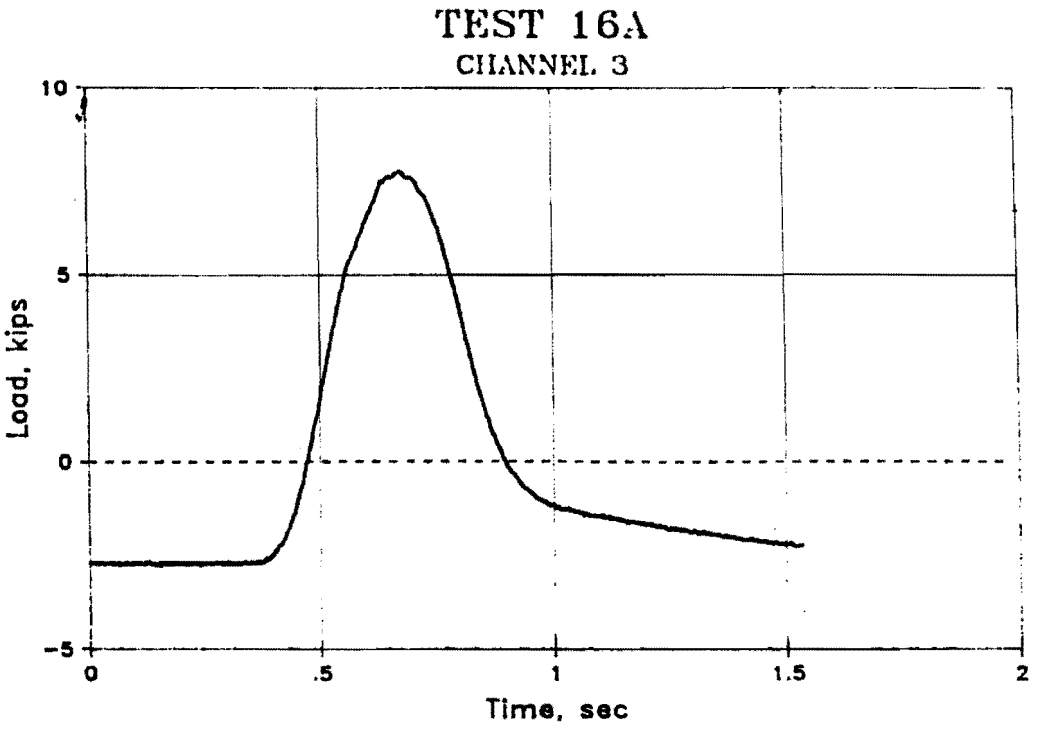
TEST 16A
CHANNEL 3
Load, kips
10
5
0
-5
0
.5
1
1.5
2
Time, sec

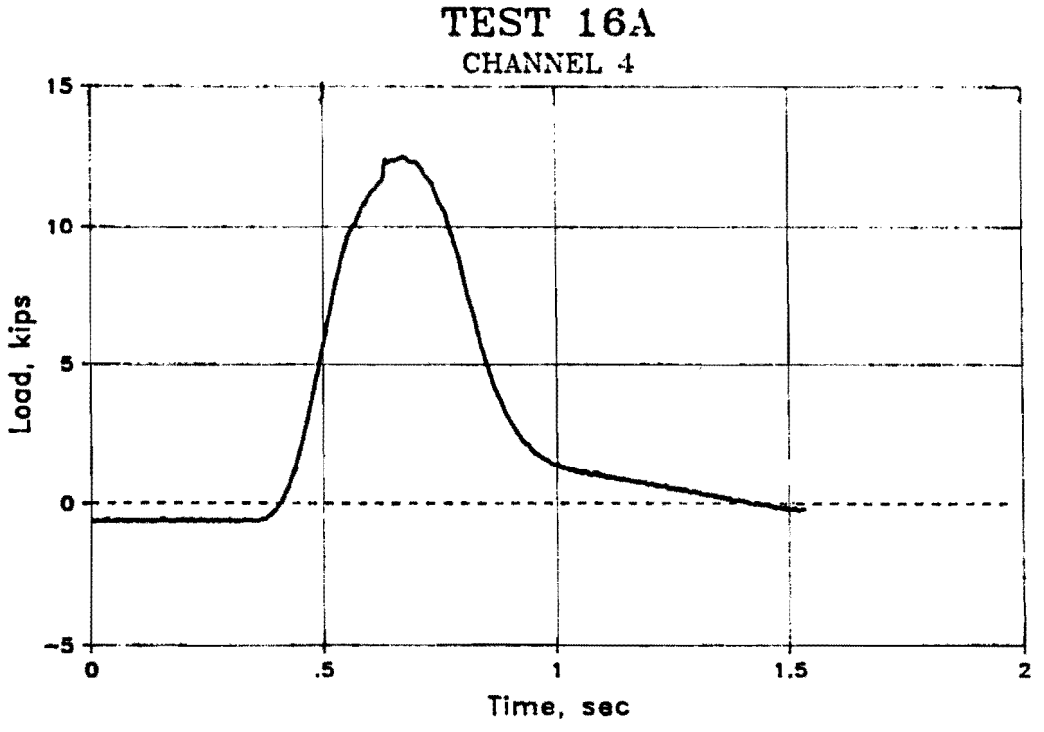
TEST 16A
CHANNEL 4
Load, kips
15
10
5
0
-5
0
.5
1
1.5
2
Time, sec

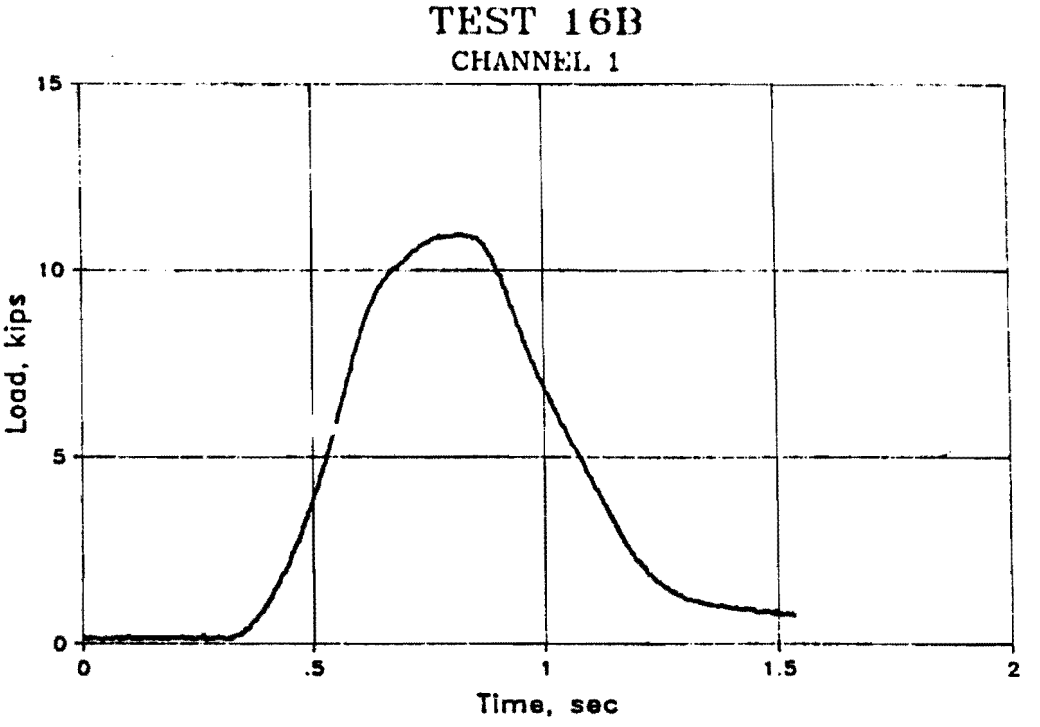
TEST 16B
CHANNEL 1
Load, kips
15
10
5
0
0
.5
1
1.5
2
Time, sec

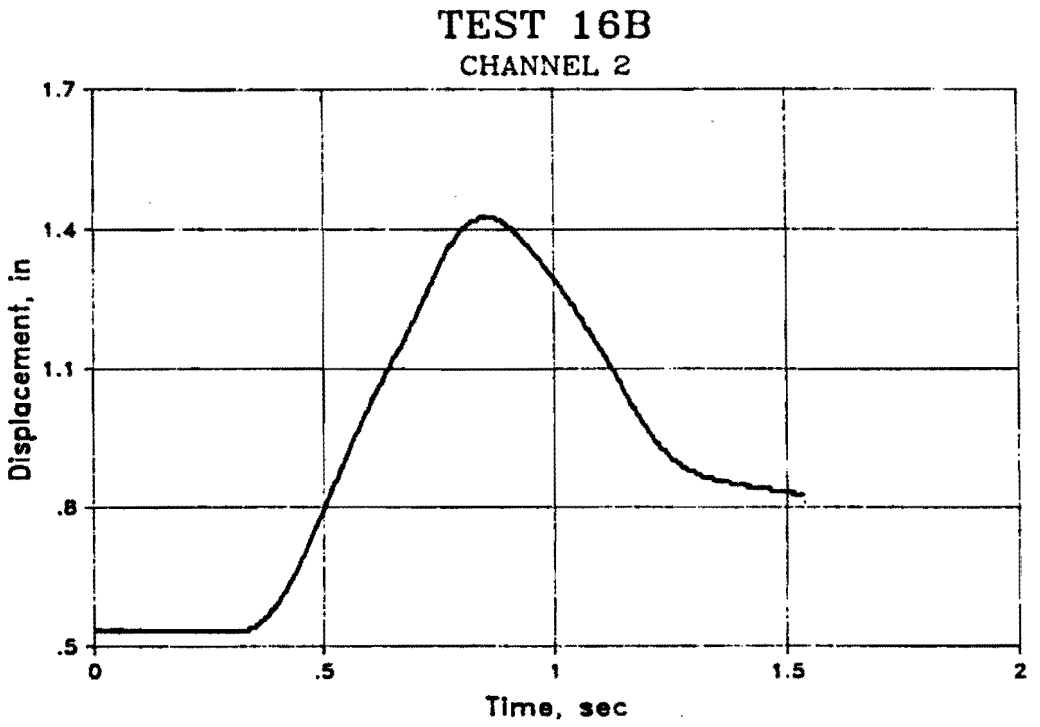
TEST 16B
CHANNEL 2
Displacement, in
1.7
1.4
1.1
.8
.5
0
.5
1
1.5
2
Time, sec

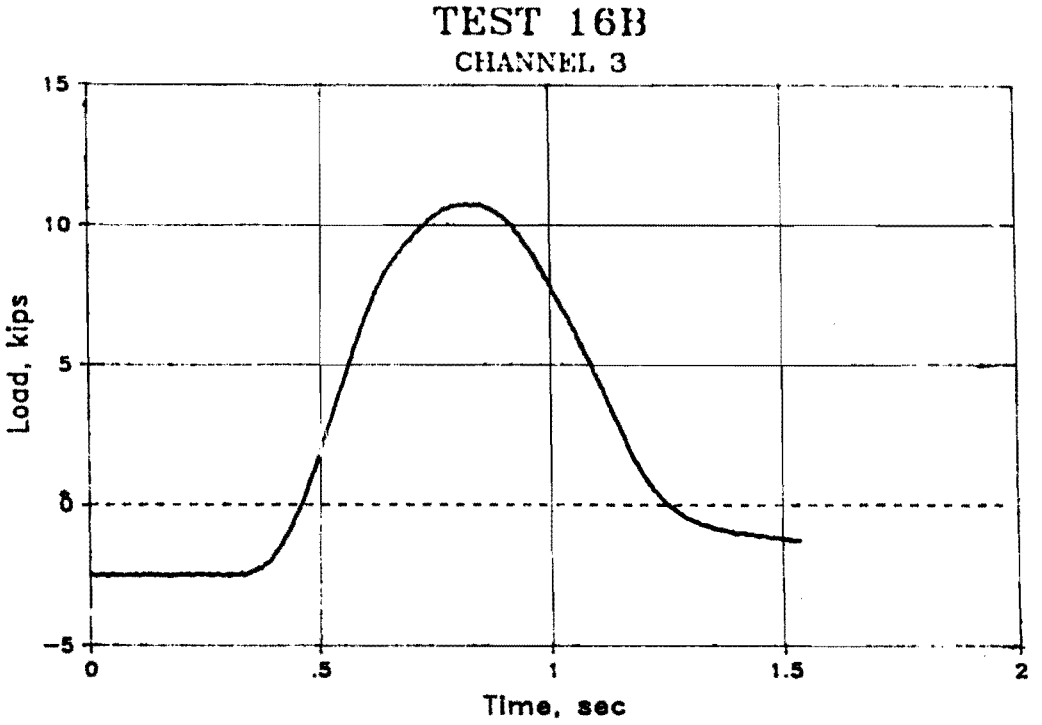
TEST 16B
CHANNEL 3
Load, kips
15
10
5
0
-5
0
.5
1
1.5
2
Time, sec

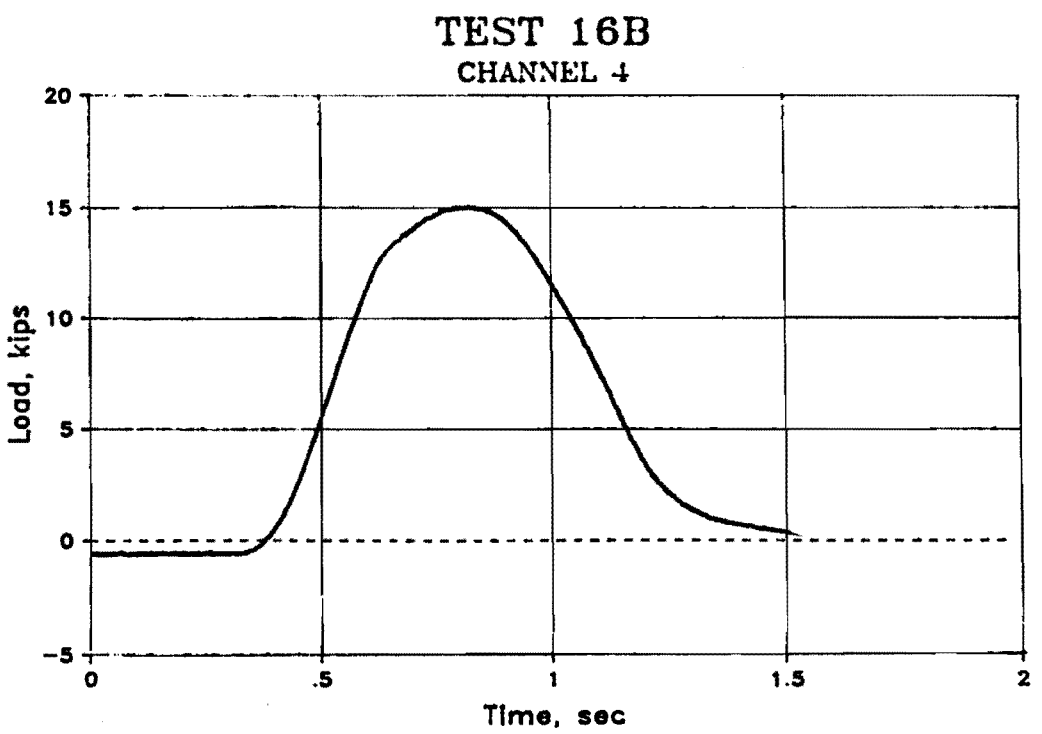
TEST 16B
CHANNEL 4
Load, kips
20
15
10
5
0
-5
0
.5
1
1.5
2
Time, sec

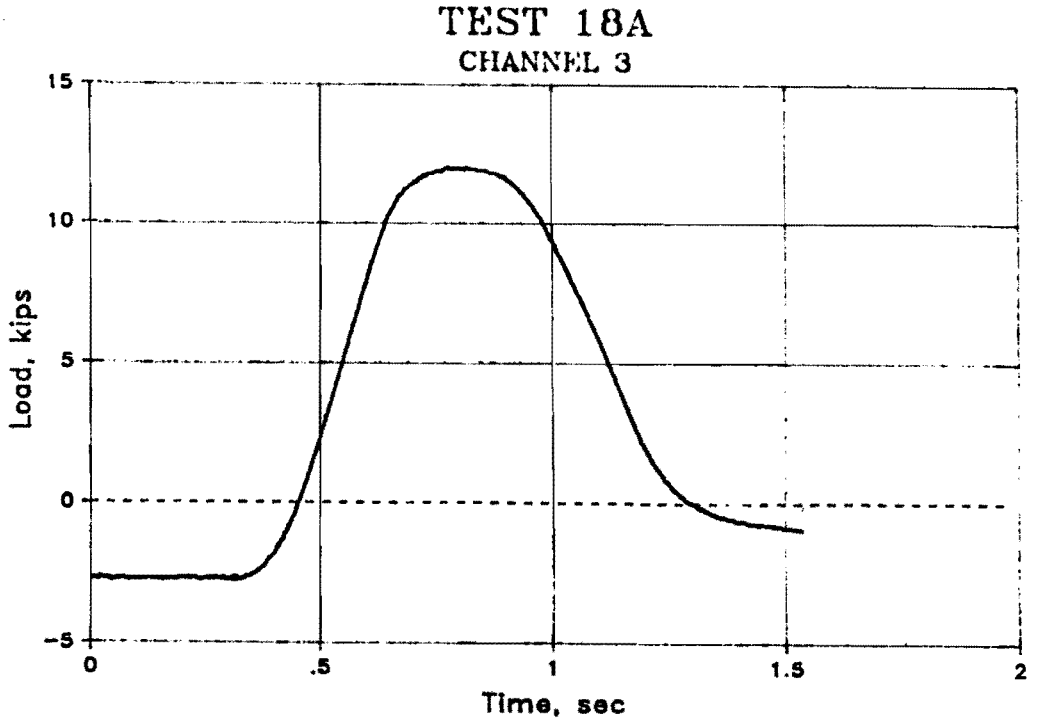
TEST 18A
CHANNEL 3
Load, kips
15
10
5
0
-5
0
.5
1
1.5
2
Time, sec

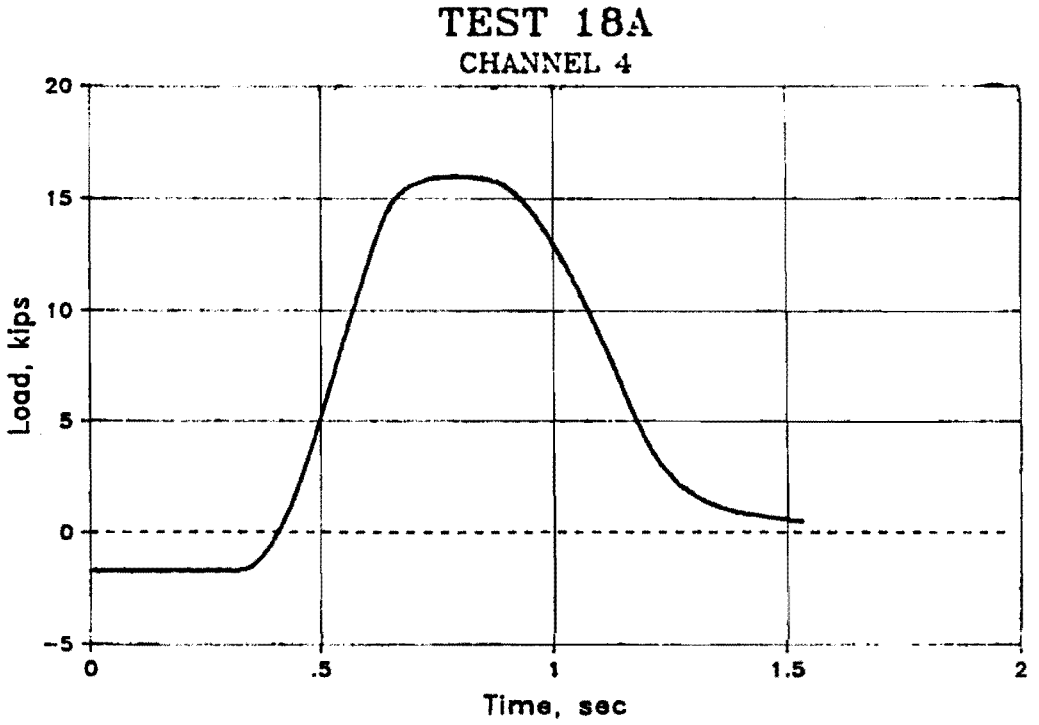
TEST 18A
CHANNEL 4
Load, kips
20
15
10
5
0
-5
0
.5
1
1.5
2
Time, sec

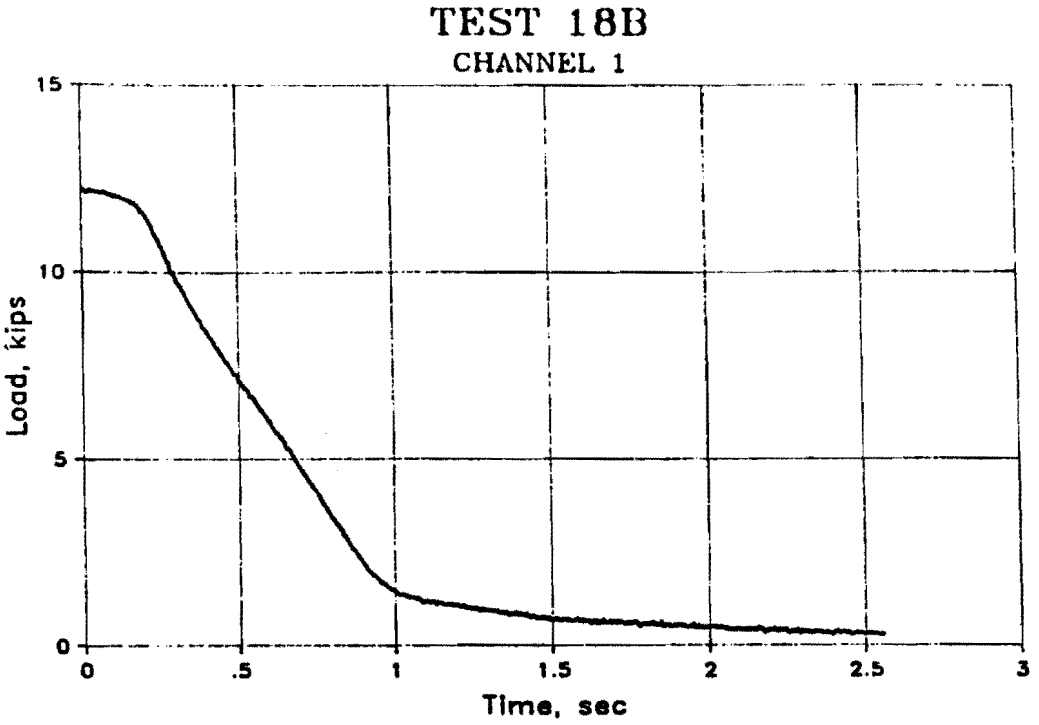
TEST 18B
CHANNEL 1
Load, kips
15
10
5
0
0
.5
1
1.5
2
2.5
3
Time, sec

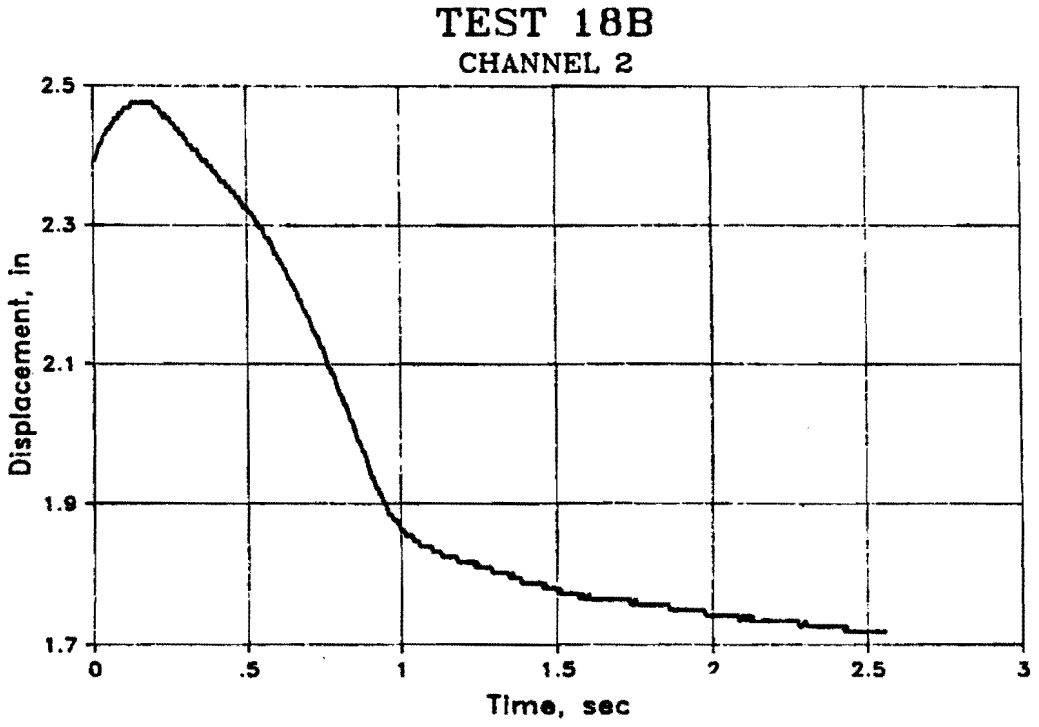
TEST 18B
CHANNEL 2
Displacement, in
2.5
2.3
2.1
1.9
1.7
0
.5
1
1.5
2
2.5
3
Time, sec

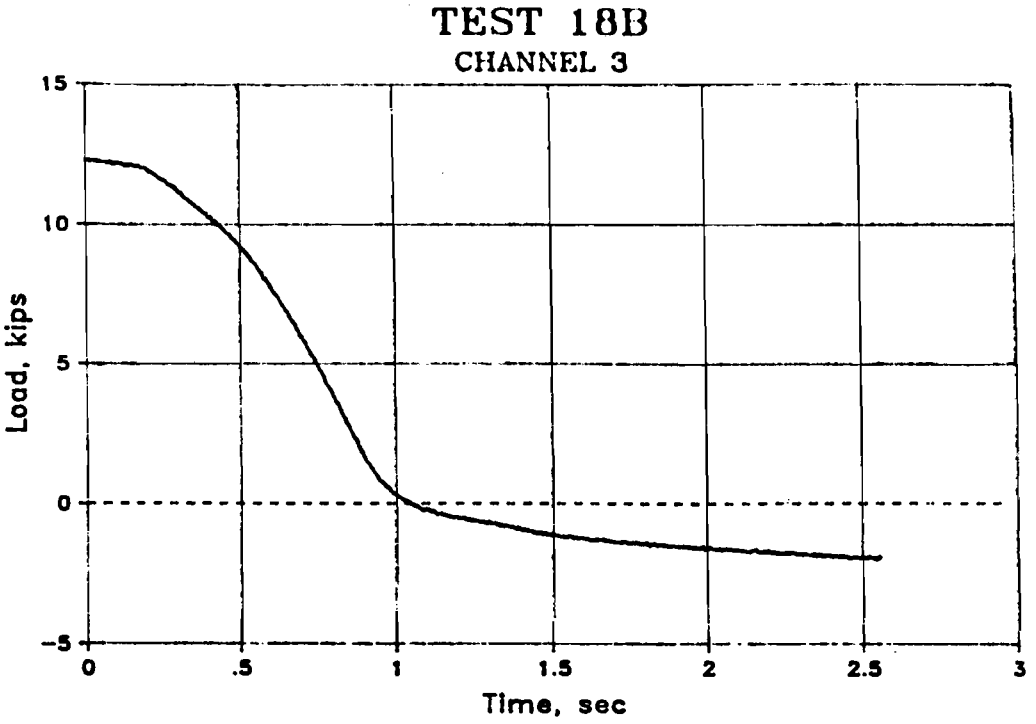
TEST 18B
CHANNEL 3
Load, kips
15
10
5
0
-5
0
.5
1
1.5
2
2.5
3
Time, sec

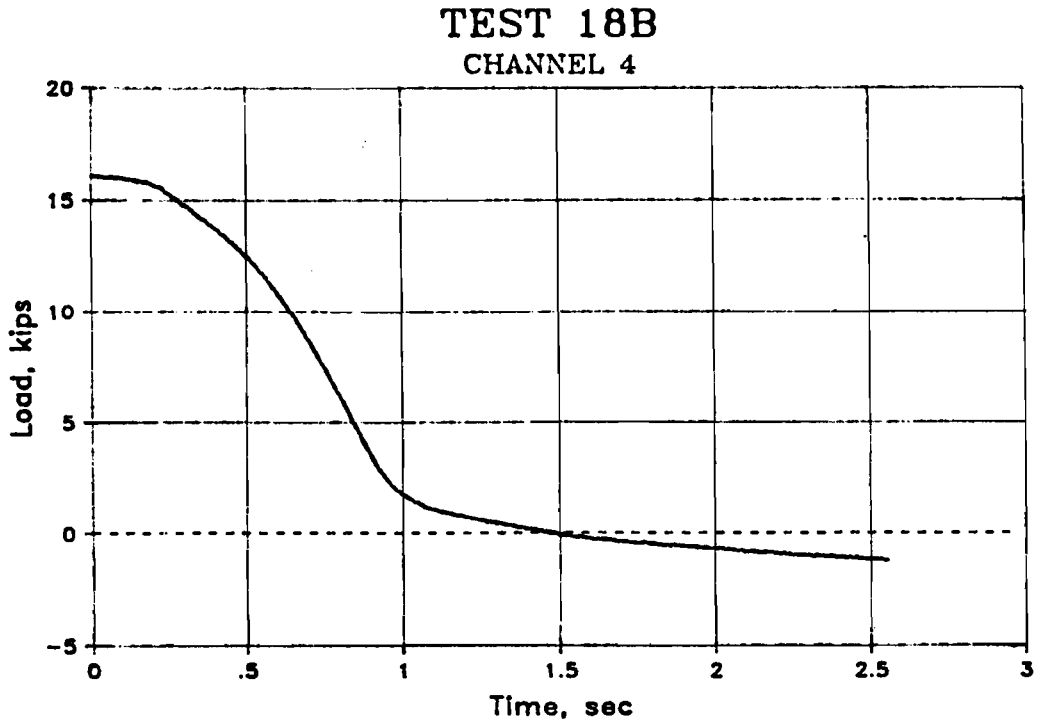
TEST 18B
CHANNEL 4
Load, kips
20
15
10
5
0
-5
0
.5
1
1.5
2
2.5
3
Time, sec

APPENDIX D

Computer Program for Calculating Flexural-Torsional Capacity

```
    1.  000000H          PROGRAM CRASH(INPUT,OUTPUT)
    2.  002131H      150 READ*,FC,F,FYS,VBARS,HBARS,AS,TH,AH,FYH,DS,DH
    3.  002147H          IF(FC.LE.0.0)GO TO 160
    4.  002151H          PRINT 170,FC,F,FYS,VBARS,HBARS,AS,TH,AH,FYH,DS,DH
    5.  002167H      170 FORMAT(1H1,/////,10X,*DATA*,//,10X,*F'C=*,F6.1,1X,
                        1        *KSI*,/,10X,*F=*,F6.1,1X,*INCHES*,/,10X,
                        1        *FYS=*,F6.1,1X,*KSI*,/,10X,** OF V. BARS=*,
                        1        F6.1,/,10X,** OF H. BARS=*,F6.1,/,10X,
                        1        *SINGLE BAR AREA=*,F6.3,1X,*SQ. IN.*,/,10X,
                        1        *SLAB THICKNESS=*,F6.1,1X,*INCHES*,/,10X,
                        1        *TOTAL HOOK AREA=*,F6.3,1X,*SQ. IN.*,/,10X,
                        1        *FYH=*,F6.1,1X,*KSI*,/,10X,*BAR DIAMETER=*,
                        1        F6.3,1X,*INCHES*,/,10X,*HOOK DIAMETER=*,
                        1        F6.3,1X,*INCHES*)
    6.  002167H          X=1.5*DS/2.
    7.  002171H          Y=2.625-DS/2.
    8.  002173H          Z=2.625*DH/2.
    9.  002174H          XX=TH*3.85-X
   10.  002200H          YY=TH-Y
   11.  002201H          ZZ=TH-Z
   12.  002203H          CT=0.75
   13.  002204H          CL=0.0
   14.  002205H          CU=0.0
   15.  002205H      120 A=0.85*CT
   16.  002207H          CC=1.4142*X
   17.  002211H          E1=0.00212*X/CT-0.0015
   18.  002214H          E2=0.00212*YY/CT-0.0015
   19.  002216H          E3=0.00212*YY/CT-0.0015
   20.  002220H          EH=0.00212*ZZ/CT-0.0015
   21.  002222H          FS1=29000.0*E1
   22.  002224H          IF(ABS(FS1).GT.FYS) FS1=FYS
   23.  002230H          IF(CT.GT.CC) FS1=-FS1
   24.  002233H          FS2=29000.0*E2
   25.  002234H          IF(FS2.GT.FYS)FS2=FYS
   26.  002237H          FS3=29000.0*E3
   27.  002240H          IF(FS3.GT.FYS)FS3=FYS
   28.  002243H          FSH=29000.0*EH
   29.  002244H          IF(FSH.GT.FYH)FSH=FYH
   30.  002247H          F1=(VBARS+HBARS)*AS*FS1
   31.  002252H          F2=VBARS*AS*FS2
   32.  002254H          F3=HBARS*AS*FS3
   33.  002257H          FH=AH*FSH
   34.  002260H          FCON=0.601*FC*(A*B-A*A)
   35.  002265H          VC=1.4142*(FCON-F2)
   36.  002267H          V=F3+FH+F1-FCON-0.7071*VC
   37.  002275H          DD=ABS(44.7-V)
   38.  002277H          IF(DD.LE.0.01)GO TO 110
   39.  002302H          IF(V.LT.44.7)GO TO 800
   40.  002304H          IF(V.GT.44.7)GO TO 700
   41.  002306H      700 CL=CT
   42.  002306H          IF(CU.NE.0.0)GO TO 900
   43.  002311H          CT=1.25*CT
   44.  002312H          GO TO 120
   45.  002313H      800 CU=CT
   46.  002314H          IF(CL.NE.0.0)GO TO 900
   47.  002317H          CT=CT/1.25
   48.  002320H          GO TO 120
   49.  002321H      900 CT=(CL+CU)/2.
```

```
50.   0023248          GO TO 210
51.   0023250      110 VCA=0.85*(A*B-A*A)
52.   0023308          PRINT 500
53.   0023358      500 FORMAT(1HO,////////,17X,*RESULTS*)
54.   0023358          PRINT 600,A,V,VC,VCA,FS1,FS2,FS3,FSH
)55.  0023508      600 FORMAT(1HO,///,10X,*A=*,F10.3,2X,*INCHES*,//,10X,*V=*,
                     1        F10.2,2X,*KIPS*,2X,*(REQUIRED V=44.7 KIPS)*,
                     1        //,10X,*V(INC)=*,F10.2,2X,*KIPS*,2X,
                     1        *(MAX. V(INC)=*,F7.2,1X,*KIPS)*,//,10X,*FS1=*,
                     1        F10.2,2X,*KSI*,//,10X,*FS2=*,F10.2,2X,*KSI*,//,
                     1        10X,*FS3=*,F10.2,2X,*KSI*,//,10X,*FSH=*,F10.2,
                     1        2X,*KSI*)
56.   0023508          GO TO 150
57.   0023508      160 STOP
58.   0023528          END
```

DATA

F'C= 4.0 KSI
B= 29.0 INCHES
FYS= 60.0 KSI
# OF V. BARS= 6.0
# OF H. BARS= 2.0
SINGLE BAR AREA= .700 SQ. IN.
SLAB THICKNESS= 10.0 INCHES
TOTAL HOOK AREA= .88 SQ. IN.
FYH= 60.0 KSI
BAR DIAMETER= .500 INCHES
HOOK DIAMETER= .750 INCHES

RESULTS

A= 1.183 INCHES

V= 44.70 KIPS (REQUIRED V=44.7 KIPS)

V(INC)= 10.04 KIPS (MAX. V(INC)= 22.37 KIPS)

FS1= 33.81 KSI

FS2= 60.00 KSI

FS3= 60.00 KSI

FSH= 60.00 KSI

REFERENCES

1. Standard Specifications for Highway Bridges, 13th Edition, American Association of State Highway and Transportation Officials (AASHTO), 1983.

2. Arnold, A. and Hirsch, T.J., "Bridge Deck Designs for Railing Impacts," Federal Highway Administration Report No. 295-1F, Nov. 1983.

3. Klingner, R.E.; Steves, M.A.; and Armstrong, K.S., "Response of Highway Barriers to Repeated Impact Loading: Concrete Barriers" Center for Transportation Research Report No. CTR 382-2F, Nov. 1985.

4. Bryden, J.E. and Hahn, K.C., "Crash Tests of Light Post Thru-Beam Traffic Barriers," Engineering Research and Development, N.Y. State Dept. of Transp., Jan. 1981.

5. "Nelson Stud Project No. 87," Report No. 1960-16: Concrete Arctests No. 5, Nelson Stud Welding Company, Lorain, 1960.

6. "Concrete Anchor Design Data," Manual No. 21, Nelson Stud Welding Company, Division of Gregory Industries, Lorain, Aug. 1961.

7. "Nelson Stud Project No. 802," Report No. 1966-5: Concrete Anchor Tests No. 7, Nelson Stud Welding Company, 1966.

8. "Embedded Properties of Headed Studs," Design Data 10, TRW Nelson Division, Lorain, 1974, 47 pp.

9. Ollgaard, J.G., Slutter, R.G., and Fisher, J.W., "Shear Strength of Stud Connectors in Lightweight and Normal Weight Concrete," AISC Engineering Journal, Vol. 8, No. 2, April 1971, pp. 55-64.

10. McMackin, P.J., Slutter, R.G., and Fisher, J.W., "Headed Steel Anchors under Combined Loading," AISC Engineering Journal, Second Quarter, April 1973, pp. 43-52.

11. PCI Design Handbook - Precast and Prestressed Concrete, 2nd Edition, Prestressed Concrete Institute, Chicago, 1978, 380 pp.

12. PCI Manual for Structural Design of Architectural Precast Concrete, Prestressed Concrete Institute, Chicago, 1977, 448 pp.

13. "Specification for the Design, Fabrication and Erection of Structural Steel Buildings, with Commentary," American Institute of Steel Construction, New York, 1978, 235 pp.

14. "Concrete Anchorages," TVA Civil Design Standard No. Ds-C6-1, Tennessee Valley Authority, Knoxville, 1975.

15. Cannon, R.W., Burdette, E.G., and Funk, R.R., "Anchorage to Concrete," Report No. CEB 75-32, Tennessee Valley Authority, Knoxville, Dec. 1975, 25 pp.

16. Bailey, J.W., and Burdette, E.G., "Edge Effects on Anchorage to Concrete," Civil Engineering Research Series No. 31, The University of Tennessee, Knoxville, Aug. 1977, 120 pp.

17. ACI Committee 349, "Proposed Addition to: Code Requirements for Nuclear Safety Related Coenrete Structures (ACI 349-76)," and "Addition to Commentary on Code Requirements for Nuclear Safety Related Structures (ACI 349-76)," ACI Journal, Proceedings, Vol. 75, No. 8, Aug. 1978, pp. 329-347.

18. Cannon, R.W., Godfrey, D.A., and Moreadith, F.L., "Guide to the Design of Anchor Bolts and Other Steel Embedments," Concrete International, July 1981, pp.28-41.

19. Klingner, R.E., and Mendonca, J.A., "Tensile Capacity of Short Anchor Bolts and Welded Studs: A Literature Review," ACI Journal, Proceedings, Vol. 79, No. 4, July-Aug. 1982, pp. 270-279.

20. Klingner, R.E., and Mendonca, J.A., "Shear Capacity of Short Anchor Bolts and Welded Studs: A Literature Review," ACI Journal, Proceedings, Vol. 79, No. 5, Sept.-Oct. 1982, pp. 339-349.

21. Klingner, R.E., Mendonca, J.A., and Malik, J.B., "Effect of Reinforcing Details on the Shear Resistance of Anchor Bolts under Reversed Cyclic Loading," ACI Journal, Proceedings, Vol. 79, No. 1, Jan.-Feb. 1982, pp. 3-12.

22. ACI Committee 318, "Building Code Requirements for Reinforced Concrete (ACI 318-83)," American Concrete Institute, Detroit, 1977, 132 pp.

23. Adihardjo, R. and Soltis, L., "Combined Shear and Tension on Grouted Base Details," AISC Engineering Journal, First Quarter, Jan. 1979, pp. 23-26.

24. Higdon, A., Ohlsen, E.H., Stiles, W.B., Weese, J.A., and Riley, W.F., Mechanics of Materials, John Wiley and Sons, Inc., New York, 1976.

25. "Riveted and Pin-connected Joints of Steel and Aluminum Alloys," L.S. Moisseif, E.C. Hartmann, and R.L. Moore, Trans. American Society of Civil Engineers, Vol. 109, 1944, pp. 1359.

26. Ferguson, Phil M., "Reinforced Concrete Fundamentals, John Wiley and Sons, Inc., New York, 1979.

27. Hawkins, N.M., Mitchell, D., and Roeder, C.W., "Moment Resisting Connections for Mixed Construction," AISC Engineering Journal, First Quarter, January, 1980, pp. 1-10.

28. Buth, C. E., personal communication, August 1984.